The Mechanism of Cytochrome c Oxidase-Catalyzed Dioxygen Reduction

Thesis by

Stephan N. Witt

In Partial Fulfillment of the Requirements

for the Degree of

Doctor of Philosophy

California Institute of Technology

Pasadena, California

1988

(Submitted April 1, 1988)

If one were only an Indian, instantly alert, and on a racing horse, leaning against the wind, kept on quivering jerkily over the quivering ground, until one shed one's spurs, for there needed no spurs, threw away the reins, for there needed no reins, and hardly saw that the land before one was smoothly shorn heath when horse's neck and head would be already gone.

The Wish to Be a Red Indian
Franz Kafka

ACKNOWLEDGEMENTS

Successful scientific research is usually a cooperative process; this was certainly the case in Sunney's research group. My scientific growth was accelerated through the association with many excellent colleagues in Sunney's laboratory. In particular, I wish to thank Dave. Dave and I labored on an oxidase project together for nearly two years. Our joint effort proved to be uniquely successful. I thank John for his patience, good humor, and for his efforts on the resonance Raman project.

The resonance Raman project was conducted in collaboration with Jerry Babcock's research group at Michigan State University. I would like to thank Bob Kean and Jose Centeno for their efforts on the Raman project. I also wish to thank Jerry for his robust skepticism. The ENDOR project was conducted in collaboration with Brian Hoffman's research group at Northwestern University. I would like to express my gratitude to Brian and Melanie Werst for their efforts on the ENDOR project.

I would like to express my gratitude to Harry Gray for the generous use of his equipment during my years at Caltech. Harry was right when he remarked that the Chan group is 12 Molar around his equipment.

My life at Caltech was enriched by many friendships. I would like to thank John, Walther, Hsin, Craig, Joe, Dayalan, and James for their friendship.

I would like to thank Sunney for his generous support during my tenure at Caltech. His unflagging insistence on excellence and his insights into biophysical chemistry will not soon be forgotten by me.

Most importantly, I thank my mother and father for their love and support. Throughout my life they encouraged me and supported me in all of my various endeavors. I owe more to them than I can ever hope to repay. I dedicate this thesis to them.

Abstract

Cytochrome *c* oxidase plays a primary role in energy transduction in most organisms. Free-energy is conserved by the oxidase in the form of a sizeable electrochemical hydrogen ion gradient across the inner mitochondrial membrane, which is generated during cytochrome *c* oxidase-catalyzed dioxygen reduction. In order to understand the energetics of cytochrome *c* oxidase-dependent energy conservation, the mechanism of cytochrome *c* oxidase-catalyzed dioxygen reduction must be understood in complete detail.

We investigated the kinetics and mechanism of cytochrome *c* oxidase-catalyzed dioxygen reduction at low temperatures (180-210 K) in order to determine the kinetic barriers to intramolecular electron transfer and to elucidate the structural details of the dioxygen intermediates which form at the dioxygen reduction site during a single turnover. Our results show that electron transfer to the dioxygen reduction site is possible from either of the low-potential metal centers. Upon transfer of the third electron to the dioxygen reduction site at low temperatures two reactive dioxygen intermediates form in sequence at the dioxygen reduction site. In both intermediates, dioxygen is at the three-electron level of reduction. The kinetics of the conversion between the two reactive intermediates were examined in detail. The conversion between these two reactive species is highly activated, although entropically assisted. Our results suggest that the cleavage of the dioxygen bond in the first three-electron-reduced intermediate results in the formation of the second three-electron-reduced intermediate. By studying the reoxidation of partially reduced cytochrome *c* oxidase at low temperatures, we also demonstrate that the rate of electron transfer within the oxidase is dependent on the nature of the trapped dioxygen intermediate at the dioxygen reduction site. Finally, the method used for the low-temperature kinetic experiments utilizes carbon monoxide as an inhibitor. Our investigation of the reoxidation of fully reduced cytochrome *c* oxidase reveals that carbon monoxide is not an innocent spectator molecule over

the course of the reoxidation of the oxidase. Specifically, the dissociation of carbon monoxide from the binuclear dioxygen reduction site is the rate-limiting step at low temperatures; and the second three-electron-reduced intermediate is thought to oxidize carbon monoxide to carbon dioxide at low temperature to produce a novel, readily detectable state of the enzyme.

We discovered that reactive partially reduced states of dioxygen may also be trapped at the dioxygen reduction site of cytochrome *c* oxidase at more ambient conditions (273-298 K) under a variety of experimental conditions. Combined chemical and spectroscopic results show that a reactive intermediate is produced at the dioxygen reduction site of cytochrome *c* oxidase when partially reduced cytochrome *c* oxidase is reoxdized with dioxygen and upon treatment of the oxidase with excess hydrogen peroxide. The trapped intermediate exhibits identical reactivity with carbon monoxide as the second three-electron-reduced intermediate which formed upon reoxidation of the fully reduced enzyme at low temperature. These results demonstrate that the same reactive three-electron-reduced dioxygen intermediate may be trapped at the dioxygen reduction site of cytochrome *c* oxidase either upon *intra*molecular electron transfer of the third electron to the peroxidic adduct, which is trapped at the binuclear site, or via an *inter*molecular reaction between the peroxidic adduct and hydrogen peroxide. This latter reaction is thought to involve the reduction of the enzymatic peroxidic adduct via a direct one-electron transfer from hydrogen peroxide. Our combined chemical and spectroscopic results are consistent with a binuclear dioxygen reduction site composed of a ferryl/cupric couple for the second three-electron-reduced dioxygen intermediate. Finally, we exploited the unique reaction between the second three-electron-reduced intermediate and carbon monoxide to probe the coordination sphere of the copper center at the reactive dioxygen reduction site of cytochrome *c* oxidase.

TABLE OF CONTENTS

CHAPTER I

Introduction

In order to survive, prokaryotic and eukaryotic organisms must catalyze hundreds, if not thousands, of endergonic biochemical reactions which are involved in such complex cellular processes as locomotion, protein synthesis and the maintenance of membrane potentials, to name only a few.* Organisms have evolved the capability to drive thermodynamically unfavorable reactions by coupling these reactions to the highly exergonic hydrolysis of ATP to ADP ($\Delta G^{\circ\prime}$ = -7.3 kcal mol^{-1}) (1). Yet, utilizing the hydrolysis of ATP to drive biochemical reactions poses a serious dilemma: organisms must be able to rapidly convert ADP back to ATP. Not surprisingly, there is in fact a magnificient diversity of biochemical processes in which ATP is produced. By understanding the chemistry by which biochemical processes generate metabolic energy, conceivably novel catalysts might

* Abbreviations used: ATP, adenosine triphosphate; NADH, nicotinamide adenine dinucleotide; $FADH_2$, flavin adenine dinucleotide; EXAFS, extended X-ray absorption fine-structure; EPR, electron paramagnetic resonance; RR, resonance Raman; ENDOR, electron nuclear double resonance; and MCD, magnetic circular dicroism.

be developed which are based on the chemical principles derived from studying the biological systems.

The inner mitochondrial membrane is composed of a complex system of integral membrane metalloproteins, referred to as respiratory enzymes. These respiratory enzymes, with an assortment of water soluble electron carriers, catalyze the transfer of electrons from NADH (and $FADH_2$) to O_2. A sizeable fraction of the redox potential difference between NADH and O_2 ($E^{o\prime} = 1.14$ V) (2) is *conserved* in the form of an electrochemical hydrogen ion gradient across the inner mitochondrial membrane via reactions that are catalyzed by the respiratory enzymes. Ultimately, the electrochemical hydrogen ion gradient is utilized by the membrane-bound ATP-synthase to synthesize ATP from ADP and inorganic phosphate. Thus, *ATP synthesis is linked to respiration*. The focus of this thesis is the primary metalloenzyme involved in respiration, cytochrome *c* oxidase.

Cytochrome *c* oxidase is the terminal electron acceptor in the respiratory chain. In eukaryotes, cytochrome *c* oxidase is a multisubunit integral metalloprotein that catalyzes the rapid four-electron reduction of dioxygen to water by accepting electrons from ferrocytochrome *c* on the cytosolic side of the membrane and transferring the electrons intramolecularly to dioxygen at the O_2 binding site (Eqn 1) (3).

$$4 \text{ Ferrocytochrome } c + 4H^+ + O_2 \longrightarrow 4 \text{ Ferricytochrome } c + 2H_2O \qquad (1)$$

Dioxygen reduction by cytochrome *c* oxidase contributes to an electrochemical hydrogen ion gradient across the inner mitochondrial membrane (4) via two distinct reactions: (A) Protons are consumed in the matrix upon the reduction of dioxygen to water (Eqn. 1), while the electrons are taken up on the cytosolic side of the membrane. This process produces charge separation ($\Delta\psi$) across the inner mitochondrial membrane. (B) Protons are vectorially translocated by a redox-linked proton pump from the matrix to the cytosol in concert with electron transfer to the dioxygen reduction site (5-6). This latter process reinforces the ΔpH established

across the inner mitochondrial membrane by the scalar reaction (Eqn 1). Since the stoichiometry in the pumping reaction appears to be $1H^+/e^-$, cytochrome *c* oxidase-catalyzed dioxygen reduction results in the consumption of up to $2H^+/e^-$ from the matrix side of the mitochondrial compartment (3). Therefore, a more appropriate description of the reaction that is catalyzed by cytochrome *c* oxidase is given in Equation 2.

$$4 \text{ Ferrocytochrome } c + 8H^+_m + O_2 \longrightarrow 4 \text{ Ferricytochrome } c + 2H_2O + 4H^+_c \quad (2)$$

Due to its primary role in energy conservation, the mechanism by which cytochrome *c* oxidase converts the electochemical potential difference between ferrocytochrome *c* and O_2 to a protonmotive energy is the subject of intense investigations in the field of bioenergetics. These investigations have naturally focused on the mechanism of cytochrome *c* oxidase-catalyzed dioxygen reduction, because the scalar dioxygen reduction reaction accounts for one-half of the sizeable electrochemical hydrogen ion gradient ($\Delta\mu_{H^+} \sim 220$ mV) (7) across the inner mitochondrial membrane, and the dioxygen molecule and its partially reduced species anchored at the dioxygen reduction site have high redox potentials and provide the driving force for the intramolecular electron transfer and proton translocation events. Furthermore, unraveling the mechanism of cytochrome *c* oxidase-catalyzed dioxygen reduction is of interest to inorganic chemists because of the importance in developing robust catalysts which can utilize O_2 as the terminal oxidant. Before embarking on the description of our investigation of the mechanism of cytochrome *c* oxidase-catalyzed dioxygen reduction, we will briefly review the essential structural and spectroscopic features of cytochrome *c* oxidase.

Spectroscopy and Structure

The mammalian cytochrome *c* oxidase is dimeric in detergent solution (8) and in two-dimensional crystalline arrays (9). It has been suggested that the enzyme is also dimeric as assembled in the mitochondrion (9). The basic structural unit of bovine cytochrome *c* oxidase consists of 12-13 non-covalently linked subunits with

a molecular weight of approximately 200 KD (7). Each monomer contains four prosthetic groups, two spectroscopically inequivalent iron atoms in the form of the unusual heme group (heme A, designated Fe_a and Fe_{a_3}) and two spectroscopically inequivalent copper atoms, designated Cu_A and Cu_B or Cu_{a_3}. Recently it was shown that cytochrome *c* oxidase also contains 1 Zn, 1 Mg per monomeric unit; there is also evidence that a third copper atom may be present per monomeric unit (10). Fe_a and Cu_A are often referred to as the low-potential centers, and serve to transfer electrons from cytochrome *c* to the high potential binuclear reduction site, namely Fe_{a_3} and Cu_B. The four metal centers are thought to be distributed through the enzyme as shown in Figure 1: Fe_a and Cu_A are approximately 13-26 Å apart, and each of these approximately 20 Å from the dioxygen reduction site (11-13). From extended X-ray absorption fine structure (14) and electron paramagnetic resonance (EPR) (15), it has been deduced that Fe_{a_3} and Cu_B are from 3.75-5 Å apart, depending upon the nature of the bridging ligand or the state of turnover of the enzyme.

The oxidized detergent solubilized enzyme is usually referred to as the "resting" enzyme. The resting enzyme is unfortunately heterogeneous, displaying a distribution of different conformational states at the binuclear reduction site (16). The variability of the Soret and α maxima observed for cytochrome *c* oxidase prepared by different isolation procedures is a reflection of the heterogeneity in the resting enzyme. There is no evidence for heterogeneity in the fully reduced solubilized enzyme. Nor is there evidence for heterogeneity in the oxidized enzyme as found in mitochondria or sub-mitochondrial particles. Thus, the conformational heterogeneity is probably an artifact of the enzyme isolation methods. Recently it has been shown that the heterogeneity associated with the isolated, detergent solubilized enzyme may be circumvented or minimized by modifications in the normal isolation procedures (17).

Because cytochrome *c* oxidase is such a large amphipathic protein it is diffi-

Figure 1

Model for the distribution of the redox centers in cytochrome *c* oxidase.

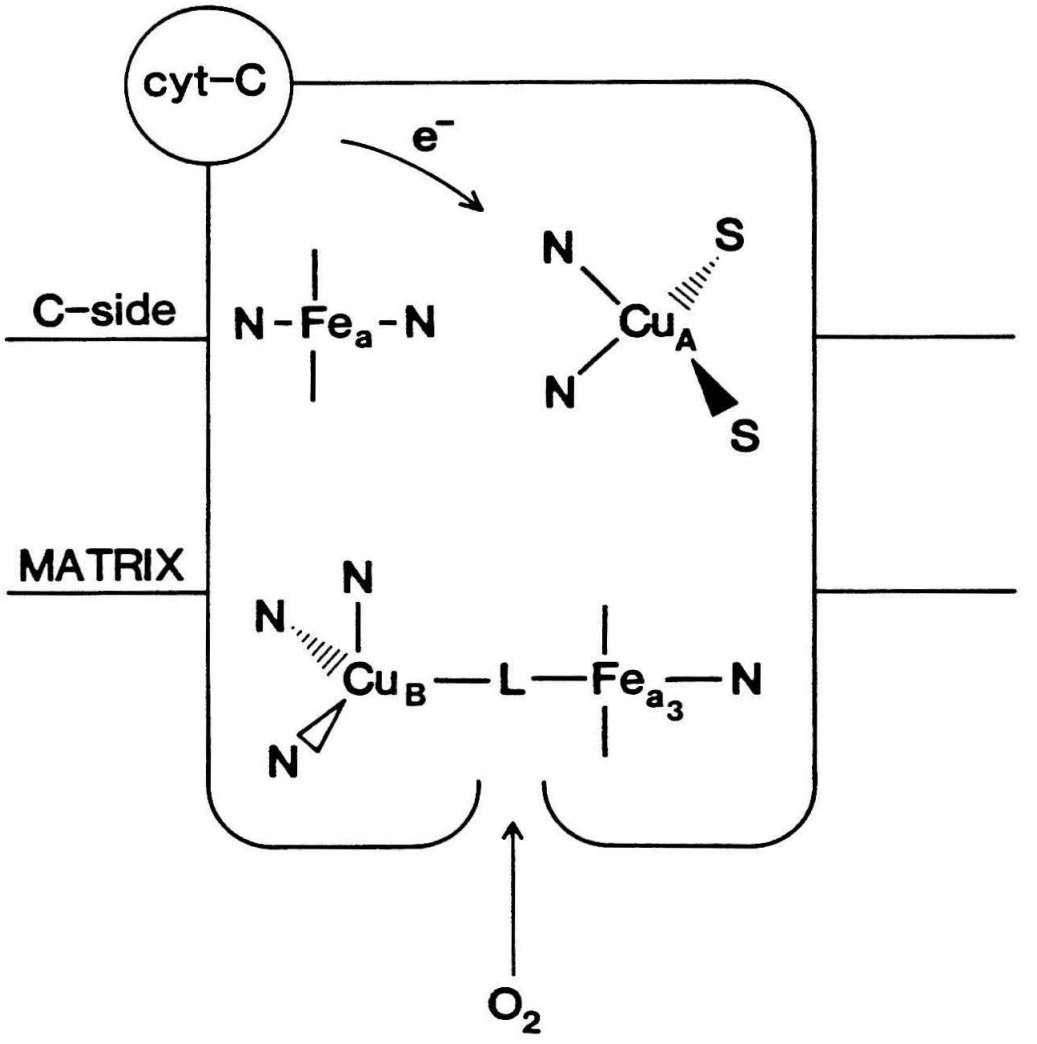
cyt–C
e⁻
C–side
N–Fe$_a$–N
N
S
Cu$_A$
N
S
MATRIX
N
N
Cu$_B$
L
Fe$_{a_3}$
N
N
O$_2$

cult to obtain diffraction quality crystals for X-ray crystollographic studies. It is unlikely that in the near future a X-ray crystal structure of cytochrome *c* oxidase with a resolution better than 10-20 Å will be forthcoming due to the difficulties in obtaining high quality crystals. This lack of structural information has necessitated the use of a variety of other spectroscopic, chemical, and genetic methods in order to deduce important structural aspects of the enzyme. Over the years, in fact, considerable progress has been made toward elucidating the architecture of cytochrome *c* oxidase, including the amino acid sequence of the major subunits, the determination of the ligand structures of the prosthetic groups, and the distance between the prosthetic groups. The structural results set functional constraints on the role of each of the metal centers in the overall scheme of electron transfers, dioxygen reduction, and proton pumping. Therefore, before proceeding to the studies on the mechanism of cytochrome *c* oxidase-catalyzed dioxygen reduction it wil be fruitful to briefly describe each metal center in turn.

Fe_a. Fe_a rapidly accepts electrons from cytochrome *c* with a similar second order rate constant ($k = 8x10^6\ M^{-1}\ s^{-1}$) (18-19), whether the experiments are conducted under anaerobic or aerobic conditions and whether the pulsed or resting enzyme is utilized. Fe_a then transfers the reducing equivalents to the dioxygen reduction site at a rate that is probably dependent on many factors. The rate of electron transfer from Fe_a to the dioxygen reduction site may be as slow as 0.5-3.0 s^{-1} as observed for the resting enzyme under anaerobic conditions (18,20); while under aerobic conditions electron transfer from Fe_a to the dioxygen reduction site may be as fast as $2x10^4 s^{-1}$ (21). These disparate rates for the oxidation of Fe_a and simultaneous reduction of the dioxygen reduction site demonstrate that the ligation, spin and redox states of Fe_{a_3} (and probably Cu_B) influence the driving force for the oxidation of ferrous Fe_a. Additionally, these same factors may modulate the kinetic barrier to electron transfer from the low potential centers to the dioxygen reduction site (20).

Since the cytochrome *c* binding site(s) is located on the cytosolic side of the inner mitochondrial membrane (22), it is likely that Fe_a is also located close to the cytosolic side of the membrane. From a combination of spectroscopic data it has been concluded that Fe_a is low-spin and magnetically isolated in both the oxidized and reduced states (22-24). One histidine has been unambiguously identified as a ligand to Fe_a in yeast cytochrome *c* oxidase (25). From comparisons of RR (26), EPR (27), ENDOR (25) and MCD (24,28) data with model compounds, it has beeen reasonably concluded that Fe_a is a bis-imidazole complex. The EPR spectrum of ferric Fe_a is typical of a low-spin heme with *g* values at 3.03, 2.21 and 1.45 (29). The ligand structure, redox properties, and the spectroscopic signatures of Fe_a are consistent with Fe_a functioning as an electron acceptor and electron donor. It is generally thought that Fe_a is the primary electron acceptor from ferrocytochrome *c*, and it mediates the transfer of electrons to Cu_A, which in turn passes them on to the dioxygen reduction site. However, this view is being challenged at the moment. Final resolution of these issues must await further experimentation. It has also been suggested by various groups that Fe_a is the site of redox-linked proton pumping (7,30).

Cu_A. Cu_A is also reduced rapidly by ferrocytochrome *c*, in parallel with the reduction of Fe_a (31). Accordingly, it has been surmised that Cu_A is also located in a subunit on the cytosolic side of the membrane (32). However, the role of Cu_A in the catalytic cycle of cytochrome *c* oxidase has been a matter of continuing debate. Originally, a sequential electron transfer pathway was proposed in which Cu_A and Fe_a are oxidized in succession at a rate of 7000 s^{-1} and 800 s^{-1}, respectively (33). Several recent kinetic studies indicate the existence of a branched pathway for the reoxidation of both Fe_a and Cu_A, as the kinetics are biphasic rather than a single exponential (21,34-35). Wikström has suggested that Cu_A does not transfer electrons to the dioxygen reduction site directly but only serves as a redox buffer for Fe_a, facilitating electron transfer to the dioxygen reduction site through Fe_a

only (7). Chan and co-workers have proposed that Cu_A is the site of redox-linked proton pumping and that reduction of Fe_a primes the protein for proton uptake and regulates the redox potential of the Cu_A site (36-37).

The structure of Cu_A is rather unusual. The copper coordination most consistent with spectroscopic experiments is CuN_2S_2, $CuNN^*S_2$ or $CuONS_2$ (38-41). EPR and ENDOR experiments on the yeast cytochrome oxidase where [1,3 $^{15}N_2$] histidine, [β, β-$^2H_2$] cysteine or [β-^{13}C] cysteine has been incorporated into the enzyme demonstrated unambiguously that at least one histidine and one cysteine are ligated to Cu_A (40); and the recent ENDOR results are consistent with two cysteines per Cu_A (41). The latter ENDOR study also suggested a symmetric coordination of the copper ion to two cysteines and that there is substantial spin density onto a cysteine sulphur in the oxidized enzyme such that the site may be considered as a Cu(I)-S_2 radical. Chan *et al.* have proposed a detailed model for the coordination of Cu_A which involves the ligation of two histidines and two cysteines per Cu_A unit (42). A recent EXAFS study on a series of samples in which Cu_A, and not Cu_B, was chemically modified by the sulphydryl reagent p-(hydroxymercuri)benzoate (p-HMB) has allowed the inner coordination spheres of Cu_B as well as Cu_A to be determined. For Cu_A, two sulphur atoms and two nitrogen (or oxygen) atoms are implicated as ligands, with Cu-N and Cu-S distances of 1.98 and 2.28 Å, respectively (43).

Cu_A is generally accepted to be bound to a region of subunit II which contans two conserved cysteine residues and several conserved histidines (44). Cu_A exhibits an intense absorption band centered at 830 nm (ϵ = 3000 M^{-1} cm^{-1}). The EPR spectrum of Cu_A is highly unusual: the spectrum is almost isotropic with no resolvable hyperfine interaction at X-band frequencies (24). The EPR spectrum of Cu_A is adequately simulated with g values of 2.18, 2.03 and 1.99 for g_z, g_y, and g_x, respectively (24,45). The g value of 1.99 has generated considerable interest because it is below the free-electron g value of 2.0023. The electron-spin relaxation

properties of Cu_A have also been shown to be significantly different than for blue copper centers (13). A possible explanation for the unusually small hyperfine interaction, the low g_z value, and the high degree of covalency is that there is significant electron delocalization to Cu_A from its associated cysteine ligands (36).

Fe_{a_3} and Cu_B. Fe_{a_3} and Cu_B comprise the binuclear dioxygen reduction site. It is generally assumed that this part of the protein complex is embedded in the bilayer membrane, closer to the matrix. The best estimates based on EPR relaxation measurements give distances of 15-20 Å for the distance of the binuclear site from either Fe_a or Cu_A (11-13). The proximal ligand to Fe_{a_3} has been unambiguously shown to be a histidine (46) based on EPR measurements on the yeast enzyme containing [1,3-^{15}N] histidine. The sixth axial position is variable; it is the site available for binding the bridging ligand between Fe_{a_3} and Cu_B. Dioxygen, carbon monoxide (CO), and nitric oxide (NO) bind to this site when Fe_{a_3} is reduced; azide, cyanide, peroxide, and formate bind when Fe_{a_3} is ferric (47).

Fe_{a_3} contributes to the intensity of the optical absorption spectrum in both the Soret and α regions (48-49). From a combination of spectroscopic studies, including resonance Raman (24,50), MCD (51) and magnetic susceptibility (52), Fe_{a_3} is a ferric heme and is high-spin in the resting enzyme. Magnetic susceptibility studies suggest that in the resting enzyme the ferric high spin Fe_{a_3} is antiferromagnetically coupled to cupric Cu_B to give a S=2 ground state ($-J \geq 200$ cm^{-1}). This antiferromagnetic coupling is thought to be mediated by a bridging ligand (16); however, the identity of this bridging ligand has been elusive. When the resting enzyme is fully reduced, ferrous Fe_{a_3} remains high-spin but goes low-spin in the presence of CO or NO.

Cu_B is the most enigmatic metal center of cytochrome *c* oxidase since it does not contribute any absorbance in the optical spectrum, nor does it have an EPR signal under most conditions. Cu_B binds NO in both the cupric and cuprous states (53); it also binds CO when Cu_B is in the cuprous state (54). The identification

of the ligands to Cu_B has been hampered by the difficulty in obtaining an EPR-detectable state of the metal center. Under some conditions, a readily saturable rhombic Cu_B EPR signal is produced (55-57), which is thought to arise from a magnetically isolated cupric Cu_B adjacent to a ferrous Fe_{a_3} stabilized in the low-spin state by dioxygen (56-57). In fact, Cline *et al.* (58) recently reported results from a comparative ENDOR study of the rhombic Cu_B EPR signal and a similar rhombic copper EPR signal from partially reduced laccase. Their ENDOR results suggest that there are two (and possibly three) nitrogen ligands to Cu_B. In Chapter III we report a new method to prepare large yields of the rhombic Cu_B EPR signal and subsequently we report the results from a recent ENDOR study of the rhombic Cu_B EPR signal (Chapter V). The most recent EXAFS measurements performed on Cu_A-depleted cytochrome *c* oxidase suggest 3 (N,O) and 1 (S,Cl) (43). If sulphur coordination is involved in Cu_B, the Cu-S distance of 2.3 Å is more consistent with sulphur from methionine than cysteine based on comparison to model compounds.

REFERENCES

1. Stryer, L. (1981) *Biochemistry* (Freeman and Co., San Francisco), p. 240.
2. Ibid. p. 311.
3. Wikström, M., Krab, K. and Saraste, M. (1981) *"Cytochrome Oxidase- A Synthesis"* (Academic Press).
4. Wikström, M. (1982) *Curr. Top. Membr. Transp.* **16**, 303-321.
5. Wikström, M (1977) *Nature* **266**, 271-273.
6. Wikström, M. and Saari, H.T. (1977) *Biochim. Biophys. Acta* **462**, 347-361.
7. Stryer, L. (1981) *Biochemistry* (Freeman and Co., San Francisco), p. 317.

8. Robinson, N.C. and Capaldi, R.A. (1977) *Biochemistry* **16**, 375-381.

9. Henderson, R., Capaldi, R.A. and Leigh, J.S. (1977) *J. Mol. Biol.* **112**, 632-648.

10. Einarsdóttir, O. and Caughey, W.S. (1985) *Biochim. Biophys. Res. Commun.* **129**, 842-847.

11. Ohnishi, T., LoBrutto, R., Salerno, J.C., Brudner, R.C. and Frey, T.G. (1982) *J. Biol. Chem.* **257**, 14821-14825.

12. Scholes, C.P., Janakkiraman, R., Taylor, H. and King, T.E. (1984) *Biophys. J.* **45**, 1027-1030.

13. Brudvig, G.W., Blair, D.F. and Chan, S.I. (1984) *J. Biol. Chem.* **259**, 11001-11009.

14. Powers, L., Chance, B., Ching, Y. and Angiolillo, P. (1981) *Biophys. J.* **34**, 465-498.

15. Stevens, T.H., Brudvig, G.W., Bocian, D.F. and Chan, S.I. (1979) *Proc. Natl. Acad. Sci. USA* **76**, 3320-3324.

16. Brudvig, G.W., Stevens, T.H., Morse, R.H. and Chan, S.I. (1981) *Biochemistry* **20**, 3912-3921.

17. Baker, G.M., Noguchi, M. and Palmer, G. (1987) *J. Biol. Chem.* **262**, 595-604.

18. Gibson, Q.H. and Greenwood, C. (1965) *J. Biol. Chem.* **240**, 2694-2698.

19. Andréasson, L.-E. (1975) *Eur. J. Biochem.* **53**, 591-597.

20. Antalis, T.M. and Palmer, G. (1982) *J. Biol. Chem.* **157**, 6194-6206.

21. Hill, B.C. and Greenwood, C. (1984) *Biochem. J.* **218**, 913-921.

22. Blum, H., Leigh, J.S. and Ohnishi, J. (1980) *Biochim. Biophys. Acta* **626**, 31.

23. Aasa, R., Albracht, S.P.J., Falk, K.-E., Lanne, B. and Vänngård, T. (1976) *Biochim. Biophys. Acta* **422**, 260-272.

24. Babcock, G.T., Vickery, L.-E. and Palmer, G. (1976) *J. Biol. Chem.* **251**, 7907-7919.

25. Martin, C.T., Scholes, C.P. and Chan, S.I. (1985) *J. Biol. Chem.* **260**, 2857-

2861.

26. Babcock, G.T., Callahan, P.M., Ondrias, M.R. and Salmeen, I. (1981) *Biochem.* **20**, 959-966.
27. Peisach, J. and Mims, W.B. (1981) *Isr. J. Chem.* **21**, 59-60.
28. Eglinton, D.G., Hill, B.C., Greenwood, C. and Thomson, A.J. (1984) *J. Inorg. Chem.* **21**, 1-8.
29. Van Gelder and Beinert, H. (1965) *Biochim. Biophys. Acta* **189**, 1-24.
30. Babcock, G.T. and Callahen, P.M. (1983) *Biochemistry* **22**, 2314-2319.
31. Wikstrõm, M., Krab, K. and Saraste, M. (1981) *"Cytochrome Oxidase- A Synthesis"* (Academic Press), p. 136.
32. Blum, H., Leigh, J.S. and Ohnishi, T. (1980) *Biochim. Biophys. Acta* **626**, 31.
33. Greenwood, C. and Gibson, Q.H. (1967) *J. Biol. Chem.* **242**, 1782-1789.
34. Clore, G.M., Andréasson, L.-E., Karlsson, B., Aasa, R. and Malmstrõm, B.G. (1980) *Biochem. J.* **185**, 139-154.
35. Blair, D.F., Witt, S.N. and Chan, S.I. (1985) *J. Am. Chem. Soc.* **105**, 7389-7399.
36. Chan, S.I., Bocian, D.F., Brudvig, G.W., Morse, R.H. and Stevens, T.H. (1979) in *"Cytochrome Oxidase"* (King, T.E. *et al.* , eds.), pp. 177-188.
37. Gelles, J., Blair, D.F. and Chan, S.I. (1986) *Biochim. Biophys. Acta* **853**, 205-236.
38. Scott, R.A., Cramer, S.P., Shaw, R.W., Beinert, H. and Gray, H.B. (1981) *Proc. Natl. Acad. Sci. USA* **78**, 664-667.
39. Hoffman, B.M., Roberts, J.E., Swanson, M., Speck, S.H. and Margoliash, E. (1980) *Proc. Ntal. Acad. Sci. USA* **77**, 1452-1456.
40. Stevens, T.H., Martin, C.T., Wang, H., Brudvig, G.W., Scholes, C.P. and Chan, S.I. (1982) *J. Biol. Chem.* **257**, 12106-12113.
41. Martin, C.T., Scholes, C.P. and Chan, S.I., unpublished results.

42. Chan, S.I., Brudvig, G.W., Martin, C.T. and Stevens, T.H. (1982) in *Electron Transport and Oxygen Utilization* (Ho, C., ed.) (Elsevier, Amsterdam), pp. 171-177.

43. Li, P.M., Gelles, J., Chan, S.I., Sullivan, R.J. and Scott, R.A. (1987) *Biochemistry* **28**, 2091-2095.

44. Buse, G., Steffens, G.J., Steffens, G.C.M., Scaher, R. and Erdweg, M. (1982) in *Electron Transport and Oxygen Utilization* (Ho., C. ed.) (Elsevier, Amsterdam), p. 157.

45. Greenaway, F.T., Chan, S.H.P. and Vincow, G. (1977) *Biochim. Biophys. Acta* **480**, 62.

46. Stevens, T.H. and Chan, S.I. (1981) *J. Biol. Chem.* **256**, 1069-1071.

47. Lemberg, M.R. (1969) *Physiol. Rev.* **49**, 48-58.

48. Vanneste, W.H. (1966) *Biochemistry* **5**, 838.

49. Blair, D.F., Bocian, D.F., Babcock, G.T. and Chan, S.I. (1982) *Biochemistry* **21**, 6928-6935.

50. Woodruff, W.H., Dallinger, R.F., Antalis, T.M. and Palmer, G. (1981) *Biochemistry* **20**, 1332-1338.

51. Thomson, A.J., Brittain, T., Greenwood, C. and Springall, J.P. (1977) *Biochem. J.* **165**, 327-336.

52. Tweedle, M.F., Wilson, L.J., Garcia-Iniquez, Babcock, G.T. and Palmer, G. (1978) *J. Biol. Chem.* **253**, 8065-8071.

53. Brudvig, G.W., Stevens, T.H. and Chan, S.I. (1980) *Biochemistry* **19**, 5275-5285.

54. Fiamingo, F.G., Altschuld, R.A., Moh, P.P. and Alben, J.O. (1982) *J. Biol. Chem.* **157**, 1639-1650.

55. Reinhammar, B., Malkin, R., Jensen, P., Karlsson, B., Andréasson, L.-E., Aasa, R., Vänngård, T and Malmström, B. (1980) *J. Biol. Chem.* **255**, 5000-5003.

56. Karlsson, B. and Andréasson, L.-E. (1981) *Biochim. Biophys. Acta* **635**, 73-80.

57. Witt, S.N. and Chan, S.I. (1987) *J. Biol. Chem.* **262**, 1446-1448.

58. Cline, J., Reinhammer, B., Jensen, P., Nenters, R. and Hoffman, P.M. (1983) *J. Biol. Chem.* **258**, 5124-5128.

CHAPTER II

The Reaction of Cytochrome c Oxidase with Dioxygen at Low Temperatures. Evidence for Two Three-Electron-Reduced Intermediates and Entropic Promotion of the Bond Breaking Step.

The mechanism of cytochrome *c* oxidase dioxygen reduction has been the subject of numerous investigations (1-7). The reaction of reduced cytochrome *c* oxidase with dioxygen is highly exothermic and is extremely rapid ($t_{1/2}$~500 μs at 298 K) (1), with a second order rate constant for the recombination of dioxygen with the reduced enzyme of approximately 8 x 10^6 M^{-1} s^{-1} (1,8). Accordingly, it is necessary to monitor the reaction using rapid kinetic techniques, or follow the formation of the intermediates at low temperatures (160-200 K) where the rate of the reaction can be slowed down dramatically.

Low temperature experiments on biological molecules have an advantage over room temperature experiments in that reactive intermediates can be generated during incubations at low temperatures and then trapped by immersing the sample into liquid nitrogen. The trapped intermediates may then be studied by a variety of techniques, such as EPR, resonance Raman, MCD, and Mössbauer spectroscopies, which provide information on the molecular structure of the reactive species. Of

course, implicit in these investigations is that the results obtained in the low temperature studies can be extrapolated to room temperature. Yet, it will become evident that biological reactions at low temperatures exhibit quite different *kinetic* behavior than (the same reaction) at room temperature.

B. Chance *et al.* pioneered the "triple-trapping" technique in 1975 (9); this technique has been widely used in the oxidase field to study the reoxidation of cytochrome *c* oxidase at low temperatures. Since carbon monoxide binds tightly to ferrous Fe_{a_3}, carbon monoxide is utilized in this method to inhibit the reoxidation of the reduced enzyme by dioxygen. Dioxygen is introduced to the fully reduced CO-inhibited enzyme while the sample is maintained at approximately 253 K as a result of the presence of 40 % solution of ethylene glycol. The dissociation of CO is so slow at 253 K that no appreciable reoxidation of the metal centers occurs during the addition of dioxygen. Samples are then frozen to 77 K and are illuminated with intense visible light to photolyze the CO from the ferrous Fe_{a_3}. The dioxygen reduction site is then exposed such that, at higher incubation temperatures, dioxygen can bind to Fe_{a_3}. When the sample is warmed to 160 K, dioxygen binds to ferrous Fe_{a_3} and intramolecular electron transfer(s) occur on the time scale of minutes. The reaction may be periodically halted by immersing the sample in liquid nitrogen, and the reaction intermediates can be studied by various spectroscopic techniques.

Clore and E. Chance demonstrated using the triple-trapping technique in conjunction with optical spectroscopy that three intermediates formed in succession at 173 K upon reoxidation of the fully reduced enzyme (Eqn. 1) (3)

$$E + O_2 \longrightarrow I \longrightarrow II \longrightarrow III\ . \qquad (1)$$

Intermediate I formed in the first phase (0-20 s) upon incubation at 173 K. Based on the optical properties and the resonance Raman spectrum of this intermediate, Clore *et al.* (3) and later Babcock *et al.* (10) suggested that the intermediate is probably a species with dioxygen bound to ferrous Fe_{a_3}, with Cu_B reduced.

Intermediate II is produced upon the transfer of one electron from the low potential centers (either Fe_a or Cu_A) to the dioxygen reduction site. The transfer of the fourth electron to the dioxygen reduction site produces intermediate III, which has dioxygen formally reduced to two equivalents of water.

Branched Pathway. Clore *et al.* (5) later extended their earlier work and employed combined optical and EPR spectroscopy to determine the redox states of Fe_a and Cu_A in intermediates I, II and III during the reoxidation of the enzyme. They showed that there was no reoxidation of either Fe_a or Cu_A in intermediate I, whereas after 250 s incubation at 173 K intermediate II was characterized by a 60 % and 40 % reoxidation of Cu_A and Fe_a, respectively. After 3000 s of continued incubation at 173 K, Intermediate III was characterized by the nearly complete oxidation of Cu_A and 60 % reoxidation of Fe_a. Analysis of their optical and EPR data with a non-linear optimization program enabled them to fit the EPR and optical data to specific kinetic models. They found that a mechanism which included a *branched* pathway was the only kinetic model that satisfactorily fit both the optical and EPR data. Thus, Clore and co-workers revised their original sequential model and proposed a mechanism containing a branched pathway (Eqn. 2).

$$\mathrm{O_2 + E \rightleftharpoons I} \begin{cases} \nearrow \mathrm{IIA} \longrightarrow \mathrm{III} \\ \searrow \mathrm{IIB} \end{cases} \qquad (2)$$

The branch point in the mechanism in Equation 2 occurs *after* the initial

complete two-electron reduction of dioxygen by Fe_{a_3} and Cu_B with transfer of the third electron to Intermediate I, $[Fe_{a_3}\text{-O-O-}Cu_B]^{+3}$, from either Fe_a or Cu_A to produce Intermediates IIA and IIB, respectively. The dioxygen reduction site may be represented for both intermediates as $[Fe_{a_3}\text{-O-O-}Cu_B]^{+2}$, with Fe_a^{III}/Cu_A^{I} and Fe_a^{II}/Cu_A^{II}, respectively, for IIA and IIB. Curiously, although both intermediates IIA and IIB were expected to have an odd-electron intermediate at the dioxygen reduction site, no EPR signal attributable to an intermediate at the dioxygen reduction site was observed. At 173 K intermediate IIB was a stable intermediate, while intermediate IIA decayed to negligible intensity with concomitant formation of intermediate III.

In 1980 Malmström *et al.* renewed their search for an EPR signal from the paramagnetic three-electron-reduced intermediate (IIA and IIB) and they discovered an unusual copper EPR signal at low temperatures and high powers (11). The discovery of this EPR signal has had a major impact on all of the subsequent work on the kinetics and mechanism of cytochrome *c* oxidase-catalyzed reduction of dioxygen which utilizes EPR in conjunction with the triple-trapping technique because the signal allows for the direct monitoring of the three-electron-reduced intermediate and the subsequent processes which occur at the dioxygen reduction site. The signal is highly anisotropic, displaying only a resolvable g_z region, and is very resistant to power saturation, even at 10 K, ($g_z = 2.25$, $A_{||} = 138$ G) (11). Experiments in which the enzyme was reoxidized with $^{17}O_2$ demonstrated a significant line broadening of the copper EPR signal as a result of ligand hyperfine splitting from the ^{17}O nucleus (12). This result showed unambiguously that the copper EPR signal originated from the copper at the dioxygen reduction site (Cu_B) and that an oxygen atom, which is derived from O_2, is ligated to Cu_B at the three-electron level of reduction. A cupric Cu_B weakly coupled to a ferryl Fe_{a_3} was suggested as the source of the anisotropic copper EPR signal (11-12). Furthermore, in this model, the unusual saturation behavior of the Cu_B EPR signal

was thought to be readily explainable, *i.e.*, the rapidly relaxing ferryl was expected to enhance the relaxation rate of the adjacent Cu_B spin (11).

Recently, we re-examined the reoxidation of fully-reduced cytochrome *c* oxidase using the triple-trapping technique in conjunction with EPR spectroscopy. In these experiments, the reoxidation was studied over an extended range of temperatures and, when possible, the temperature dependences of the rate of the individual reaction steps were detemined in order to estimate the kinetic barriers. As a result of this work, new reaction sequences in the reduction of dioxygen by cytochrome *c* oxidase were discovered, and the initial reaction sequence was clarified. First, the new evidence which shows that the dissociation of CO from cuprous Cu_B is the rate-limiting step in the initial electron tranfer events to dioxygen will be discussed; then the evidence for *two* three-electron-reduced dioxygen intermediates will be presented.

MATERIALS and METHODS

Sample Preparation. Beef heart cytochrome *c* oxidase was isolated by the method of Hartzell and Beinert (13). The enzyme was typically dissolved in 50 mM phosphate buffer with 0.5 % Tween-20 at pH 7.4. The purified enzyme contained 8 nM heme *a* ((mg protein)$^{-1}$) and its activity was 9.0 nmol of O_2 reduced min^{-1} (μg of protein)$^{-1}$ (or 120 mole cyt-*c* oxidized (mole cytochrome *c* oxidase)$^{-1}$ s^{-1}). Heme *a* concentrations were determined by the pyridine hemochromogen assay (14). Protein concentration was determined by a modification of the Lowry procedure which includes 1 % sodium docecyl sulfate to solubilize integral membrane proteins (15). Enzyme concentrations used for EPR experiments were typically 0.2-0.3 mM in cytochrome *c* oxidase.

EPR samples for low temperature kinetic study were prepared in 5 mm o.d. (3.4 mm i.d.) quartz EPR tubes. Prior to reduction, the samples were deoxygenated by four to five cycles of evacuation and flushing with argon that had been

scrubbed of oxygen by passage through a column containing 0.1 M vanadous ion on 2 N HCl followed by passage through a solution of 0.02 M NaOH. A small excess (ca. 1.2 equiv) of NADH (nicotinamide adenine dinucleotide) (Sigma type VI) and 0.01 equiv of phenazine methosulphate were added to the samples under an argon atmosphere, causing complete reduction within 30 min. An equal volume of 80/20 (v/v) ethylene glycol, which had been previously degassed by four to five cycles of freezing, evacuation, thawing, and stirring, was mixed thoroughly with the reduced enzyme at 4 °C. The argon atmosphere was then exchanged for a 25 %/75 % mixture of carbon monoxide (CO) (Matheson 99.99 %) and scrubbed argon. The samples were cooled to -20 °C and evacuated. One atmosphere of pure dioxygen was admitted to the samples in the dark, and they were vigorously agitated for 15-20 s and then frozen in liquid nitrogen. The frozen solution formed an optically transparent glass. Because CO is bound to the dioxygen reduction site, very little reoxidation of the metal centers occurred during the course of the addition of dioxygen (less then 5 % in most cases), as judged by the intensities of Fe_a and Cu_A EPR signals prior to incubation at temperatures which allow reaction with dioxygen.

In order to remove CO from Fe_{a_3}, the samples were photolyzed in a finger Dewar at 77 K by irradiation with a 200-W Hg-Xe arc lamp for 30-40 min with frequent rotation of the sample so that all sides were equally exposed to the light. The reaction with dioxygen was initiated by immersing the sample tubes in a n-pentane bath kept at the desired temperature by immersion in methanol/ethanol solutions cooled by the addition of liquid nitrogen. The reaction was quenched by returning the sample to liquid nitrogen, and the n-pentane which solidified to the outside of the EPR tube was scraped off prior to examination of the sample by EPR.

Partially reduced cytochrome *c* oxidase samples were prepared by similar methods as those described previously, with the exception that enough NADH was

added to reduce the enzyme by approximately 3 electrons per oxidase molecule. The extent of reduction was determined from the EPR spectrum obtained after reduction but prior to the incubations at elevated temperatures.

EPR Spectroscopy. EPR spectra were recorded on a Varian E-line Century Series X-band spectrometer operating in the absorption mode. The modulation amplitude was 16 G and the modulation frequency 100 kHz. Microwave powers used were 0.02 mW for the Cu_A EPR signal, 0.02 and 0.2 mW for the Fe_a signal, and 20 mW for the anisotropic Cu_B signal.

Sample temperature was controlled with an Air Products Heli-Tran cryostat. The temperature at the sample position was measured before and after spectra were acquired, using a gold-chromel thermocouple in a glycerol-filled EPR tube. The temperature was typically 9 K. Data were rejected if significant (0.5 K) temperature changes occurred during spectrum acquisition.

For most purposes, EPR intensities were measured as peak heights (Fe_a at $g = 3$) or peak to trough distances (Cu_A). For the purposes of absolute comparisons between signal intensities, Cu_A signal was double integrated, using a base line which was determined by the requirement that the first integral be zero, and the Fe_a signal was integrated by the method of Aasa and Vänngård (16) by using the peak at $g = 3$ to estimate the the total area. The unusual Cu_B signal was integrated by using the lowest-field hyperfine peak to estimate the total area, using the assumption that the g_x and g_y values are both 1.3 as suggested by line shape simulations (12). This integration verified that the observed Cu_B signal intensity corresponded to the number of spins expected on the basis of the kinetic models postulated. For routine relative measurements of the Cu_B EPR signal, the height of the lowest-field hyperfine peak was used; the line width of this peak was observed to remain constant within the uncertainty of the determination.

Data Analysis. The rate of the decay of the unusual Cu_B EPR signal was investigated over a limited range of tempertures to determine the activation pa-

rameters for the reaction. The kinetic data for the decay of the Cu_B signal were not well-fitted by a single exponential function. It is currently thought that non-exponential kinetics for processes in proteins at low temperatures result from the presence of multiple conformations which have different activation barrier heights for the kinetic process (17-19). At low temperatures there is insufficient thermal energy to promote interconversions between the various conformational states. Thus, all of the various activation enthalpies for the rate process are manifested in the kinetics. Experimentally, a distribution of activation enthalpies is observed, instead of a single, well-defined value.

Austin *et al.* (17-18) first demonstrated that the nonexponential kinetics for the rebinding of CO to myoglobin at low temperatures following photolysis could be fitted to a power law (Eqn. 3)

$$N(t) = C\ (1 + t/t_o)^{-n} \tag{3}$$

where N(t) is the fraction of unbound heme at time t, and C, t_o, and n are constants; it should be noted that t_o and n are actually temperature dependent constants, so it is more accurate to write $t_o(T)$ and $n(T)$.

Austin *et al.* related the fraction of unbound heme to a distribution of activation barriers according to Equation 4

$$N(t) = \int_0^\infty dE^* g(E^*) \exp(-k(E^*)t) \tag{4}$$

where $g(E^*)$ is the probability of finding a molecule with an activation energy between E^* and dE^*, and $k(E^*)$ is

$$k(E^*) = A \exp(-E^*)/k_B T \tag{5}$$

Equation 4 may be expressed as a function of k using equation 5 (Eqn. 6)

$$N(t) = k_B T \int_0^A dk\ [g(k)/k]\ \exp(-kt)\ . \tag{6}$$

The prefactor A is assumed to be temperature independent and is sufficiently large ($\sim 10^{13}$ s^{-1}) such that the upper limit of integration is infinity. Equation 6 is then the Laplace transform (L) of g(k)/k (Eqn. 7)

$$N(t) = k_B T \, L\{g(k)/k\} \, . \tag{7}$$

The distribution function (g(k)) is then determined by taking the inverse Laplace transform (L^{-1}) of the power law function (Eqns. 8-9)

$$L^{-1}\{N(t)\} = k_B T \, g(k)/k \tag{8}$$

$$g(k) = n(t_o k)^n \exp(-t_o k)/k_B T \Gamma(n+1) \, , \tag{9}$$

where Γ is the Gamma function. The most probable rate constant in the distribution is $k_p = n/t_o$, which occurs at $dg(k)/dk = 0$. The activation parameters ΔH^* and ΔS^* are obtained by fitting the peak rate constants to the Arrhenius equation (Eqn. 10)

$$\ln k_p = \ln \omega + \Delta S^*/R - \Delta H^*/R(1/T) \, . \tag{10}$$

The Cu_B kinetic data were fitted to the power law by using a nonlinear least-squares program which computes estimates of C, n, and t_o. Activation enthalpies and entropies were determined by fitting the ln k_p vs. 1/T data to the linear form of the Arrhenius relation (Eqn. 10), employing a linear least-squares program. The standard deviation in the slope and the y-intercept of the Arrhenius equation (Eqn. 10) was calculated according to Bevington (20). Error bars on the graphs represent twice the sample standard deviation of the data points from the best fit line in the nonlinear least-squares fit of the kinetic data at each temperature. The reported uncertainty in the magnitude of the activation parameters ΔH^* and Δs^* is equal to one standard deviation.

The same linear least-squares analysis was also applied to the Arrhenius plot of the kinetic data for the Cu_A oxidation. For this process, the rate was estimated by measuring the initial slope to the EPR intensity vs. time curves.

RESULTS

Oxidation of Fe_a and Cu_B. Following photolysis of CO from Fe_{a_3} at 77 K, cytochrome *c* oxidase samples were first incubated at temperatures between 166 and 186 K to initiate the intramolecular electron transfers to dioxygen. Optically monitored low temperature kinetic studies have established that the binding of dioxygen to Fe_{a_3} takes place with a bimolecular rate constant of 81 M^{-1} s^{-1} (5) at 173 K, therefore this binding step is not expected to be rate-limiting in our experiments, where the oxygen concentration is ca. 1 mM and the initial electron transfers take place with rates of appproximately $2x10^{-3}$ s^{-1} at 173 K. The intermediate which is formed upon oxygen binding, designated I by Clore *et al.* , exhibits no EPR signals (5). Upon incubation between 166 and 186 K, electron transfers from Cu_A and Fe_a to the dioxygen reduction site take place, causing the appearance of the expected EPR signals that are characteristic of the oxidized states of these metal centers.

The magnitudes of Cu_A and Fe_a EPR signals after various times of incubation at 181 K are plotted in Figure 1. The oxidation of Cu_A during the first 30 min. at 181 K takes place in at least two phases, as evidenced by the poor quality of a single exponential fit to the data. If the analysis is restricted to only the first 3 min. of oxidation at 181 K and if the data points are taken at shorter intervals, the Cu_A data are satisfactorially fitted by a single exponential (data not shown), indicating that a prior step is not partially rate-limiting. Fits to the Fe_a data are not conclusive with respect to the question of whether the oxidation is monophasic or biphasic owing to the poorer signal-to-noise ratio of this signal. The ratio of the intensities of the Cu_A and Fe_a signals during the inital phase of oxidation is also shown in Figure 1 and demonstrates that the two sites are not oxidized in parallel. After 55 min. at 181 K, the intensity of Fe_a signal corresponded to only ca. 30 % of the intensity of Cu_A signal. In samples which had been thoroughly oxygenated prior to freezing, the intensity of the Cu_A signal corresponded to nearly 100 %

Figure 1

Intensities of the EPR signals due to Cu_A and Fe_a during incubation of a reduced cytochrome *c* oxidase sample in the presence of dioxygen at 181 K. Conditions of EPR spectroscopy: temperature 9 K; microwave frequency 9.172 GHz; modulation amplitude 16 G; microwave power 0.02 mW (Cu_A) or 0.20 mW (Fe_a). Sample preparation, incubation methods, and quantitation of the EPR signals are described in the Materials and Methods Section. Bottom: the ratio of the intensities of the Cu_A and Fe_a signals during incubations at the same temperature, showing that the two sites do not follow parallel courses of oxidation.

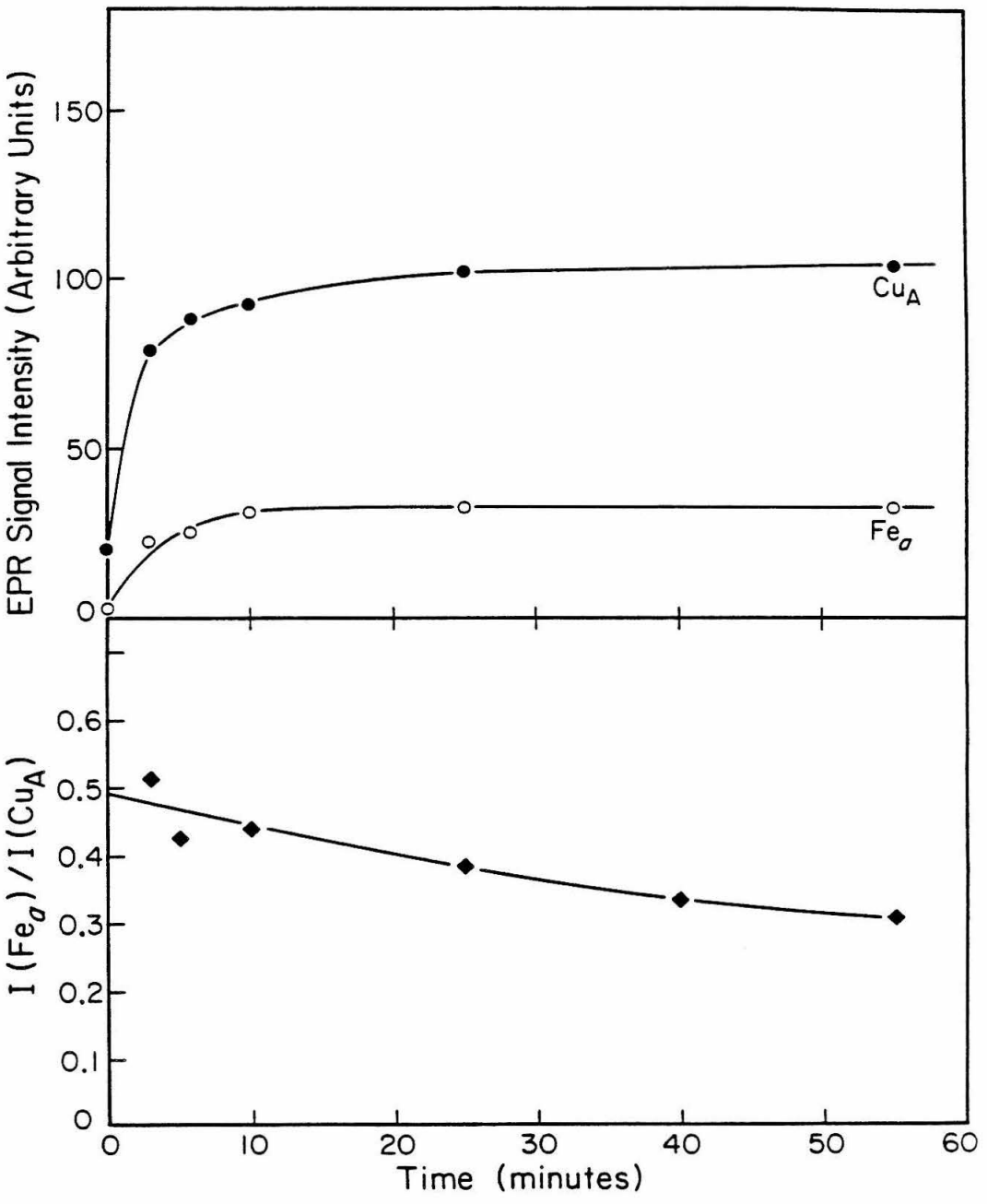
EPR Signal Intensity (Arbitrary Units)
150
100
50
0
Cu_A
Fe_a
$I(Fe_a)/I(Cu_A)$
0.6
0.5
0.4
0.3
0.2
0.1
0
0
10
20
30
40
50
60
Time (minutes)

of the enzyme molecules, as judged by the effect of thawing the samples and remeasuring the Cu_A EPR signal. All of these observations agree qualitatively with the results of the combined optical/EPR study of Clore *et al.* (5). Their results and ours are most satisfactorally accounted for by the reaction sequence shown in Scheme I.

The oxidation of Cu_A was investigated at several temperatures between 166 and 186 K. Because this process is not well-fitted by a single exponential, the rate of the first oxidation step was estimated by measuring the initial slopes of the EPR intensity vs. time curves. The rate constants and corresponding temperatures are presented in Table I. An Arrhenius plot of the data is linear within the experimental uncertainty and gives an activation enthalpy and entropy for this reaction step of 13 $\pm$ 2 kcal mol^{-1} and 3 $\pm$ 8 cal mol^{-1} K^{-1}, respectively, assuming a preexponential factor of 10^{13} s^{-1}. This result confirmed the earlier work of B. Chance and co-workers who determined an activation enthalpy of 12.5 kcal mol^{-1} for the same reaction step (9). The level of Fe_a oxidation which was attained in this early phase of the reaction (and therefore its rate of oxidation) relative to that of Cu_A did not vary significantly over the temperature range examined, indicating that the activation enthalpies for the Fe_a and Cu_A oxidation are similar.

In an infrared absorption study of the photolysis of CO from cytochrome *c* oxidase, Fiamingo *et al.* (21) have shown that when CO is photolyzed from the enzyme at low (ca. 180 K) temperatures, it first binds to Cu_B and subsequently recombines with Fe_{a_3} in a relatively slow process. While CO remains bound to Cu_B, the binding and the reaction of dioxygen to form an electron accepting intermediate is likely to be inhibited. These authors in fact pointed out that the rate of CO dissociation from cuprous Cu_B at 183 K paralleled the rate of oxidation of Cu_A in the low temperature kinetic study of Clore *et al.* Thus, they suggested that the dissociation of CO from cuprous Cu_B may be rate-limiting in the initial electron transfer step of the dioxygen reduction reaction as studied

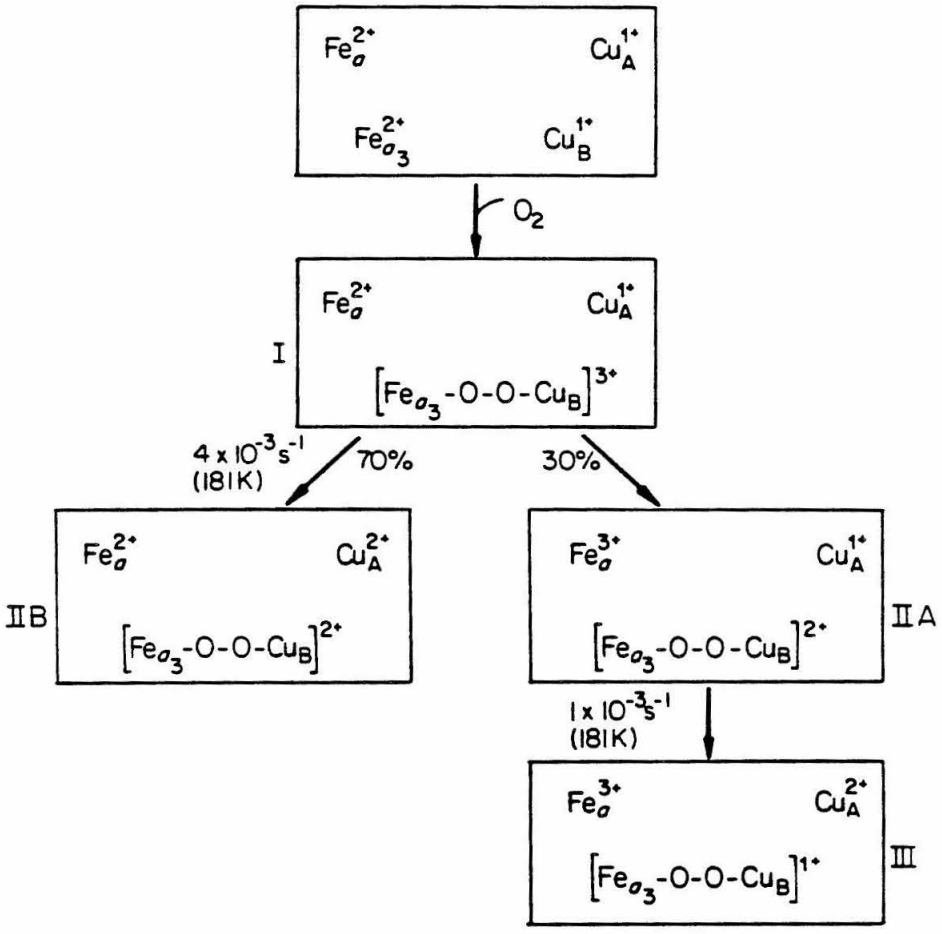
$Fe_{a_3}^{2+}$ Cu_B^{1+}
Fe_a^{2+} Cu_A^{1+}
O_2
I
$[Fe_{a_3}\text{-}O\text{-}O\text{-}Cu_B]^{3+}$
$4 \times 10^{-3} s^{-1}$ (181K)
70%
30%
IIB
Fe_a^{2+} Cu_A^{2+}
$[Fe_{a_3}\text{-}O\text{-}O\text{-}Cu_B]^{2+}$
IIA
Fe_a^{3+} Cu_A^{1+}
$[Fe_{a_3}\text{-}O\text{-}O\text{-}Cu_B]^{2+}$
$1 \times 10^{-3} s^{-1}$ (181K)
III
Fe_a^{3+} Cu_A^{2+}
$[Fe_{a_3}\text{-}O\text{-}O\text{-}Cu_B]^{1+}$

Scheme I

Table I

First-Order Rate Constants and Corresponding Temperatures for the Formation of the Cu_A EPR Signal

Temp (K)	$k(Cu_A)$ $(s^{-1})^a$
186.0	$(1.7 \pm 0.2) \times 10^{-2}$
181.0	$(4.4 \pm 0.2) \times 10^{-3}$
180.5	$(4.6 \pm 0.1) \times 10^{-3}$
176.0	$(1.3 \pm 0.1) \times 10^{-3}$
173.0	$(1.9 \pm 0.1) \times 10^{-3}$
171.0	$(5.0 \pm 0.2) \times 10^{-4}$
166.0	$(1.9 \pm 0.2) \times 10^{-4}$

[a] First-order rate constants were determined by measuring the initial slopes to the formation curves of the Cu_A signal ($\Delta H^* = 13 \pm 2$ kcal mol^{-1}, $\Delta S^* = 3 \pm 8$ cal mol^{-1} K^{-1}).

at low temperatures by the triple-trapping technique. The rate of recombination of CO with Fe_{a_3} (which parallels its rate of dissociation from cuprous Cu_B) is $7.4x10^{-3}$ s^{-1} at 181 K; the activation enthalpy for this process is 9.2 kcal mol^{-1} (21). Comparison with our measurements (Table I) shows that the rate of Cu_A oxidation at 181 K is similar (within a factor of 2) at this temperature, whereas the activation enthalpy for Cu_A oxidation is significantly greater.

Production of the Unusual Cu_B EPR Signal. The initial transfer of an electron from either Cu_A or Fe_{a_3} to the dioxygen reduction site produces an intermediate which contains an odd number of electrons at the dioxygen reduction site. This species gives rise to a copper EPR signal which is distinguished by two unusual properties: It is very difficult to saturate, even at 9 K, and only one of its g values is evident in the spectrum (11-12). This signal has been assigned to Cu_B in close proximity to another paramagnetic ion which undergoes more rapid spin relaxation (11-12). In Figure 2, the intensity of this signal after various times of incubation at 181 K is shown. The Cu_B EPR spectrum in the g_x region is shown in Figure 3. In agreement with earlier findings (11), we observe that the early growth of this signal roughly parallels the initial oxidation of Cu_A and Fe_a. This result is consistent with the assignment of the signal to an intermediate at the Fe_{a_3}/Cu_B site which is at the three-electron level of dioxygen reduction. The intensity of this signal reaches its maximum after approximately 5 min. at 181 K; it then decays somewhat, leveling off after approximately 20 min. At times between 30 and 90 min., the signal intensity does not change appreciably; assuming g_x and g_y values of 1.3 (as suggested by line shape simulations described in ref. 12), the Cu_B signal intensity at this time corresponds to ca. 80 % of that of Cu_A, consistent with Scheme I.

Decay of the Unusual Cu_B EPR Signal. Subsequent steps in the dioxygen reduction reaction, which have not been previously investigated, were studied by raising the sample incubation temperature. The intensities of the Cu_A, Fe_a, and

Figure 2

Intensity of the unusual Cu_B EPR signal during incubation of a reduced cytochrome *c* oxidase sample in the presence of dioxygen at 181 K. Conditions of EPR spectroscopy were as noted in Figure 1, except the microwave power was 20 mW. Sample preparation, incubation methods, and EPR signal quantitation are described in the Material and Methods Section. Assuming $g_\perp$ values of 1.3 for the Cu_B signal (12), its intensity after 25 min. corresponds to 80 % of that due to Cu_A.

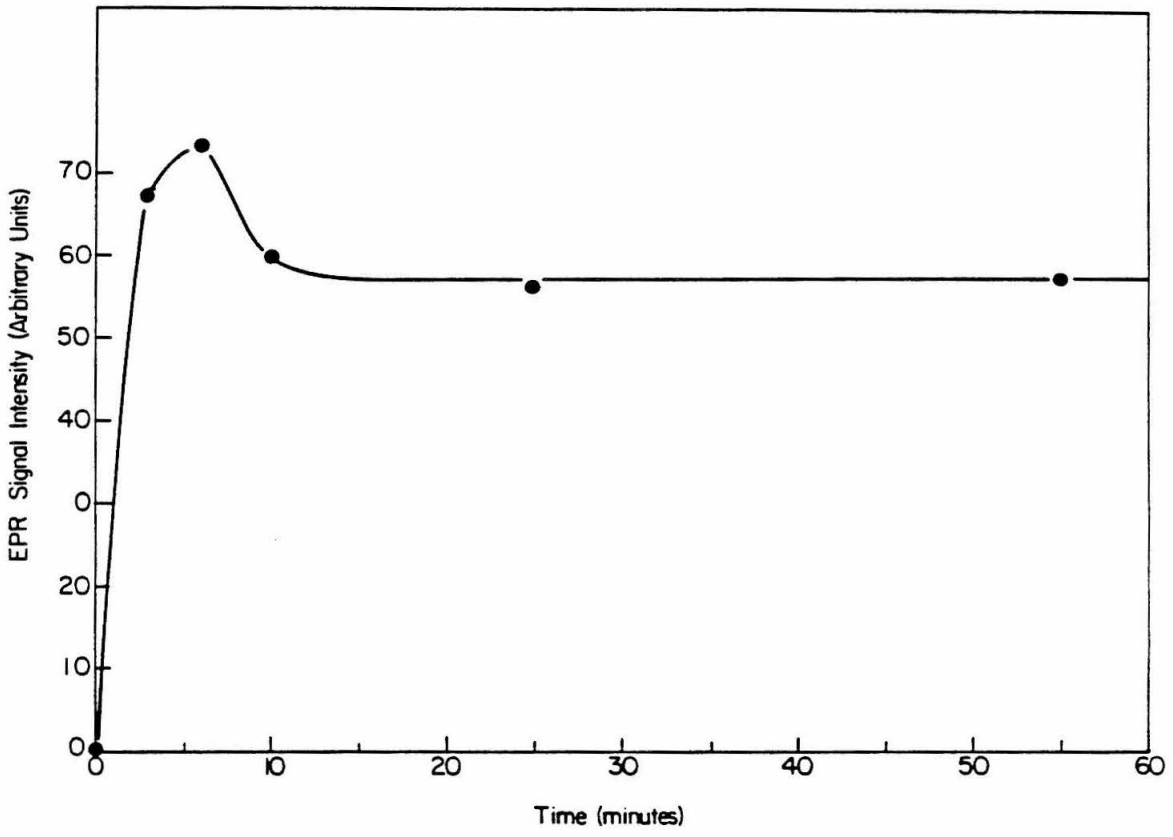
EPR Signal Intensity (Arbitrary Units)
70
60
50
40
0
20
10
0
0
10
20
30
40
50
60
Time (minutes)

Figure 3

Unusual Cu_B EPR spectrum observed after incubation of a cytochrome *c* oxidase sample (initially fully reduced) for 45 s at 191 K. Conditions of EPR spectroscopy as in Figure 2. The observed hyperfine coupling is 137 G. Only the four features indicated are associated with the Cu_B signal; the remaining features are due to Cu_A, and to a lesser extent, Fe_a.

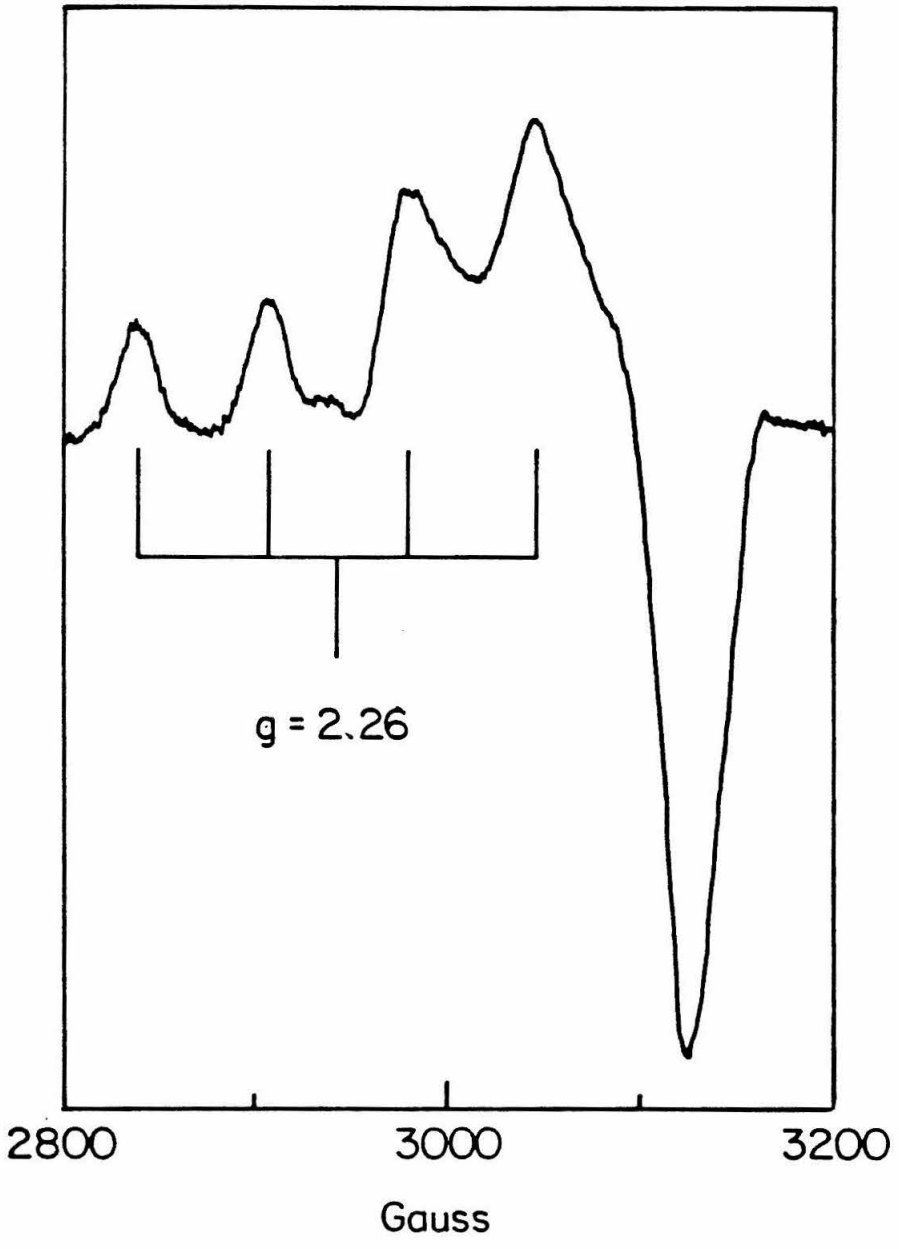
g = 2.26
2800
3000
3200
Gauss

Cu_B EPR signals after various times of incubation at 191.5 K are plotted in Figure 4. This sample was preincubated at lower temperature (177 K) to produce the Cu_A, Fe_a, and the Cu_B EPR signals. At 191.5 K, the unusual Cu_B EPR signal decays to negligible intensity at a conveniently monitored rate (ca. $1.8x10^{-3}$ s^{-1}). During the same period, the level of Fe_a oxidation changes by less than 20 % (in terms of the total number of oxidase molecules present) and that of the Cu_A by less than 10 %. The changes in the Fe_a and Cu_A EPR signal intensities do not parallel the decay of the unusual Cu_B EPR signal. After 1 hour at 198 K, Fe_a is still less than 50 % as oxidized as is Cu_A, yet the unusual Cu_B signal is almost completely gone. These observations imply that a process occurs at the Fe_{a_3}/Cu_B site which is *independent* of the transfer of the fourth electron from either Cu_A or Fe_a and which causes the disappearance of the unusual Cu_B EPR signal. This would imply the existence of a second, EPR-silent intermediate at the three-electron level of dioxygen reduction.

The decay of the unusual Cu_B EPR signal is clearly nonexponential at all temperatures at which we examined it. Nonexponential processes in proteins at low temperatures have previously been attributed to the existence of multiple conformations which have different activation enthalpies for the process and which do not rapidly interconvert (17-19). The data for the decay of the unusual Cu_B signal were fitted to the power law expression (Eqn. 3) (ref. 17 cf. Materials and Methods Section), which are thought to be appropriate to such a situation. The line drawn through the Cu_B points in Figure 4 is the best power law fit.

When the activation enthalpy takes on a range of values, its most probable value may be determined from the power law treatment if the process is examined over a range of temperatures (17). Following the incubation at 177 K for 90 min. to produce the unusual Cu_B signal, its decay was investigated at temperatures between 181-207 K. The decay curve at each temperature was fitted to the power law; the best fit kinetic parameters for the Cu_B decay at various temperatures are

Figure 4

Intensities of the EPR signals due to Cu_A, Fe_a, and Cu_B during incubation of a cytochrome *c* oxidase sample at 191.5 K. Initally reduced samples were preincubated at a lower temperature (177 K) for 2 hours to produce the intermediate which exhibits the Cu_B EPR signal. The lines through the Cu_A and Fe_a data points are drawn to guide the eye. The line through the Cu_B data points is the best power law fit. Conditions of EPR spectroscopy were as described in the legends to Figures 1 and 2.

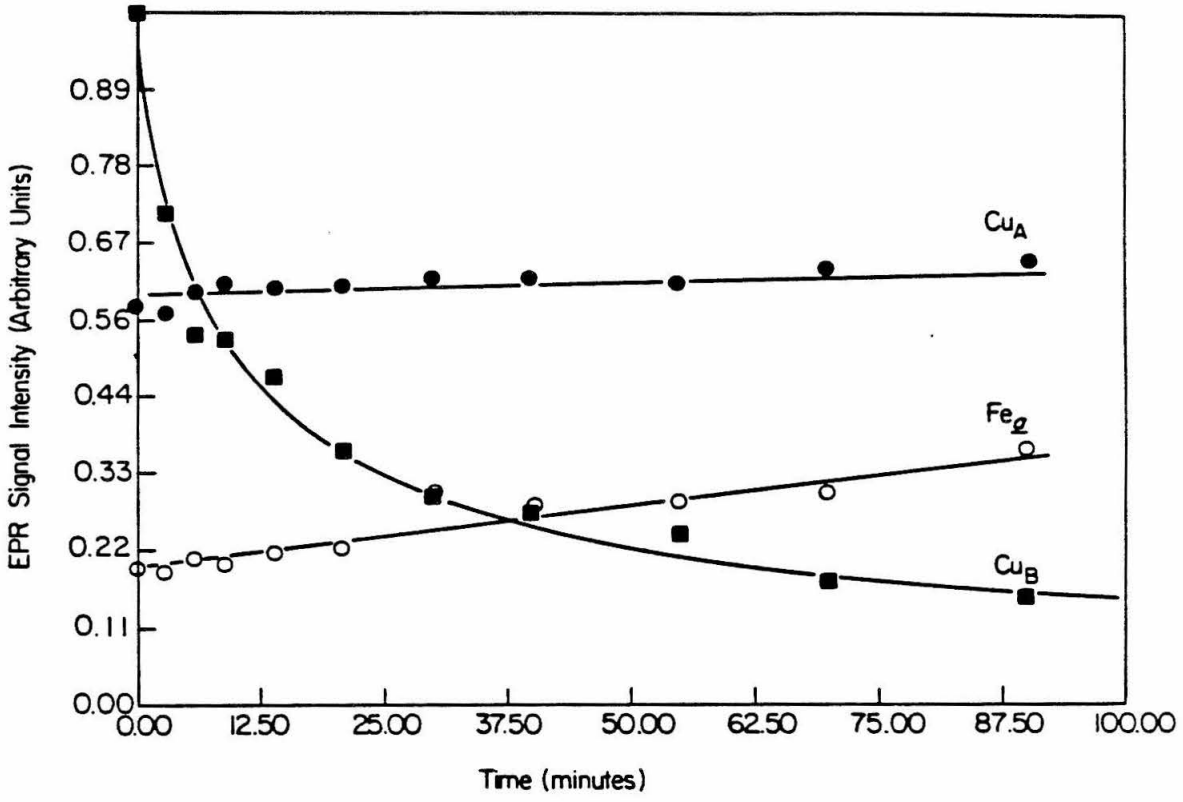
EPR Signal Intensity (Arbitrary Units)
0.89
0.78
0.67
0.56
0.44
0.33
0.22
0.11
0.00
0.00
12.50
25.00
37.50
50.00
62.50
75.00
87.50
100.00
Time (minutes)
Cu_A
Fe_2
Cu_B

Table II

First-Order Rate Constants and Corresponding Temperatures for the Decay of the Cu_B EPR Signal

Temp (K)	k_p $(s^{-1})^a$
207.0	$(3.4 \pm 0.6) \times 10^{-2}$
203.0	$(1.8 \pm 0.4) \times 10^{-2}$
203.0	$(3.4 \pm 0.1) \times 10^{-2}$
202.5	$(6.8 \pm 0.3) \times 10^{-3}$
197.0	$(4.5 \pm 0.7) \times 10^{-3}$
193.0	$(1.4 \pm 0.3) \times 10^{-3}$
191.5	$(1.8 \pm 0.4) \times 10^{-3}$
187.0	$(5.2 \pm 1.3) \times 10^{-4}$
183.0	$(8.1 \pm 2.2) \times 10^{-5}$

[a] k_p is the first order rate constant for the decay of the unusual Cu_B EPR signal, where $k_p = n/t_o$ (see Materials and Methods).

Figure 5

Arrhenius plot of the measured rate of decay of the unusual Cu_B signal. The Cu_B EPR signal intensities were fitted to a power law expression (see Material and Methods). The best linear least-squares fit to the data yields an activation enthalpy and entropy of 18 kcal $mol^{-1} \pm 2$ kcal mol^{-1} K^{-1} and 21 ± 8 cal mol^{-1} K^{-1} (assuming a preexponential factor of 10^{13} s^{-1}).

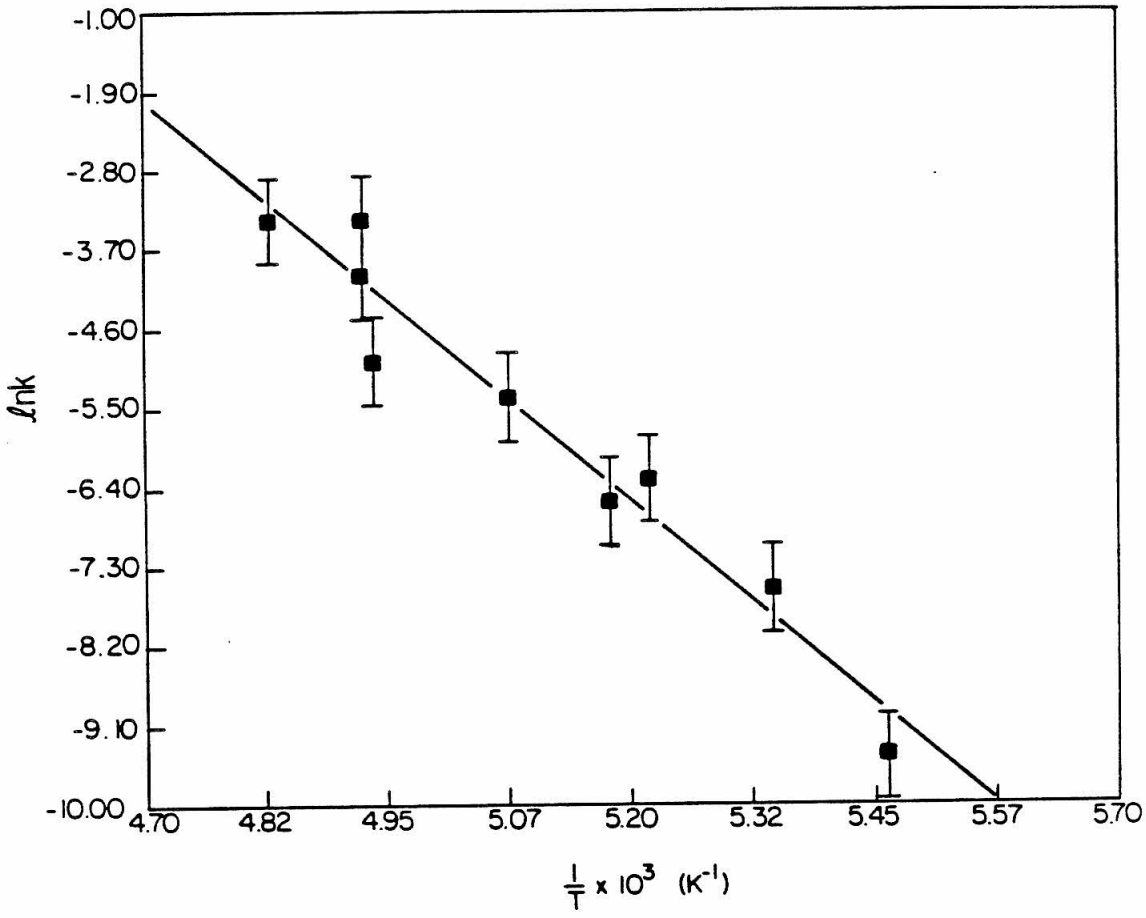
-1.00
-1.90
-2.80
-3.70
-4.60
-5.50
-6.40
-7.30
-8.20
-9.10
-10.00
lnk
4.70
4.82
4.95
5.07
5.20
5.32
5.45
5.57
5.70
1/T x 10^3 (K^-1)

Figure 6

Plot of the activation enthaply distribution for the decay of the unusual Cu_B EPR signal at 203 K. The distribution function was calculated by inserting the best-fit parameters ($\Delta H_p^* = 18$ kcal mol^{-1}, n = 0.65 and T = 203 K) into the following equation (18,21):

$$g(H^*) = \frac{n^n}{RT\,\Gamma(n)}\, exp\{-n[(H^* - H_p^*)/RT + e^{-(H^* - H_p^*)/RT}]\}\ .$$

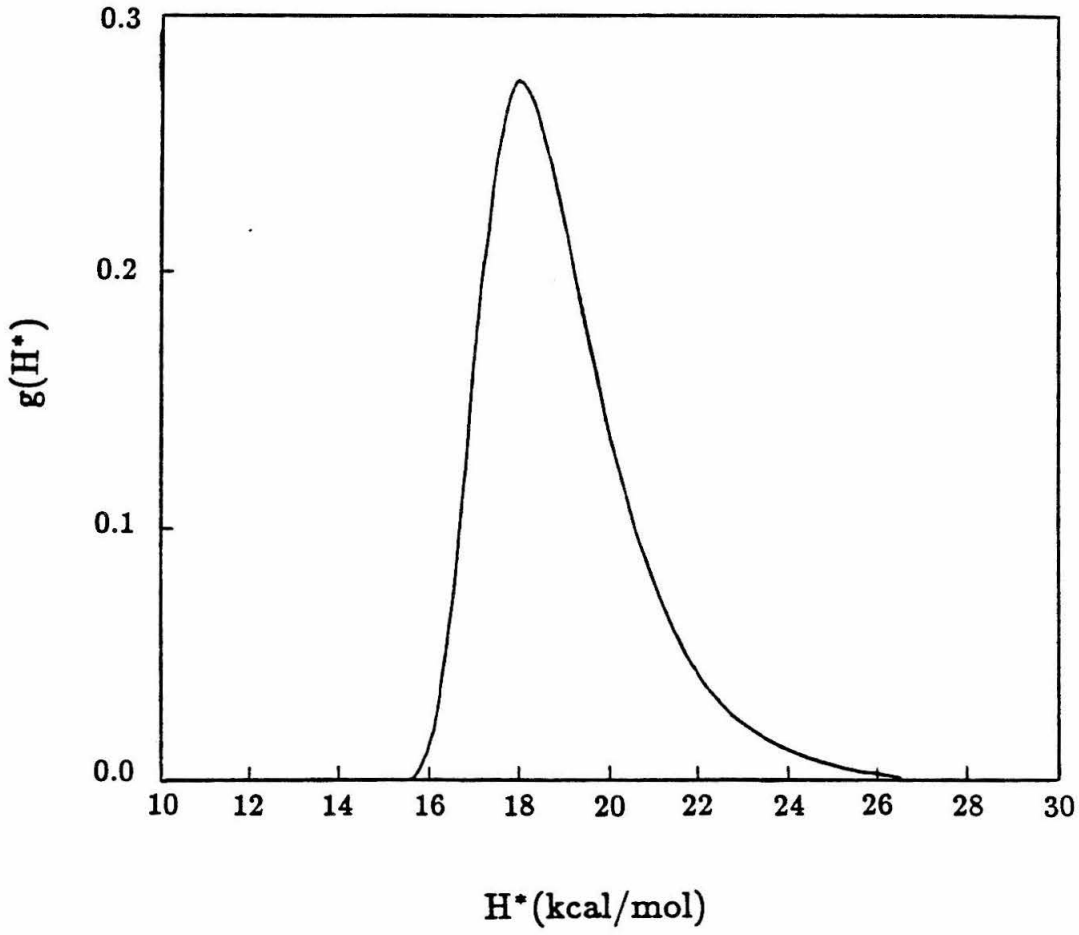
0.3
0.2
0.1
0.0
g(H*)
10
12
14
16
18
20
22
24
26
28
30
H*(kcal/mol)

compiled in Table II. The data in Table II were used to construct the Arrhenius plot in Figure 5. From the Arrhenius plot, we obtained a value of 18 kcal mol^{-1} for the most probable activation enthalpy and a corresponding activation entropy of 21 $\pm$ 8 cal mol^{-1} K^{-1}, assuming a preexponential factor of 10^{13} s^{-1}. The determination of the most probable activation enthalpy (18 kcal mol^{-1}) allows us to construct an activation enthalpy distribution for the decay of the unusual Cu_B EPR signal at a given temperature. For example, in Figure 6 we display a plot of the activation enthalpy distribution for the decay of the Cu_B EPR signal at 203 K. The activation enthalpy distribution was calculated by inserting the best-fit parameters ($\Delta H_p^* = 18$ kcal mol^{-1}, $n = 0.65$ and T = 203 K) into the appropriate equation for the distribution function (see legend to Figure 6).

Further Oxidation of Fe_a. As noted above, Fe_a oxidation is not complete even after incubations which cause the nearly complete disappearance of the unusual Cu_B signal. Continued incubation at 203 K causes further oxidation of Fe_a to take place at a rate of approximately $8x10^{-4}$ s^{-1} (Figure 7). A comparison of the Fe_a oxidation with the decay of the unusual Cu_B EPR signal again shows clearly that the two processes are not correlated: Most of the increase in the Fe_a signal takes place *after* the unusual Cu_B EPR signal has decayed; however, even after prolonged incubation (more than 1 hour) at 203 K, Fe_a oxidation is still not complete, as evidenced by a further increase in its intensity upon incubation at a somewhat higher temperature (211 K). Judging from the slowness of Fe_a oxidation at 193 K (not shown) relative to that at 203 K, this process is rather highly activated. The activation enthalpy for this process was not determined, owing to the occurrence of other, complicating processes to be described below.

Appearance of New Signals from Magnetically Isolated Cu_B and Fe_{a_s}. In an attempt to induce the complete oxidation of Fe_a and measure its rate at a higher temperature, several samples with different histories were incubated at 211 K or higher. EPR spectra of a typical sample after incubation at 183

Figure 7

Intensity of the Fe_a EPR signal during incubation of a cytochrome *c* oxidase sample at 203 K. Prior to the 203 K incubation, the sample was incubated at 177 K for 2 hours. The behavior of the unusual Cu_B signal during the 203 K incubation is also shown. The lines through the data points are drawn to guide the eye. Conditions of EPR spectroscopy were as described in the legends to Figures 1 and 2.

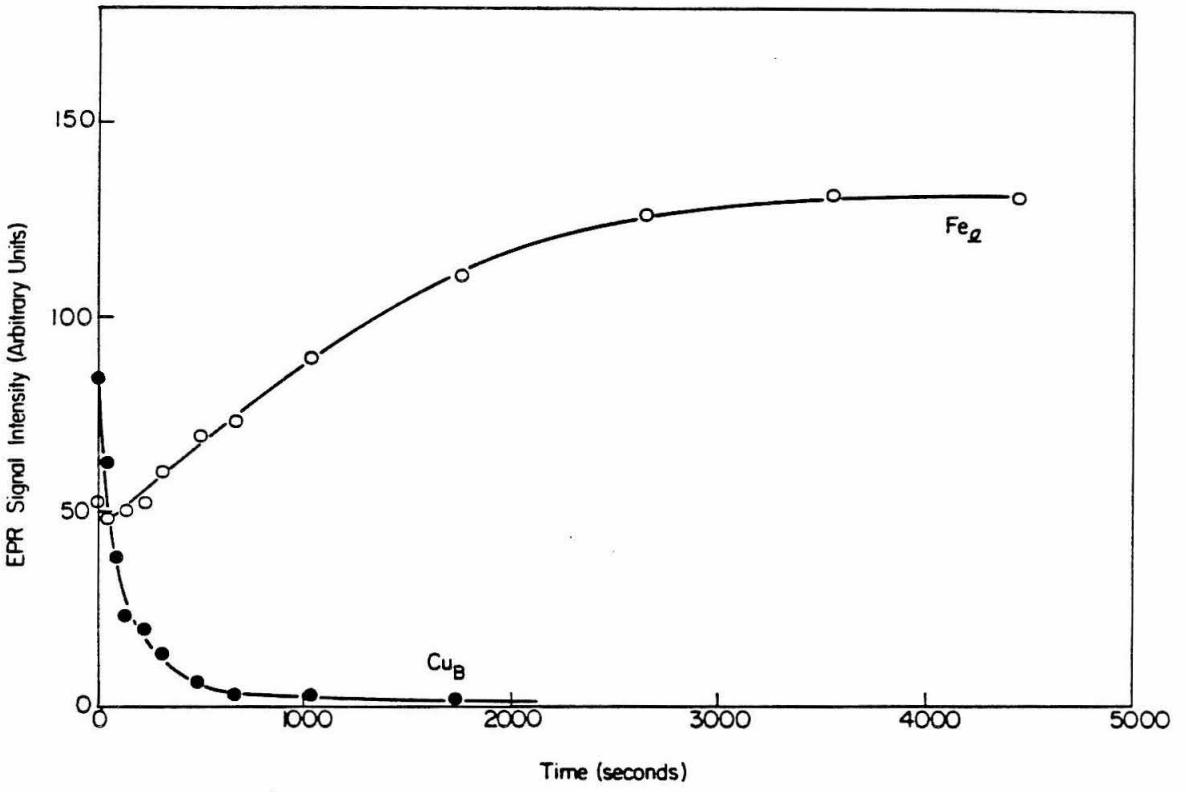
150
100
50
0
EPR Signal Intensity (Arbitrary Units)
0
1000
2000
3000
4000
5000
Time (seconds)
Fe_a
Cu_B

Figure 8

Development of new, magnetically isolated copper and iron EPR signals upon incubation at 211 K and higher temperatures. A: Spectrum of an initially reduced cytochrome *c* oxidase sample after incubation at 183 K for ca. 11 hours. B: Spectrum after incubation at 211 K for 20 min. C: Spectrum after incubation at 211 K for 60 min, 216 K for 20 min, 223 K for 65 min and 228 K for 16 min. For spectra A, B, and C, conditions of EPR spectroscopy were as described in the legend to Figure 1. The expansion of the low-field region is for the same sample as C but with microwave power of 0.20 mW and 4-fold higher gain.

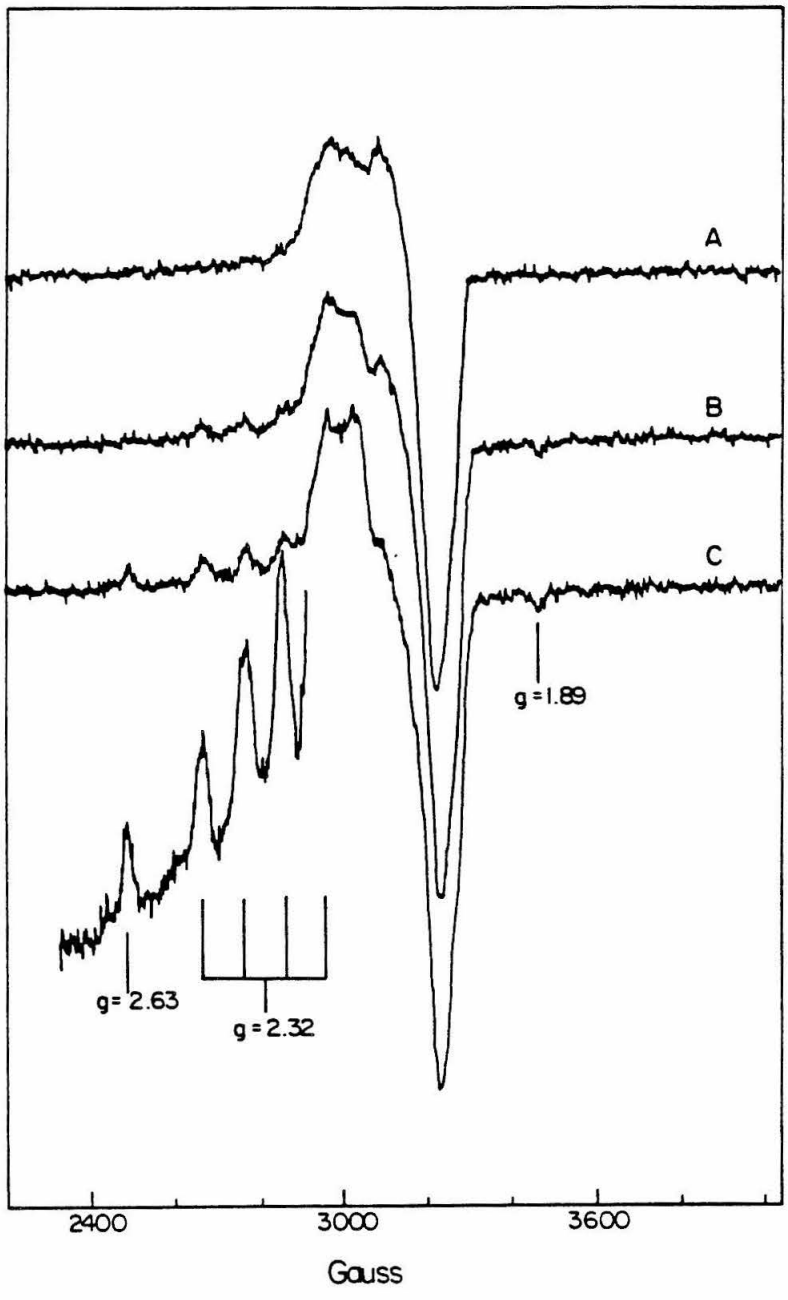
A
B
C
g = 1.89
g = 2.63
g = 2.32
2400
3000
3600
Gauss

K, 211 K, and higher temperatures are shown in Figure 8. A new signal with splittings characteristic of a cupric ion appears upon incubation at 211 K. The g values and hyperfine coupling of this signal are the same of those of a signal assignable to Cu_B which has been previously observed by Karlsson and Andréasson (22) using a different sample preparation. This Cu_B EPR signal will be referred to as the "rhombic" Cu_B EPR signal since the g tensor is definitely rhombic (23). During later stages of incubation at 211 K, and more so upon incubation at higher temperatures, another signal appears with features at $g = 2.63$ and $g = 1.89$, which is most plausibly assigned to a low-spin Fe_{a_3} coordinated by imidazole and hydroxide. (24-25). These signals exhibit no resolved dipolar splittings and are readily saturated, which indicates that they are due to magnetically isolated species. Concomitant with the appearance of these signals, Fe_a undergoes some oxidation but again not to completion (as judged by the effect of thawing the samples, which causes a further increase in the signal intensity).

Low Temperature Oxidation of ca. Three-Fourths Reduced Cytochrome c Oxidase. The role played by the fourth electron in the reaction of cytochrome oxidase with dioxygen may be investigated in the low-temperature kinetic experiments using enzyme samples which are reduced by fewer than four electrons. The results of such an experiment are displayed in Figure 9, where we plot the intensities of the Cu_A, Fe_a, and the unusual Cu_B EPR signals during incubation at 181 K of a sample initially reduced by only 3.4 electrons. In this situation, most of the enzyme molecules contain only 3 reducing equivalents at the beginning of the reaction. The important observations are Fe_a oxidation during this initial reaction step takes place to a much greater extent and at a slower apparent rate, as compared to the situation in the fully reduced enzyme (compare with Figure 1) and that the unusual Cu_B EPR signal shows no early decay phase (compare with Figure 2).

The next step of the reaction, namely the decay of the unusual Cu_B EPR

Figure 9

Intensities of the Cu_A, Fe_a, and the unusual Cu_B EPR signals during incubation of a partially (3.4 equiv) reduced cytochrome *c* oxidase sample at 181 K. The lines through the data points are drawn to guide the eye. Conditions were as noted in the legends to Figures 1 and 2. This figure should be compared with Figures 1 and 2, which depict an experiment which is identical except that it employs fully reduced enzyme.

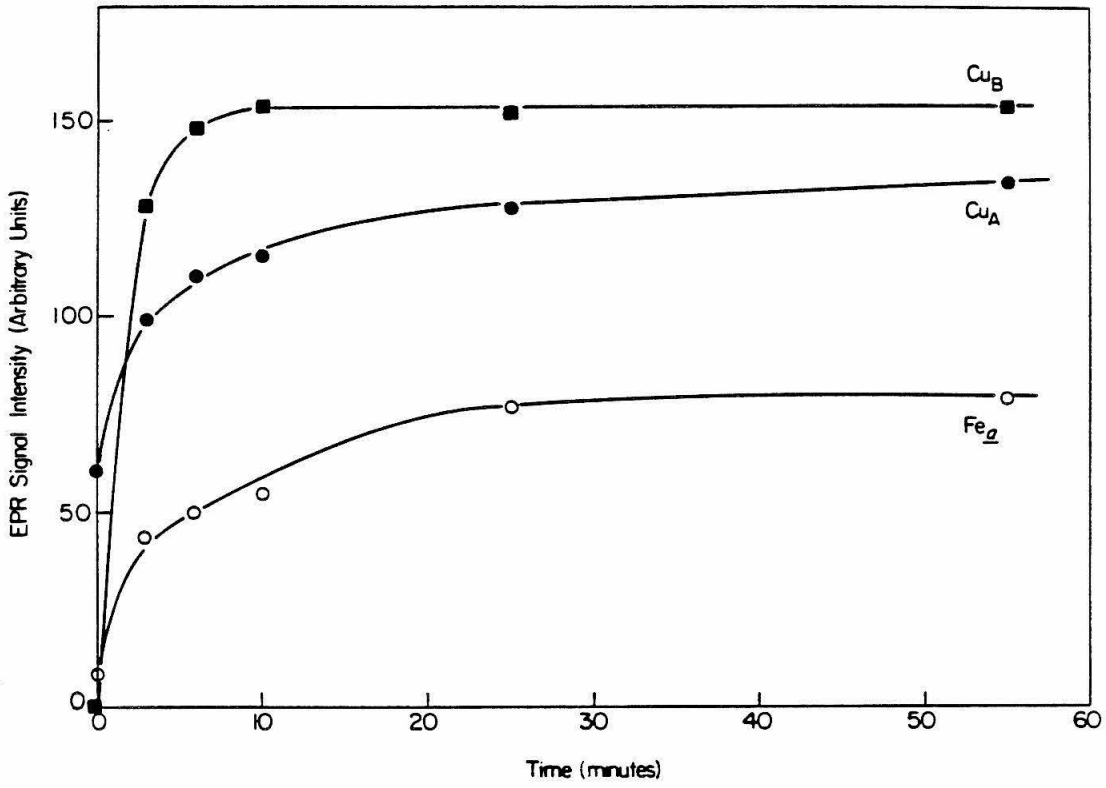
EPR Signal Intensity (Arbitrary Units)
150
100
50
0
0
10
20
30
40
50
60
Time (minutes)
Cu_B
Cu_A
Fe_a

signal, was investigated by incubating the sample at 205 K. The unusual Cu_B signal decays to near completion at a rate which is in agreement with rates measured with the fully reduced enzyme (Figure 10). This observation confirms that the transfer of the fourth electron to the dioxygen reduction site is not required for the elimination of the unusual Cu_B signal, since most of the oxidase molecules do not contain a fourth electron.

The role of the fourth electron in producing the magnetically isolated Cu_B and Fe_{a_3} EPR signals was examined by incubating a three-electron-reduced sample at 203 K for 6 min followed by repeated incubations at 211 K or higher. The new copper and iron signals are produced in somewhat higher yield relative to the Cu_A signal in the four-electron-reduced samples, particularly after 222 K incubation (Fig. 11). Some low-temperature kinetics samples were thawed for ca. 1 min at ice temperature to measure the changes in the Cu_A and Fe_a EPR signals. After the samples were thawed and refrozen, the magnetically isolated, rhombic Cu_B EPR signal appeared in appreciably higher yield in a 3.4-electron-reduced sample than in a fully reduced sample (spectra not shown).

Solvent Dependence. The solvent dependence of the low-temperature dioxygen reduction reaction was examined by conducting some experiments in 50 % glycerol rather than in 40 % ethylene glycol. The results of these experiments may be summarized as follows: The first reaction step, which involves the oxidation of Fe_a and Cu_A to produce the intermediate which exhibits the unusual copper EPR signal, was not substantially affected by the change in the solvent. The unusual copper EPR signal was identical in appearance and was produced in similar yield. By contrast, the next step, which involves the decay of the unusual copper signal, was significantly affected: In 50 % glycerol, this process was approximately 100 times slower than in 40 % ethylene glycol, requiring incubation temeperatures some 15 °C higher to achieve comparable rates.

Figure 10

Decay of the unusual Cu_B EPR signal during 205 K incubation of a cytochrome *c* oxidase sample initially reduced by 3.4 electrons. The sample was preincubated at 181 K for 55 min to generate the unusual Cu_B EPR signal. Conditions for EPR spectroscopy were as described in the legends to Figures 1 and 2.

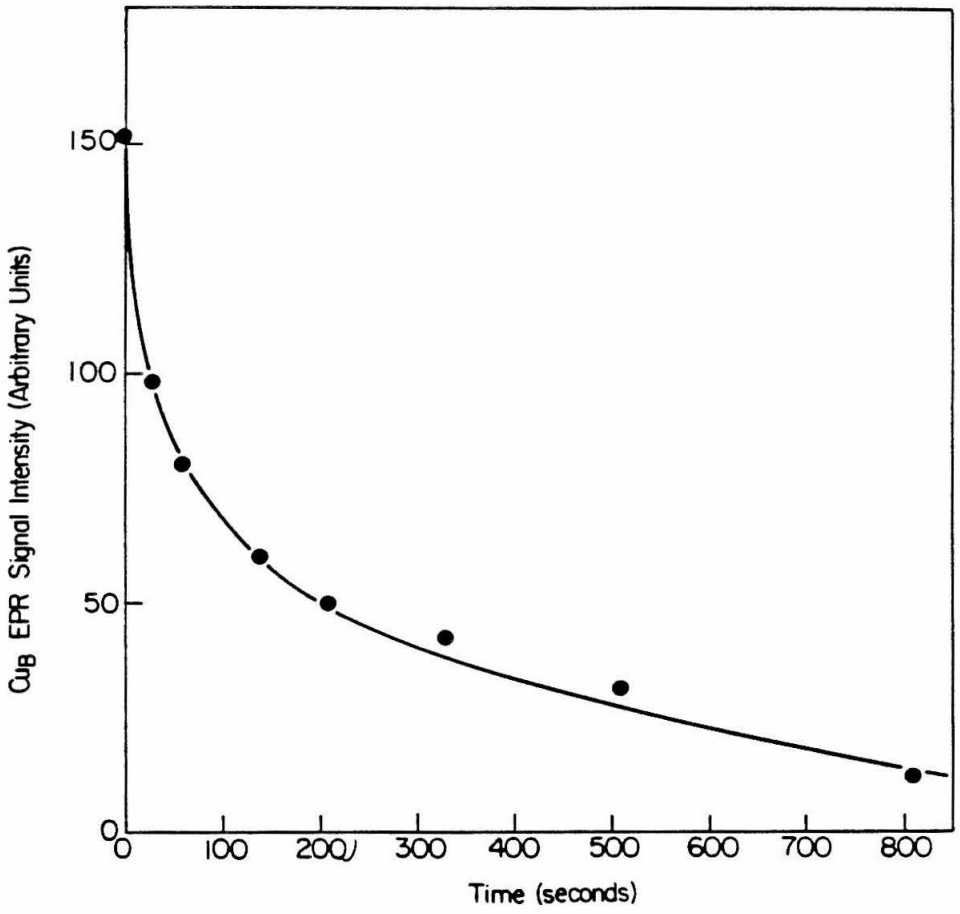
150
100
50
0
0
100
200
300
400
500
600
700
800
Time (seconds)
Cu_B EPR Signal Intensity (Arbitrary Units)

Figure 11

Development of the new, magnetically isolated copper and iron EPR signals in ca. three-electron-reduced cytochrome *c* oxidase sample. Conditions for EPR spectroscopy were as described in the legends to Figures 1 and 9.

A. Spectrum after incubation at 203 K for 6 minutes.

B. After incubation at 211 K for 135 minutes.

C. After incubation at 211 K for 135 minutes and 222 K for 50 minutes.

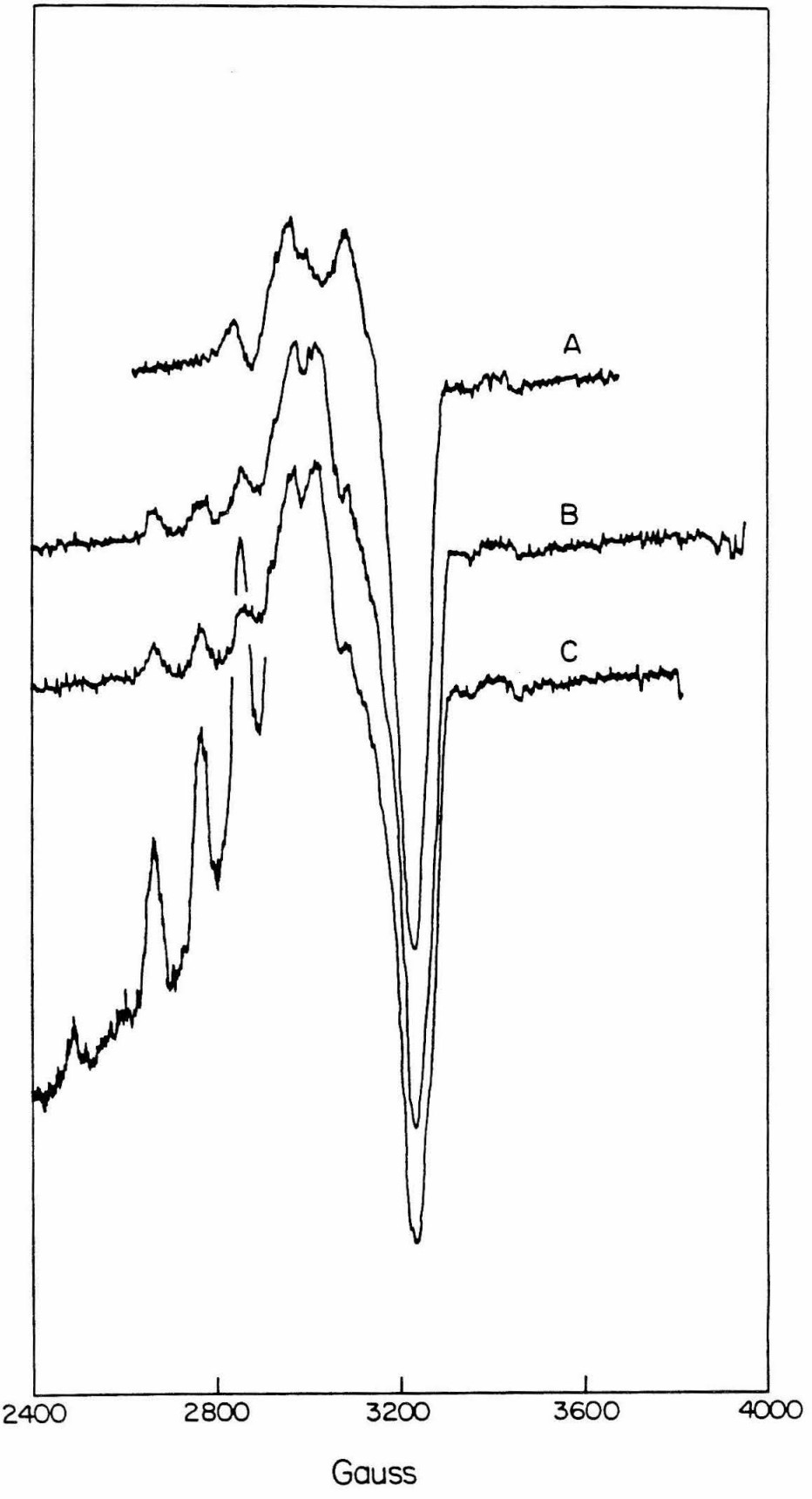
A
B
C
2400
2800
3200
3600
4000
Gauss

DISCUSSION

Initial Reaction Step. The overall reaction scheme which best accounts for the initial electron-transfer events is shown above in Scheme I and is essentially identical with that deduced by Clore *et al.* (5). This scheme involves first the transfer of an electron from *either* Cu_A or Fe_a with similar apparent rates, to produce an intermediate at the Fe_{a_3}/Cu_B site which is formally at the three-electron-reduced level of dioxygen reduction. The three-electron-reduced intermediate gives rise to the unusual Cu_B EPR signal which exhibits only the features associated with one g value and which is unusually resistant to power saturation. At 181 K, both of these electron-transfer processes have an apparent first order rate constant of ca. 4.4 $x10^{-3}$ s^{-1}. Approximately 30 % of Fe_a and 70 % of Cu_A are oxidized in this step. The reduced Cu_A which remains is oxidized in a somewhat slower process (k = ca. $1x10^{-3}$ s^{-1}). At 181 K, Fe_a is still about 70 % reduced after 2 hours. Thus, after 2 hours at 181 K, 70 % of the Fe_{a_3}/Cu_B sites are at the three-electron level of dioxygen reduction and exhibit the unusual Cu_B EPR signal, while the remaining 30 % are at the four-electron (formally, water) level.

The evidence for the reaction scheme consists of the following observations: (A) The careful kinetic analysis of Clore *et al.* showed convincingly that Fe_a is oxidized in a single first-order step during incubation at a comparable temperature (173 K) and that Cu_A oxidation is well-fitted by the expression appropriate to the two-step mechanism in Scheme I. All our data on the oxidations of Fe_a and Cu_A are consistent with this scheme: In numerous experiments at 181 K, the overall time course of Cu_A oxidation was not well-fitted by a single exponential, and the oxidation of Fe_a did not parallel that of Cu_A. After 2 hours of incubation at 181 K, integration of the Cu_A and Fe_a signals shows that the amount of oxidized Fe_a corresponds to much less than (approximately 30 % of) the amount of oxidized Cu_A. (B) After subsequent incubation for 30 min at 203 K, the Fe_a signal increases to approximately 80 % of Cu_A. This indicates that a substantial percentage of the

Fe_{a_3}/Cu_B sites were in fact still at the three-electron level of dioxygen reduction after the incubation at 181 K, as required by scheme I. At the same time, the Cu_A signal does not increase appreciably, indicating that the oxidation of this site was very nearly complete at the lower temperature. (C) The Cu_B EPR signal, which is associated with an intermediate of dioxygen reduction at the three-electron level, shows a small but reproducible *decrease* at times between 5 and 10 min of incubation at 181 K. In the present reaction scheme, this decrease is caused by the elimination of some three-electron-reduced intermediate by the transfer of the fourth electron from Cu_A to the Fe_{a_3}/Cu_B site (the conversion from intermediate IIA to intermediate III). In samples initially reduced by only three electrons, in which the transfer of the fourth electron may not take place in most of the enzyme molecules, this early phase of Cu_B decay was not observed.

The causes underlying the branched reaction scheme are in part revealed by the experiments using partially (ca. 3.5 equiv) reduced enzyme samples. In ca. 3.5-equiv reduced samples, Fe_a is approximately 10 % oxidized and Cu_A is approximately 50 % oxidized at the beginning of the experiment. In these samples, Fe_a is oxidized to a much greater extent (approaching 80 %) in the first electron transfer step. This step is analogous to the conversion from intermediate I to intermediate IIA in Scheme I, differing only in that Cu_A is already largely oxidized. In the partially reduced samples, the Fe_a oxidation exhibits an apparent first order rate constant which is approximately 2-fold smaller than that observed in the fully reduced samples. These observations are readily interpreted in terms of Scheme I. In the initial electron-transfer step of this scheme, the apparent rate constants for Fe_a or Cu_A oxidation in the case of the fully reduced enzyme will be the *sum* of the rate constants for the oxidation of these sites (26), whereas in the case of the three-electron-reduced enzyme the apparent rate constants will be the same as the actual rate constants. The more extensive oxidation of Fe_a in the ca. three-electron-reduced enzyme indicates that the electron transfer from Fe_a

is relatively fast if the electron is the third electron to be transferred to dioxygen but slow if it is the fourth. In the fully reduced enzyme, Fe_a must compete with Cu_A to be the donor of the this third electron. It was previously suggested (5) that the trapping of the fourth electron in Fe_a is due to an Fe_a-Cu_A interaction, in which the oxidation of Cu_A blocks the Fe_a to Fe_{a_3}/Cu_B electron transfer. The experiment using three-electron reduction shows that the contrary is the case: The presence of initially oxidized Cu_A *increases* the amount of Fe_a oxidation.

The first electron transfer from Cu_A was examined over a range of temperatures between 166 and 186 K. The rate was estimated by using the slope of the early portion of the Cu_A oxidation data, since at later times the curve is complicated by the second electron transfer step (the conversion from intermediate IIA to intermediate III), in which some 30 % of the Cu_A oxidizes more slowly to yield the four-electron product at the Fe_{a_3}/Cu_B site. The activation parameters deduced for the first electron transfer step from Cu_A are $\Delta H^* = 13 \pm 1$ kcal mol^{-1} and $\Delta S^* = 3 \pm 8$ cal mol^{-1} K^{-1} (in a 40 % ethylene glycol glass). This electron transfer step showed only a weak dependence upon the nature of the medium: in a 50 % glycerol glass, the rate was not markedly different from that in 40 % ethylene glycol.

Nature of the First Reaction Step. Employing Fourier transform infrared spectroscopy, Fiamingo *et al.* (21) recently demonstrated that CO coordinated to cuprous Cu_B after the photolysis of CO from ferrous Fe_{a_3}. CO relaxed back completely to Fe_{a_3} within a few minutes at 210 K and above after removal of the excitation source, while the Cu_B-CO complex was stable overnight at 140 K and below. The reformation of a $Fe^{II}_{a_3}$ – CO complex was a first order process, exhibiting a distribution of activation enthalpies below 210 K: the peak activation enthalpy of the distribution was 9.2 ± 0.2 kcal mol^{-1}, with an activation entropy of -18.4 ± 1.4 cal mol^{-1} K^{-1} (21). From these results, evidently a sizeable fraction of cuprous Cu_B would be complexed with CO over the same temperature range in

which the triple trapping experiments are conducted (170-200 K). The reoxidation of Cu_B (and Fe_{a_3}) is unlikely to proceed until CO dissociates from cuprous Cu_B. Accordingly, Fiamingo *et al.* proposed that the rate-limiting step for the proper binding of O_2 and the subsequent oxidation of the fully reduced enzyme was the dissociation of CO from cuprous Cu_B.

Our investigation of the initial rate of reoxidation of Cu_A revealed that over a limited temperature range (166-186 K), the rate of reoxidation of Cu_A paralleled the rate of dissociation of CO from Cu_B. The activation enthalpy and entropy for the initial reoxidation of Cu_A are $\Delta H^* = 13 \pm 1$ kcal mol^{-1} and $\Delta S^* = 3$ cal mol^{-1} K^{-1}. It should be noted that in our study, samples were in 40 % ethylene glycol, whereas in the study of Fiamingo *et al.* the samples were in 100 % glycerol. Therefore, although the activation energies for the dissociation of CO from cuprous Cu_B and the reoxidation of Cu_A are indeed different, the similarity in the rates of these two processes leads us to agree with Fiamingo *et al.* that the rate limiting step in the reoxidation of the enzyme is likely to be the dissociation of CO from cuprous Cu_B (Scheme II). The activation parameters from our study and from the study of Fiamingo *et al.* may be different because of the quite different solvents which were employed, or the differences may reflect the fact that the activation parameters determined by Fiamingo *et al.* are for dissociation of CO from Cu_B and for the *rebinding* to ferrous Fe_{a_3}. In our study, CO does not rebind to ferrous Fe_{a_3} after dissociation from cuprous Cu_B. The correspondence is close enough to suggest that the first process under examination in our experiments may in fact be the dissociation of CO fron cuprous Cu_B, followed by relatively rapid reaction with iron-bound dioxygen to generate a peroxidic intermediate and enable electron transfer from Fe_a or Cu_A (Scheme II).

If Scheme II is correct, then the first intermediate in the low temperature dioxygen reaction (probably a dioxygen adduct of ferrous Fe_{a_3}) may differ from the physiologically relevant intermediate due to the involvement of the CO molecule

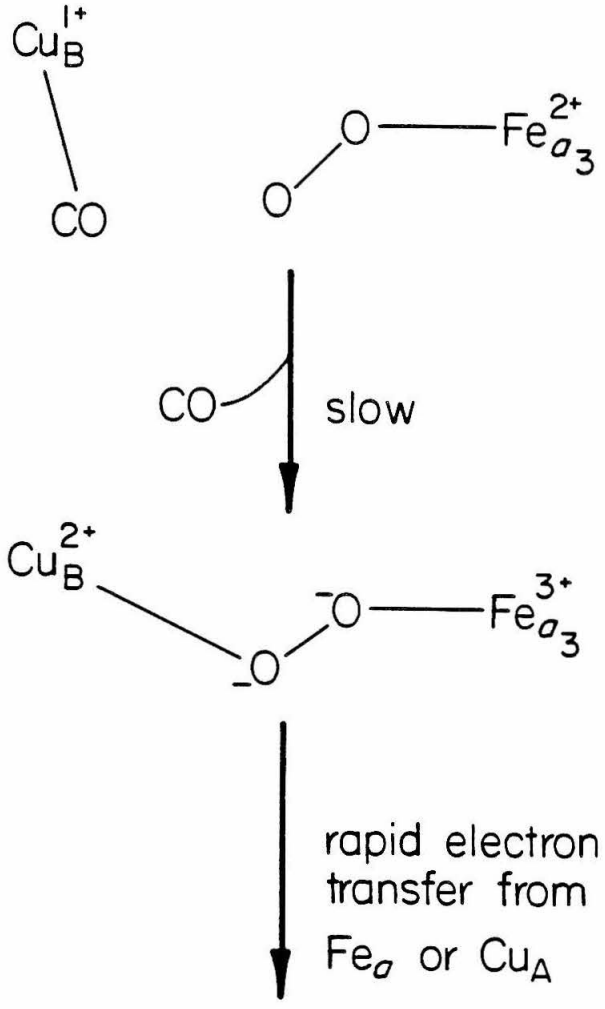
Cu_B 1+
CO
O
O
Fe_a3 2+
CO
slow
Cu_B 2+
O
O
Fe_a3 3+
rapid electron
transfer from
Fe_a or Cu_A

Scheme II

bound to Cu_B. In the absence of CO, such an intermediate may never be formed or may have a very short lifetime. This posssibility emphasizes the need to devise kinetic experiments, both at low and physiological temperatures, in which inhibitory ligands are not present.

Second Reaction Step. As noted above, an unusual EPR signal from Cu_B appears in concert with the early oxidation of Cu_A and Fe_a. Subsequent electron transfer from Cu_A in the subpopulation of molecules which underwent initial oxidation at Fe_a causes a portion of the signal to disappear, but most of the unusual Cu_B signal, which is assigned to intermediate IIB in Scheme I, remains after 1 hour at 181 K. The next distinct reaction step which is observed, after prolonged incubation at 181 K or much shorter incubation at temperatures ca. 10 deg higher, is the disappearance of this unusual Cu_B signal. During this process, very little further oxidation of Cu_A or Fe_a takes place, and the time courses of the Cu_A and Fe_a oxidation do not parallel the disappearance of the unusual EPR signal. In samples which are initially reduced by only ca. 3.4 electrons, the unusual Cu_B signal disappears to near completion and at the same rate as observed in fully reduced samples, indicating that the transfer of a fourth electron is not required for the elimination of the three-electron-reduced intermediate which gives rise to the unusual Cu_B EPR signal. These observations imply that there are *two* intermediates at the three-electron level of dioxygen reduction, the first EPR-detectable and the second EPR-undetectable under the conditions of our experiments.

The conversion from the first to the second three-electron-reduced intermediate was characterized in considerable detail. At all temperatures studied, the decay of the unusual Cu_B EPR signal was nonexponential, which we attribute to the existence of multiple conformations which have different activation enthalpies for this step and which interconvert only slowly, if at all, at these low temperatures. Analogous behavior has been observed in the recombination of CO with myoglobin (17-18) or with cytochrome *c* oxidase following photolysis (21). The

progress of these reactions was satisfactorially fit by the power law expression (Materials and Methods). The power law also gives satisfactory fits for the conversion between the first and second three-electron-reduced intermediates. The power law analysis was used in conjunction with examination of this process over a range of temperatures to estimate the most probable activation enthalpy. The value which we deduce is 18 kcal mol^{-1}. The corresponding activation entropy is 21 cal mol^{-1} K^{-1}, assuming a prefactor of 10^{13} s^{-1}, which may be an overestimate.† These activation parameters indicate that this step is entropically promoted to a substantial degree: An activation entropy of 21 cal mol^{-1} K^{-1} corresponds to a rate enhancement of approximately 4 x 10^4.

We should consider some factors which may cause an overestimation of the most probable activation enthalpy and the activation entropy for the conversion between the two three-electron-reduced dioxygen intermediates. When the decay of the unusual Cu_B EPR signal was studied, typically the initial population of the EPR-detectable three-electron-reduced intermediate was ~70-80 % of the total enzyme molecules. (Recall that from 20-30 % of the initial population of the EPR-detectable three-electron-reduced species was eliminated by the transfer of the fourth electron to the dioxygen reduction site. See Scheme I.) Since the decay of only ~70-80 % of the initial population of the EPR-detectable three-electron-reduced intermediate was observed in this study, what effect might this have on the determined activation parameters ΔH^* and ΔS^*?

(i) To answer this question we must consider two alternative models for the decay of the 20 % subpopulation of the EPR-detectable three-electron-reduced

† At 200 K, the Eyring prefactor kT/h is approximately 0.4 x 10^{13} s^{-1}; so 1.0 x 10^{13} s^{-1} is likely to be an over estimate. Also, the transmission coefficient κ has been taken to be 1.0, the maximum possible. The effect of these assumptions, which probably overestimate the effective frequency prefactor, will be to underestimate the activation entropy.

dioxygen intermediate. (a) The distribution of barrier heights ($g(H^*)$) after the preincubation period, which is representative of ~70-80 % of the initial population, may in fact be identical to the initial distribution of barrier heights. Specifically, the distribution of barrier heights after the preincubaton period will be the same as the initial distribution *if* the transfer of the fourth electron to the dioxygen reduction site (step IIA to III in Scheme I) does not preferentially reduce those conformations of the EPR-detectable three-electron-reduced intermediate which have the smallest barrier height (for conversion to the EPR-silent three-electron-reduced intermediate). If the activation enthalpy distribution after the preincubation period is similar to the initial distribution, the experimentally determined parameters (ΔH_p^* and ΔS^*) will reflect the initial distribution of barrrier heights. (b) In contrast, it is plausible that the transfer of the fourth electron to the dioxygen reduction site (step IIA to III in Scheme I) is actually more favorable in the subset of molecules in which the activation barrier (for the conversion of the EPR-detectable species to the EPR-silent species) is lowest. If this is the case, the subpopulation of the most rapidly reacting EPR-detectable three-electron-reduced intermediate will be eliminated before the start of our experiment. We then expect that the peak of the activation enthalpy distributon will be skewed to larger barrier heights. Thus, in the latter case, ΔH_p^* and ΔS^* will be *overestimated*.

(ii) It is now appreciated that at temperatures below 120 K the multitude of conformational substates, which are accessible to a protein, do not interconvert. However, at more elevated temperatures, specifically near the freezing temperature ($T_f \sim 200$ K)) of mixtures of water and ethylene glycol, it is known that some conversion between the conformational substates can occur (19,27). In fact, Agmon and Hopfield (27) have suggested that there is an increased rate of interconversion between conformational substates near the freezing temperature, and the increased rate of conversion has the unusual effect of *increasing* the most probable barrier height for the recombination of carbon monoxide with myoglobin. Our

experiments do not involve the recombination of CO with ferrous Fe_{a_3}; however, since our experiments were conducted close to the T_f of the solvent (183-207 K), a similar increase in the most probable activation barrier may have occurred. Again, an increase in the most probable activation enthalpy would also tend to cause an overestimation of the activation entropy.

The conversion between the two three-electron-reduced intermediates was also examined by conducting some experiments in 50 % glycerol rather than in 40 % ethylene glycol. In the glycerol glass, this step was much (ca. 100-fold) slower, taking place at an appreciable rate only at temperatures some 15 deg higher than the reaction in ethylene glycol. This result may reflect a change in the conformation of the enzyme, or its conformational flexibility, in the glycerol glass. The intensity and position of the Cu_B signal are the same in the glycerol and ethylene glycol glasses, which suggests that the structure of the dioxygen reduction site is *not* substantially different. If the rate difference is caused by a difference in conformational flexibility, this would suggest that significant protein conformational change is involved in this step.

The two three-electron-reduced intermediates are at the same formal oxidation level, but they must be structurally different since one exhibits an unusual copper EPR signal while the other does not. Various structures which contain the correct number of electrons may be envisioned, depending upon the state of the dioxygen bond and the extent of protonation. The activation parameters for the conversion and the sensitivity of the process to conformation (which is implied by its distributed activation enthaly) suggest that this process corresponds to the cleavage of the dioxygen bond. The first of the three-electron-reduced intermediates would then contain a peroxidic adduct of ferrous Fe_{a_3} and cupric Cu_B, while the second intermediate would contain a ferryl ion and a cupric ion. Adopting this hypothesis, shown in Scheme III, we may say that the cleavage of the O-O bond is promoted largely by a positive entropy change. Such a favorable

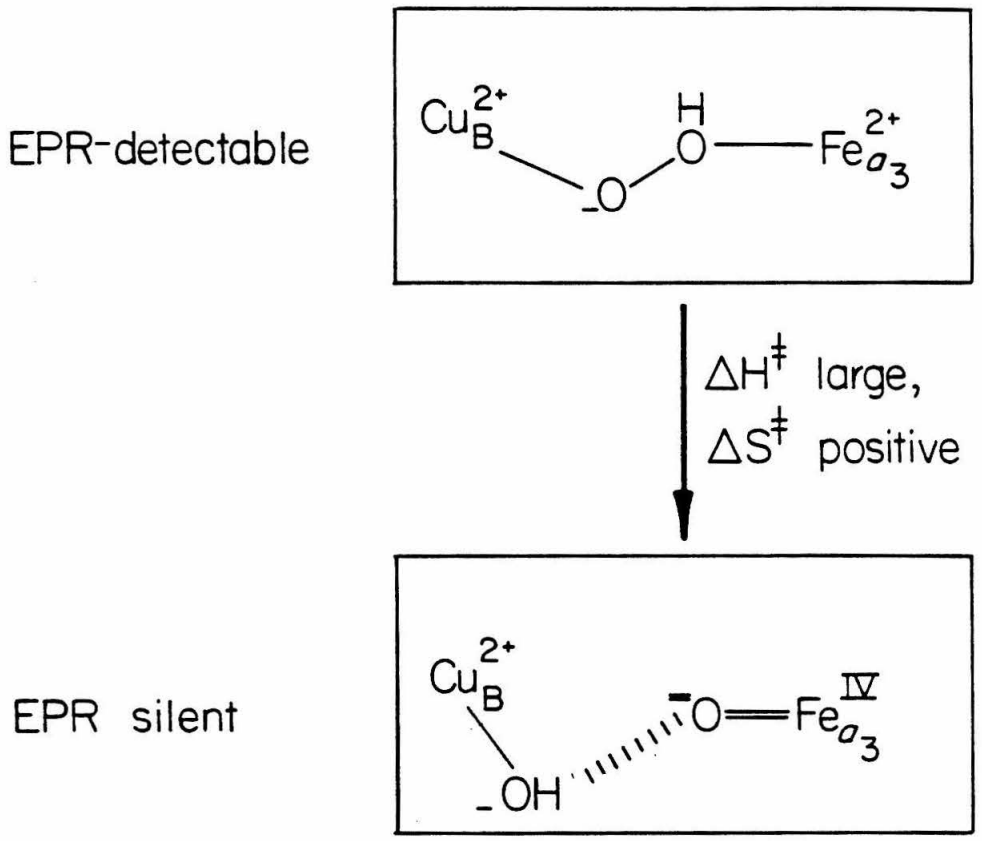
EPR-detectable
Cu_B^{2+}
H
O
$Fe_{a_3}^{2+}$
O
$\Delta H^{\ddagger}$ large,
$\Delta S^{\ddagger}$ positive
EPR silent
Cu_B^{2+}
O
$Fe_{a_3}^{IV}$
OH

Scheme III

entropy of activation could be achieved through ordering of the reactant state, in which the hydroperoxide is coordinated to both the copper and the iron. If the intermetal distance is appropriate, the metals may act as a "rack" on which the hydroperoxide is stretched and is thereby ordered (28). Conversely, the hydroperoxide binding is expected to constrain the intermetal distance, thus decreasing the motional freedom of the surrounding protein.

The description shown in Scheme II applies to intermediate IIB only, since intermediate IIA is eliminated by a different pathway which involves the transfer of a fourth electron to the dioxygen reduction site. Following this electron transfer, the oxygen-oxygen bond may be broken, via a mechanism which is different from that in Scheme III or it may be intact until the temperature is raised further. Since intermediate III is EPR-silent, other approaches will be required to study this alternate pathway. We only note here that the highly activated character of the reaction step in Scheme III makes it very likely that this path, which proceeds via two three-electron-reduced intermediates, will be the dominant one at physiological temperature, since the postulated bond-breaking step is predicted to be very rapid (10^6-10^8 s^{-1}) at 37 °C (by extrapolation of the Arrhenius plot in Figure 5).

Nature of the Unusual Cu_B EPR Signal. If Scheme III is correct, it must somehow account for the unusual EPR spectroscopic properties of the two three-electron-reduced intermediates. With regard to the first intermediate, we must explain why only a small portion of the copper EPR spectrum is observed and why this signal is very difficult to saturate relative to magnetically isolated copper ions. Previously, in the absence of evidence for two different three-electron-reduced intermediates, this unusual Cu_B EPR signal was proposed to arise from a cupric ion in proximity to a ferryl ion (the *second* three-electron intermediate in our reaction scheme). Additionally, it was proposed that a hydroxide ion coordinated to the copper is hydrogen-bonded to the ferryl oxygen, facilitating a superexchange interaction between the copper and the iron spins (12). The rapid relaxation of the

copper spin and the absence of g_x and g_y features were ascribed to dipolar and/or superexchange coupling to the S = 1 (low-spin) ferryl ion, which is expected to relax very rapidly (11,29-30).

In our reaction scheme, the unusual Cu_B signal is proposed to arise from a hydroperoxide-bridged cupric/ferrous intermediate. In this intermediate, the hydroperoxide coordination to the copper may be stronger than its coordination to iron; consequently, we propose that the ferrous iron is high-spin (S = 2) or intermediate-spin (S = 1). Niether of these spin-states would be surprising given that the hydroperoxide coordination to copper could substantially weaken its coordination to iron. The peroxidic bridge between the copper and iron ions will facilitate a superexchange coupling between the ions. If the superexchange coupling parameter J is small relative to the axial zero-field splitting D of the high- or intermediate-spin heme, then perturbation theory may be used to calculate the g values of the coupled cupric/ferrous spin system. This perturbation treatment shows that the superexchange coupling affects g_x and g_y to first order in J/D but g_z only to second order. The shape and intensity of the resolvable portion of the spectrum at g_z is consistent with values for g_x and g_y less than or equal to 1.3 (11). Assuming an axial zero-field splitting of 20 cm^{-1} and iron g values of 2.0, the superexchange coupling required to give g_x and g_y values of 1.3 is calculated to be 3.5 cm^{-1} if the iron is intermediate-spin, or 1.1 cm^{-1} if the iron is high-spin. Using these values for J, the value of g_z (which is perturbed only to second order in J/D) is predicted to be typical for copper, even if the g values of the iron are quite anisotropic (*e.g.*, g_z(Fe) = 3.0), which is itself unlikely. Similarly, the copper hyperfine coupling parameter A_z(eff) will not be significantly reduced relative to the isolated copper ion.

The absence of observable inflections near $g = 1.3$ could be caused by inhomogeneously broadening of the resonance, either by g anisotropy in the iron (which would cause g_y to be greater than 1.3 and g_x to be less than 1.3) and/or "J-strain",

a distribution in the value of the superexchange coupling parameter J caused by conformational heterogeneity. The resistance of the unusual Cu_B EPR signal to power saturation also follows as a consequence of weak superexchange coupling to the iron ion. The presence of nearby high-lying states in the iron spin manifold, which are admixed with the copper spin states, will facilitate the relaxation of the copper spin via the Orbach mechanism (31). The temperature dependence of the Cu_B relaxation rate is consistent with relaxation via an Orbach mechanism which involves spin excited states ca. 20 cm^{-1} higher in energy (32). Thus, all of the properties of the unusual Cu_B signal are accounted for by adopting the structure proposed in Scheme III and postulating a fairly weak (1.1 or 3.5 cm^{-1}, depending on the iron spin state) superexchange interaction between the copper and the iron.

With regard to the second intermediate at the three-electron level of reduction, which we suggest is in the cupric/ferryl oxidation state, we must explain why no EPR spectrum assignable to this intermediate is observed. The perturbation treatment described above, as well as the analogous treatment in which a very strong superexchange interaction is assumed and the zero field splitting is treated as a perturbation, indicates that in the limits of very strong or very weak coupling, the superexchange interaction cannot make the expected resonance so anisotropic or so inhomogeneously broadened that all its spectral features, particularly those at g_x, are undetectable. However, at intermediate strengths of the superexchange coupling (which would require a higher order calculation for quantitative characterization), it is possible that the g_x and g_y values could be lowered, shifting these resonances to much higher field, so that even the resonance at g_x became undetectable. Using the formulas of Aasa and Vänngård (16), we calculate that a shift in $g_{x,y}$ from 1.3 to ca. 0.5 would result in a ten-fold reduction in the area of the peak at g_x. In the $S(\mathrm{Fe}) = 1$, $S(\mathrm{Cu}) = 1/2$ system, this would require a superexchange coupling of 8 cm^{-1}, using the above perturbation treatment. (However, since $J/D = 0.4$ in this case, this calculation must be considered approximate).

We note that if there is even a weak bond between the ferryl oxygen and the copper ion, the superexchange coupling between the metal centers could be much stronger in the ferryl-containing intermediate than in the hydroperoxide-bridged intermediate and quite possibly as strong as 8 cm^{-1}. Another possible explanation for the absence of an EPR signal from the second three-electron-reduced intermediate is that spin relaxation in this cupric/ferryl system is very rapid ($1/T_2 = 10^{10}$ s^{-1}), so that the spectral features are broadened beyond detection.

Third Reaction Step. In the third step of the reaction, an additional fraction of Fe_a is oxidized. This takes place at conveniently monitored rates at temperatures near 203 K. At ca. 193 K, Fe_a oxidation takes place much more slowly, so this step is rather highly activated. Precise measurement of the activation enthalpy was not made. As discussed above, the slowness of this oxidation is related to the fact that the electron in Fe_a at this step is the *fourth* electron to take part in the dioxygen reaction; when it is the third electron, the transfer occurs more rapidly. This indicates that the different electron transfers which take place during the dioxygen reduction reaction can have significantly different rates, even when the donor is the same. This is not surprising in view of the changes which are necessarily taking place at the dioxygen reduction site during the reaction cycle.

Fourth Reaction Step: Generation of a Magnetically Isolated Cu_B EPR Signal. In samples which had previously been incubated at 203 K or lower temperature, subsequent incubation at 211 K for 20-40 min caused the appearance of a new, rhombic EPR signal with hyperfine splittings which indicate that it is due to copper. The saturation behavior of this signal was not unusual for copper, *i.e.*, it was significantly saturated by submilliwatt microwave powers at 9 K, and it exhibits no dipolar splittings to suggest that it is in proximity to another paramagnet. This signal has been observed previously under different sample preparation conditions and was assigned to Cu_B (22). Since complete recovery of the normal Cu_A signal intensity is observed after incubation at the low temperatures, we

also conclude that the signal is due to Cu_B. The absence of splittings or unusual saturation behavior indicates that the nearby Fe_{a_3} is diamagnetic, *i.e.*, low-spin ferrous. If the incubation was continued at 211 K or higher, another signal appears at $g = 2.63$ and 1.89, which may be assigned to low-spin ferric Fe_{a_3} (24-25). This signal, like the magnetically isolated, rhombic Cu_B signal, exhibits no splittings to suggest the proximity of another paramagnet, indicating that the nearby Cu_B is reduced. Both of the EPR signals from the dixoxygen reduction site which appear upon incubation at 211 K thus arise from states in which the site contains a single reducing equivalent.

Because we have proposed that the dioxygen reduction site is already highly oxidized (ferryl/cupric) state after the low-temperature incubations, its partial reduction at 211 K is at first somewhat puzzling. A source for the electrons, apart from Fe_a and Cu_A, is required to explain the reduction. A variety of evidence suggests that this electron source is carbon monoxide, which reduces the site via the reaction in Scheme IV.

After the lower temperature incubations, and after the 211 K incubations which lead to the generation of the new signals, Fe_a oxidation was still not complete. These observations are as required by Scheme IV. In a sample initially reduced by ca. only 3.4 electrons, incubation at 211 K led to the generation of the magnetically isolated Cu_B and Fe_{a_3} EPR signals in higher yield. Upon thawing samples which had been used in the kinetic studies at 200 K or lower for 1 min at ice temperature, little of the magnetically isolated Cu_B signal was seen if the samples had been initially reduced almost completely, but a substantial quantity was produced in the samples which had been initially reduced by only 3.4 equiv. These results suggest that a three-electron-reduced intermediate is involved in the production of the magnetically isolated Cu_B EPR signal.

Alternative explanations for the appearance of the magnetically isolated EPR signals which do not involve the re-reduction of this site must postulate that the

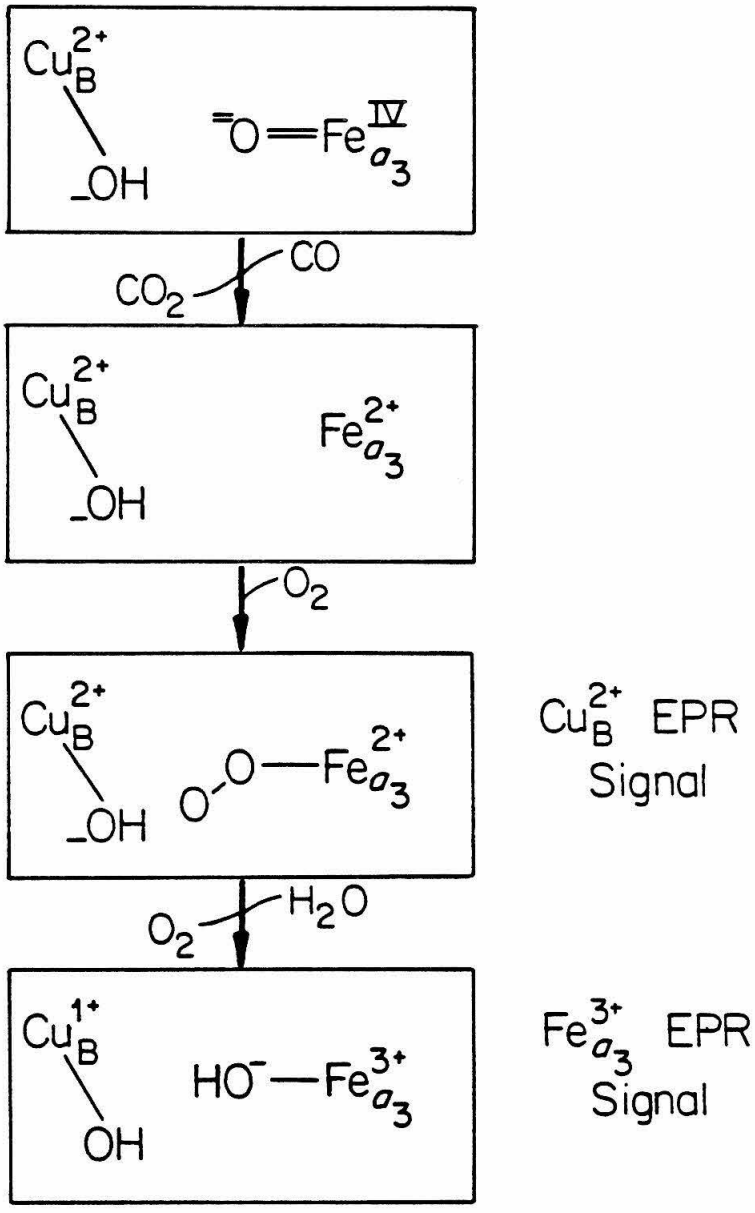
Cu$_B^{2+}$
$^{=}$O=Fe$^{IV}_{a_3}$
OH
CO$_2$
CO
Cu$_B^{2+}$
Fe$^{2+}_{a_3}$
OH
O$_2$
Cu$_B^{2+}$
O-O-Fe$^{2+}_{a_3}$
OH
Cu$_B^{2+}$ EPR Signal
O$_2$
H$_2$O
Cu$_B^{1+}$
HO$^-$-Fe$^{3+}_{a_3}$
OH
Fe$^{3+}_{a_3}$ EPR Signal

Scheme IV

iron-cooper pair was not oxidized to the ferryl-cupric level at low lower incubation temperatures. Such explanations would require that there be *three* intermediates at the three-electron level of dioxygen reduction and that the dixoygen bond be intact in all three of them. The different EPR properties of the three intermediates would then be due to changes in the iron-cooper coupling and the iron spin state. This kind of explanation appears unlikely to be true, especially in view of the stability of the new Cu_B signal for at least 1 min at 273 K.

The oxidation of carbon monoxide which is proposed in Scheme IV is noteworthy because it takes place at an appreciable rate ($t_{1/2} \sim 20$ min) at relatively low temperature (211 K) and significantly faster at ice temperature ($t_{1/2}$ less than 1 min). This is perhaps surprising in view of published reports on the reduction of cytochrome *c* oxidase (33) or hemin by carbon monoxide (34). However, the latter reactions take place in ferric/cupric or ferric systems, in contrast to the reaction in Scheme IV, which involves a ferryl ion. The ferryl ion, with the structure proposed, is well suited to this reaction in two respects: It is able to accept two electrons at once, and it contains an oxygen atom which is not protonated.

Electron-Transfer Pathways. We conclude by noting one of the implications of the scheme describing the early electron-transfer events. This scheme involves the partitioning of the oxidase molecules into two distinct populations by the transfer of this first electron from either Fe_a or Cu_A. The occurrence of this partitioning indicates that both Cu_A-to-Fe_{a_3}/Cu_B site and Fe_a-to-Fe_{a_3}/Cu_B site electron-transfer pathways are approximately equally competent at these temperatures. The similarity of the rates via the two path indicates that one is not very much better than the other with respect to the distance of the transfer or the suitability of the intervening material (35). The existence of two competent electron pathways to the dioxygen reduction site may have implications for the mechanisms of energy conservation by the oxidase. It is now well established that the cytochrome *c* oxidase-catalyzed transfer of electrons from cytochrome *c* to

dioxygen is coupled to the active transport of protons across the mitochondrial membrane (36), and it appears most likely that either Fe_a or Cu_A is involved in this proton pumping function. If, for example, Cu_A were the proton pump, then the Fe_a-to-Fe_{a_3}/Cu_B electron-transfer path would bypass the pump. Such a bypass mechanism might be important at steps in dioxygen reduction where the Cu_A-to-Fe_{a_3}/Cu_Btransfer, which is linked to proton pumping, is relatively slow because these steps are not sufficiently exothermic. It has been suggested (37) that proton pumping might be uncoupled from electron transfer at some steps in the cytochrome *c* oxidase reaction cycle. The existence of two competent electron-transfer pathways to the dioxygen reuduction site may reflect the need for this uncoupling.

REFERENCES

1. Gibson, Q.H. and Greenwood, C. (1963) *Biochem. J.* **86**, 541-554.
2. Chance, B. and Leigh, J.S., Jr. (1977) *Proc. Natl. Acad. Sci. USA* **74**, 4777-4780.
3. Clore, G.M. and Chance, E.M. (1978) *Biochem. J.* **173**, 811-820.
4. Clore, G.M. and Chance, E.M. (1978) *Biochem. J.* **175**, 709-725.
5. Clore, G.M., Andréasson, L.-E., Karlsson, B., Aasa, R. and Malmström, B.G. (1980) *Biochem. J.* **185**, 139-154.
6. Hill, B.C. and Greenwood, C. (1984) *Biochem. J.* **218**, 913-921.
7. Blair, D.F., Witt, S.N. and Chan, S.I. (1985) *J. Am. Chem. Soc.* **107**, 7389-7399.
8. Greenwood, C. and Gibson, Q.H. (1967) *J. Biol. Chem.* **242**, 1782-1787.
9. Chance, B., Saronio, C. and Leigh, J.S., Jr. (1975) *J. Biol. Chem.* **250**, 9226-9237.
10. Babcock, G.T., Jean, J.M., Johnston, L.N., Palmer, G. and Woodruff, W.H. (1984) *J. Am. Chem. Soc.* **106**, 8305-8306.
11. Karlsson, B., Aasa, R., Vänngård, T. and Malmström, B.G. (1981) *FEBS*

Lett. **131**, 186-188.

12. Hansson, O., Karlsson, B., Aasa, R., Vänngård, T. and Malmström, B.G. (1982) *EMBO J.* **1**, 1295-1297.
13. Hartzell, C.R. and Beinert, H. (1974) *Biochim. Biophys. Acta* **368**, 318-338.
14. "Laboratory Methods in Porphryrin and Metalloporphyrin Research", Fuhrop, J.-H., Smith, K.M., Eds. (Elsevier, New York) 1975, p. 48.
15. Markwell, M.A.K., Haas, S.M., Bieber, L.L. and Tolbert, N.E. (1978) *Anal. Biochem.* **87**, 206-210.
16. Aasa, R. and Vänngård, T. (1975) *J. Magn. Res.* **19**, 308-315.
17. Austin, R.H., Beeson, K., Eisenstein, L., Frauenfelder, H., Gunsalus, I.C. and Marshall, V.P. (1974) *Phys. Rev. Lett.* **32**, 403-405.
18. Austin, R.H., Beeson, K.W., Eisenstein, L., Frauenfelder, H. and Gunsalus, I.C. (1975) *Biochemistry* **14**, 5355-5373.
19. Agmon, N. and Hopfield, J.J. *J. Chem. Phys.* **79**, 2042-2053.
20. Bevington, P.R. "Data Reduction and Error Analysis for the Physical Sciences" (McGraw-Hill, New York) 1969, p. 114.
21. Fiamingo, F.G., Altsculd, R.A., Moh, P.P. and Alben, J.O. (1982) *J. Biol. Chem.* **257**, 1639-1650.
22. Karlsson, B. and Andréasson, L.-E., (1981) *Biochim. Biophys. Acta* **635**, 73-80.
23. Reinhammer, B., Malkin, R., Jensen, P., Karlsson, B., Andréasson, L.-E., Aasa, R., Vänngård, T. and Malmström, B. (1980) *J. Biol. Chem.* **255**, 5000-5003.
24. Lanne, B., Malmström, B.G. and Vänngård, T. *Biochim. Biophys. Acta* **545**, 205-214.
25. Tang, J.A., Koch, S., Papaefthymiou, G.C., Foner, S., Frankel, R.B., Ibers, J.A. and Holm, R.H. (1976) *J. Am. Chem. Soc.* **98**, 2414-2434.
26. Espenson, J.H. "Chemical Kinetics and Reaction Mechanisms" (McGraw-Hill,

New York), 1981, p. 55.

27. Young, R.D. and Bowne, S.F. (1984) *J. Chem. Phys.* **81**, 3730-3737.
28. Lumry, R. and Eyring, H. (1954) *J. Phys. Chem.* **58**, 110-120.
29. Theorell, H. and Ehrenberg, A. (1952) *Arch. Biochem. Biophys.* **41**, 442-461.
30. Schulz, C.E., Rutter, R., Sage, J.T., Debrunner, P.G. and Hager, L. (1984) *Biochemistry* **23**, 4743-4754.
31. Orbach, R. (1961) *Proc. R. Soc. London, Ser. A* **264**, 458-484.
32. Malmström, B.G., unpublished results.
33 Nicholls, P. and Chanady, G.A. (1981) *Biochim. Biophys. Acta* **634**, 256-265.
34. Bickar, D., Bonaventura, C. abd Bonaventura, J. (1984) *J. Biol. Chem.* **259**, 10777-10783.
35. Hopfield, J.J. *Proc. Natl. Acad. Sci. USA* **71**, 3640-3644.
36. Wikström, M., Krab, K. and Saraste, M. (1981) *Cytochrome Oxidase-A Synthesis*, (Academic Press, New York)
37. Blair, D.F., Gelles, J. and Chan, S.I. (1986) *Biophys. J.* **50**, 713-733.

CHAPTER III

The Reoxidation of Partially Reduced Cytochrome c Oxidase, and Reactions with Hydrogen Peroxide: Evidence for a Ferryl Fe_{a_3}/cupric Cu_B Binuclear Site in Cytochrome c Oxidase.

Introduction

After completion of the low temperature kinetic study, which is described in chapter II, I was convinced that the second EPR-silent, three-electron-reduced dioxygen intermediate ($Fe^{IV}_{a_3}$=O Cu^{II}_B) could be trapped at the dioxygen reduction site of cytochrome *c* oxidase under more physiological conditions, that is, at more ambient temperatures (273-298 K), in the absence of ethylene glycol; after all, it was well established that other highly reactive ferryl enzymatic intermediates are kinetically stable at room temperature. Horse radish peroxidase compound I (HRP-I), for example, is composed of a reactive ferryl porphyrin π-radical cation (1), yet displays remarkable kinetic stability at room temperature in the absence of reducing substrates (2). Because of its kinetic stability, HRP-I is one of the best characterized enzymatic intermediates. There was no reason *a priori* to rule

out that the EPR-silent, three-electron-reduced dioxygen intermediate could be successfully trapped at the dioxygen reduction site of cytochrome *c* oxidase at room temperature, although we did rule out the possibility of trapping the first EPR-detectable, three-electron-reduced intermediate, the proposed ferrous Fe_{a_3}/cupric hydroperoxide, since the half-time for the decay of the unusual anisotropic Cu_B EPR signal is approximately 10 μs (as extrapolated from the low temperature Arrhenius plot in chapter II, Figure 6) (3).

In order to trap a subpopulation of the EPR-silent, three-electron-reduced intermediate at the dioxygen reduction site, substoichiometrically reduced cytochrome *c* oxidase samples were reoxidized with dioxygen. We reasoned that this procedure would produce subpopulations of (i) a two-electron-reduced species (Compound C), (ii) a three-electron-reduced species, and (iii) the pulsed enzyme at the dioxygen reduction site. In fact, we found that when partially reduced (65-85 %) cytochrome *c* oxidase samples were reoxidized with dioxygen, the second three-electron-reduced intermediate is trapped at the dioxygen reduction site. The intermediate has novel spectral features at 580 and ~537 nm in the reoxidized minus resting difference spectrum. Moreover, combined optical and EPR results revealed that this trapped reactive species reacts rapidly with carbon monoxide (CO) at 277-290 K causing the abolition of the spectral features at 580 and 537 nm, with the concomitant formation of a rhombic Cu_B EPR signal.

The discovery of the novel spectral features due to the subpopulation of the second three-electron-reduced intermediate ultimately led us to study the reactions of cytochrome *c* oxidase with hydrogen peroxide (H_2O_2). We observed that when excess H_2O_2 is added to the oxygenated or reduced states of cytochrome *c* oxidase, a more homogeneous population of the second, EPR-silent, three-electron-reduced intermediate is produced at the dioxygen reduction site of cytochrome *c* oxidase, as judged by the intense spectral features at ca.580 and 537 nm in the reoxidized minus resting difference spectrum. (The reactive species which is produced upon the

addition of hydrogen peroxide to the reduced or oxygenated state of cytochrome *c* oxidase will be referred to as the 428/580 nm species, or the H_2O_2-treated enzyme.) Furthermore, the 428/580 nm species reacts rapidly with CO at 277 K to produce large yields (~60 %) of the rhombic Cu_B EPR signal, originally observed in the low temperature study (Chapter II), which is attributed to a state of the enzyme in which Fe_{a_3} is thought to be stabilized in a low-spin ferrous-dioxygen (or possibly CO) adduct adjacent to cupric Cu_B (4-5).

We will present evidence which shows that the same reactive intermediate is produced at the dioxygen reduction site of cytochrome *c* oxidase (i) when partially reduced cytochrome *c* oxidase is reoxidized with dioxygen at room temperature; and (ii) upon treatment of oxygenated (or reduced) cytochrome *c* oxidase with excess hydrogen peroxide, based on the reactivity of these species (i-ii) with carbon monoxide (CO). We propose that these disparate preparative procedures produce the same reactive binuclear dioxygen reduction site, which contains a ferryl Fe_{a_3}/cupric Cu_B binuclear dioxygen reduction site, *i.e.*, the same species which is thought to form upon reoxidation of fully reduced cytochrome *c* oxidase at low temperature (Chapter II).

Materials and Methods

Beef-heart cytochrome *c* oxidase was prepared by the method of Hartzell and Beinert (6). The enzyme was dissolved in 50 mM phosphate buffer containing 0.5 % (w/v) Tween-20 at pH 7.4 unless specified otherwise. Enzyme concentration was determined by measuring the absorbance at 604 nm in the reduced minus oxidized difference spectrum ($\Delta\epsilon^{r-o}$(604 nm) = 24 mM^{-1} cm^{-1}) (7).

Partially Reduced Samples. Enzyme concentrations for the EPR experiments were typically 150-250 μM. EPR samples for the trapping experiments were prepared in 3.8 mm o.d. quartz EPR tubes fitted with vacuum line joints. Samples were deoxygenated by repeated flushing with argon which had been passed

through a 1-meter long scrubbing column containing manganese dioxide supported on vermiculite. Appropriate amounts of deoxygenated NADH (Sigma) were added to achieve the desired extent of reduction. Phenazine methosulfate (PMS) (0.01 equiv) and horse heart cytochrome *c* (0.001-0.003 equiv, Sigma type VI) were added to facilitate reduction via one-electron mediation. After partial or complete reduction, samples were incubated at ice temperature for a minimum of two hours to allow for complete redox equilibration. Samples were then frozen to 77 K and EPR spectra were recorded at low temperatures (ca. 10 K).

To initiate the reoxidation of the partially reduced samples, samples were evacuated while frozen at 77 K and one atmosphere of dioxygen was admitted. By running tap water (288 K) over the outside of the frozen EPR tubes, the samples were rapidly thawed (10 sec), without rupturing the EPR tubes. The thawed samples were shaken and immediately refrozen to 77 K. The interval from thawing to refreezing was made as short as possible to minimize the loss of any relatively unstable trapped intermediates. Typical intervals between thawing and refreezing were 45-60 seconds.

For the optical experiments, samples were degassed and reduced in precision 2 mm path-length cells using a modification of the methods described above. Typical enzyme concentrations were 60-70 μM. After the samples were partially reduced they were incubated for 4-12 hours at ice temperature to ensure redox equilibrium. The fully reduced sample was prepared by reducing with excess NADH containing approximately 0.02 eq of PMS and then was incubated for 96 hours at ice temperature to ensure complete reduction. The samples were then evacuated and one atmosphere of dioxygen was admitted as before. Following reoxidation of the partially or fully reduced samples with dioxygen, carbon monoxide was admitted to reoxidized samples at 277 K within 10-15 minutes. No freeze-thaw cycles were necessary for the UV-VIS experiments. Optical spectra of the reoxidized samples before and after addition of CO were recorded at 275 K on a Beckman Acta CIII

which was interfaced to a Spex Industries SC-31 SCAMP data processor. All optical absorption difference spectra were smoothed by a computer routine on the SCAMP data processor.

H_2O_2 Treatment of Cytochrome c Oxidase. Sample preparation procedures for the H_2O_2-treated samples were the same as for the partially reduced samples with the modification that the samples were reduced with NADH only; no PMS was used as a mediator because it inhibits catalase (8). In the absence of a mediator, the reduction of cytochrome *c* oxidase is very slow and typically requires 2-3 days of incubation at ice temperature. Typically, from 4-5 equiv of NADH (i.e., ~25 % excess) was added to reduce the samples. If dithionite (Baker) was used to reduce the samples, the samples were deoxygenated according to the methods described above, and then solid dithionite (ca. 0.1 mg) was introduced into the sample either by removing the stopcock or by adding the dithionite through the straightbore stopcock. The atmosphere above the sample was immediately evacuated and then replaced with an atmosphere of argon. All optical samples were contained in precision 2 mm path-length Quartz cuvettes, and all the optical absorption difference spectra were smoothed by averaging over a window of seven absorbance points.

Hydrogen peroxide stock solutions were prepared in phosphate buffered solution at pH 7.4, typically containing 1 mM EDTA (Baker). The concentration of the hydrogen peroxide stock solution was determined using an enzymatic assay which utilizes horse radish peroxidase (Boehringer Mannheim, Grad I) (9). Reduced cytochrome *c* oxidase samples in EPR tubes were reoxidized with sufficient H_2O_2 (Baker) to give a final concentration of approximately 4 mM. Unless otherwise specified, bovine liver catalase (0.01-0.10 %) (Sigma, C-10) was added within ca. 100 sec from the addition of H_2O_2 in order to remove the excess H_2O_2. (Catalase decomposes 2 equivalents of hydrogen peroxide to two (and one) equivalents of H_2O (and O_2).) After recording optical spectra of samples from 750-450

nm which were contained in the EPR tubes, the samples were refrozen to 77 K. A special cylindrical sample holder was employed to hold the EPR tube in place during the optical absorption measurement. Due to the intense absorbance of the EPR samples, transmittance filters (16-50 %) were used to attenuate the reference beam when the EPR samples were examined by optical spectroscopy. To initiate the reaction of the reoxidized samples with CO, carbon monoxide (99.99 % pure, Matheson Co.), or argon as a control, was admitted to the samples according to the procedure described above. Samples were maintained at ice temperature throughout the sample manipulations and the recording of optical spectra.

Activity assays of cytochrome *c* oxidase samples were measured polarographically with a YSI Model 53 O_2-electrode after the long incubation period to ensure that the lengthy incubation period did not adversely affect the enzyme. Similarly, to ensure that the brief exposure to high concentrations of hydrogen peroxide did not irreversibly inactivate the enzyme, activity assays were conducted on the H_2O_2-treated enzyme, which had an initial lengthy preincubation period required to reduce the samples. The lengthy incubation period and the brief exposure to millimolar levels of hydrogen peroxide did not adversely affect the activity of the enzyme: The activity of the enzyme after 67 hours incubation at ice temperature was 103 $\pm$ 9 mole cyt-*c* oxidized (mole cytochrome *c* oxidase)$^{-1}$ s^{-1}; samples with the same 67 hours incubation period, but which were exposed to 3 mM H_2O_2 for 60 sec at ice temperature to reoxidize the reduced enzyme, displayed an activity of 120 $\pm$ 7 mole cyt-*c* oxidized (mole cytochrome *c* oxidase)$^{-1}$ s^{-1}. These activities fall well within the range of the activity of the resting enzyme without any prior incubation period (125 $\pm$ mole cyt-*c* oxidized (mole cytochrome *c* oxidase)$^{-1}$ s^{-1}).

EPR. Low-temperature EPR was used to ascertain whether a reaction had occurred between the reoxidized samples and CO. When CO was added to reoxidized samples that were initially reduced from 60 % to 90 %, a rhombic CuB EPR signal ($A_{||}$ = 10.5 mT, g_z = 2.29) was observed. Such a signal has been reported

previously (4,10), although under different reaction conditions, and was attributed to a cupric Cu_B adjacent to a ferrous Fe_{a_3}-dioxygen adduct (4-5). In other cases, the production of the rhombic Cu_B EPR signal was examined at 77 K.

Integrations of the rhombic Cu_B ERR signal were carried out following the method of Aasa *et al.* (11) in which the area under the low-field hyperfine line is compared to the double integral of a standard sample, in this case, Cu(II)-o-phenanthroline. In some cases, Fe_a was used as an internal standard, and the ratio of Cu_B/Fe_a was determined by measuring the area under the low-field hyperfine peak of the rhombic Cu_B EPR signal and comparing that to the area under the "absorption" peak at $g = 3$ of Fe_a (10). The g values used in the integration of the Cu_B EPR signal were determined from computer simulations of the spectrum ($g_x = 2.28$, $g_y = 2.109$, and $g_z = 2.052$) (10).

EPR spectra were recorded on a Varian E-line Century series X-band spectrometer. Either an Oxford low-temperature system or a Air Products Heli-Trans low-temperature system was used for temperature control. A modulation amplitude of 1.6 mT and a modulation frequency of 100 kHz were used to obtain the spectra. The microwave power was typically 0.02 mW. A carbon-glass resistor was used to measure the temperature inside the cavity after each spectrum was recorded. To facilitate data manipulation, the analog data were digitized and collected on a Compaq-Plus PC. For recording EPR spectra at liquid nitrogen temperature, a liquid nitrogen dewar was inserted into the cavity to maintain samples at 77 K.

RESULTS

Partially Reduced Cytochrome *c* Oxidase.

EPR—A typical EPR spectrum for a cytochrome *c* oxidase sample that was approximately 75-80 % reduced is shown in Figure 1*a*. The intensity of the g = 6 component of the high-spin Fe_{a_3} EPR signal provides an indication of the

level of reduction. After the partially reduced sample was reoxidized at 277 K, it exhibited the typical Fe_a and Cu_A EPR signals with the expected intensities when the sample was refrozen (spectrum not shown). The very anisotropic Cu_B EPR signal which we attributed to the hydroperoxide-bridged cupric Cu_B/ferrous Fe_{a_3} adduct was *not* observed at 10 K even with 20 mW of microwave power (3), nor was the readily saturated rhombic Cu_B EPR signal. If, as a control, argon was admitted to the reoxidized sample, there was no evidence of the rhombic Cu_B EPR signal (Fig. 1*b*). When CO was admitted to the same reoxidized sample, however, the rhombic Cu_B EPR signal appeared (Fig. 1*c*). These observations are in agreement with the results from the low-temperature kinetic study which suggested that the species exhibiting the rhombic Cu_B EPR signal was produced via a reaction of an EPR-silent intermediate with CO.

In a series of samples we attempted to correlate the yield of the rhombic Cu_B EPR signal with the initial level of reduction. When a half-reduced sample (Fig. 2*a*) was reoxidized and CO admitted, no rhombic Cu_B EPR signal was observed (Fig. 2*b*). Negative results were also obtained when the sample was initially 100% reduced (spectrum not shown). However, when an 80% reduced sample (Fig. 2*c*) was reoxidized and incubated with CO we observed the rhombic Cu_B EPR signal (Fig. 2*d*). The intensity corresponds to less than 10% of the total amount of Fe_a. These EPR results demonstrate that a subpopulation of the species with the rhombic Cu_B EPR signal is formed when CO is added to a reoxidized sample that had been initially reduced by >2 but <4 equivalents.

Optical—Although EPR spectroscopy has allowed us to monitor a paramagnetic product formed by a reaction between CO and the three-electron-reduced dioxygen intermediate, the method does not shed light on the nature of the intermediate, apart from its reactivity with CO, since this species is apparently EPR-silent. We have therefore carried out parallel optical experiments on the reoxidized cytochrome *c* oxidase samples to augment the EPR studies.

Figure 1

EPR spectra of partially reduced and reoxidized cytochrome *c* oxidase. A sample that was initially reduced by ca. 75-80 % (3.0-3.2 equiv) (*a*) and reoxidized with 1 atm of O_2 was incubated with 1 atm of argon, as a control, for 30-45 sec and then frozen to 77 K (*b*) and then with 1 atm of CO (*c*) for 30-45 sec at 298 K before refreezing. The *insets* beneath *b* and *c*, respectively, show the $g = 2.3$ region of the spectrum at increased power and gain. The *inset* to *b* verifies that no rhombic Cu_B EPR signal was produced as a result of freezing and thawing cycles. Conditions for obtaining EPR spectra were : temperature, 16 K; microwave power, 0.02 milliwatts (*a-c*), 0.2 milliwatts (*b*, *inset*), and 0.04 milliwatts (*c*, *inset*); gain, 3.2×10^4 (*a*), 8×10^3 (*b*), 2.5×10^4 (*b*, *inset*), 1×10^4 (*c*), and 3.2×10^4 (*c*, *inset*).

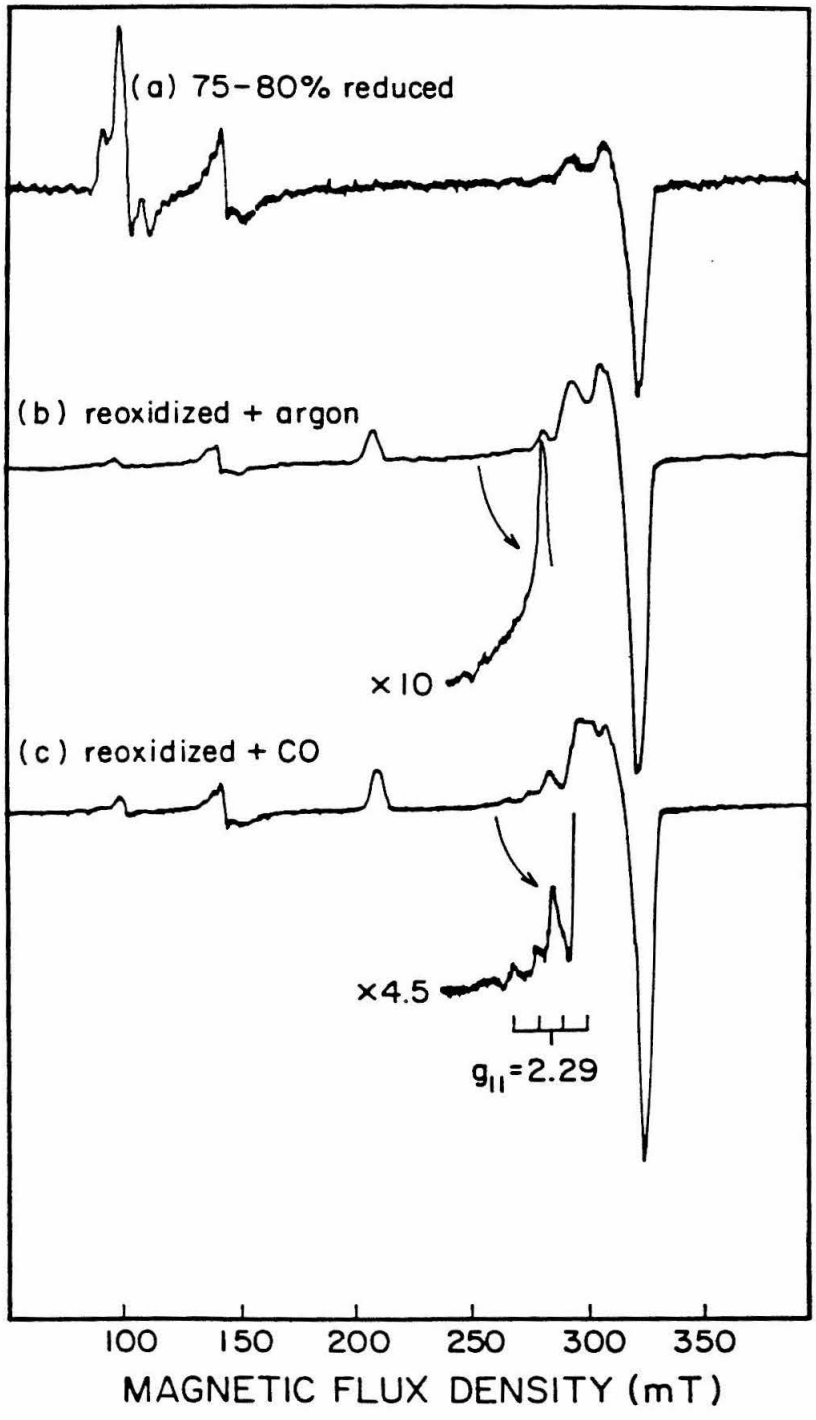
(a) 75-80% reduced
(b) reoxidized + argon
×10
(c) reoxidized + CO
×4.5
g_{11}=2.29
100
150
200
250
300
350
MAGNETIC FLUX DENSITY (mT)

Figure 2

EPR spectra of partially reduced and reoxidized cytochrome *c* oxidase. Samples that were initially reduced by 50 % (2 equiv) (*a*) and 80 % (3.2 equiv) (*c*) and reoxidized with 1 atm of O_2 were incubated with 1 atm of CO at 298 K (*b* and *d*) for 30-45 sec before freezing. The *inset* below Fig. 2*d* shows the $g = 2.3$ region of the spectrum at a ten-fold higher power and a two-fold higher gain. Conditions for obtaining EPR spectra were: temperature, 10-13 K; microwave power, 0.02 milliwatts (*a-d*) and 0.20 milliwatts (*d*, *inset*); gain, 1.6×10^4 (*a*), 1.0×10^4 (*b*), 4.0×10^4 (*c*), 2.0×10^4 (*d*), and 4×10^4 (*d*, *inset*).

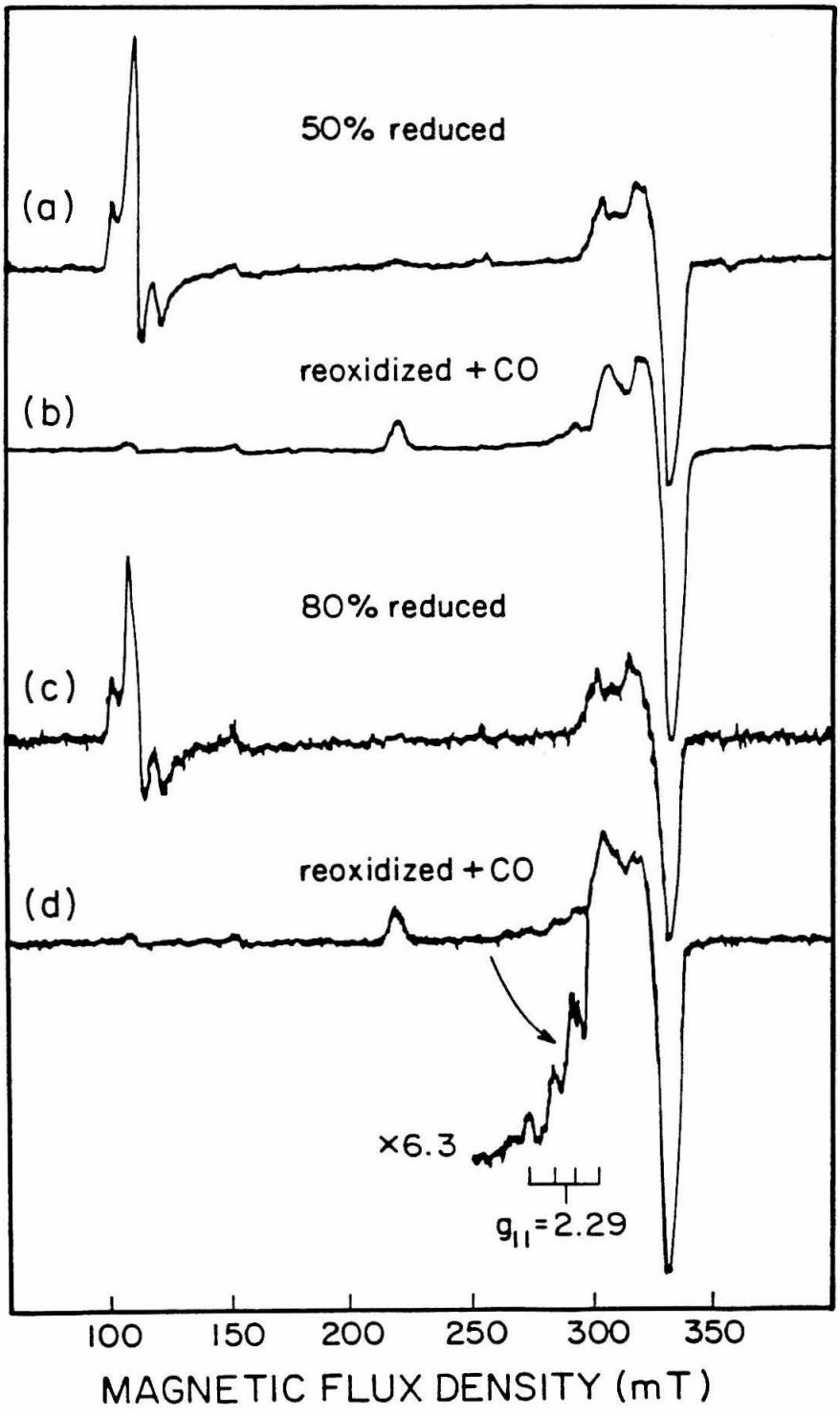
50% reduced
(a)
reoxidized + CO
(b)
80% reduced
(c)
reoxidized + CO
(d)
×6.3
g_{11}=2.29
100
150
200
250
300
350
MAGNETIC FLUX DENSITY (mT)

A difference spectrum (reoxidized-resting) for a reoxidized cytochrome *c* oxidase sample that was initially reduced between 35-45 % is shown in Figure 3*a*. The peak at 604 nm may be assigned to the peroxidic adduct at the dioxygen reduction site, namely, Compound C by reference to earlier work (12). Similarly, the corresponding difference spectrum for a reoxidized sample that was initially completely reduced is shown in Figure 3*b*. The peak at 601 nm in Figure 3*b* is characteristic of the pulsed enzyme; a similar spectrum for the pulsed enzyme has been reported by Armstrong *et al.* (13). However, when a sample that was initially 85 % reduced was reoxidized, the difference spectrum (Figure 3*c*) revealed a number of novel spectral features (580 and 537 nm) that were not assignable to the peroxide adduct or the pulsed enzyme. A broad trough centered at 668 nm was present in both the sample which was fully reduced and then reoxidized and the sample which was initially reduced by 85% and then reoxidized (Figs. 3*b* and 3*c*).

Assignments of the spectral features at 668, 580 and 537 nm has been aided by examining the reactivity of the sample toward CO. Addition of CO resulted (within minutes, the time taken to record the spectrum through the 500 nm region) in the loss of the peak at 580 nm and a diminution of intensity of the 537 nm peak and a concomitant shift to 545 nm (Fig. 3*d*). The observed shift in the Soret from 425 to 427 nm after the addition of CO also suggests a reaction involving Fe_{a_3}, possibly the reduction of Fe_{a_3} from the ferryl to the ferrous state. There was no noticeable change in position or intensity of the 668 nm trough when CO was added to the sample; thus, this feature, which was also observed in the pulsed species produced by oxidation of the fully reduced enzyme, is not due to the EPR-silent precursor species.

Concomitant with the loss of intensity of the 580 and 537 nm peaks, we also observed increased intensity at 605 nm upon the addition of CO, which we ascribe to formation of the peroxidic adduct at the dioxygen reduction site (Compound

Figure 3

Difference spectra (reoxidized-resting) for cytochrome *c* oxidase samples with varying initial levels of reduction. Difference spectra obtained after reoxidation of samples that were initially 35-45 % (*a*) and 100 % (*b*) reduced. The ***solid difference spectrum*** in *c* was obtained immediately after reoxidation of a sample that was initially ca. 85 % reduced. The ***dashed difference spectrum*** shown in *c* was obtained after 23 min of continued incubation at 277 K. When 1 atm of CO was admitted 28 min after reoxidation, the difference spectrum shown in *d* was obtained within 2-3 min (the earliest acquisition time). Spectra of the reoxidized samples were recorded within 2-3 min from the addition of O_2. Resting spectra were recorded before reduction of the samples.

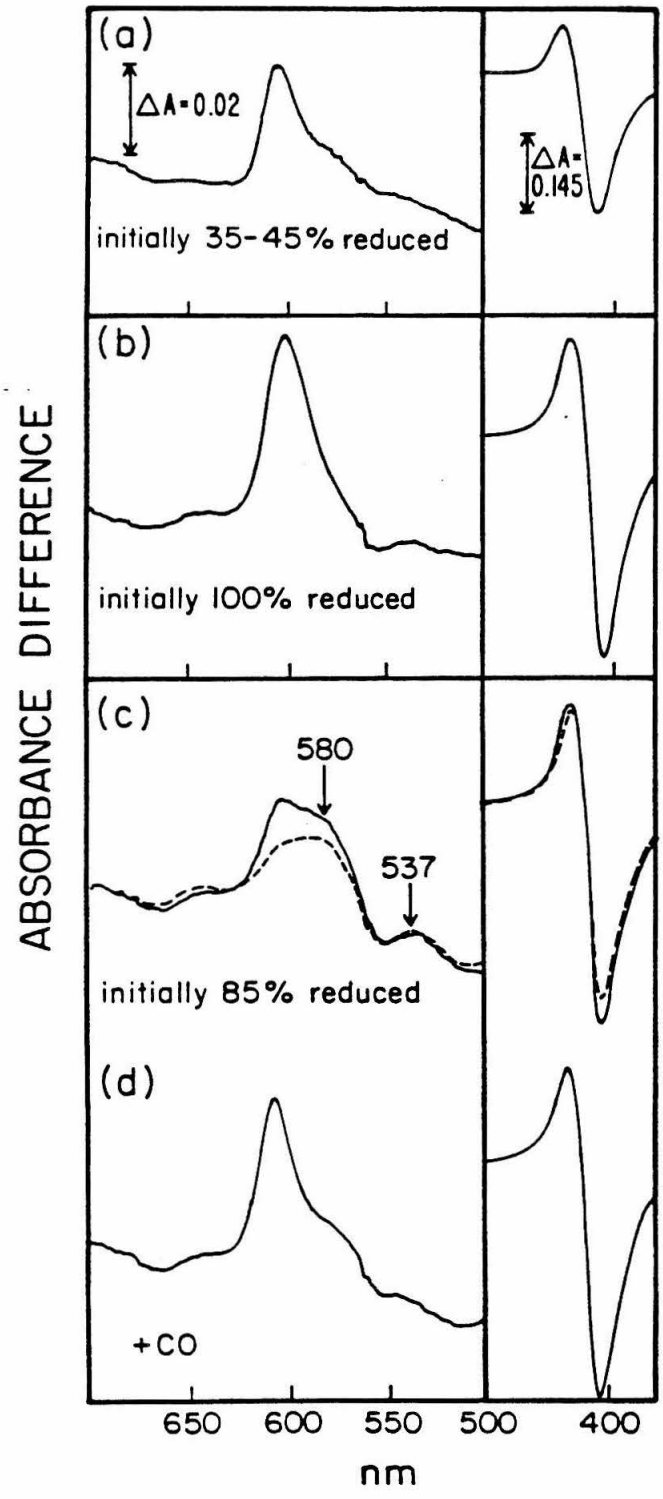
(a)
ΔA=0.02
ΔA=0.145
initially 35-45% reduced
(b)
initially 100% reduced
(c)
580
537
initially 85% reduced
(d)
+CO
ABSORBANCE DIFFERENCE
650
600
550
500
400
nm

C) (12). The latter species is expected when CO reacts, in the presence of dioxygen, with the pulsed subpopulation which is formed when fully reduced enzyme molecules are reoxidized (14). The ferrous Fe_{a_3}-L/cupric Cu_B species formed from the reaction of the three-electron-reduced dioxygen species with CO might also contribute to this intensity (4).

We have noted that the intermediate giving rise to the 580 and 537 nm peaks is quite stable in solution. On prolonged incubations the intermediate decayed to the resting state. However, the half-time for this decay varied considerably from sample to sample, ranging from minutes to hours. This variability in stability is not surprising considering the varying amounts of reducing contaminants and denatured enzyme present in different samples.

Reactions of Cytochrome *c* Oxidase with Hydrogen Peroxide

Formation of the 428/580 nm Species. We found that the 428/580 nm species is produced under a variety of experimental conditions. The conditions under which the 428/580 nm is formed and its spectral signatures are summarized as follows. (i) When excess H_2O_2 is added to the reoxidized cytochrome *c* oxidase (dithionite-reduced + O_2 + excess H_2O_2) and is followed after ca. 60 sec by the addition of a trace amount of catalase, a species is produced which exhibits a Soret maximum at 428-427 nm with two intense broad bands in the visible region of the absorption spectrum at 596-595 nm and ~535 nm, which we assign to the α and β bands, respectively. The position of the α band in the optical spectrum of the 428/580 nm species is unusually blue-shifted, relative to the optical spectrum of the resting state of cytochrome *c* oxidase (Fig. 4*a*). In the difference spectrum (reoxidized minus resting), prominent optical bands are observed in the reoxidized minus resting difference spectrum at 580-582 ($\Delta\epsilon_{580} \approx 5\ mM^{-1}\ cm^{-1}$) and 535-537 nm (Fig. 4*b*). Lastly, the charge transfer electronic transition in the near-infrared (~660 nm), observed in the optical absorption spectrum of the resting enzyme

(Fig. 4*a*), is absent in the spectrum of the 428/580 nm species (Fig. 4).

When the 428/580 nm species was examined by electron paramagnetic resonance (EPR) spectroscopy, the typical EPR signals from ferric Fe_a and cupric Cu_A were observed at their expected intensities (data not shown): no unusual EPR resonances attributed to either Fe_{a_3} or Cu_B were observed, even at 2 K. In the resting state of cytochrome *c* oxidase, an unusual EPR resonance is observed at $g' = 12$ (15). The EPR resonance has been suggested to arise from a transition between the magnetic sublevels of an excited spin state of an S = 2 state, formed as a result of a strong antiferromagnetic superexchange coupling between high-spin ferric Fe_{a_3} and cupric Cu_B (15-17). The $g' = 12$ transition is absent in the 428/580 nm state of the enzyme (data not shown). We also observed a radical EPR signal at $g = 2.0$ of variable intensity upon the treatment of the reduced enzyme with excess hydrogen peroxide (see Fig. 9*f*).

(ii) The same species is produced when excess H_2O_2 is added to stoichiometrically reduced (NADH) cytochrome *c* oxidase (followed by the addition of catalase after ca. 60-90 sec) (Figures 6 and 9) and when excess H_2O_2 is added to the peroxidic adduct (Compound C) (Fig. 5), as judged by the appearance of similar spectral features. If catalase is omitted, the 428/580 nm species is still produced. Catalase was employed in these studies to minimize the exposure to high concentrations of hydrogen peroxide, and because excess H_2O_2 in solution can obscure the detection of any reaction products of the 428/580 nm species with reductants (vide infra). Evidently the 428/580 nm species is also produced by the addition of ethyl hydrogen peroxide to the oxygenated state of the enzyme, as recently reported by Chance and co-workers (18).

We consistently observed an absorption maximum at 595-596 nm in the H_2O_2-treated cytochrome *c* oxidase, with prominent α and β bands at ~580 and ~537 nm, respectively, in the difference spectrum. The position of the Soret maximum and the the two bands at 580 and 537 nm agree well with published results, al-

Figure 4

Absorbance spectra of resting and the 428/580 nm form of cytochrome *c* oxidase (H_2O_2-treated). A sample of resting cytochrome *c* oxidase prior to the activation with H_2O_2 is shown in *a* (*dashed* trace). The absorbance spectrum of H_2O_2-treated cytochrome *c* oxidase (*solid* trace) was recorded 90 sec from the addition of H_2O_2. A difference spectrum is shown in *b* (H_2O_2-treated minus resting). Sample concentration was 50 μM. The sample was contained in a 2 mm path length, quartz precision cuvette. Conditions for obtaining the optical spectra were: temp., 277 K; scan speed, 2 nm/sec; bandwidth, 1.0 nm. The difference spectrum (*b*) was smoothed by averaging around an individual point with a window of 7 points. Spectra were corrected for dilution.

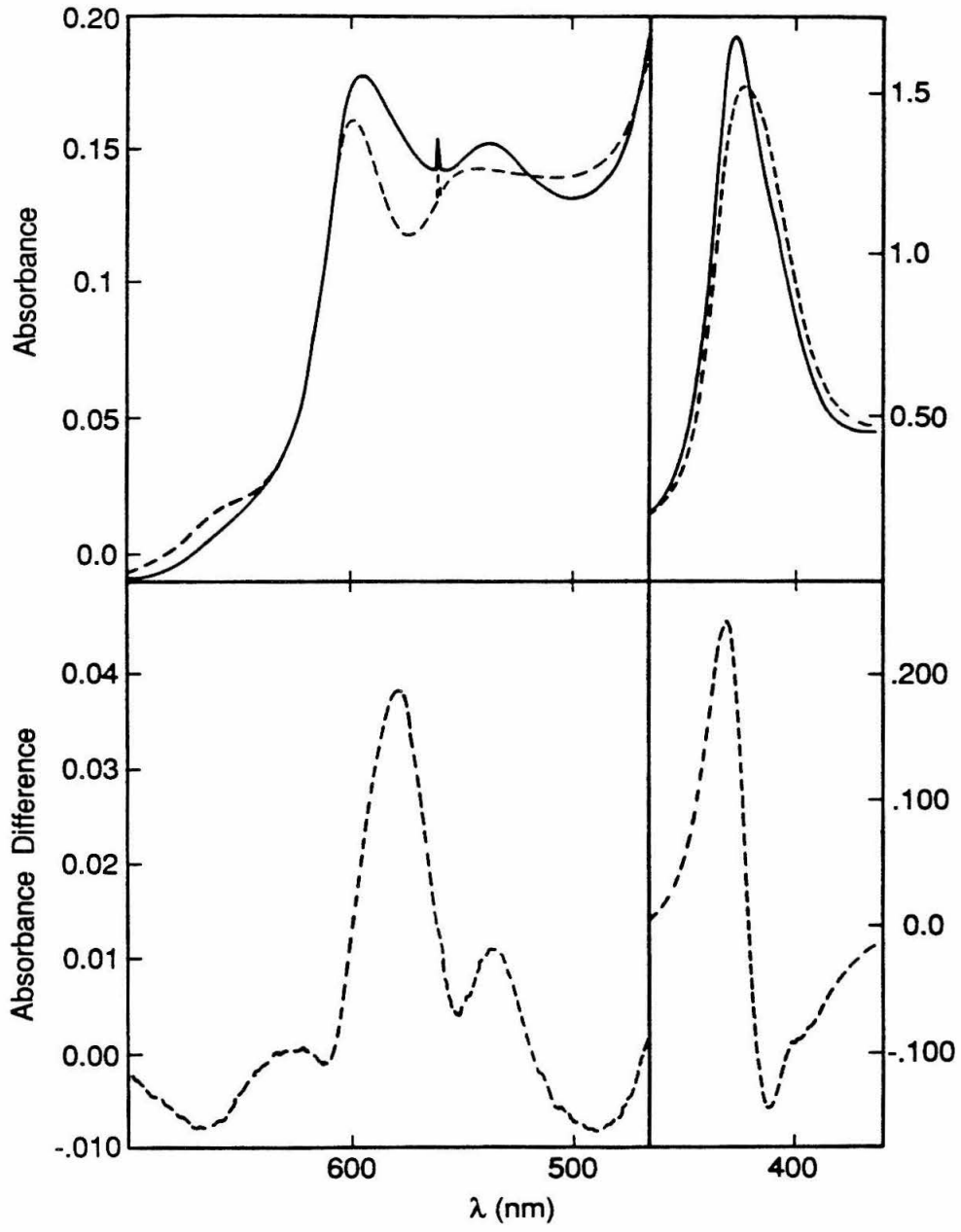
0.20
0.15
0.1
0.05
0.0
Absorbance
1.5
1.0
0.50
0.04
0.03
0.02
0.01
0.00
-.010
Absorbance Difference
.200
.100
0.0
-.100
600
500
400
λ (nm)

though the α maximum at 595-596 nm differs substantially from the value of 601 and 600 nm as reported by Wrigglesworth (19) and Kumar *et al.* (20), respectively. This discrepancy in the α region for samples prepared in this laboratory and in the laboratory of Chance and co-workers and others is most likely related to the incomplete formation of the 428/580 nm species. Incomplete formation of the 428/580 nm species might result when excess H_2O_2 is added to the resting state of the enzyme (19), since all of the molecules are probably not activated, and when excess H_2O_2 is added to the pulsed enzyme in the presence of catalase in the solution (20). In the latter case, due to the presence of catalase, the effective concentration of H_2O_2 is lower than expected; thus, the complete activation of all of the molecules may not be achieved. By reoxidizing fully reduced cytochrome *c* oxidase with excess H_2O_2, we ensure that all of the enzyme molecules are activated, and indeed, the difference spectrum in Fig. 4*b*, does not contain the component at ~606 nm which is found in the spectra reported by Kumar *et al.* and Wrigglesworth. Therefore, the α maximum of 595-596 nm reported herein is probably closer to the actual value for this state of the enzyme.

Bickar *et al.* (21) demonstrated that cytochrome *c* oxidase binds hydrogen peroxide reversibly ($K_d \sim 10^{-6}$ M^{-1}) at low concentrations of hydrogen peroxide. The peroxidic adduct, referred to as Compound C, has an intense absorption band at 607 nm in the reoxidized minus resting difference spectrum, with a less intense broad shoulder centered at approximately 570-580 nm. A similar, if not identical, species is produced upon the aeration of the mixed-valence CO-inhibited state of the enzyme (MV-CO) (Fe_a^{III}, Cu_A^{II}, $Fe_{a_3}^{II}$-CO, Cu_B^{I}) (14). Typically when we added low levels of hydrogen peroxide (50 μM) to the reoxidized enzyme, we observed a Soret maximum at 427-428 nm, with an α band at 600 nm (Fig.5*a*). In the difference spectrum (reoxidized minus resting), a band is observed at 605 nm, with two broad shoulders centered at ca.580 nm and 540 nm (Fig. 5*b*) in the difference spectrum. When the level of hydrogen peroxide is increased from

Figure 5

Absorbance spectra of cytochrome *c* oxidase in the presence of micromolar (50-150 μM) and millimolar (3.5 mM) levels of hydrogen peroxide. Hydrogen peroxide was added to the pulsed form of cytochrome *c* oxidase, the resultant optical spectra are shown in *a* and *b*: *solid* trace (50 μM); *dashed* trace (150 μM); and *dotted* trace (3.5 mM). Difference spectra are shown in *b* (pulsed plus H_2O_2 minus resting). Sample concentration was 55 μM. All spectra were corrected for dilution. Instrumental conditions are the same as in the legend to Figure 4.

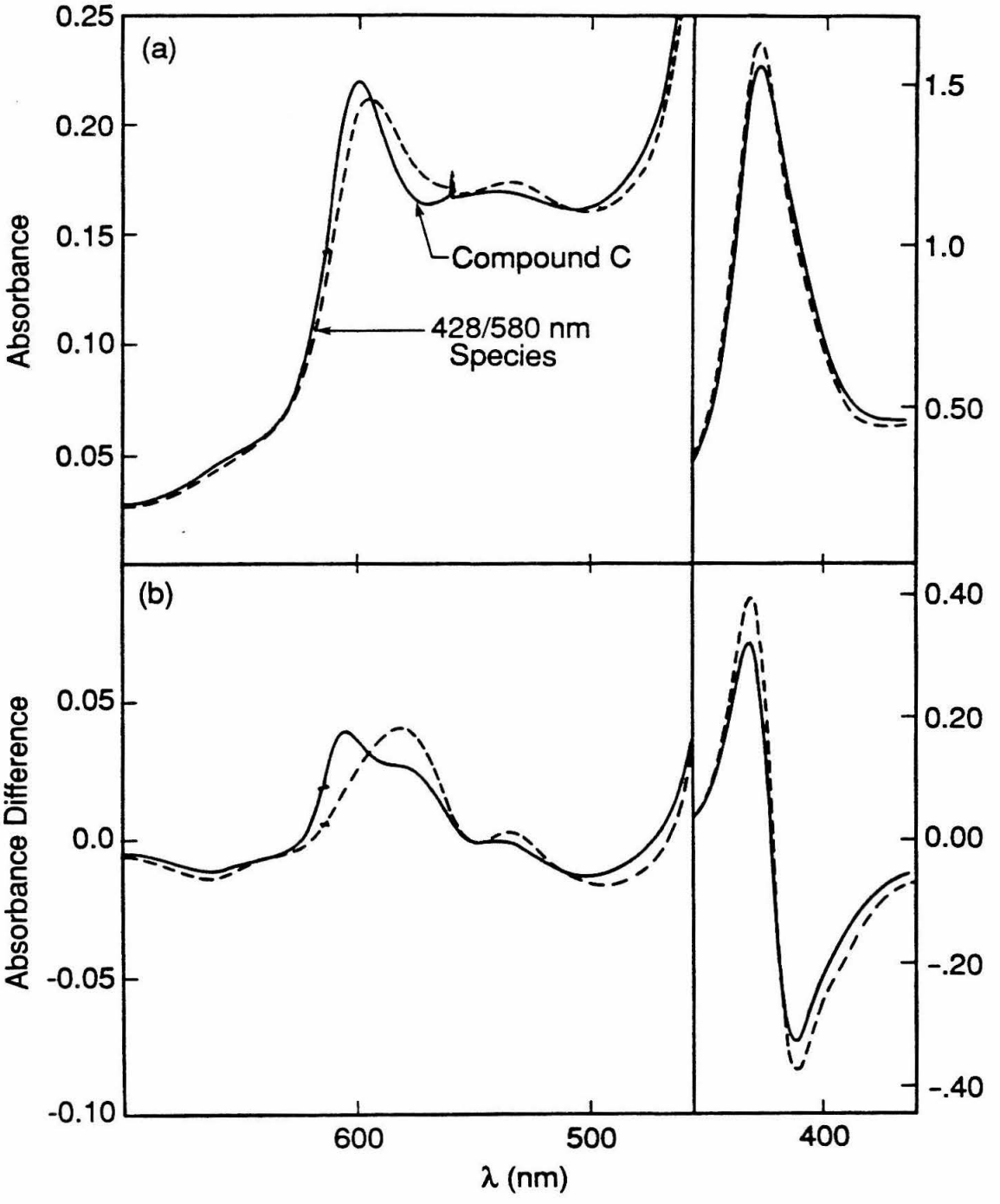
(a)
(b)
Compound C
428/580 nm
Species
Absorbance
Absorbance Difference
λ (nm)
0.25
0.20
0.15
0.10
0.05
1.5
1.0
0.50
0.40
0.20
0.00
-.20
-.40
0.05
0.0
-0.05
-0.10
600
500
400

50 to 150 μM, no significant changes were observed in either the positions or intensities of the α or Soret bands (data not shown). However, when excess H_2O_2 (ca. 4 mM) was added to the sample of the peroxidic adduct, several prominent spectral changes were observed. The α band shifted from 600 to 595-596 nm upon the addition of excess H_2O_2 (Fig. 5*a*), while the position of the Soret maximum remains nearly unchanged, at 428 nm. In the difference spectrum (Fig. 5*b*), the band at 605 nm decreased in intensity with a concomitant increase in the intensity of the band centered at 580 nm. Furthermore, the plateau centered at ca. 540 nm in the difference spectrum of the peroxidic adduct (Fig. 5*b*) also sharpens upon the addition of excess H_2O_2, revealing a more pronounced band centered at ca. 534 nm.

It is noteworthy that the spectral features at 580 and 537 nm which are produced upon the addition of excess H_2O_2 to (i) the oxygenated enzyme (Fig. 4), (ii) the peroxidic adduct, Compound C (Fig. 5) and (iii) to reduced cytochrome *c* oxidase (Figs. 5,9) are similar to the spectral features which formed upon reoxidation of partially reduced cytochrome *c* oxidase (Fig. 3*c*).

It is evident from the optical spectra in Figure 6 that the 428/580 nm species eventually converts to a species with spectral features that are characteristic of the resting state of cytochrome *c* oxidase. The optical spectrum of a sample of resting cytochrome *c* oxidase, prior to the reduction and activation to the 428/580 nm species, displays a Soret maximum at 420 nm, with an α band at 598 nm (Fig. 6*a*). When excess H_2O_2 was added to the reduced sample (spectrum not shown), the Soret and α maxima shifted to 428 and 596 nm, respectively (Fig. 6*b*). After the reoxidation of the reduced sample with excess H_2O_2, the sample was incubated for 28 hours at 273 K. The optical spectrum obtained after the 28 hour incubation period is similar, but not identical, to the optical spectrum of the initial resting state of the enzyme (Fig. 6*c*). The Soret maximum is observed at 417 nm, with the α band at 599 nm. An inspection of Figure 6 shows that although there are

Figure 6

Absorbance spectra of cytochrome *c* oxidase before and after the treatment with concentrated hydrogen peroxide. The optical spectrum of resting cytochrome *c* oxidase is shown in the *dotted* (*a*) trace. Following the reduction and reoxidation of the sample with excess H_2O_2 (3.5 mM), the optical spectrum of the 428/580 nm species was obtained (*b*, *solid* trace). A final optical spectrum was recorded after a 28 hour incubation period (*c*, *dashed* trace). Sample concentration was 54 μM. Spectra were corrected for dilution. Instrumental conditions same as in the legend to Figure 4.

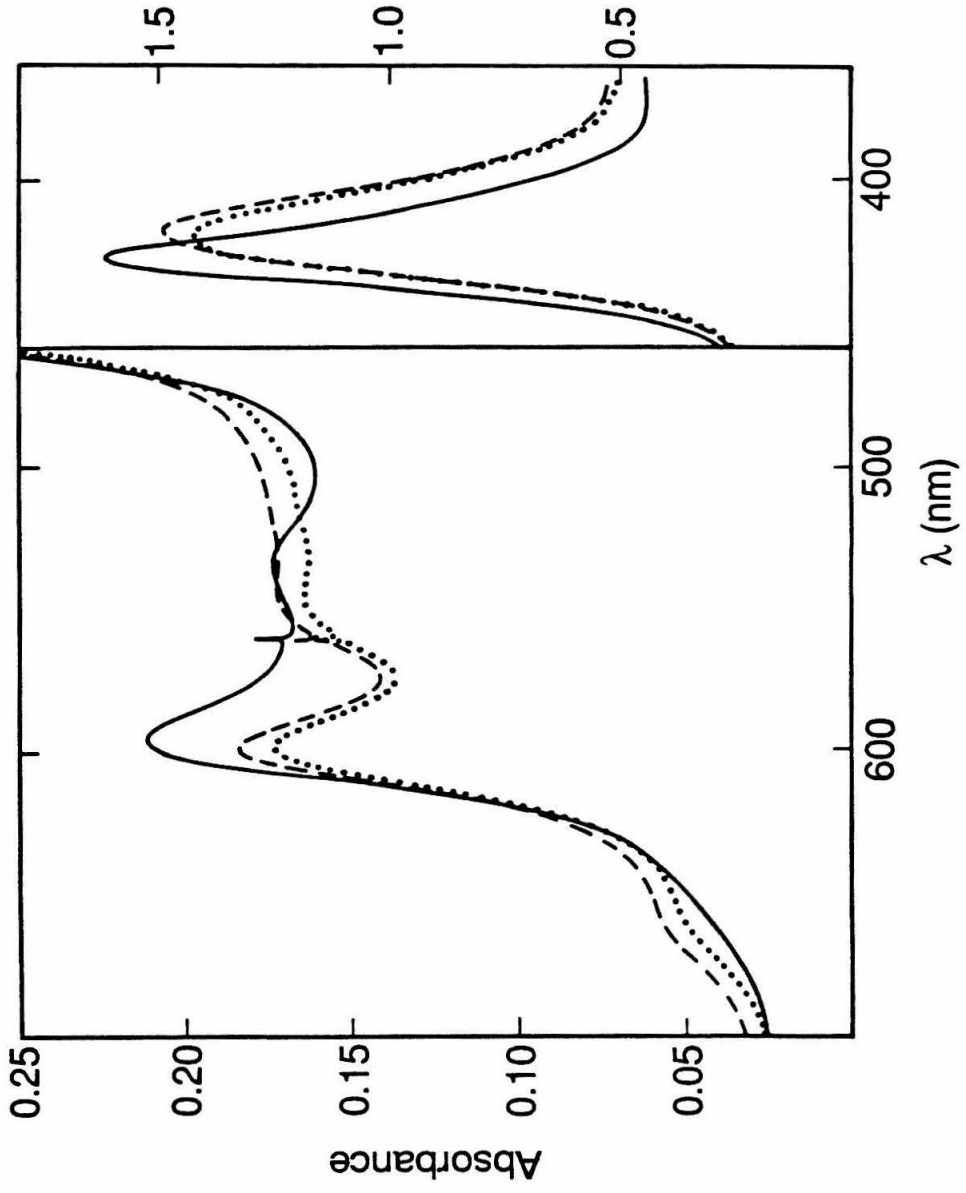
1.5
1.0
0.5
400
500
600
λ (nm)
0.25
0.20
0.15
0.10
0.05
Absorbance

differences in the positions and intensities of the initial and final optical spectra, the subtle spectral features which are observed in the initial resting spectrum at ~670 and 546 nm are regained after the 28 hour incubation period. The spectral features in the final optical spectrum are consistent with the conversion of the 428/580 nm species to the resting state of the enzyme.

It is noteworthy that the optical spectrum of the 428/580 nm species resembles the optical spectrum of the cyanide-inhibited enzyme ($Fe^{III}_{a_3}$-CN Cu^{II}_B) (Fig. 7). Both species exhibit a blue-shifted α-band relative to the resting enzyme, display prominent β bands at ca. 540 nm, and have a Soret maximum at 427-428 nm. Because of the similar spectral properties of the 428/580 nm species and the cyanide-inhibited enzyme, Ericińska (22) and later Wrigglesworth (19) concluded that the dioxygen reduction site in the H_2O_2-treated enzyme is composed of a low-spin hydroxy ferric Fe_{a_3} complex adjacent to cupric Cu_B ($Fe^{III}_{a_3}$-OH Cu^{II}_B). We consider it quite improbable that a homogeneous population of a low-spin hydroxy-ferric Fe_{a_3} adduct would be formed at pH 7.4. On the other hand, the spectral properties of the 428/580 nm species are also similar to the subpopulation of the EPR-silent, three-electron-reduced species that is trapped at the dioxygen reduction site when the partially reduced enzyme is reoxidized (see Fig. 3*c*). Therefore, to determine whether the 428/580 nm species contained a low-spin hydroxy ferric Fe_{a_3} or a ferryl Fe_{a_3}, the reactivity of the species with carbon monoxide was investigated. The reaction between the pulsed form of the enzyme, which is thought to be composed of an intermediate-spin ferric Fe_{a_3} adjacent to cupric Cu_B (23), and CO results in the formation of the EPR-silent, mixed-valence CO-inhibited form of the enzyme (24-26). Analogously, if the 428/580 nm species contains a low-spin hydroxy ferric Fe_{a_3}/cupric Cu_B binuclear dioxygen reduction site, a two-electron reduction by CO would result in an even spin intermediate at the dioxygen reduction site that is expected to be EPR-silent. In contrast, a two electron reduction of an odd electron intermediate, such as the proposed ferryl Fe_{a_3} adjacent to cupric

Figure 7

Absorbance spectra of 50 μM cyanide-inhibited and H_2O_2-treated cytochrome *c* oxidase. Optical spectra of the cyanide-inhibited enzyme (*dashed* trace) and the 428/580 nm form of the enzyme (*solid* trace) are shown in panel *a*. Difference spectra are shown in *b*: cyanide-inhibited cytochrome *c* oxidase minus resting (*b*, *dashed* trace) and H_2O_2-treated cytochrome *c* oxidase minus resting (*solid* trace). Same instrumental conditions as in the legend to Figure 4.

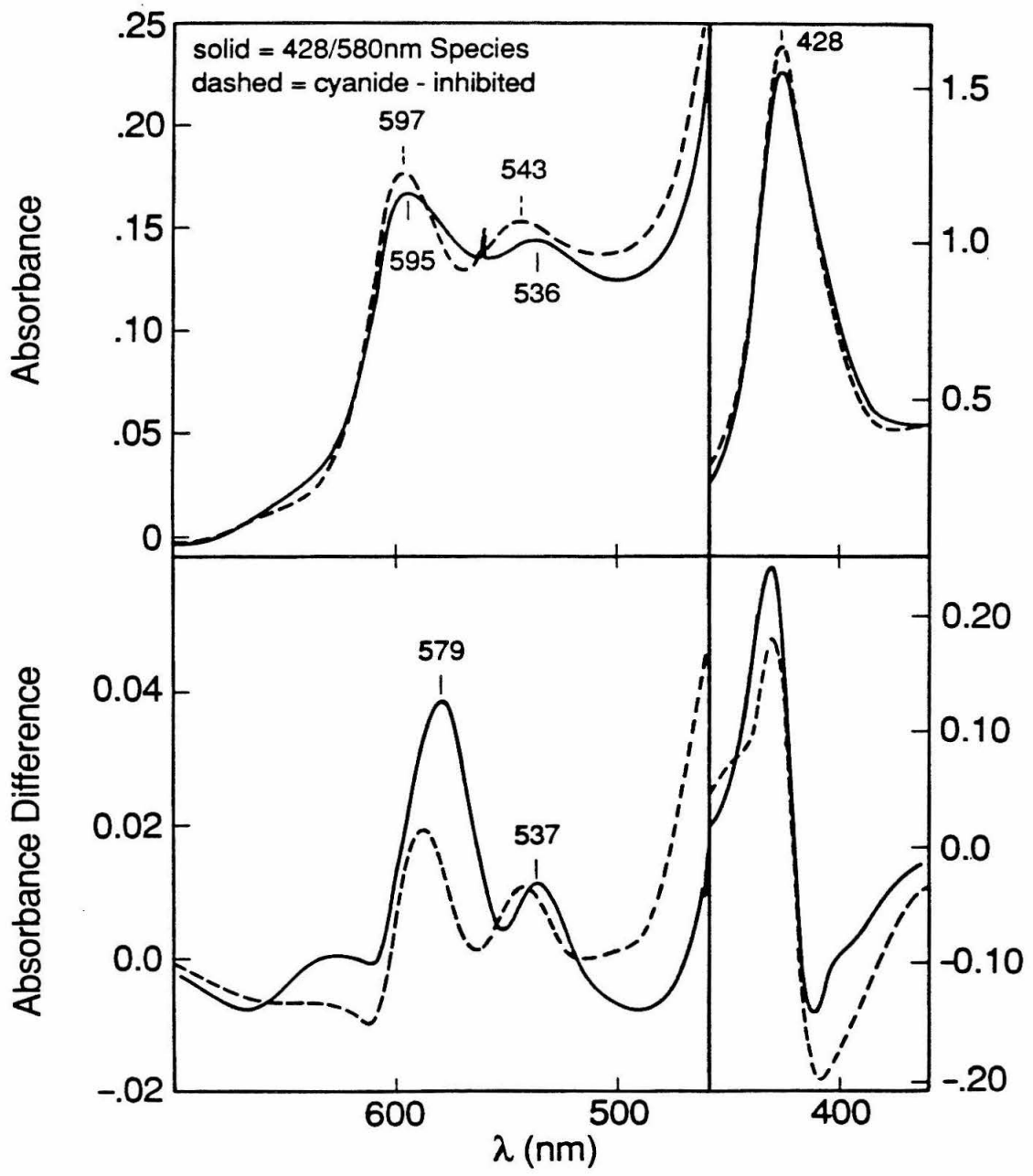
solid = 428/580nm Species
dashed = cyanide - inhibited
597
543
595
536
428
579
537
Absorbance
Absorbance Difference
λ (nm)
.25
.20
.15
.10
.05
0
1.5
1.0
0.5
0.04
0.02
0.0
-.02
0.20
0.10
0.0
-0.10
-.20
600
500
400

Cu_B, is expected to result in the formation of the rhombic Cu_B EPR signal, similar to the reaction observed at low temperatures (Chapter II).

Reaction of the 428/580 nm Species with CO. A sample of the 428/580 nm species was prepared by adding excess H_2O_2 to the oxygenated enzyme, followed by the addition of a trace amount of catalase after ca. 60 sec (Fig. 8). Upon the addition of carbon monoxide to the 428/580 nm species the Soret maximum shifted from 428 nm to ca. 425 nm, with a concomitant shift of the α band maximum from 595 nm to 601 nm (Fig. 8*a*). A difference spectrum (reoxidized minus resting) of the 428/580 nm species plus CO minus the 428/580 nm species reveals that the spectral features at 580 and 535 nm are abolished upon the addition of CO, with the formation of a new optical feature at ca. 607 nm (Fig. 8*b*). There was also an increase in the intensity at ~660 nm following the addition of CO. (The broad band centered at 660 nm is probably due to the pulsed enzyme (13).) For comparison purposes, one atmosphere of CO was admitted to the cyanide-inhibited enzyme. As expected, due to the tight binding of cyanide to ferric Fe_{a_3}, the addition of CO caused no significant spectral changes (data not shown). This result indicates that the 428/580 nm species undergoes a fairly rapid reaction with carbon monoxide to produce a subpopulation of the pulsed enzyme and another species which exhibits substantial intensity at 605-610 nm in the absorption difference spectrum (reoxidized minus resting).

Insights into the nature of the 428/580 nm species and the product of the reaction with carbon monoxide were derived from additional optical and parallel EPR experiments designed to monitor the reactivity of this species towards CO. An optical spectrum of the resting enzyme is shown in Fig. 9. After reoxidation of the reduced sample (spectrum not shown) with excess H_2O_2, the optical spectrum in Fig. 9*b* was obtained following the addition of catalase. Comparison of the optical spectrum of the resting enzyme sample (Fig. 9*a*) to the spectrum of the H_2O_2-treated enzyme sample (Fig. 9*b*) shows the chacteristic shift of the α band

Figure 8

Absorbance spectra of 50 μM H_2O_2-treated and H_2O_2-treated cytochrome *c* oxidase plus CO. The absorbance spectrum of the 428/580 nm species, recorded 90 sec after the addition of H_2O_2, is shown in panel *a* (*solid* trace). One atm of CO was then admitted to the H_2O_2-treated sample (ca. 7 min after the addition of H_2O_2), and an absorbance spectrum was obtained (7.5 min after the addition of H_2O_2) (*a*, *dashed* trace). A difference spectrum is shown in *b* (H_2O_2-treated cytochrome *c* oxidase plus CO minus H_2O_2-treated enzyme). Instrumental conditions were the same as in the legend to Figure 4.

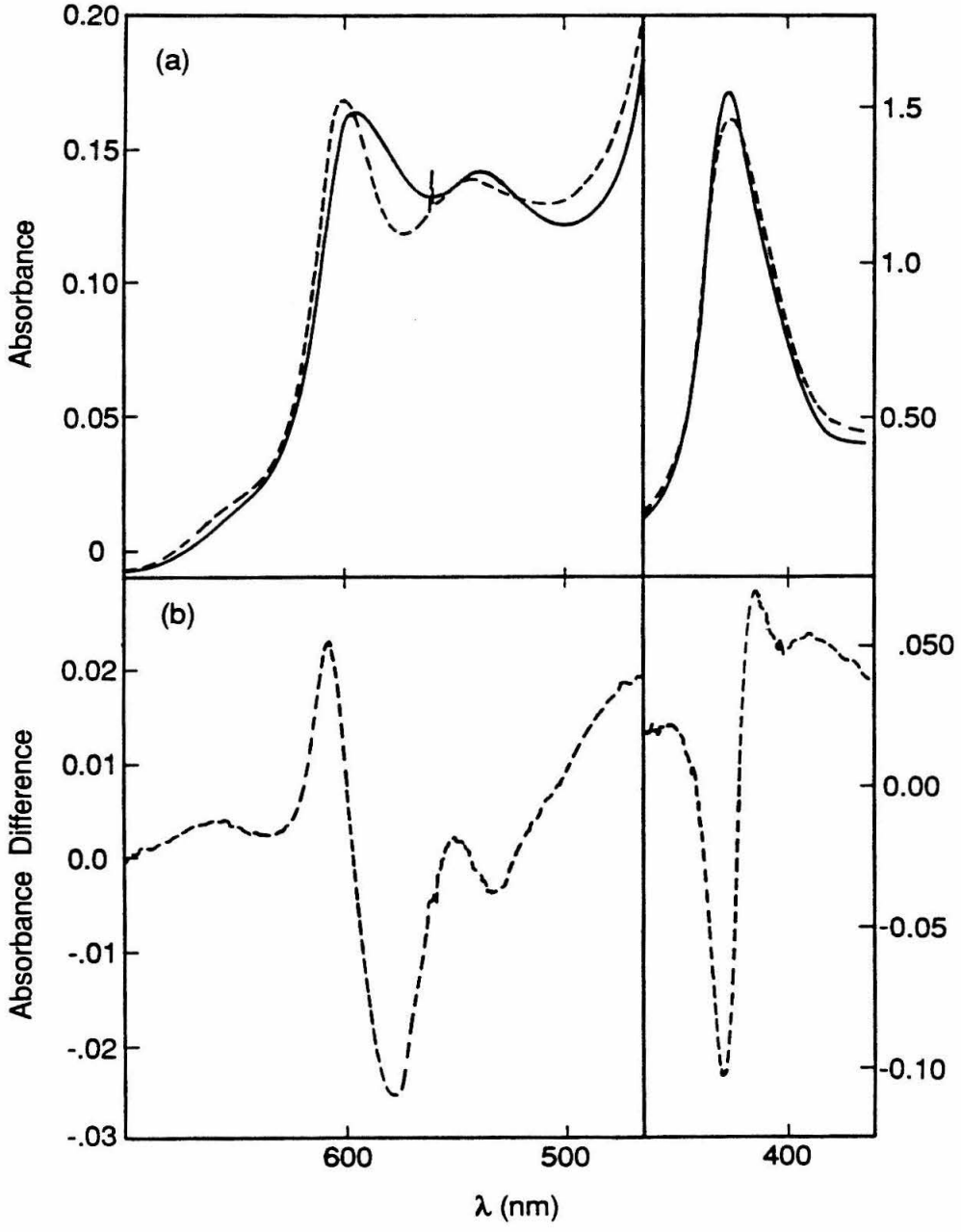
(a)
(b)
Absorbance
Absorbance Difference
0.20
0.15
0.10
0.05
0
1.5
1.0
0.50
0.02
0.01
0.0
-.01
-.02
-.03
.050
0.00
-0.05
-0.10
600
500
400
λ (nm)

from 600 nm to 596 nm and the corresponding shift of the β band from 547 to 534 nm, respectively. An optical spectrum was recorded within approximately 20 sec after the addition of CO to the 428/580 nm species (Fig. 9*d*) to verify that the reaction between the 428/580 nm species and CO had occurred. In fact, the difference spectrum in Fig. 9*e* shows that, upon the addition of CO to the reoxidized species, the 580/537 nm spectral features (Fig. 9*c*) are abolished and the band at 604 nm becomes more intense.

An EPR spectrum at 77 K after the reoxidation of the fully reduced sample with excess H_2O_2 (Fig. 9*h*) consists of the typical EPR spectrum of Cu_A (g_z = 2.18, g_y = 2.03, and g_x = 1.99), with a slight yield of a radical EPR signal at g = 2. The addition of CO to this sample resulted in the formation of the rhombic Cu_B EPR signal (g = 2.28, $A_{||}$ = 0.0106 cm^{-1}) (Fig. 9*g*). After recording the optical spectrum (Fig. 9*d*,*e*) the sample was immediately refrozen to 77 K and another EPR spectrum was recorded (Fig. 9*h*) to verify that the intermediate exhibiting the rhombic Cu_B EPR signal was present during the optical measurements. The EPR spectra in Figures 9*g* and *h* are a superposition of the EPR signals from Cu_A and Cu_B. A consequence of this superposition is that the positive component of the Cu_A EPR spectrum at g_y = 2.08 (Fig. 9*f*) is reduced in intensity because that region of the spectrum is dominated by the intense broad negative feature at g_x = 2.07 of the rhombic Cu_B EPR signal. After warming the sample to 277 K to obtain an optical spectrum, a decrease in the concentration of the species which gives rise to the rhombic Cu_B EPR signal is observed. Thus, the overall intensity of the rhombic Cu_B EPR signal is diminished, as evidenced by the decrease in intensity of the hyperfine lines, while the g = 2.08 component of Cu_A has become more prominent (Fig. 9*h*). The increased intensity in the α band upon the addition of CO with the simulataneous formation of the rhombic Cu_B EPR signal is consistent with a two-electron reduction of a ferryl Fe_{a_3}/cupric Cu_B couple to a low-spin ferrous-dioxygen (or possibly CO) Fe_{a_3}/cupric Cu_B couple.

Figure 9

Absorption and EPR spectra of the 428/580 nm species before and after the addition of CO. After the addition of CO to the H_2O_2-treated enzyme, the sample was flushed with dioxygen and then incubated at 277 K for 8 hours to obtain a resting spectrum (*a*). The reduced sample was reoxidized with a 24-fold molar excess of H_2O_2, followed in 105 sec by the addition of 0.1% catalase (*b* and *c*), and then frozen (360 sec from the addition of H_2O_2) to 77 K to record an EPR spectrum (*f*). The resultant reoxidized sample was incubated under 1 atm of CO for 20 sec, at approximately 283 K, and then refrozen to 77 K. After recording an EPR spectrum (*g*), the sample was thawed again to obtain the optical spectra in *d* and *e* and subsequently refrozen (620 sec from the addition of H_2O_2) to obtain a final EPR spectrum (*h*). The latter EPR spectrum verifies that the species exhibiting the rhombic Cu_B EPR signal was present during the optical measurement. The difference spectra (*c* and *e*) are the 428/580 nm species minus resting and the 428/580 nm species plus CO minus resting, respectively. Sample concentration was 146 μM. The samples were obtained in 3.4 mm (inner diameter) quartz EPR tubes. Conditions for obtaining EPR spectra were: temperature, 77 K; microwave power, 4 milliwatts; modulation amplitude, 10 Gauss; and gain, 1.25 x 10^4 (*f*-*h*).

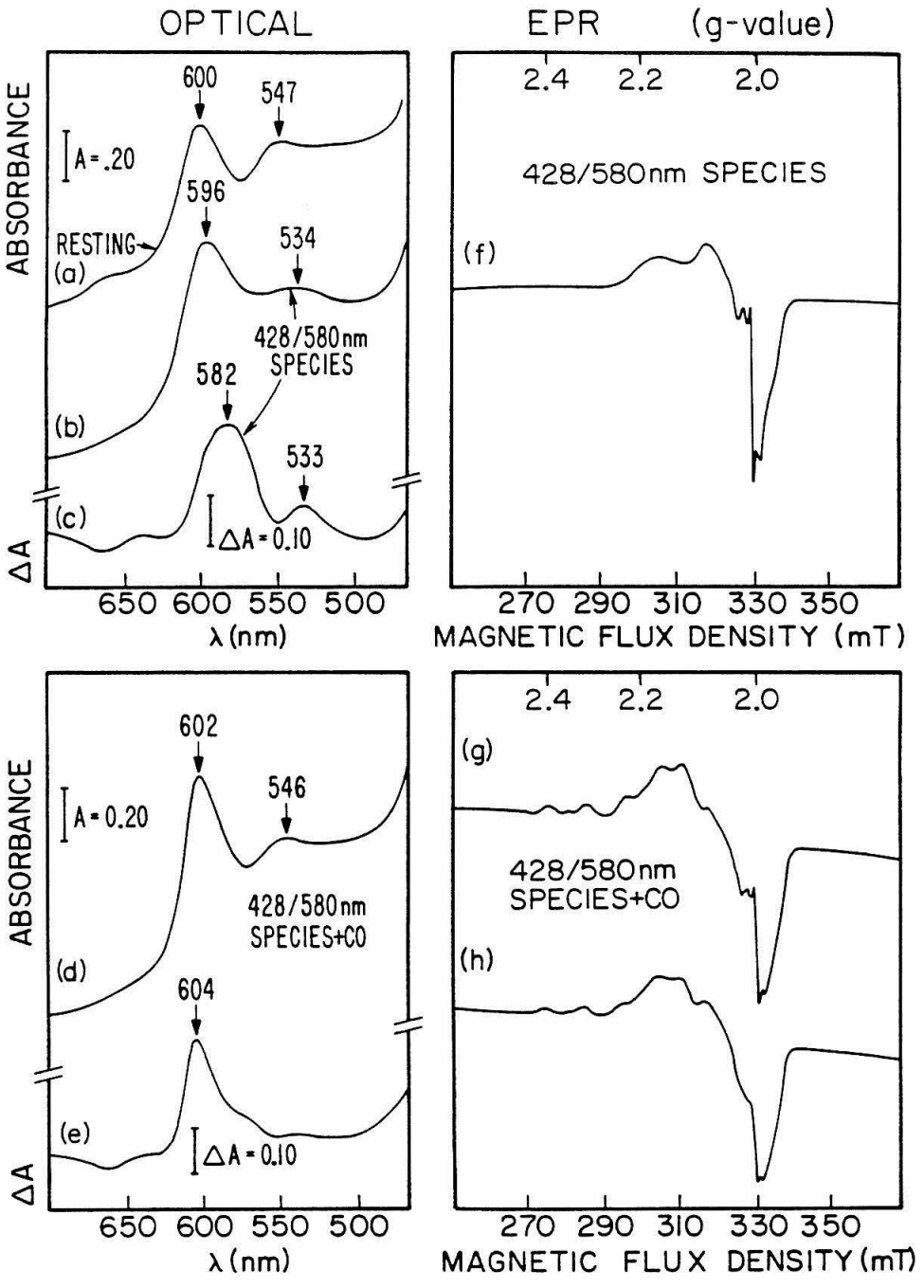
OPTICAL
EPR (g-value)
ABSORBANCE
600
547
A=.20
596
RESTING
(a)
534
428/580nm
SPECIES
582
(b)
533
(c)
ΔA=0.10
ΔA
650 600 550 500
λ(nm)
2.4 2.2 2.0
428/580nm SPECIES
(f)
270 290 310 330 350
MAGNETIC FLUX DENSITY (mT)
602
546
A=0.20
428/580nm
SPECIES+CO
(d)
604
(e)
ΔA=0.10
(g)
(h)
MAGNETIC FLUX DENSITY(mT)

Figure 10

The low-temperature EPR spectrum of the 428/580 nm species following the addition of 1 atm of CO. A sample of NADH-reduced cytochrome *c* oxidase was reoxidized with excess H_2O_2 (4 mM). A trace amount of catalase was added after a 54 sec incubation period in order to remove the excess H_2O_2 from solution. After recording an optical spectrum of the H_2O_2-treated sample (spectrum not shown), the sample was frozen to 77 K (277 sec from the addition of H_2O_2). While the sample was frozen, the EPR tube was evacuated and the atmosphere above the sample was replaced with 1 atm of CO. The sample was rapidly thawed, shaken and refrozen within 60 sec of thawing (337 sec from the addition of H_2O_2). Sample concentration was ca. 160 μM. The sample was contained in a 3.4 mm (inner diameter) quartz EPR tube. Conditions for obtaining the EPR spectrum were: temperature, 10 K; microwave power, 0.02 milliwatts; modulation amplitude, 16 Gauss; and gain, 1.25×10^4.

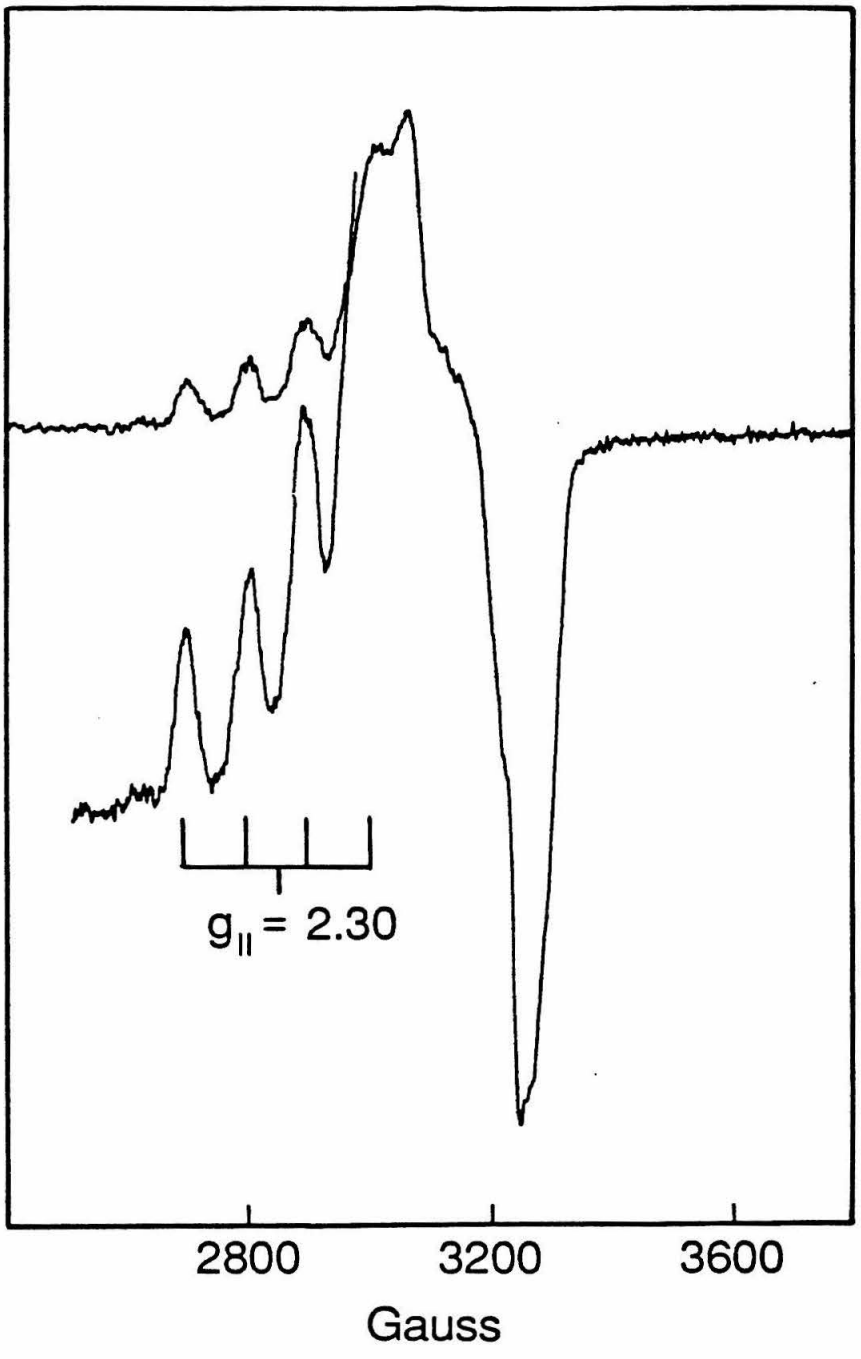
$g_{||}$ = 2.30
2800
3200
3600
Gauss

A low-temperature EPR spectrum of the rhombic Cu_B EPR signal is shown in Figure 10. We integrated the low-field hyperfine line of the rhombic Cu_B EPR signal in Figure 10, using the area under the $g_z = 3.03$ absorption peak of Fe_{a_3} as an internal standard. The integrated intensity of the rhombic Cu_B EPR signal corresponds to 0.6 spins per molecule of cytochrome *c* oxidase. Significantly, the rhombic Cu_B EPR signal which was produced upon the addition of CO to the 428/580 nm species is identical, within our experimental uncertainty, to the rhombic Cu_B EPR signal which was produced in the low temperature kinetic study (see Fig. 8, Chap. II).*

Additional experiments were conducted to investigate the role of catalase on the production of the rhombic Cu_B EPR signal. A reduced cytochome *c* oxidase sample was reoxidized with excess H_2O_2, but catalase was not added after the 100 sec incubation period in order to quench the the excess hydrogen peroxide. Carbon monoxide (1 atm) was admitted to the sample, and the sample was then rapidly frozen to 77 K for examination by EPR. In the absence of nanomolar amounts of catalase, the yield of the rhombic Cu_B EPR signal was negligible (Fig. 11*b*) in comparison to the yield when catalase was employed (Fig. 11*a*). In an independent optical experiment, the H_2O_2-treated enzyme, in which catalase was not added after the 100 sec incubation with H_2O_2, exhibited the spectral features at 428 and 580 nm in the optical absorption spectrum. Thus, the negligible yield of the rhombic Cu_B signal must be related to the presence of excess hydrogen peroxide in solution. The species which is thought to give rise to the rhombic Cu_B EPR signal ($Fe^{II}_{a_3}$-L Cu^{II}_B, where L = O_2 or possibly CO) is probably rather

* We believe that the rhombic Cu_B EPR signal that was produced in the low temperature experiments (Chap. II) ($A_{||} = 105$ Gauss, with $g_z = 2.32$) is identical to the rhombic Cu_B EPR signal that was produced when CO was added to the 428/580 nm species ($A_{||} = 105$ Gauss, $g_z = 2.28$). The g_z values from the two experiments agree within experimental uncertainty ($\Delta g = \pm 0.02$).

Figure 11

EPR spectra of H_2O_2-treated cytochrome *c* oxidase in the presence or absence of trace amounts of catalase. A fully reduced cytochrome *c* oxidase sample was reoxidized with excess H_2O_2 (4mM), and was followed by the addition of a trace amount of catalase after 100 sec of reaction time. The sample was then rapidly frozen to 77 K and the atmosphere above the sample was replaced with one atmosphere of CO. The sample was thawed, shaken, and refrozen to 77 K within 45 sec. The EPR spectrum at 77 K is shown in Fig. 5*a*. A companion sample was treated identically as described above except that catalase was not added to quench the excess H_2O_2. The EPR spectrum following the addition of one atm of CO is shown in Fig. 5*b*. A sample of resting enzyme was incubated with excess H_2O_2 for 100 sec and then the excess H_2O_2 was quenched by the addition of catalase. One atm of CO was added to the H_2O_2-treated resting enzyme, and the EPR spectrum at 77 K was obtained (*c*). Conditions for obtaining the EPR spectra were: temperature, 77 K; modulation amplitude, 10 Gauss; power, 4 milliwatts; frequency, 9.278 GHz; gain, 1.25 x 10^4 (*a*), 1 x 10^4 (*b*-*c*).

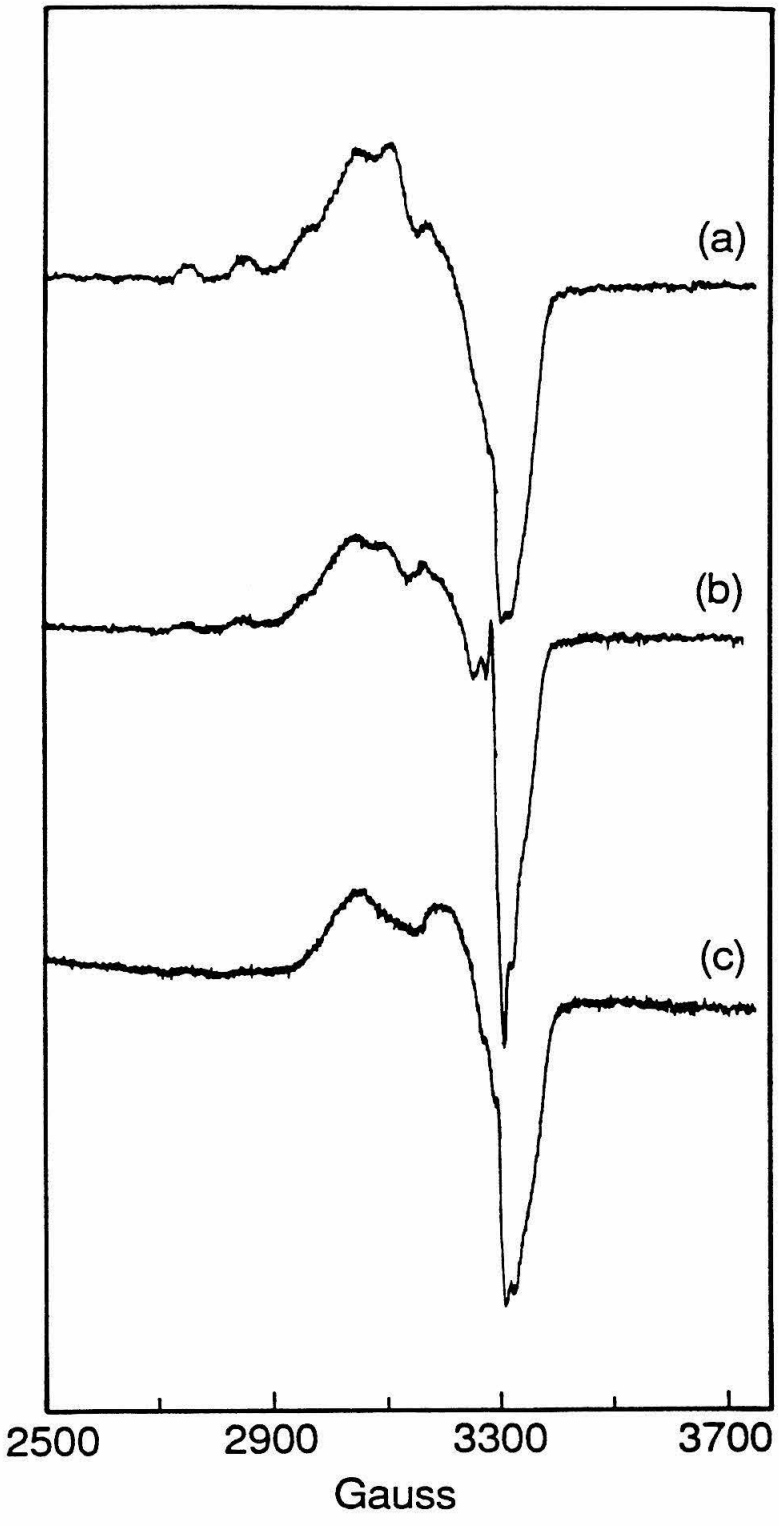
(a)
(b)
(c)
2500
2900
3300
3700
Gauss

susceptible to oxidation by H_2O_2, which would result in diminished yields of the species when catalase was not employed.

When the resting enzyme was briefly (~60 sec) exposed to millimolar levels of hydrogen peroxide, the 428/580 nm species was not produced in sizeable yields as judged by comparison of the optical difference spectrum of the H_2O_2-treated resting sample to the optical difference spectrum of a sample that was initially reduced and then treated with excess H_2O_2 (data not shown). Furthermore, no rhombic Cu_B signal was produced upon the addition of 1 atmosphere of CO (Fig. 11*c*). These results are consistent with the experiments of Wrigglesworth (19), who found that only long incubation times with excess hydrogen peroxide resulted in the formation of the 428/580 nm species.

Reductive Titration of the 428/580 nm Species

The reactivity of the 428/580 nm species with carbon monoxide suggests that the species contains an EPR-silent ferryl Fe_{a_3}/cupric Cu_B binuclear dixoygen reduction site, or another species at the same formal level of reduction. If this hypothesis is correct, a substantial population of the pulsed enzyme should be produced upon the addition of an equivalent of reductant to the 428/580 nm species, and since the pulsed enzyme has distinct spectral features its formation may be conveniently monitored. Therefore, in order to test the hypothesis that the 428/580 nm species contains one more oxidizing equivalent than the resting enzyme, a reductive titration was conducted under aerobic conditions. The titration was monitored by optical and EPR spectroscopies.

Optical—The reductive titration of the 428/580 nm species consisted of three related experiments: (1) To determine the spectral changes which result in the *absence* of added reducing equivalents, the 428/580 nm species was incubated at ice temperature and optical spectra were periodically recorded over a 34 min interval; (ii) In a parallel experiment, NADH was sequentially added to a sample of the 428/580 nm species, and optical spectra were recorded over approximately 30

min; (iii) to rule out the possibility that the binding of cytochrome *c* (or NAD^+) accelerated the decay of the 428/580 nm species, aliquots of NAD^+ (plus PMS) were added to a sample of the 428/580 nm species. In all cases, the 428/580 nm species was prepared by reoxidizing stoichiometrically reduced (NADH) cytochrome *c* oxidase with excess H_2O_2, followed by the addition of catalase. The typical population of the 428/580 nm species was estimated as ~70-80 %, based on the absorbance at 580 nm (ϵ_{580}~5 mM^{-1} cm^{-1}) in the difference spectrum (reoxidized minus resting). With regard to the absorption difference spectra in Figures 12-14*b*, typically, the first optical spectrum of the 428/580 nm species, which was recorded immediately after the treatment with excess H_2O_2 and reflects the largest population of the 428/580 nm species, was *subtracted* from the successive optical spectra which were recorded at later time points. Therefore, the difference spectra may be represented at (H_2O_2-treated(t) minus H_2O_2-treated(t_o)), where t_o is the time at which the first optical spectrum of the 428/580 nm species was recorded.

(i) The optical spectrum of the 428/580 nm species, recorded immediately after the addition of catalase, is shown in Figure 12. After a 34 min incubation at ice temperature, the Soret and α bands shifted from 428 and 596 nm to 427 and 597 nm, respectively (Fig. 12*a*). There is also an increase in the intensity of the near-infrared band centered at ~660 nm after the 34 min incubation period. The optical difference spectra (H_2O_2-treated(t) minus H_2O_2-treated(*initial*)) reveal the spectral changes which occurred during the incubation period (Fig. 12*b*). Upon incubation at ice temperature, there is a gradual increase in the intensity of the negative features at 580 and ~537 nm ($t_{1/2}$~60 min), with a parallel increase in the intensity of the broad positive feature at 660 nm. Similarly, in the Soret region of the difference spectrum (Fig. 12b), we see a gradual increase in the intensity of the sharp negative feature at 430 nm, with a parallel increase in the intensity of the positive feature in the difference spectrum at ca. 414 nm. These spectral changes are consistent with the conversion of the 428/580 nm species,

Figure 12

Absorbance spectra of the 428/580 nm species upon incubation at 273 K. Absorbance spectra were recorded 250 sec (*a*, *solid line*) and 34 min (*a*, *dashed line*) from the addition of H_2O_2. Difference spectra (H_2O_2-treated(t) minus H_2O_2-treated(250 sec)) are shown in *b*: t = 585 sec (*solid line*), 1320 sec (*dashed line*), and 2040 sec (*dotted line*). Sample concentration was ca. 55 μM. All spectra were corrected for dilution. Same instrumental conditions as those described in the legend to Figure 4.

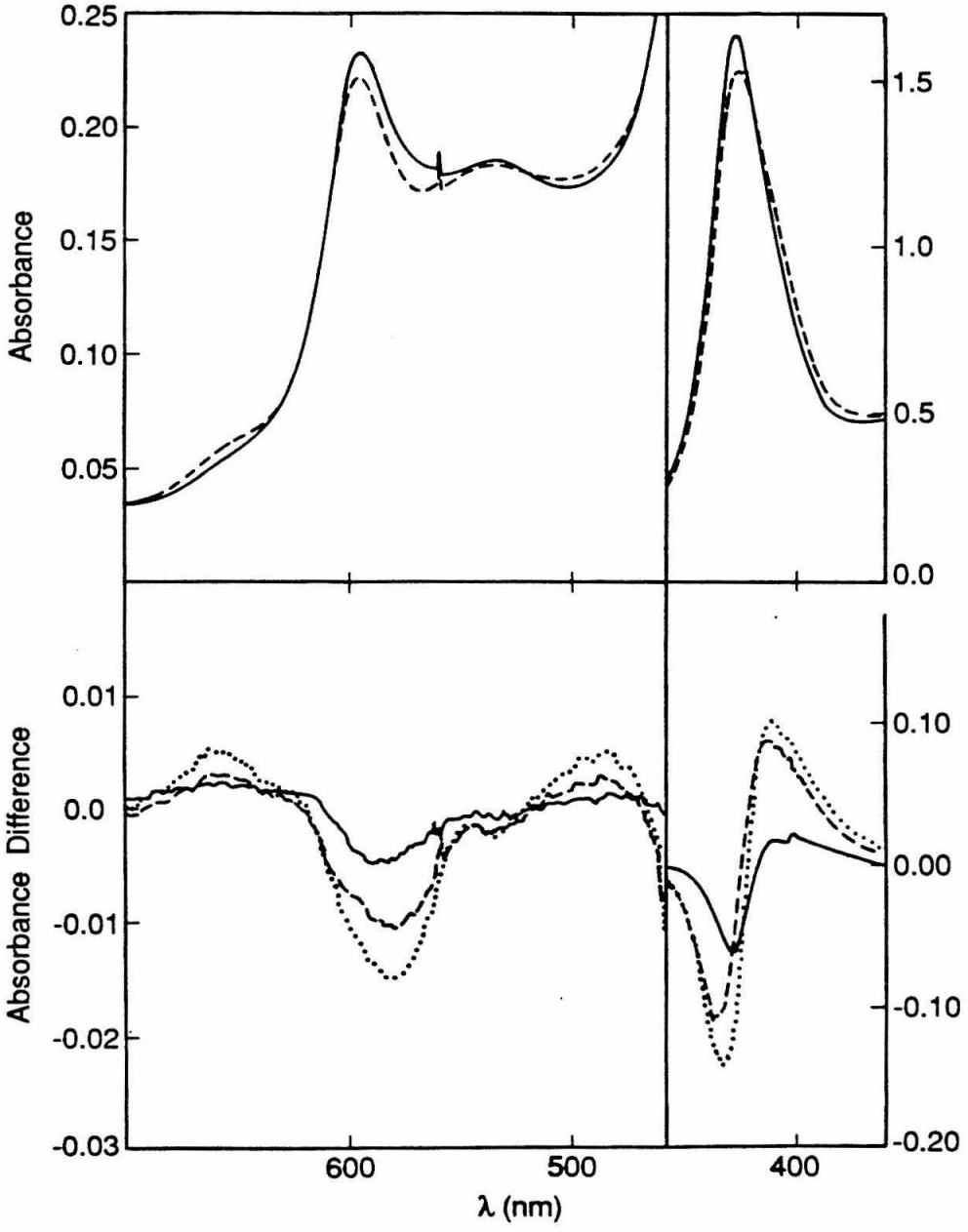
0.25
0.20
0.15
0.10
0.05
Absorbance
1.5
1.0
0.5
0.0
0.01
0.0
-0.01
-0.02
-0.03
Absorbance Difference
0.10
0.00
-0.10
-0.20
600
500
400
λ (nm)

which displays spectral signatures in the difference spectrum at 580, 537, and 430 nm (the 428/580 nm species), to an intermediate with spectral features at 660, possibly 480, and 414 nm upon incubation of the 428/580 nm form of the enzyme at ice temperature. By reference to earlier work (7), these optical changes which take place over the course of the incubation period are consistent with the conversion of a low-spin species (the 428/580 nm species) to a high-spin (or possibly intermediate-spin) species.

(ii) When 1 equiv (1.0 e^-)/oxidase molecule) of NADH was added to the 428/580 nm species, the Soret maximum shifted from 428 to 427 nm, the α band shifted from 596-597 to ca. 598 nm (Fig. 13*a*), and a weak band formed in the near infrared region of the spectrum at ~660 nm. An examination of the visible region of the optical difference spectra (Fig. 13*b*) shows that the addition of reductant to the 428/580 nm form of the enzyme caused an increase in the intensities of the negative features at 580 and 537 nm, with a corresponding increase in the intensity of the broad positive band in the difference spectrum at ~660 nm. Relative to the reference difference spectra shown in Figure 12*b*, the addition of 1 equiv of NADH (Fig, 13*b*, dotted trace) caused an approximate two-fold increase in the intensity of the two negative peaks at 580 and ~537 nm, with a parallel ~two-fold increase in the intensity of the broad positive band in the near-infrared (660 nm), which is due to the pulsed enzyme (13). In the Soret region of the optical difference spectra (Fig. 13*b*), similar changes are observed as those seen in the difference spectra of Figure 12*b*; however, the magnitudes of the changes are greater by a factor of ca. 1.3-2.0. In the difference spectrum in Figure 13*b*, a sharp band is observed at ~605-610 nm. This band may arise from either the peroxidic adduct, Compound C (12,21), or from the species which is thought to give rise to the rhombic Cu_B EPR signal, i.e., $Fe^{II}_{a_3}$-O_2 Cu^{II}_B (4). The reductive titration shows that the conversion to the pulsed form of cytochrome *c* oxidase is accelerated by the addition of reducing equivalents.

Figure 13

Absorbance spectra of the 428/580 nm species before and after the addition of NADH. The optical spectrum of the 428/580 nm species was obtained 256 s from the addition of H_2O_2 (*a*, *solid* trace). Following the addition of 1 equiv of NADH, the *dashed* optical spectrum was obtained (950 sec from the addition of H_2O_2). In total, 4 equiv of NADH were added incrementally to the 428/580 nm species over a period of 40 min from the initial reoxidation (t) with H_2O_2. The first, second, third, and fourth equivalents were added at 950, 1655, 2035, and 2390 sec from the reoxidation with H_2O_2. Difference spectra (H_2O_2-treated(t) minus H_2O_2-treated(256 sec)) are shown in *b*, where, t = 950 sec (*solid* trace), 1655 sec (*dashed* trace), and 2390 sec (*dotted* trace). Sample concentration was ca. 55 μM. All spectra were corrected for dilution. Same instrumental conditions as those described in the legend to Figure 4.

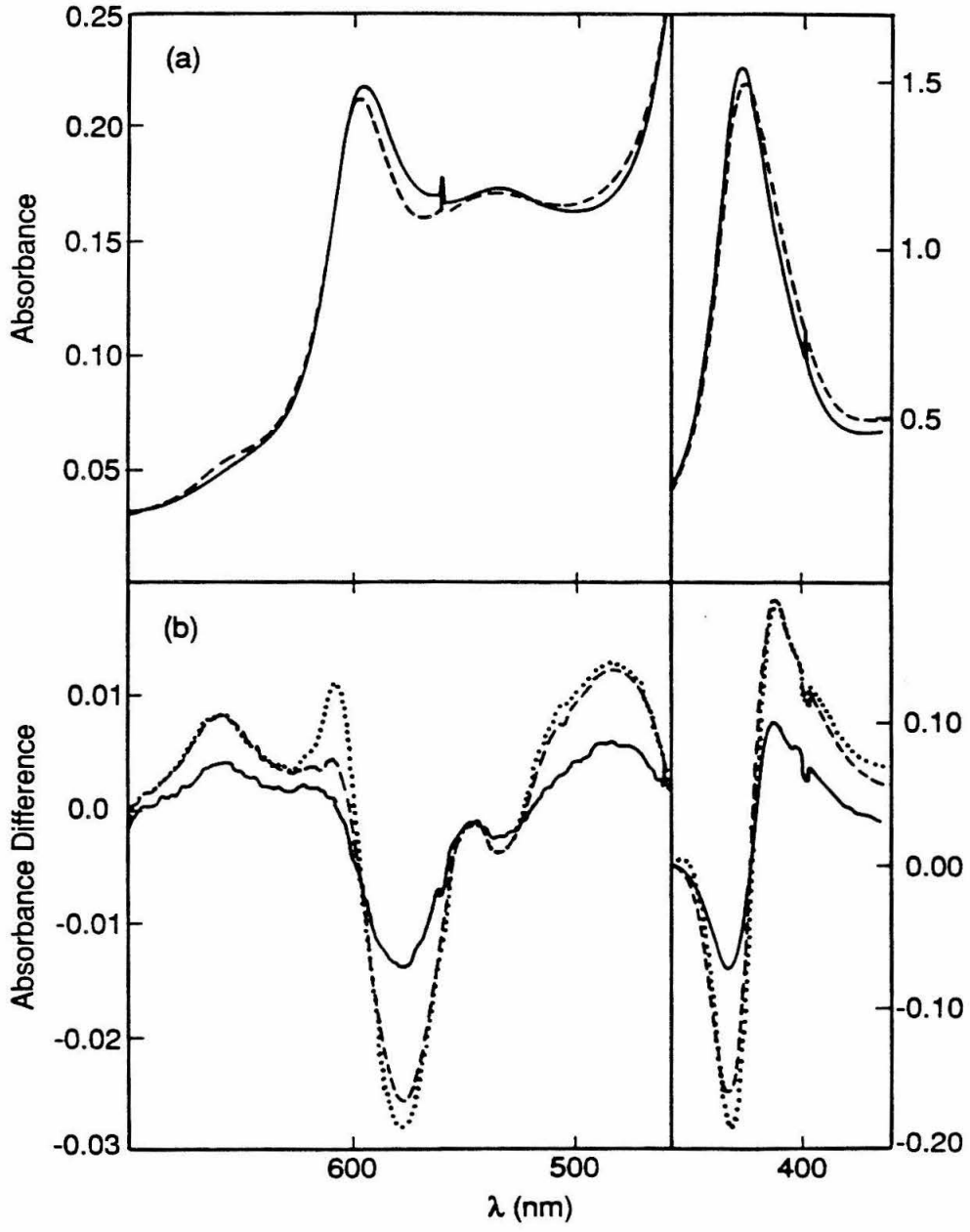
(a)
(b)
Absorbance
Absorbance Difference
λ (nm)
0.25
0.20
0.15
0.10
0.05
1.5
1.0
0.5
0.01
0.0
-0.01
-0.02
-0.03
0.10
0.00
-0.10
-0.20
600
500
400

Figure 14

Absorbance spectra of the 428/580 nm species before and after the addition of NAD^+. The optical spectrum of the 428/580 nm species was obtained 240 sec after the addition of the H_2O_2 (*a*, *solid line*). Following the addition of 1 equiv of NAD^+, the *dashed* optical spectrum was obtained (935 sec from the addition of H_2O_2). In total, 4 equiv of NAD^+ were added incrementally to the 428/580 nm species over a period of ca. 34 min from the initial reoxidation (t) with H_2O_2. The first, second, third, and fourth equivalents were added at 935, 1293, 1632, and 2005 sec from the reoxidation with H_2O_2. Difference spectra are shown in *b* (H_2O_2-treated(t) minus H_2O_2-treated(240 sec)): t = 935 sec (*solid* trace); t = 1632 sec (*dashed* trace); and t = 2005 sec (*dotted* trace). Sample concentration was ca. 55 μM. All spectra were corrected for dilution. Same instrumental conditions as those described in the legend to Figure 4.

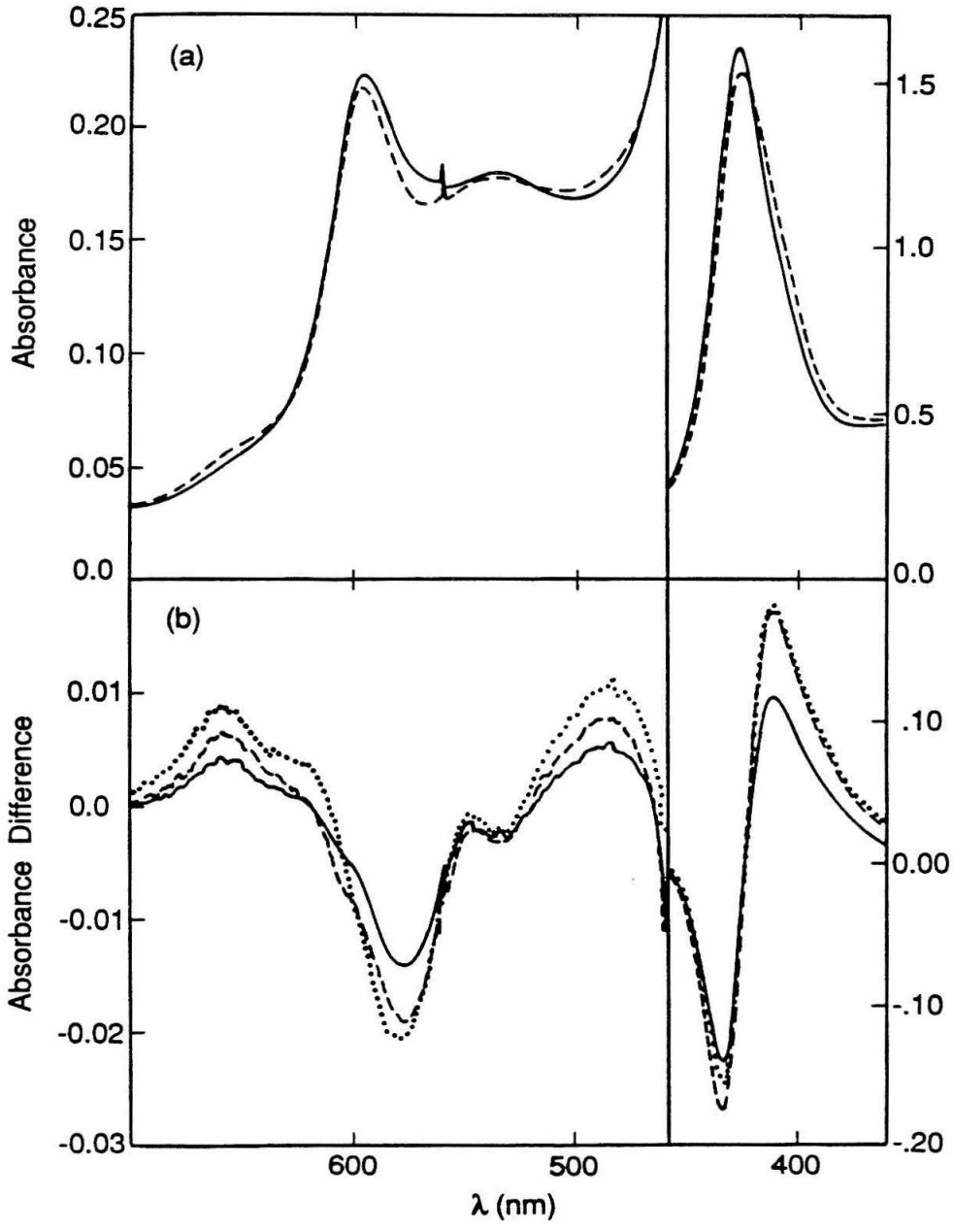
(a)
(b)
Absorbance
Absorbance Difference
λ (nm)
0.25
0.20
0.15
0.10
0.05
0.0
1.5
1.0
0.5
0.0
0.01
0.0
-0.01
-0.02
-0.03
.10
0.00
-.10
-.20
600
500
400

(iii) When 1 equiv of NAD^+ (including 1 % cyt-*c*, and 0.01% PMS) was added to a sample of the 428/580 nm species, the Soret and α maxima shifted from 428 and 596-597 nm to 427 and 597-598 nm (Fig. 14*a*). Examination of the difference spectra (Fig. 14*b*) shows that NAD^+ (plus mediator) caused a substantial decay of the population of the 428/580 nm species; however, the extent of the decay was never as great as when NADH was added (Fig. 13*b*, and Fig. 16). The effect of the added mediator and ferricytochrome *c* is probably to facilitate the entry of endogenous reducing equivalents into the enzyme.

EPR—To confirm that the pulsed enzyme is in fact produced upon the addition of NADH to the 428/580 nm species, we repeated the reductive titration of the 428/580 nm species and monitored the formation of the pulsed enzyme by EPR.

It is thought that a homogeneous population of pulsed cytochrome *c* oxidase is produced upon the reoxidation of the dithionite-reduced enzyme, which contains a trace amount of catalase (27). When we prepared a sample of the pulsed enzyme by this procedure the expected EPR resonances at $g = 5$, 1.8, and 1.7 were observed at low temperature (10 K) and high powers (10 mW) (Fig. 15*a*). In Figure 15*a* we show the two unusual EPR resonances which occur at high field. Quantitation of the EPR resonances associated with the pulsed enzyme is not possible at present due to the uncertainty of the spin multiplicity of the system and because of the unusual temperature dependence of the resonances (13). Therefore, the EPR spectrum of the pulsed enzyme shown in Figure 15*a* was used for comparison purposes, that is, to ascertain whether a sizeable population of the pulsed enzyme was produced when a reducing equivalent was added to the 428/580 nm species. The broad feature at high field ($g = 1.45$) in traces *a*-*e* (Fig. 15) is due to the g_x value of ferric Fe_a (28).

When the 428/580 nm species was examined by EPR at low temperatures and high microwave powers (10-20 mW), no unusual EPR resonances were observed

either in the low-field or the high-field region of the spectrum (Fig. 15*b*). However, the addition of 1 equiv of NADH (1 % ferricyt-*c*, 0.01 % PMS) to the 428/580 nm species resulted in the formation of a subpopulation of the pulsed enzyme as judged by the appearance of the unusual resonances at $g = 5$ (spectrum not shown), 1.8 and 1.7 (Fig. 15*c*). (The addition of reductant to the 428/580 nm species did not result in the formation of the rhombic Cu_B EPR signal.) In a parallel sample, when NAD^+ and mediator were added to the 428/580 nm species (Fig. 15*d*) only a negligible population of the pulsed enzyme was produced (Fig. 15*e*). This result ruled out the possibility that the formation of the pulsed enzyme is dependent on the binding of NAD^+ (or ferricytochrome *c*). The EPR results demonstrate that a subpopulation of the pulsed enzyme is produced upon the addition of a reducing equivalent to the 428/580 nm species.

The results from the optically monitored titration of the 428/580 nm species are summarized in Figure 16, which show the approximate populations of the 428/580 nm species over the course of the incubation at 273 K, with and without added reducing equivalents. Inspection of Figure 16 shows that the decay of the 428/580 nm species is accelerated by the addition of reducing equivalents. This result substantiated the earlier work of Orii and King (29), who showed that the decay of the 428/580 nm component of the oxygenated enzyme was accelerated by reductant. Specifically, the approximate half-time for the decay of the 428/580 nm species in the presence (and absence) of added reducing equivalents may be extrapolated from the data shown in Figure 16. The addition of reducing equivalents to the 428/580 nm species resulted in a decrease in the half-time for the decay of the spectral features associated with the 428/580 nm species from approximately 60 min to 20 min. We stress, however, that the reductive titration was conducted in the presence of low concentrations of mediator (phenazine methosulfate). When similar levels of mediator (and reductant) are used to reduce the resting enzyme, several hours are required for complete reduction. Therefore, although the opti-

Figure 15

EPR spectra of the pulsed enzyme, the 428/580 nm species, and the 428/580 nm species plus NADH (or NAD^+). The high-field EPR spectra of the pulsed form of cytochrome *c* oxidase and the 428/580 nm form of the enzyme are shown in *a* and *b*, respectively. After recording an EPR spectrum of the 428/580 nm species, the sample was rapidly thawed to ice temperature and aliquots of ferricytochrome *c*, catalase, and 1 equiv of NADH (plus PMS) were introduced into the sample (180 sec from the addition of H_2O_2), and the sample was frozen to 77 K (240 sec from the addition of H_2O_2) for examination by EPR (*c*). As a control, 1 equiv of NAD^+ (plus PMS) were added to an identically treated sample of the 428/580 nm species. The corresponding EPR spectra for the 428/580 nm species and the 428/580 nm species plus NAD^+ are shown in *d* and *e*, respectively. Traces *c* and *e* were not corrected for dilution. Sample concentrations were 310 μM (*a*) and 250 μM (*b*-*e*). For the two samples of the 428/580 nm species, the final catalase, ferricytochrome *c*, and phenazine methosulfate concentrations were approximately 3 μM, 4 μM, and 1 μM, respectively. Conditions for obtaining EPR spectra were (*a*-*e*); temp., 10 K; modulation amplitude, 16 Gauss; power, 20 milliwatts; frequency, 9.228 GHz; gain, 3.2×10^4; number of scans, 3.

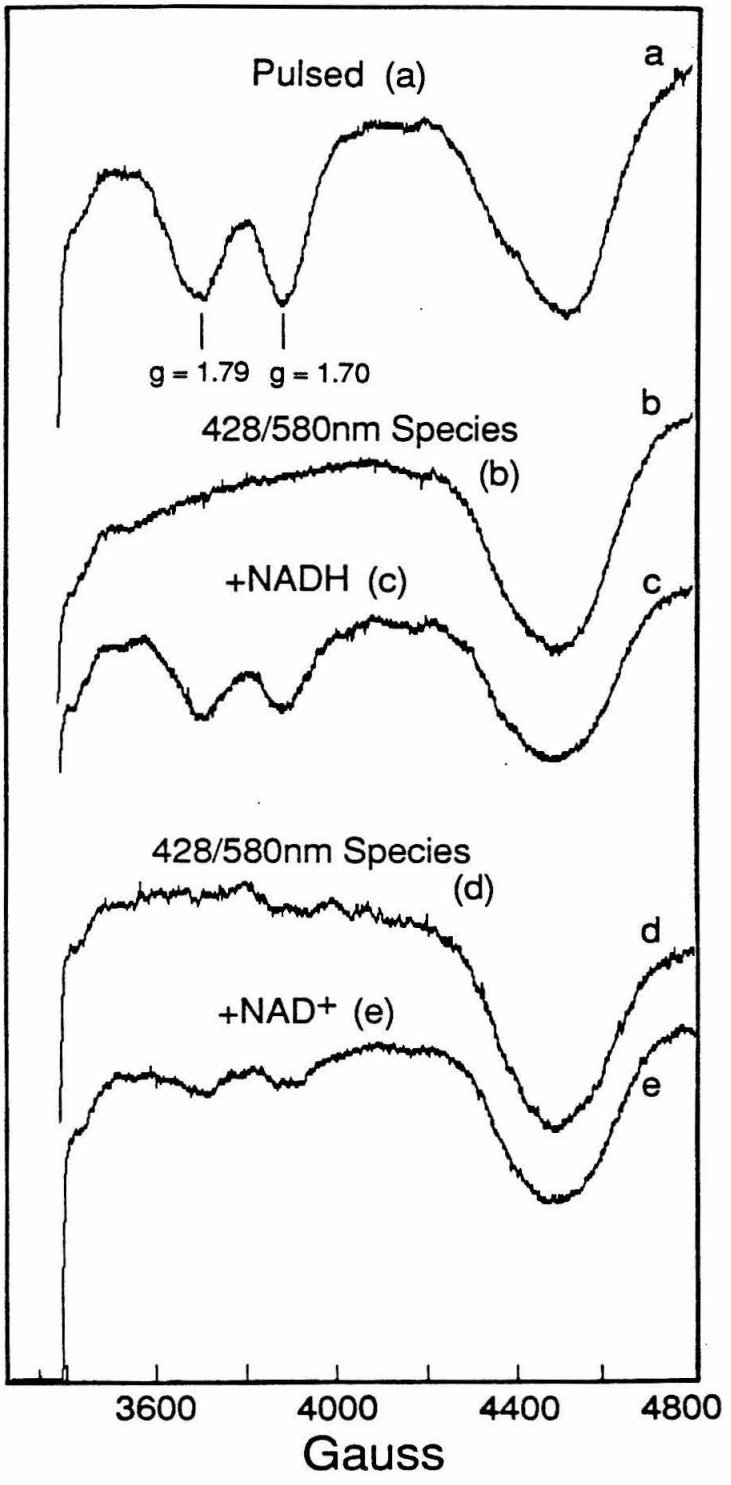
Pulsed (a)
a
g = 1.79
g = 1.70
428/580nm Species
(b)
b
+NADH (c)
c
428/580nm Species
(d)
d
+NAD+ (e)
e
3600
4000
4400
4800
Gauss

Figure 16

Population of the 428/580 nm species upon incubation at 273 K, in the presence and absence of reducing equivalents (NADH). The decay of the population of 428/580 nm species in the absence of added reductant is shown in Figure 16 (00). The decay of the 428/580 nm species was also monitored in a control sample in the presence of NAD^+ (00): t = 4 min, no NAD^+; t~10 min, 0.5 equiv NAD^+; t~16 min, 1 equiv NAD^+; t~22 min, 2 equiv NAD^+; t~27 min, 3 equiv NAD^+; t~33 min, 4 equiv NAD^+. The decay of the 428/580 nm species in the presence of NADH (00): t = 4 min, no NADH; t~11 min, 0.5 equiv NADH; t~16 min, 1 equiv NADH; t~27 min, 2 equiv NADH; t~34 min, 3 equiv NADH; t~40 min, 4 equiv NADH. A value of 1.0 corresponds to a 100 % population.

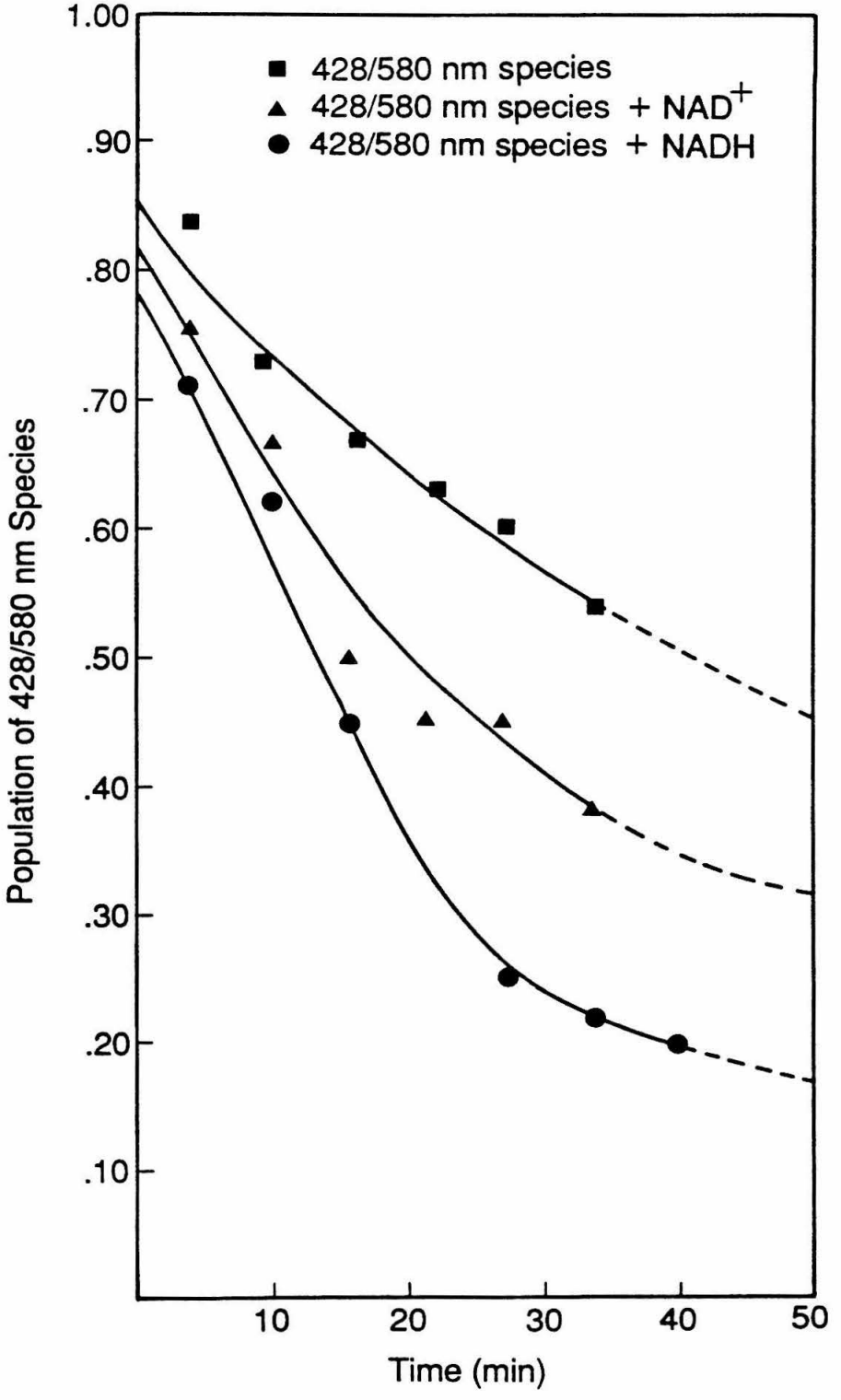
1.00
.90
.80
.70
.60
.50
.40
.30
.20
.10
Population of 428/580 nm Species
428/580 nm species
428/580 nm species + NAD+
428/580 nm species + NADH
10
20
30
40
50
Time (min)

cally monitored titration consisted of the addition of 4 equivalents of NADH (Fig. 13*a*,*b*), it is possible that only a fraction of the reductant was actually consumed during the course of the reduction. The results from the optically monitored reductive titration provide a relative gauge of the susceptibility of the 428/580 nm species to reduction. Since the largest population of the pulsed form of the enzyme was produced upon the addition of reductant to the 428/580 nm species, as evidenced by the most pronounced intensity at ca. 660 and 414 nm in the difference spectrum in Figure 13*b*, by implication the 428/580 nm species must contain more oxidizing equivalents than the pulsed enzyme.

Low Temperature EPR of the 428/580 nm Species. The reactive 428/580 nm species does not exhibit any unusual EPR resonances from either Fe_{a_3} or Cu_B, yet the reactivity studies reported herein suggest that the binuclear site is composed of an odd-electron species. A possible explanation for the lack of an EPR signature from the binuclear dioxygen reduction site is that rapid spin relaxation of one of the paramagnetic centers, such as a ferryl Fe_{a_3}, could enhance the electron-spin relaxation of a nearby less rapidly relaxing paramagnetic species, such as cupric Cu_B (30) and preclude the observation of an EPR signal from the cupric ion. To test this hypothesis, the 428/580 nm species was examined by EPR at 2 K, where the electron-spin relaxation is expected to be sufficiently slow to allow observation of an EPR signal from cupric Cu_B. Unfortunately, no resonances attributable to either Fe_{a_3} or Cu_B were observed in the low-temperature experiments.

DISCUSSION

Reoxidation of Partially Reduced Cytochrome c Oxidase.

In order to trap a three-electron-reduced dioxygen intermediate at the dioxygen reduction site of cytochrome *c* oxidase, *partially* reduced samples were reoxidized. If a sample of cytochrome *c* oxidase that is initially reduced between 50-100

% is reoxidized there will be, at minimum, three subpopulations of intermediates initially present at the dioxygen reduction site: (i) the peroxidic adduct, Compound C (a two-electron-reduced species); (ii) a three-electron-reduced species; and (iii) the pulsed species (formally a four-electron-reduced dioxygen species). Since the optical features of the peroxidic adduct and the pulsed enzyme are well characterized, examination of the optical difference spectra of partially reduced and reoxidized samples enabled the optical features associated with the subpopulation of trapped, three-electron-reduced intermediate to be deconvoluted from the spectral contributions from the other subpopulations.

Unique optical features were observed in the optical difference spectrum (reoxidized minus resting) at ~580 and ~537 nm in samples that were initially only partially reduced (65-85 %) and then reoxidized. These spectral features are not assignable to either the pulsed enzyme or Compound C; therefore, a reasonable conclusion is that the optical features at 580 and 537 nm arise from the subpopulation of three-electron-reduced species. The examination of the partially reduced and reoxidized samples by EPR spectroscopy revealed no unusual spectral signatures. Evidently, the subpopulation of three-electron-reduced species is EPR-silent. Alternatively, with such low populations of the trapped, three-electron-reduced species, it is possible that the species is in fact EPR active, but the poor yields of the intermediate precluded observation of an EPR signal.

The reactivity between the subpopulation of EPR-silent, three-electron-reduced intermediate and CO was investigated. Upon the addition of CO to the reoxidized sample all three subpopulations of intermediates can react with CO. Since CO is a two-electron donor, reduction by CO of the two subpopulations of even-electron intermediates, namely Compound C and pulsed, must result in products with integer spin, which are EPR-silent. In fact, it is now generally recognized that carbon monoxide can reduce cytochrome *c* oxidase to produce the EPR-silent,

CO-mixed-valence compound by the following reaction (Eqn. 1) (24-26).

$$[Fe^{III}_{a_3}\ Cu^{II}_B] + 2CO + H_2O \longrightarrow [Fe^{II}_{a_3} - CO\ Cu^{I}_B] + CO_2 + 2H^+ \qquad (1)$$

However, when CO reacts with the three-electron-reduced dioxygen intermediate another odd-electron intermediate must necessarily be produced. Thus, only the product of the reaction involving the odd-electron manifold of intermediates is visible by EPR.

We observed only modest yields (~10 %) of the rhombic Cu_B EPR signal upon the addition of CO to samples which were initially reduced (65-85 %) and then reoxidized. No rhombic Cu_B EPR signal formed after the addition of CO to either the pulsed enzyme or to samples which were initially half-reduced and then reoxidized. These experiments with CO suggest that the subpopulation of the EPR-silent, three-electron-reduced intermediate is involved in a reaction with CO. Control experiments implicated CO as the source of electrons. Carbon monoxide is a two-electron donor. Because the dioxygen reduction site became reduced to only the ferrous/cupric state upon the addition of CO, while Cu_A and Fe_a remained oxidized, the intermediate that reacted with CO is by implication a ferryl Fe_{a_3}/cupric Cu_B (or a species at the same formal level of oxidation).

The low yield of the rhombic Cu_B EPR signal in the present room temperature incubation experiments is probably a consequence of the three different subpopulations of intermediates present at the dioxygen reduction site after reoxidation of a partially reduced sample. Furthermore, the intermediate might be short-lived in the EPR experiments because of the many cycles of freezing and thawing, which can contribute to enzyme denaturation and thus the production of endogenous reducing equivalents.

Reactions with Hydrogen Peroxide

The evidence for the assignment of the redox states of Fe_{a_3} and Cu_B in the

428/580 nm state of the enzyme and the proposed schemes for the formation and decay of the reactive state of the enzyme will be discussed.

(i) When the H_2O_2 concentration is approximately equivalent to the enzyme concentration, a peroxidic adduct (Compound C) is produced at the dioxygen reduction site (21). However, when excess H_2O_2 is added to Compound C, or is added initially to the reduced (or oxygenated) enzyme, a population of the 428/580 nm species is produced. The homogeneity of the population is evidenced by the lack of any appreciable intensity at 607 nm in the reoxidized minus resting difference spectrum due to Compound C (Fig. 4*b*), which certainly might be expected to form under such reaction conditions. Two observations regarding the optical spectrum of the 428/580 nm species are worth noting. (a) A comparison of the Soret region of the optical spectra of the resting enzyme and the 428/580 nm species shows that the intense Soret band is narrower in the 428/580 nm species than in the resting enzyme (Fig. 4*a*). The optical spectrum of the cyanide-inhibited enzyme also exhibits a sharpened Soret, relative to the resting enzyme (Fig. 7). The reason for the narrow Soret in the cyanide-inhibited enzyme is that there is a homogeneous population of low-spin ferric iron in the cyanide-inhibited enzyme. Because low-spin ferric Fe_a and Fe_{a_3} have absorption maxima at 426 and 428 nm, respectively, the observed Soret band is quite narrow (7). Analogously, the 428/580 nm species exhibits a narrow Soret, with a Soret maximum at 428 nm, suggesting that the intermediate contains a low-spin ferric (or ferryl) Fe_{a_3} complex. (b) The 428/580 nm species and the cyanide-inhibited enzyme also share spectral features in the visible region of the optical spectrum (500-600 nm). In contrast to the quite narrow bands observed in the Soret region of the spectrum for both derivatives, in the visible region the α-region of the spectrum (~600 nm) is rather broad, relative to the resting enzyme. Does this fact suggest inhomogeneity? Recall that both Fe_a and Fe_{a_3} contribute intensity in the Soret and α regions of the optical spectrum of cytochrome *c* oxidase. Evi-

dently, cyanide binding to ferric Fe_{a_3} results in an increase in the intensity and a red-shift of the α and β bands associated with Fe_{a_3}, hence an overall broadening of the composite optical spectrum of the cyanide-inhibited enzyme is observed. Analogous to the cyanide-inhibited enzyme, the intense and blue-shifted optical spectrum of the of 428/580 nm species may signify a homogeneous population of a low-spin ferric Fe_{a_3} complex.

(ii) The reactivity of the 428/580 nm species with carbon monoxide was investigated in order to aid in the assignment of the redox states of the metal centers at the binuclear site. Although the 428/580 nm species and the cyanide-inhibited enzyme share common spectral features, they exhibit dramatically different reactivity with carbon monoxide. As expected, the cyanide-inhibited enzyme is *inert* to ligand substitution reactions at the binuclear site because cyanide tightly binds to ferric Fe_{a_3}. In contrast, the 428/580 nm species contains a reactive binuclear site, as evidenced by its reactivity with carbon monoxide. The 428/580 nm species catalyzes a fairly rapid reaction with CO. (The reaction was complete within the time required to obtain an optical spectrum, ~3 min.) The optical difference spectrum in Figure 8 shows that the optical bands at 580 and 537 nm are abolished upon the introduction of CO into the sample of the 428/580 nm species. The difference spectrum also shows that the pulsed enzyme is produced in the reaction due to the formation of the absorption band at ~660 nm.

Further insights into the nature of the reaction between the 428/580 nm species and CO were derived from a parallel EPR investigation of the reaction. Examination of the reaction by EPR demonstrated that a rhombic Cu_B EPR signal is produced upon the addition of CO to a sample of the 428/580 nm species. This rhombic Cu_B EPR signal is the same signal that was produced upon prolonged incubation of samples in the low-temperature experiments described in Chapter II, as judged by the correspondence between the g values and the hyperfine coupling constant ($A_{||}$ = 105 Gauss). Quantitation of the 428/580 nm species using the

estimated extinction coefficient ($\Delta\epsilon_{580}$~5 mM^{-1} cm^{-1}) and parallel quantitation of the Cu_B EPR signal revealed that typically an ~80 % population of the 428/580 nm species produced approximately 40-60 % of the rhombic Cu_B EPR signal when CO was admitted into the sample. The discrepancy between the two populations may be related to (a) the loss of the reactive 428/580 nm species in the interval between obtaining the optical spectrum and adding CO, which is also accompanied by a freeze/thaw cycle, and (b) the intermolecular transfer may occur between two oxidase molecules containing the 1/4 reduced state ($[Fe^{II}_{a_3}$-L $Cu^{II}_B]$), resulting in the production of the pulsed enzyme and Compound C. This latter reaction might be quite fast in a sample of very concentrated cytochrome *c* oxidase, which is known to be highly aggregated.

The 428/580 nm species catalyzes a reaction with CO which produces a half-reduced dioxygen reduction site in which the low-potential centers are oxidized (Fe^{III}_a, Cu^{II}_A, $Fe^{II}_{a_3}$-L, Cu^{II}_B). Because CO is a two-electron reductant, this result implies that the 428/580 nm species contains *five* oxidizing equivalents, with the extra oxidizing equivalent located on Fe_{a_3}. A proposed reaction sequence for the formation of a low-spin ferrous-dioxygen adduct adjacent to cupric Cu_B upon the addition of CO to the ferryl Fe_{a_3}/cupric Cu_B binuclear couple is shown in Scheme IV.

(iii) Since we have not detected the formation of carbon dioxide to substantiate the proposed oxidation of CO to CO_2, we conducted an aerobic reductive titration of the 428/580 nm species to confirm that the species contains more oxidizing equivalents than the normal resting state of the enzyme. The titration results indicate that the decay of the 428/580 nm species is accelerated by the addition of reducing equivalents, and the decay of the 428/580 nm species is accompanied by the parallel formation of the *pulsed* enzyme, which contains *four* oxidizing equivalents. The latter result provides additional evidence that the 428/580 nm is in fact in a higher oxidation state than the pulsed enzyme.

Formation of the 428/580 nm Species. The reactivity of the 428/580 nm species with carbon monoxide and NADH established that the binuclear dioxygen reduction site contains more oxidizing equivalents than the pulsed form of cytochrome *c* oxidase. We observed that when the concentration of hydrogen peroxide is approximately equivalent to the concentration of the enzyme, a species is produced which exhibits spectral signatures that are similar, but not identical, to those reported by others for the peroxidic adduct, Compound C (Fig. 5) (14,19,21). Most notably, we never observed an intense band at 607 nm (in the difference spectrum) if hydrogen peroxide is added to the pulsed enzyme; instead, we typically observed only a moderately intense band at 605 nm, with a pronounced shoulder at ~580 nm and a weak plateau centered at ~540 nm (Fig. 5*b*). This discrepancy may indicate that our samples were heterogeneous, with contributions from the peroxidic adduct and the 428/580 nm species. However, the 428/580 nm species certainly could not have been populated to a great extent because at low concentrations of hydrogen peroxide (50-150 μM) the α band is observed at 600 $\pm$ 1 nm. If the 428/580 nm species was significantly populated at low concentrations of hydrogen peroxide we would expect a more blue-shifted α band. Therefore, we conclude that some of the intensity at ~580 nm in the difference spectrum, at low levels of hydrogen peroxide, is probably due to the peroxidic adduct, Compound C. It has been suggested that the intense band at 607 nm in the difference spectrum of the peroxidic adduct is due to a ligand to metal charge transfer (CT) electronic transition from the peroxidic adduct to ferric Fe_{a_3} (31). If this hypothesis is correct, presumably the intensity of the proposed CT transition is dependent on the protonation state of the peroxidic group. Thus, the relatively low intensity at 607 nm in our optical spectrum of the peroxidic adduct (Fig. 5*b*) may suggest that the protonation state of our samples of the peroxidic adduct is different than the work of others.

In Scheme I and II we propose reaction sequences to account for the formation

of a ferryl Fe_{a_3}/cupric Cu_B binuclear couple by the activation of cytochrome *c* oxidase with hydrogen peroxide. In each scheme we have omitted the reaction steps involving the reoxidation of the reduced enzyme with hydrogen peroxide. However, Orii *et al.* (32) in fact demonstrated that hydrogen peroxide is almost as catalytically competent as O_2 in reoxidizing reduced cytochrome *c* oxidase. When the H_2O_2 concentration is approximately equivalent to the enzyme concentration, a peroxidic adduct, Compound C, is produced at the dioxygen reduction site as shown in Scheme I. (Although a bridging anionic peroxidic group is indicated in Scheme I, we stress that the degree of protonation and the number of oxygen atoms from H_2O_2 which actually bridge Cu_B and Fe_{a_3} are not known.) However, if large excesses of H_2O_2 are added initially to the pulsed or reduced enzyme, it is proposed that the extra H_2O_2 can act as a direct one-electron donor to Compound C to produce the ferryl Fe_{a_3}/cupric Cu_B binuclear couple and superoxide.

Alternatively, we cannot rule out that under conditions of excess hydrogen peroxide, an equivalent of hydrogen peroxide directly oxidizes ferric Fe_{a_3} to the ferryl oxidation state with the concomitant formation of the hydroxyl radical. A similar reaction has been reported for the formation of ferryl myoglobin by the oxidative action of hydrogen peroxide (33). In Scheme II we propose a reaction sequence which incorporates the ideas outlined above.

The proposed schemes (Schemes I and II) for the formation of a ferryl Fe_{a_3}/ cupric Cu_B binuclear dioxygen reduction site includes the production of a reactive radicals (superoxide and hydroxyl radicals). Although the 428/580 nm species was produced in every different batch of cytochrome *c* oxidase that we tested, as judged by the formation of the characteristic optical features, the formation of the radical EPR signal was completely batch-dependent. In some cases we observed a sizeable population of a radical EPR signal at ca. $g = 2.0$. Specifically, in those cases, the intensity of the narrow radical signal would extend above the the intense g_y feature of Cu_A observed at $g = 2.08$ (Fig. 9*f*). In other experiments,

Scheme I

Proposed reaction sequence to account for the formation of a ferryl Fe_{a_3}/cupric Cu_B couple at the dioxygen reduction site of cytochrome *c* oxidase via one-electron reduction of the peroxidic adduct, Compound C, by hydrogen peroxide.

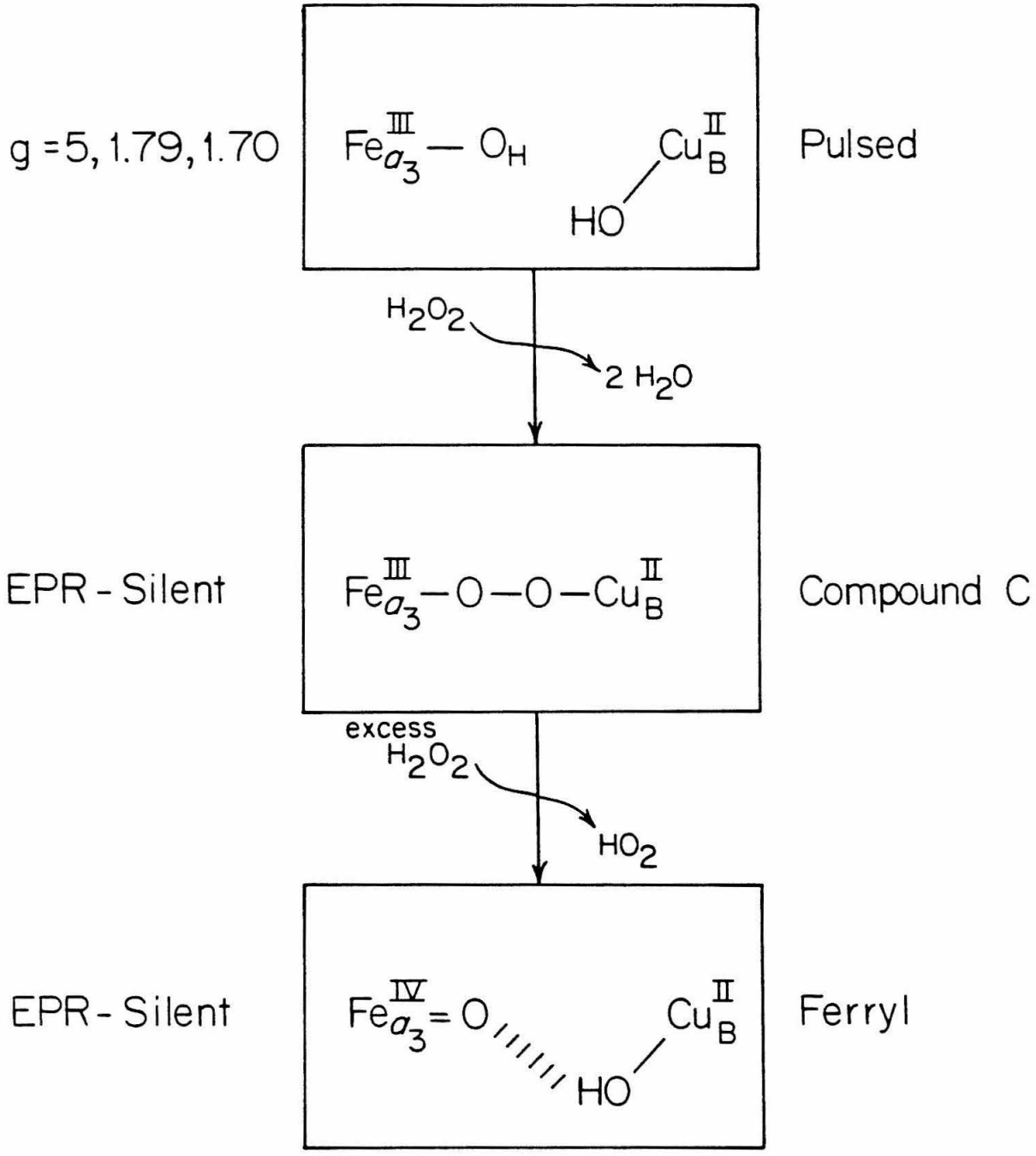
g =5, 1.79, 1.70
$Fe^{III}_{a_3}$ — O_H
Cu^{II}_B
HO
Pulsed
H_2O_2
2 H_2O
EPR - Silent
$Fe^{III}_{a_3}$—O—O—Cu^{II}_B
Compound C
excess
H_2O_2
HO_2
EPR - Silent
$Fe^{IV}_{a_3}$= O
Cu^{II}_B
HO
Ferryl

Scheme II

Proposed reaction sequence to account for the formation of a ferryl Fe_{a_3}/cupric Cu_B couple at the dioxygen reduction site of cytochrome *c* oxidase via one-electron *oxidation* of ferric Fe_{a_3} by hydrogen peroxide.

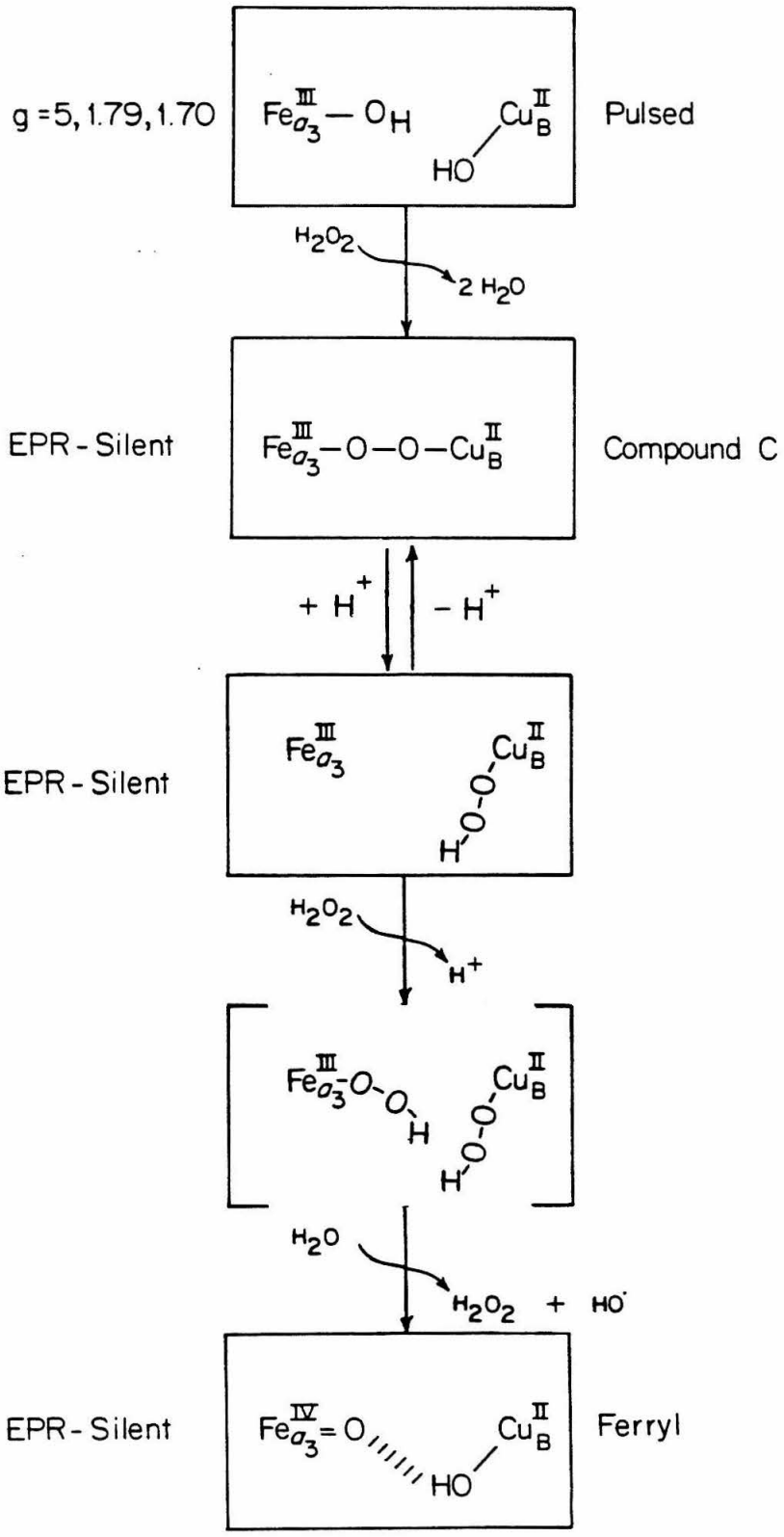
g = 5, 1.79, 1.70
Pulsed
HO
H_2O_2
2 H_2O
EPR - Silent
Compound C
+ H^+
- H^+
EPR - Silent
H_2O_2
H^+
H_2O
H_2O_2 + HO·
EPR - Silent
Ferryl

we observed a population of a radical EPR signal similar to that seen in Figure 9*f*, or in many instances, no radical EPR signal was observed. The superoxide radical and the hydroxyl radical are expected to be powerful oxidants and to exhibit kinetic lability (34). If these reactive species are produced upon the addition of excess H_2O_2 to a sample of cytochrome *c* oxidase, they probably would undergo a rapid hydrogen-abstraction reaction with amino acids located near the binuclear dioxygen reduction site. If a protein radical is formed upon treatment of the enzyme with hydrogen peroxide, the protein radical might be magnetically coupled to the metal centers at the dioxygen reduction site, which could preclude the observation of an EPR signal.

Decay of the 428/580 nm Species. The reductive titration of the 428/580 nm species revealed that the 428/580 nm species converts to the pulsed (and eventually resting) states of the enzyme upon incubation at ice temperature, in the absence of exogenous reducing equivalents, with a half-time of approximately 60 min. We also demonstrated that the addition of a reducing equivalent to the 428/580 nm species caused the rapid (~60 sec) formation of a population of the pulsed state of the enzyme, as judged by the appearance of the EPR resonances at $g = 5$, 1.8, and 1.70, which are diagnostic of the pulsed form of cytochrome *c* oxidase (Fig. 15*b*,*c*). In Scheme III, we propose a reaction sequence which accounts for the accelerated formation of the pulsed enzyme upon the addition of an equivalent of reductant to the 428/580 nm species. Scheme III incorporates the well known fact that the pulsed enzyme slowly converts to the resting state of the enzyme upon incubation at ice temperature (15). In the absence of reducing equivalents, the 428/480 nm species probably converts to the resting enzyme as a result of reduction by endogenous reducing equivalents.

The Reaction Between CO and the 428/580 nm Species

The first indication we had that Cu_B played a primary role in the catalysis of CO to CO_2 by the 428/580 nm species was the fact that no reduction of the

Scheme III

A proposed reaction sequence for the conversion of the reactive, EPR-silent 428/580 nm species to the pulsed (and resting) states of the enzyme by the action of exogenous reductants, such as NADH.

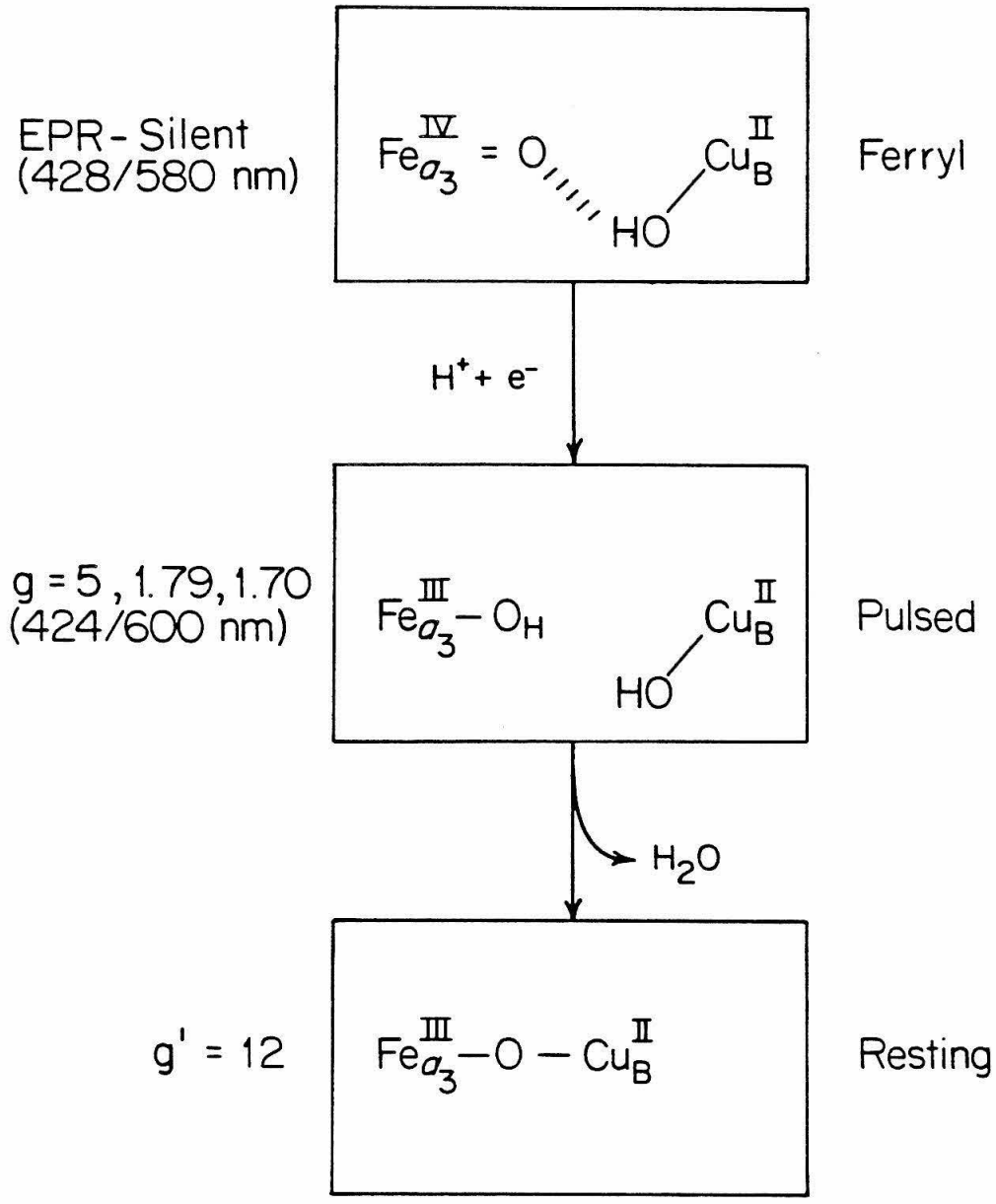
EPR - Silent
(428/580 nm)
$Fe^{IV}_{a_3}$ = O
Cu^{II}_{B}
HO
Ferryl
$H^+ + e^-$
g = 5 , 1.79, 1.70
(424/600 nm)
$Fe^{III}_{a_3}$ – O_H
Cu^{II}_{B}
HO
Pulsed
H_2O
g' = 12
$Fe^{III}_{a_3}$ – O – Cu^{II}_{B}
Resting

Scheme IV

Proposed scheme for the oxidation of carbon monoxide by the ferryl Fe_{a_3}/cupric Cu_B binuclear dixoygen reduction site of the 428/580 nm species, with the concomitant formation of a half-reduced dioxygen reduction site.

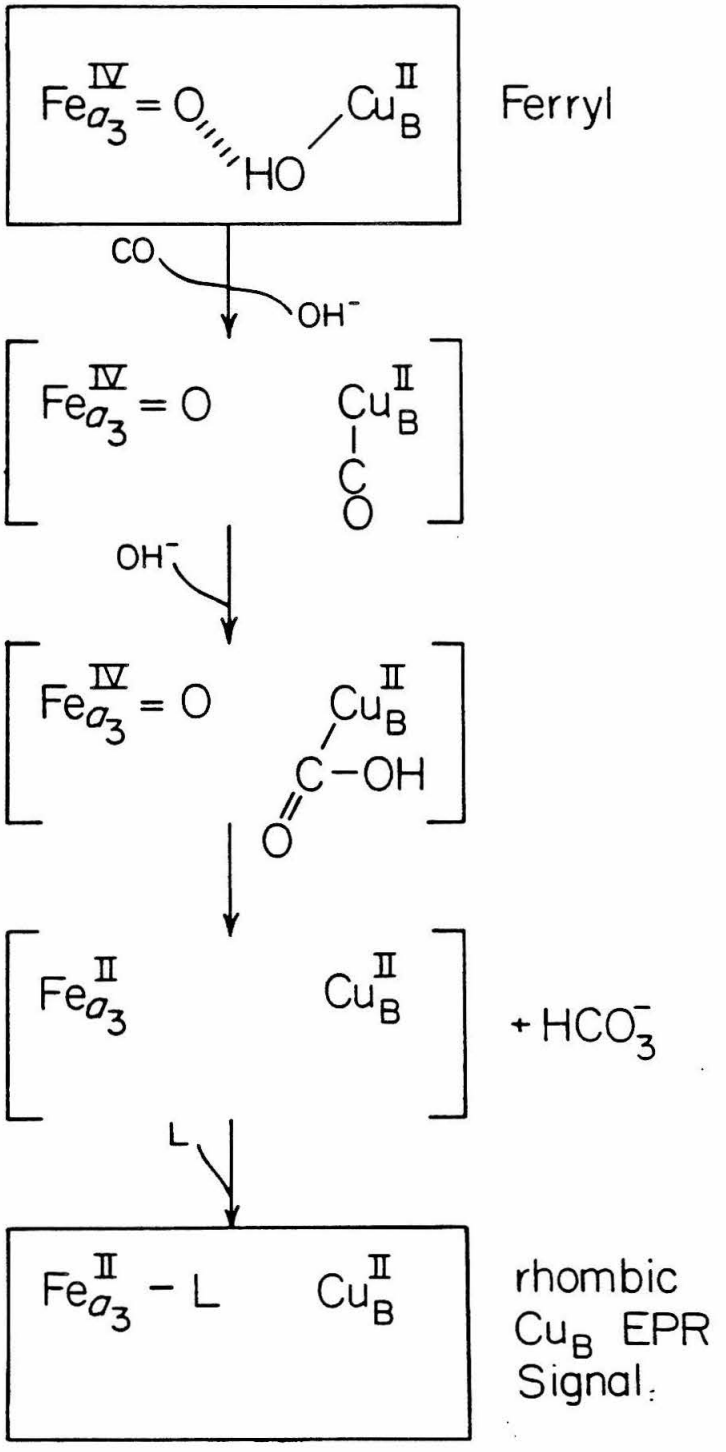
Fe a3 IV = O
HO
Cu B II
Ferryl
CO
OH-
Fe a3 IV = O
Cu B II
C
O
OH-
Fe a3 IV = O
Cu B II
C-OH
O
Fe a3 II
Cu B II
+ HCO3-
L
Fe a3 II - L
Cu B II
rhombic
Cu B EPR
Signal

reactive HRP-I (ferryl prophyrin π-radical cation) occurred upon the addition of an atmosphere of CO to the sample. The lack of reactivity of HRP-I suggested that Cu_B must play a role in the catalysis of CO by cytochrome *c* oxidase, alternatively carbon monoxide may be excluded from approaching the iron center of horse radish peroxidase.

Early investigations by Harkness and Halpern (35) into the oxidation of CO by aqueous solutions of Ag(I) and Hg(II) salts implicated the formation of a reactive metal-carbonyl species. It was suggested that the binding of CO to these metals activates the CO to nucleophilic attack by H_2O (or OH^-) and results in the formation of a reactive metal hydroxycarbonyl (M-COOH). This reactive species undergoes rapid decarbonylation to produce CO_2 and reduced metal ion. Similarly, reactive cupric and cuprous hydroxycarbonyls have been suggested to play a primary role in the oxidation of CO by copper salts (36). Bercaw and co-workers (37) suggested that the reduction of the cobalt(III) cofactor of vitamin-B_{12} by carbon monoxide might also proceed via a pathway which includes a reactive metal carbonyl insertion complex.

Byerley and Peters (36) showed that Cu(II) salts are also capable of oxidizing CO to CO_2, although the reactions conditions are quite severe (pCO = 1360 atm). They proposed two mechanisms for the oxidation of CO by copper salts in aqueous solution. One reaction pathway was suggested to be independent of the carbon monoxide pressure and involved the initial formation of a copper(I)-CO complex. The other pathway involved the activation of CO by the cupric ion. Interestingly, they suggested that both reaction pathways have a common rate-determining step, which is the decomposition of a reactive carbon monoxide insertion complex (M-COOH).

Based on the ability of either copper(I) or copper(II) to activate CO to nucleophilic attack by either H_2O or hydroxide, a reasonable mechanism for the oxidation of carbon monoxide by the 428/580 nm species could involve (i) the

transient binding of CO to cupric Cu_Bfollowed by; (ii) the nucleophilic attack of H_2O (or OH^-) to produce a reactive copper hydroxycarbonyl resulting in; (iii) either the decarbonylation of the hydroxycarbonyl complex to produce CO_2 and a two-electron-reduced site, or direct oxygen atom transfer occurs from the oxy-ferryl to the reactive metal hydroxycarbonyl complex to produce HCO_3^-. A proposed scheme for the oxidation of CO to HCO_3^-, which incorporates these features, is shown in Scheme IV.

The Nature of the Reactive Binuclear Dioxygen Reduction Site in the 428/580 nm Species

The lack of an EPR signal from the binuclear dioxygen reduction site of the 428/580 nm species is puzzling, although it does not rule out that the site is composed of a paramagnetic species. There are other examples in the literature of paramagnetic enzymatic intermediates which are EPR-silent (38). In a recent study by Pyrz *et al.* Mössbauer spectroscopy was used to examine the EPR-silent phosphate-inhibited complex of the purple acid phosphatase enzyme uteroferrin (38). Their results showed that the phosphate-inhibited uteroferrin is composed of a high-spin (S = 5/2) ferric ion magnetically coupled to a high-spin (S = 2) ferrous ion. An EPR signal is expected from such a species, yet, surprisingly, no EPR resonances were observed under the conditions of their experiment. Pyrz *et al.* suggested that a ground state of S = 1/2 was consistent with the Mössbauer data, and that an EPR signal might not be observed from such a coupled spin system under the conditions of their experiments. Alternatively, analogous to the arguement put forth by Blair *et al.* (3) to explain the EPR-silence of the proposed ferryl Fe_{a_3}/cupric Cu_B couple of cytochrome *c* oxidase, even if the binuclear center of the phosphate complex of uteroferrin has a ground state of S = 1/2, it is conceivable that the species could still be EPR-silent if the magnitude of the superexchange coupling is comparable to the zero-field splitting of the iron centers.

An alternative proposal for the reactive species at the dioxygen reduction site in the 428/580 nm species might be considered. Instead of a ferryl Fe_{a_3}/cupric Cu_B binuclear couple, an equally plausible model, at first glance, is that the site contains a ferryl Fe_{a_3} associated with a heme A π-radical cation adjacent to cuprous Cu_B. This latter species also contains three oxidizing equivalents. What is the likelihood that the site is composed of a ferryl heme A π-radical cation/cuprous Cu_B species?

There are several examples of very reactive, yet kinetically stable, enzymatic intermediates which contain a ferryl porphyrin π-radical cation (39). Typically, these rather unusual intermediates are formed by the two-electron oxidation of the native ferric peroxidases (such as horse radish peroxidase (HRP) or Japanese radish) and catalase (CAT) by hydrogen peroxide (Eqn. 2), yielding an intermediate which is formally Fe(V) (2, 39) (These high-valent enzymatic intermediates are referred to as Compounds I)

$$HRP(PFe^{III}) + H_2O_2 \longrightarrow HRP - I(^{\cdot+}PFe^{IV} = O) + H_2O \; . \qquad (2)$$

Unlike cytochrome *c* oxidase, the active site of the native peroxidases and catalases is mononuclear, containing a ferric heme. Curiously, all of the enzymes which form ferryl porphyrin π-radical cations contain iron protoporphyrin IX as the prosthetic group. Naturally, this porphyrin must possess specific chemical properties which facilitate the formation of a stable, reversibly-oxidized porphyrin. Studies on model compounds have elucidated some of the factors which govern the formation of a stable, reversibly-oxidized/reduced porphyrin (40). The porphyrin must have electron-donating substituents which stabilize the cation by hyperconjugation in order to form stable porphyrin π-radical cations. Protoporphyrin IX is well suited for the formation of a stable π-radical cation because it is methylated in the 5th and 8th positions of the porphyrin ring and has vinyl substituents at the 2nd and 4th positions (Fig. 17). The methyl (and vinyl) group can readily stabilize a π-radical cation by an electron-releasing effect. Conversely, substituents such as the formyl, halides, and alkoxides would be expected to destabilize a cationic

porphyrin by an electron-withdrawing effect. Cytochrome *c* oxidase contains a rather unusual porphyrin termed heme A. Heme A contains an isoprenoid chain and a formyl group at the 2nd and 8th positions of the porphyrin ring, in place of the methyl and vinyl groups found on protoporphyrin IX (Fig. 17). Because of the powerful electron-withdrawing effect of the formyl group, Chan and co-workers (41) concluded that heme A is probably resistant to reversible one-electron oxidation, making it rather unlikely that a porphyrin π-radical cation of heme A is formed upon the reaction of cytochrome *c* oxidase with hydrogen peroxide.

There is another reason to favor the ferryl Fe_{a_3}/cupric Cu_B model for the dioxygen reduction site in the 428/580 nm species over the alternative model, namely, the ferryl Fe_{a_3} heme A π-radical cation/cuprous Cu_B couple. Clearly, Cu_B must have an inordinately high reduction potential in order to remain in the cuprous oxidation state when in close proximity to an oxidant as powerful as a ferryl porphyrin π-radical cation, which could have a reduction potential as high as 1 V. Certainly, there are examples of copper complexes exhibiting high reduction potentials. For example, the multi-copper metalloenzyme laccase has a measured reduction potential for the type-1 copper complex which is approximately 0.8 V (42). What makes the ferryl heme A π-radical cation/cuprous Cu_B model untenable is that following the oxidation of CO, a low-spin dioxygen (or CO) ferrous Fe_{a_3} complex is produced which is adjacent to *cupric* Cu_B. Therefore Cu_B must have a lower reduction potential than ferric Fe_{a_3} in order for the observed species to be produced. This model requires an enormous shift in the reduction potential of Cu_B over the course of the reaction with CO, from a high potential form capable of resisting oxidation by the ferryl porphyrin π-radical cation, to a low potential form, which displays a lower reduction potential than ferric Fe_{a_3}. A copper complex which displays such a variation in reduction potentials seems improbable. Moreover, coupled with the expected resistance of heme A to reversible oxidation/reduction, we conclude that the reactive species trapped at the dioxy-

Figure 17

The structure of heme A.

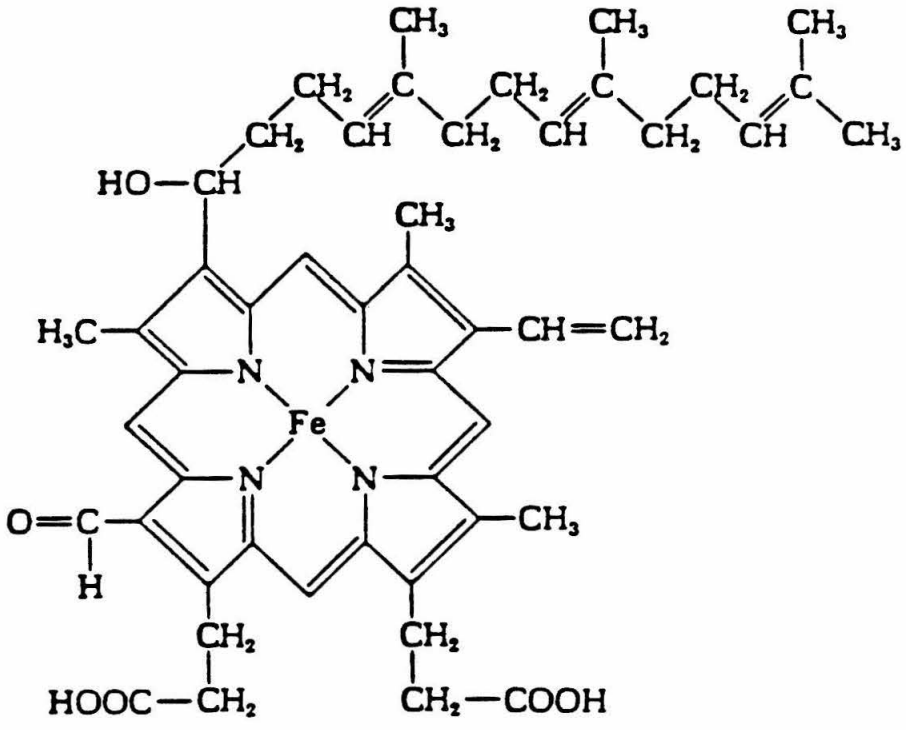
CH3
CH3
CH3
CH2
C
CH2
C
CH2
C
CH2
CH
CH2
CH
CH2
CH
CH3
HO—CH
CH3
H3C
CH=CH2
N
N
Fe
N
N
O=C
H
CH3
CH2
CH2
HOOC—CH2
CH2—COOH

gen reduction site in the 428/580 nm species is more convincingly explained by a ferryl Fe_{a_3}/cupric Cu_B binuclear couple.

An experiment to distinguish a ferryl Fe_{a_3}/cupric Cu_B binuclear couple from the alternate species, a ferryl heme A π-radical cation adjacent to cuprous Cu_B, should be mentioned. X-ray absorption edge measurements on the 428/580 nm species should be able to determine whether Cu_B is in the cupric or cuprous oxidation state.

"Oxygenated" Cytochrome c Oxidase. The work described in this chapter sheds light on the nature of the heterogenous reoxidized state of cytochrome *c* oxidase, referred to as the "oxygenated" enzyme. For several years it has been recognized that there are multiple forms of reoxidized cytochrome *c* oxidase. This was best exemplified by the early work of Okunuki and co-workers (43) and later by the work of Orii and King (29), who showed that when dithionite-reduced cytochrome *c* oxidase is reoxidized with dioxygen, three intermediates form in sequence at the dioxygen reduction site; the intermediates were designated by Orii and King as Compounds I, II and III, based on the order of their appearance. Collectively, these intermediates have been lumped together into a form of the enzyme termed the "oxygenated" enzyme. Compound I is characterized by an α band maximum in the reoxidized minus resting difference spectrum at 605 nm, Compound II has an α and β band at $\sim$ 578 and $\sim$535 nm in the difference spectrum and Compound III has two bands at 600 nm and 580 nm in the optical difference spectrum. Over the years there has been considerable speculation about the nature of the reoxidized species which comprise the oxygenated enzyme.

Recent experiments from several laboratories have clarified the relationship between the multiple forms of the reoxidized enzyme. Evidently, the heterogeneity observed in the oxygenated enzyme is related to the reduction procedure. Chance *et al.* recently suggested that significant levels of H_2O_2 may be generated *in situ*

by the reaction of O_2 with dithionite (18).* In fact, Kumar *et al.* (27) demonstrated that the reoxidation of the dithionite reduced enzyme, in the strict absence of hydrogen peroxide (which was accomplished by adding a trace amount of catalase), produced a homogeneous population of the EPR-detectable intermediate, originally reported by Beinert *et al.* (44). The addition of *excess* hydrogen peroxide (millimolar levels) to the pulsed enzyme resulted in the abolition of the unusual EPR resonances and a simultaneous shift in the Soret maximum from 424 to 428 nm (20). Coupled with these changes, there was a shift in the α band maximum in the difference spectrum from 605 nm to 580 nm, respectively (20). Interestingly, Kumar *et al.* showed that both the 420 nm and 428 nm forms of cytochrome *c* oxidase displayed enhanced catalytic activity in the presence of ferrocytochrome *c*, clearly establishing *both* forms as activated states of oxidized cytochrome *c* oxidase. Bickar (21) and later Wrigglesworth (19) showed that at micromolar levels of hydrogen peroxide another intermediate forms which exhibits a red-shifted Soret maximum and an α maximum in the difference spectrum at 606 nm and a less intense broad shoulder centered at 580 nm.

Three enzymatic states are produced at the dioxygen reduction site upon reoxidation of the reduced enyme depending on the concentration of H_2O_2 in solution, where we are disregarding the possible spectral differences which might arise due to different degrees of protonation of these three species. (In all three of the enzymatic states to be described, the low potential centers are oxidized.) The conditions under which these species are produced and the probable assignment of the redox states of Fe_{a_3} and Cu_B are summarized as follows.

(i) In the complete absence of H_2O_2, the pulsed enzyme is produced upon the reoxidation of the dithionite-reduced enzyme (27). Alternatively, the pulsed

* In a typical experiment in which optical spectroscopy is utilized, 0.1 mg of dithionite will give a ten-fold molar excess, although usually as much as 1 mg is actually added to samples.

form of the enzyme is also produced when stoichiometrically reduced cytochrome *c* oxidase is reoxidized with O_2, or even with porphyrexide (13). Based on the combined results from EPR (13,44), resonance Raman (23), EXAFS (45), and ligand binding studies of the pulsed enzyme (46), it has been concluded that the bridging ligand is absent in the pulsed enzyme, and that Fe_{a_3} is in the ferric oxidation state (S = 3/2) and is weakly superexchange (or dipolar) coupled to cupric Cu_B. In the absence of reducing equivalents, this reactive form of the enzyme eventually converts to the resting state of the enzyme (15).

ii(2) There is general agreement that at micromolar levels of H_2O_2 a true peroxidic adduct is produced at the binuclear dixoygen reduction site (19,21,32), although the exact nature of the coordination of the oxygen atoms to the metal centers at the binuclear site is not known (31) (Eqn. 3)

$$[Fe^{III}_{a_3}\ Cu^{II}_B] + H_2O_2 \rightleftharpoons [Fe^{III}_{a_3} - O - O - Cu^{II}_B] + 2H^+ . \qquad (3)$$

The EPR-silent peroxidic adduct prepared by the addition of micromolar concentrations of H_2O_2 to the pulsed or resting enzyme is spectroscopically identical to the species which is produced upon photolysis of the mixed-valence CO-inhibited state of the enzyme in the presence of O_2, which was termed Compound C by Chance and Leigh (12) (Eqn. 4). The peroxidic adduct, Compound C, is spectroscopically equivalent ot Compound I of Orii and King (29)

$$[Fe^{II}_{a_3} - CO\ Cu^{I}_B] + O_2 \rightleftharpoons [Fe^{III}_{a_3} - O - O - Cu^{II}_B] + CO . \qquad (4)$$

In our study, the addition of micromolar amounts of H_2O_2 to the pulsed enzyme produced a species with similar, but not identical, spectral features (in the difference spectrum) as those previously reported (19,21). We deduced that a sizeable population of the 428/580 nm species was not produced at low levels of hydrogen peroxide since the α band was observed at 600 nm, rather than at the expected position of 597-596 nm for a reasonable population of the 428/580 nm species. This discrepancy in the reported optical spectra of the peroxidic adduct, Compound C, may reflect different protonation states of the bridging peroxidic group.

(iii) At millimolar levels of H_2O_2 another intermediate is produced based on the shift of the α band in the reoxidized minus resting difference spectrum from 607 nm to ca. 580 nm upon the addition of excess H_2O_2 to Compound C (or the pulsed enzyme). This state of the enzyme is probably a major component of the oxygenated enzyme if excess dithionite is used (Compound II of Orii and King (29)), since substantial concentrations of H_2O_2 would be produced. There has been considerable speculation regarding the spin and redox states of Fe_{a_3} in this state of the enzyme. Wrigglesworth (19) suggested that Fe_{a_3} is a low-spin ferric complex in this derivative. Chance *et al.* (18) on the other hand suggested that cytochrome *c* oxidase was capable of a catalase-like reaction with hydrogen peroxide to generate a ferryl Fe_{a_3} porphyrin π-radical cation adjacent to cupric Cu_B; they designated this species as "pulsed-peroxide I". Our combined optical and EPR study demonstrated that the 428/580 nm species, produced upon the addition of excess H_2O_2 to the oxygenated or reduced enzyme, contains a reactive binuclear dioxygen reduction site, proposed to contain a ferryl Fe_{a_3}/cupric Cu_B couple, or another species at the same formal level of oxidation.

Ubiquity of the 428/580 nm Species

Wikström (47) has reported that when mitochondria are poised in a highly oxidized state with ferricyanide, the addition of ATP induces the formation of two intermediates which are similar, if not identical, to two of the intermediates that are formed when O_2 reacts with fully reduced cytochrome *c* oxidase. It was proposed that a partial reversal of the dioxygen reaction had occurred. The first intermediate Wikström observed upon stepwise reversal of the dioxygen reduction reaction displays an intense broad band centered at 580 nm in the difference spectrum (reoxidized minus resting) ($\Delta\epsilon_{580}$ = 6 mM^{-1} cm^{-1}).* The second intermediate had intense absorption at 607 nm, making it spectroscopically similar

* Personal communication from Prof. M. Wikström

to Compound C. Wikström (47) suggested that the 580-nm species was a one-electron oxidation product of ferric Fe_{a_3}/cupric Cu_B, namely, a ferryl Fe_{a_3}/cupric Cu_B couple. In the light of our results, this conclusion appears correct; evidently the 580/537 nm species may be produced either by reducing dioxygen by three electrons or by reversing the O_2 reaction by a single electron transfer step.

It is evident from this study that similar spectral features are produced in the α, β region of the difference spectrum (i) when partially reduced samples of cytochrome *c* oxidase are reoxidized with dioxygen; and (ii) upon the addition of excess H_2O_2 to the oxygenated enzyme, Compound C, and the fully reduced state of the enzyme. Similar spectral features in the absorption difference spectrum are also observed upon a one-electron reversal of the dioxygen reduction reaction as reported by Wikström (47) and upon reoxidation of the dithionite reduced state of cytochrome *c* oxidase (Compound II of Orii and King (29)). In addition, combined optical and EPR results revealed that the trapped, EPR-silent, three-electron-reduced dioxygen intermediate, as prepared by both methods (i and ii), reacts rapidly with CO at 277-298 K, causing the abolition of the spectral features at 580 and ~537 nm and the appearance of a rhombic Cu_B EPR signal. The same rhombic Cu_B EPR signal was previously observed to form at low temperatures, in the presence of 40 % ethylene glycol, upon the reaction of the second EPR-silent, three-electron-reduced intermediate with CO (3). Moreover, the reductive titration of the 428/580 nm state of cytochrome *c* oxidase demonstrated that the reactive binuclear dioxygen reduction site contains more oxidizing equivalents than the pulsed form of the enzyme. Based on these chemical and spectroscopic similarities, we conclude that the same reactive, EPR-silent, ferryl Fe_{a_3}/cupric Cu_B binuclear couple is formed at the dioxygen reduction site, when the reduced enzyme is reoxidized with O_2, and upon the addition of excess H_2O_2 to reduced (or oxygenated) cytochrome *c* oxidase.

In the previous chapter we showed that an EPR-silent, three-electron-reduced

intermediate is formed via intramolecular transfer of a third electron to the two-electron-reduced dioxygen intermediate (Compound C) from either Cu_A or Fe_a (3). In that study, the transfer of the third electron to the dioxygen reduction site at low temperature (180 K) first produced an EPR-detectable intermediate, suggested to be a ferrous Fe_{a_3}/cupric Cu_B hydroperoxide, which at higher temperatures (183-210 K) decayed to the EPR-silent intermediate, proposed to be a ferryl Fe_{a_3}/cupric Cu_B couple. In this chapter, we showed that the EPR-silent, three-electron-reduced intermediate is produced via an intermolecular reaction at the dioxygen reduction site with hydrogen peroxide. The reaction may involve either the one-electron reduction of the peroxidic adduct, Compound C, by hydrogen peroxide, or hydrogen peroxide may oxidize ferric Fe_{a_3} directly; both reactions involve the net one-electron oxidation of the binuclear dioxygen reduction site of cytochrome *c* oxidase to produce the proposed ferryl Fe_{a_3}/cupric Cu_B binuclear couple.

REFERENCES

1. Schulz, C.E., Devaney, P.W., Winkler, H., Debrunner, P.G., Doan, N., Chiang, R., Rutler, R. and Hager, L.P. (1975) *FEBS Lett.* **103**, 102-105.
2. Dunford, H.B. and Stillman, J.S. (1976) *Coordination Chem. Rev.* **19**, 187-251.
3. Blair, D.F., Witt, S.N. and Chan, S.I. (1985) *J. Am. Chem. Soc.* **107**, 7389-7399.
4. Karlsson, B. and Andréasson, L.-E. (1981) *Biochim. Biophys. Acta* **635**, 73-81.
5. Blair, D.F., Martin, C.T., Gelles, J., Wang, H., Brudvig, G.W., Stevens, T.H. and Chan, S.I. (1983) *Chemica Scripta* **21**, 43-53.
6. Hartzell, C.R. and Beinert, H. (1974) *Biochim. Biophys. Acta* **368**, 318-338.

7. Blair, D.F., Bocian, D.F., Babcock, G.T. and Chan, S.I. (1982) *Biochem.* **21**, 6928-6935.

8. Dawson, R.M.C., Elliot, D.C., Elliot, W.H. and Jones, K.M. (eds) (1969) in *Data for Biochemical Research* 2nd Ed., (Oxford Univ. Press, Oxford), p. 441.

9. Cotton, M.L. and Dunford, H.B. (1973) *Can. J. Chem.* **51**, 582-587.

10. Reinhammer, B., Malkin, R., Jensen, P., Karlsson, B., Andréasson, L.-E., Aasa, R., Vänngård, T. and Malmström, B. (1980) *J. Biol. Chem.* **255**, 5000-5003.

11. Aasa, R. and Vänngård, T. (1975) *J. Magn. Res.* **19**, 308-315.

12. Chance, B. and Leigh, J.S. (1977) *Proc. Natl. Acad. Sci. USA* **74**, 4777-4780.

13. Armstrong, F., Shaw, R.W. and Beinert, H. (1983) *Biochim. Biophys. Acta* **722**, 61-71.

14. Nicholls, P. and Chanady, G.A. (1981) *Biochim. Biophys. Acta* **634**, 256-265.

15. Brudvig, G.W., Stevens, T.H., Morse, R.H. and Chan, S.I. (1981) *Biochem.* **20**, 3912.

16. Hagen, W.R. (1982) *Biochim. Biophys. Acta* **708**, 82-98.

17. Brudvig, G.W., Morse, R.H. and Chan, S.I. (1986) *J. Magn. Res.* **67**, 189-201.

18. Chance, B., Kumar, C., Powers, L. and Ching, Y.C. (1983) *Biophys. J.* **44**, 353-363.

19. Wrigglesworth, J.M. (1984) *Biochem. J.* **217**, 715-719.

20 Kumar, C., Naqui, A. and Chance, B. (1984) *J. Biol. Chem.* **259**, 11668-11671.

21. Bickar, D., Bonaventura, J. and Bonaventura, C. (1982) *Biochem.* **21**, 2661-2666.

22. Erecińska, M. and Chance, B. (1977) *Arch. Biochem. Biophys.* **188**, 1-14.

23. Carter, K.R., Antalis, T.M., Palmer, G., Feris, N.S. and Woodruff, W.H. (1981) *Proc. Natl. Acad. Sci.* **78**, 1652-1655.

24. Bickar, D., Bonaventura, C. and Bonaventura, J. (1984) *J. Biol. Chem.* **259**,

10777-10783.

25. Brzezinski, P. and Malmström, B.G. (1985) *FEBS Lett.* **187**, 111-114.
26. Morgan, J.E., Blair, D.F. and Chan, S.I. (1985) *J. Inorg. Biochem.* **23**, 295-302.
27. Kumar, N., Naqui, A. and Chance, B. (1984) *J. Biol. Chem.* **259**, 2073-2076.
28. Aasa, R., Albracht, S.P.J., Falk, K.-E., Lanne, B. and Vänngård, T. (1976) *Biochim. Biophys. Acta* **422**, 260-272.
29. Orii, Y. and King, T.E. (1976) *J. Biol. Chem.* **251**, 7487-7493.
30. Schulz, C.E., Rutter, R., Sage, J.T., Debrunner, P.G. and Hager, L.P. (1984) *Biochemistry* **23**, 4743-4754.
31. Wikström, M., Krab, K. and Saraste, M. (1981) *Cytochrome Oxidase -A Synthesis* (Academic Press, NY), pp. 124-128.
32. Orii, Y. (1982) *J. Biol. Chem.* **257**, 9246-9248.
33. George, P. and Irvine, D.H. (1952) *Biochem. J.* **52**, 511.
34. Taube, H. (1986) *Prog. Inorg. Chem.* **34**, 607-625.
35. Harkness, A.C. and Halpern, J. (1961) *J. Am. Chem. Soc.* **83**, 1258.
36. Byerley, J.J. and Peters, E. (1969) *Can. J. Chem.* **47**, 313-321.
37. Bercaw, J.E., Goh, L.-Y. and Halpern, J. (1972) *J. Am. Chem. Soc.* **94**, 6534-6536.
38. Pyrz, J.W., Sage, J.T., Debrunner, P.G. and Que, L., Jr. (1986) *J. Biol. Chem.* **261**, 11015-11020.
39. Dolphin, D. (1981) *Israel J. Chem.* **21**, 67-71.
40. Groves, J.T., Haushalter, R.C., Nakamura, M., Nemo, T. and Evans, B.J. (1981) *J. Am. Chem. Soc.* **103**, 2884-2886.
41. Chan, S.I., Witt, S.N. and Blair, D.F. *Chemica Scripta, in press.*
42. Fee, J.A. (1975) *Structure and Bonding* **23**, 1-60.
43. Sekuzu, I., Tamemori, S., Yonetani, T. and Okunuki, K. (1959) *J. Biochem. (Tokyo)* **46**, 43-49.

44. Beinert, H., Hansen, R.E. and Hartzell, C.R. (1976) *Biochim. Biophys. Acta* **423**, 339-355.

45. Chance, B. and Powers, L. (1985) *Curr. Top. in Bioenerg.* **14**, 1-19, (Academic Press).

46. Brittain, T. and Greenwood, C. (1976) *Biochem. J.* **155**, 453-455.

47. Wikström, M. (1981) *Proc. Natl. Acad. Sci. USA* **78**, 4051-4054.

CHAPTER IV

A Resonance Raman Investigation of the Oxidized Forms of Cytochrome c Oxidase

Introduction

Based on a series of chemical results, in Chapter III we established that a reactive, EPR-silent, three-electron-reduced species is trapped at the binuclear dioxygen reduction site of cytochrome *c* oxidase upon the addition of excess H_2O_2 to the reduced or oxygenated enzyme. Following the reoxidation of the reduced enzyme, the activation of the pulsed enzyme by hydrogen peroxide was proposed to occur, with the formation of a ferryl Fe_{a_3}/cupric Cu_B binuclear couple (Eqns. 1-2)

$$[Fe^{III}_{a_3}\ Cu^{II}_B]\ + H_2O_2 \rightleftharpoons [Fe^{III}_{a_3} - O\ - O\ - Cu^{II}_B]\ + 2H^+ \qquad (1)$$

$$\textit{excess}\ H_2O_2\ + [Fe^{III}_{a_3} - O - O - Cu^{II}_B] \longrightarrow [Fe^{IV}_{a_3} = O\ Cu^{II}_B(OH)]\ + HO_2\ . \qquad (2)$$

Of the three cytochrome *c* oxidase intermediates depicted in Equations 1 and 2, only the pulsed enzyme ($[Fe^{III}_{a_3}\ Cu^{II}_B]$) has EPR resonances which are assigned to one of the metal centers at the dioxygen reduction site. Unfortunately, no

EPR resonances are observed from Fe_{a_3} or Cu_B in either Compound C or the 428/580 nm species; therefore, another spectroscopic method was needed to probe the structure of the binuclear dioxygen reduction site for the latter two EPR-silent species. In this chapter we describe our recent resonance Raman (RR) investigation of three reactive forms of cytochrome *c* oxidase, in which the low potential centers (Fe_a and Cu_A) are oxidized: (i) the pulsed form of cytochrome *c* oxidase, (ii) the peroxidic adduct, Compound C, and (iii) the 428/580 nm species. These three states of cytochrome *c* oxidase are quite reactive and typically decay to the resting enzyme; therefore, in order to retard the rate of conversion to the resting state of the enzyme, each reactive form of the enzyme was examined at low temperature (~150 K). By this procedure we were able to obtain high quality resonance Raman spectra. Herein we report the first resonance Raman spectrum of a nearly homogeneous population of the 428/580 nm species, which displays novel spectral features that may be unambiguously assigned to a low-spin Fe_{a_3} species. The low frequency iron-oxygen vibrational mode, ν(FeO), which is sensitive to isotopic substitution, was not detected in these experiments. However, the frequencies and intensities of the skeletal modes of Fe_{a_3} (cytochrome a_3) in the spectrum of the 428/580 nm species provide support for the assignment of a low-spin (S = 1) ferryl Fe_{a_3} at the dioxygen reduction site of the 428/580 nm species, although we cannot rule out a low-spin ferric Fe_{a_3} species. Models for the reactive binuclear dioxygen reduction site of the 428/580 nm species are discussed which are consistent with these two alternative species.

Resonance Raman Spectroscopy

Resonance Raman spectroscopy is a powerful spectroscopic technique which has provided important structural information for heme enzymes such as myoglobin, hemoglobin, and cytochrome *c* oxidase. Unlike infrared spectroscopy on biological molecules, in which the allowed vibrations arising from the entire ensemble of amino acids and prosthetic groups are observed, in resonance Raman

spectroscopy only those vibrations are enhanced which contribute intensity to the electronic absorption (1). Because only vibronically active modes are resonance enhanced, great selectivity is achieved. The theory of Raman and resonance Raman has been thoroughly reviewed (1-3). The great utility of resonance Raman as a structural probe of heme proteins is that the vibrational modes of the porphyrin are sensitive to the redox and spin state of the iron, and thus provide an *indirect* probe of these aspects of the metal center. To understand what information regarding the iron center may be extracted from an analysis of the high frequency vibrational modes of the porphyrin macrocycle, we must first describe some of the optical properties of porphyrins and then the mechanism by which the iron interacts with the porphyrin.

A remarkable number of proteins contain iron porphyrin (heme) as a prosthetic group. These heme proteins function in such disparate roles as (i) oxygen carriers, (ii) electrons carriers and (iii) oxygen activators. Despite their functional diversity, heme proteins have common optical absorption features since they all contain a heme chromophore. These common spectroscopic features are summarized as follows. Two purely electronic transitions ($(0\rightarrow0)\pi\rightarrow\pi^*$) of the porphyrin dominate the optical spectrum of heme proteins (4). The higher energy transition is referred to as the Soret band ($\epsilon\sim10^5$ M^{-1} cm^{-1}) and typically occurs near 400 nm. The less intense electronic transition, designated the α band, is observed at approximately 550 nm ($\epsilon\sim10^4$ M^{-1} cm^{-1}). Usually, porphyrins also exhibit a weak absorption band $\sim$1300 cm^{-1} higher than the α band, which arises from a vibronic transition ($(0\rightarrow1)\pi\rightarrow\pi^*$); this band is referred to as the β band. Cytochrome *c* oxidase is unusual because its Soret (420 nm), α (600 nm), and β ($\sim$580 nm) bands fall at much lower energy than for most heme proteins (5). It is now appreciated that the formyl substituent extends the conjugation of the heme A macrocycle, thereby lowering the energy of the electronic transitions (6). Because our experiments employed Soret excitation, we must now consider the porphyrin

vibrations that are vibronically active, *i.e.*, which contribute to the intensity of the Soret absorption band.

When Soret excitation is used in resonance Raman studies of heme proteins, intense scattering is observed from totally symmetric vibrational modes of the porphyrin (1). According to Champion and Albrecht (7), the totally symmetric vibrational modes derive intensity from two different scattering processes, referred to as *A*-term and *B*-term sources (see Spiro, ref. 1). The x,y polarized Soret electronic states undergo *B*-term coupling with similarly polarized electronic states of the α-band, where the strength of the coupling depends on the product of the transition dipoles of the electronic states to be mixed (7). In this report, we will be examining the vibrational modes of the porphyrin in the high frequency region between 1200-1700 cm^{-1} because these modes are sensitive to the spin state and oxidation state of the iron. In this spectral region, the porphyrin vibrations are due mainly to in-plane C-C and C-N stretching motions of the porphyrin (8-9). Two vibrational modes in particular have been implicated as being sensitive indicators of the redox and spin state of the iron; these porphyrin skeletal modes are referred to as ν_4 and ν_2, respectively. The frequency of the oxidation state marker band, ν_4, is thought to be inversely related to the electron population in the vacant porphyrin π^* molecular orbitals (8,10,11). Importantly, the electron population in the π^* molecular orbitals may be increased as a result of backbonding from the iron d-π orbitals: as the electron population in the π^* molecular orbitals increases, the C-C and C-N bonds weaken and thus the vibrational frequency decreases. Because the extent of backbonding between the iron and the porphyrin is greatest for Fe(II) and the least for Fe(IV), the vibrational frequency of ν_4 tends to increase in the following manner: $\nu_4(Fe^{IV})>\nu_4(Fe^{III})>\nu_4(Fe^{II})$. It is also known that the frequency of the oxidation state marker band is also affected by any ligands to the iron which are strong π acids, such as O_2 and CO, because these ligands compete with the porphyrin π^* molecular orbitals for electron density from the metal d-π

orbitals. The normal mode which is sensitive to the oxidation state of the metal is depicted in Figure 1. Diagnostic values for ν_4 are 1358 cm^{-1} (PFe^{II}), 1372 cm^{-1} (PFe^{III}), and 1380 cm^{-1} (PFe^{IV}) (12).

It is generally recognized that the frequency of all porphyrin skeletal modes above 1450 cm^{-1} are influenced by the core size of the porphyrin, that is, the C_t-N (center-to-pyrrole-nitrogen) distance (13). In fact, Spiro and Strekas (8) demonstrated that there is a negative linear dependence on the C_t-N distance and the frequency of the skeletal mode. It is also well known that the spin state of the iron will have a profound effect on the core size of the porphyrin (13). For example, when ferric iron is stabilized in the high-spin state by a weak field ligand such as fluoride, the five d electrons are distributed over the five d-orbitals. Occupation of the $d_{x^2-y^2}$ orbital will result in a measurable expansion of the porphyrin core because this orbital is antibonding and is directed at the four pyrrole nitrogen atoms. An increase in the core size results in a weakening of the force constants of the bonds that comprise the porphyrin backbone, which lowers the frequency of the vibrational mode. In contrast, when ferrous or ferric heme is stabilized in the low-spin state by a strong field ligand, only the d-π orbitals are occupied, which are directed away from the ligands. Under this condition usually the metal ligand bonds are quite strong and the core is contracted because no antibonding electrons are directed at the pyrrole (and axial) ligands, and thus the frequency of the vibrational mode is increased in energy relative to the high-spin case. The normal mode (ν_2) which is sensitive to the spin state of the iron is depicted in Figure 1. Diagnostic values for this mode are: ~1572 cm^{-1} (high-spin) and ~1590 cm^{-1} (low-spin).

Resonance Raman investigations of cytochrome *c* oxidase have made important contributions to our understanding of the spin and redox states of Fe_{a_3} and Fe_a in a variety of different states of the enzyme (14-15). (We will continue to refer to the two iron centers of cytochrome *c* oxidase as Fe_{a_3} and Fe_a in this chapter,

Figure 1

Schematic depiction of the structure-sensitive normal vibrational modes of a symmetric metalloporphyrin (8). The oxidation state marker band (ν_4) is due to mainly C-N stretching (*a*). The core-size marker mode (ν_2) is primarily due to the asymmetric stretch of the α-methine carbon (C_m) bonds of the porphyrin (*b*). The heme A macrocycle is shown in *c*.

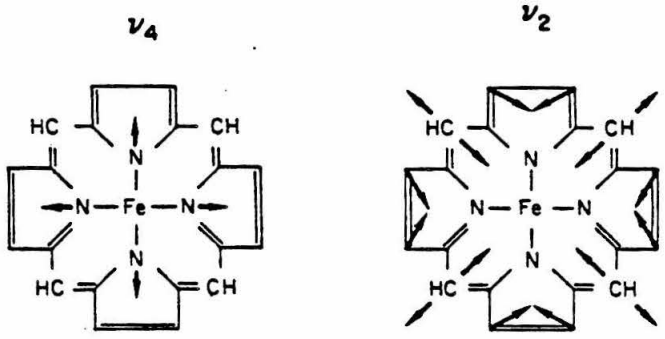

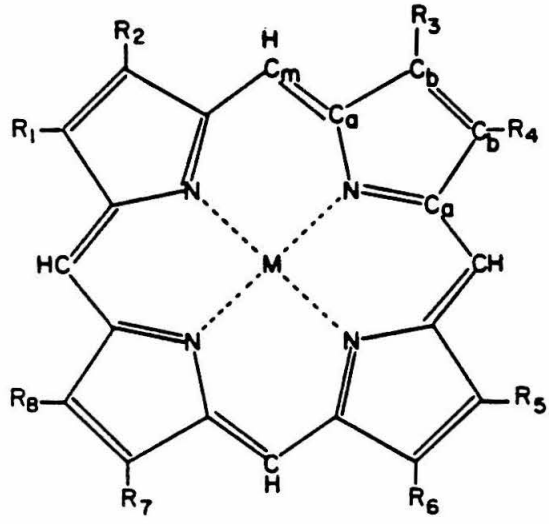

Me = CH_3

I = isoprenoid chain ($C_{17}H_{29}O$)

V = $C_\alpha H{=}C_\beta H_2$

P = C_2H_4COOH

C = COH

	R_1	R_2	R_3	R_4	R_5	R_6	R_7	R_8
heme A	Me	I	Me	V	Me	P	P	C

even though this terminology deemphasizes the fact that both iron centers are embedded within a porphyrin macrocycle. We stress, however, that the designations Fe_a and Fe_{a_3} refer to not only the iron centers but to the heme A macrocycles as well.) Significantly, Fe_a and Fe_{a_3} have distinct absorption envelopes in the Soret and α regions of the absorption spectrum, with Soret maxima at 414 and 426 nm for Fe_{a_3} and Fe_a, respectively, in the resting enzyme (16). There are important implications of the distinct absorption maxima of Fe_a and Fe_{a_3}. By a judicious choice of excitation frequency, the vibrations due to either Fe_a or Fe_{a_3} may be selectively enhanced. When 406.7 nm excitation frequency is employed, selective enhancement of the vibrational modes associated with Fe_{a_3} is achieved because Fe_{a_3} has the dominant spectral contribution at 406.7 nm, whereas when a 441.4 excitation wavelength is employed, a selective enhancement of the vibrational modes of Fe_a is achieved since Fe_a has the predominant absorption in that region of the absorption spectrum of the resting enzyme. In contrast, if the absorption bands of Fe_a and Fe_{a_3} overlap significantly, as is the case when ferric Fe_{a_3} is stabilized in the low-spin state by the appropriate strong field ligand, then both hemes will contribute to the resonance Raman spectrum when 406.7 nm (or 428 nm) excitation is used.

MATERIALS and METHODS

Cytochrome *c* oxidase was isolated by the method of Hartzell and Beinert (17) and was dissolved in 50 mM phosphate buffer containing 0.5 % Tween-20 at pH 7.4. The enzyme was stored at 193 K prior to use. Isolated, detergent-solubilized cytochrome *c* oxidase typically displayed an activity of ca. 125 moles ferrocytochrome *c* reoxidized/mole of cytochrome *c* oxidase/sec. The concentration of the enzyme was determined spectrophotometrically ($\Delta\epsilon^{r-o}$(604 nm) = 24 mM^{-1} cm^{-1}). For some of the resonance Raman experiments the enzyme was dialyzed into D_2O (Cambridge Isotope, 99.9 %) buffered with 50 mM phosphate (0.5 % Tween-20) at pD = 7.8-8.2.

Sample Preparation. All samples for resonance Raman were contained in 4 mm O.D. quartz EPR tubes, and samples were deoxygenated by 6-7 cycles of evacuation followed by the addition of one atmosphere of argon, which had been deoxygenated by passage through a 1 m column column containing manganous dioxide supported on vermiculite. After each flushing cycle, the sample was allowed to incubate at ice temperature for ca. 10 min. Cytochrome *c* oxidase samples were reduced by adding stoichiometric amounts of NADH (Sigma), containing no mediator. The NADH was thoroughly deoxygenated by the procedure outlined above, and the concentration of the NADH was determined spectrophotometrically ($\epsilon(330\ \text{nm}) = 6220\ \text{M}^{-1}\ \text{cm}^{-1}$. Samples were incubated from 48-65 h at 277 K to ensure complete reduction . Enzyme concentration was typically 300 μM.

The preparation of the 428/580 nm species was accomplished by the addition of excess H_2O_2 (4-6 mM) to samples of the fully reduced enzyme. After a brief incubation period with H_2O_2 (~60 sec), a trace amount of catalase (Sigma, C-10) was was added to quench the excess H_2O_2, and the samples were then immediately frozen to 77 K by immersion into liquid nitrogen. Typically, the interval from the reoxidation of the samples to freezing was approximately 120-150 sec. Alternatively, if an optical spectrum was recorded after the addition of catalase, the interval from the initial reoxidation to freezing was ca. 240-270 sec. Samples of the 428/580 nm species typically displayed a Soret maximum at 427-428, a blue-shifted α band at 595-596 nm, with an intene band at ~580 nm in the reoxidized minus resting difference spectrum. Hydrogen peroxide solutions were prepared by diluting 30 % H_2O_2 (Baker) into a solution of phosphate buffer containing 1 mM EDTA (Baker). An enzymatic method, which utilizes horse radish peroxidase (Boerringer Mannheim), was used to determine the concentration of the H_2O_2 stock solution (18). The brief treatment of the reduced enzyme with excess hydrogen peroxide did not significantly perturb the pH of the enzyme solution. For example, a resting sample of cytochrome *c* oxidase initially buffered

to pH 7.35 exhibited no change in pH (or a small decrease ΔpH = 0.06) after the addition of excess H_2O_2 to the NADH-reduced enzyme (or the dithionite-reduced enzyme).

The pulsed form of cytochrome *c* oxidase and the peroxidic adduct, referred to as Compound C, were prepared by the following procedures. Fully reduced samples of cytochrome *c* oxidase were reoxidized with 1 atm of O_2 and then immediately frozen to 77 K (~60 sec from the addition of O_2). Low temperature EPR measurements verified that the reoxidized samples exhibited the unusual EPR resonances at $g = 5$, 1.79, and 1.7, which are diagnostic features of the pulsed enzyme. Typically, our samples of the pulsed enzyme displayed a Soret maximum at 424 nm with a symmetric band in the reoxidized minus resting difference spectrum at 600 nm. Samples of Compound C were prepared by two different procedures. (i) Upon the addition of 1-2 equiv H_2O_2 to the pulsed enzyme, the peroxidic adduct is produced (19-20). After the addition of near stoichiometric amounts H_2O_2 to the pulsed enzyme, the samples were immediately frozen to 77 K and examined by EPR. Samples produced by this procedure displayed only EPR resonances from Fe_a^{III} and Cu_A^{II}, at their expected intensities. Furthermore, the diagnostic EPR resonances associated with the pulsed enzyme were abolished by the addition of the H_2O_2. No unusual EPR resonances associated with either Fe_{a_3} or Cu_B were observed. Samples of the peroxidic adduct prepared by this procedure exhibited a Soret maximum at 427-428 nm with a moderately intense band at 602-604 nm in the reoxidized minus resting difference spectrum. (ii) The peroxidic adduct may also be prepared by the addition of 1 atm of O_2 to the mixed-valence CO-inhibited state of the enzyme (MV-CO) (Fe_a^{III}, Cu_A^{II}, $Fe_{a_3}^{II}$-CO, Cu_B^{I}) (21-22). It is well known that carbon monoxide reduces resting cytochrome *c* oxidase, and that under anaerobic conditions, the MV-CO state of the enzyme is produced (23). To prepare the MV-CO state of cytochrome *c* oxidase, 1 atm of CO (Matheson, 99.99 %) was added to samples of the deoxygenated enzyme. Complete formation

of the MV-CO-inhibited species was achieved after a 24 hour incubation at 273 K. (During the incubation period the samples were kept in the dark.) Finally, 1 atm of O_2 was admitted to the MV-CO samples and the samples were subjected to a brief period (~30 sec) of irradiation with intense visible light (200 W Hg-Xe Oriel Lamp) in order to photolyze carbon monoxide from ferrous Fe_{a_3}. Evidently, following photolysis, dioxygen enters the binuclear dioxygen reduction site and is reduced to the level of peroxide (Fe_a^{III}, Cu_A^{II}, $Fe_{a_3}^{III}$-O-O-Cu_B^{I}). Samples of the peroxidic adduct produced by this procedure typically displayed a Soret maximum at 424 nm with an intense band at 607 nm in the reoxidized minus resting difference spectrum.

An aqueous solution of isotopically labeled hydrogen peroxide ($H_2{}^{18}O_2$) was synthesized by the reaction of $^{18}O_2$ (ICON, 98 %) with 2-ethylanthrahydroquinol, which was prepared by the *in situ* catalytic hydrogenation (Pt/charcoal) of 2-ethylanthraquinone (24). We found that it was essential to remove the Pt/charcoal catalyst from the solution of 2-ethylanthrahyroquinol prior to the addition of the $^{18}O_2$, otherwise only low yields of the isotopically labeled hyrogen peroxide were produced (~5-10 mM). The Pt/charcoal was removed from the solution by filtration under vacuum through a fine frit. After reoxidation of the 2-ethylanthraquinol, which was free of the Pt catalyst, approximately 6 ml of H_2O (or D_2O) (50 mM phosphate buffer at pD = 8, 1 mM EDTA) was added to the final reaction mixture to extract the hydrogen peroxide from the organic phase. It was essential to remove residual organic compounds from the solution of hydrogen peroxide, otherwise the reduced enzyme was not completely activated to the 428/580 nm state, probably as a result of reduction of the reactive binuclear site by the residual organic compounds. Isotopically labeled hydrogen peroxide was purified by passage through a short (5 cm) C_{18} (octadecyl bonded to silica, Baker) column. The isotopic enrichment of the $H_2{}^{18}O_2$ was determined by Raman spectroscopy ($\geq$95 % $H_2{}^{18}O_2$), and the concentration of the hydrogen peroxide

(46 mM) was determined by the enzymatic assay described above. Aliquots of the isotopically labeled hydrogen peroxide were stored at 193 K until ready for use.

A special cylindrical sample holder was used to hold the EPR tubes in place during the optical measurements. Due to the intense absorbance of the samples, transmittance filters (16-50 %) were used to attenuate the reference beam. Optical spectra were recorded on a Beckman Acta CIII which was interfaced to a Spex Industries SC-31 SCAMP data processor. Samples were maintained at 273 K throughout the sample manipulations and when optical spectra were recorded.

Resonance Raman. In the resonance Raman experiments to be described, a polarization scrambler was used so that unpolarized scattering was detected. When resonance Raman spectra were obtained from liquid samples, the sample was maintained at ca. 277 K by passing a chilled stream of gaseous nitrogen over the sample. Resonance Raman spectra were obtained from spinning samples employing a 90 degree scattering geometry. Spectra were recorded on a Spex 1401 scanning monochrometer with an RCA 31034 C photomultiplier tube using ~3mW of incident power at 406.7 nm (Spectra-physics model 164 Kr ion laser). Laser power was measured with a Coherent Radiation power meter (Model No. 210).

Resonance Raman spectra were also obtained from frozen samples, which were maintained from 193 to 148 K by a steady stream of chilled gaseous nitrogen. In order to avoid prolonged irradiation of only one face of the sample (contained in the EPR tube), the sample was continuously rotated during the irradiation period (45-200 min). This low temperature system utilized a 135 degree backscattering geometry. Typical incident powers were ca. 5 mW. The data collection time varied with each sample and are noted in the individual figures. None of the spectra were smoothed, although a linear sloping baseline was subtracted from the raw data. Some of the spectra exhibit unusual baselines. This is a consequence of subtracting a linear baseline from spectra which displayed large non-linear fluorescence backgrounds. Subtraction of a linear baseline did not introduce artifacts

into the spectra since the peak positions remained unchanged from the raw data. The spectral resolution is 6 cm^{-1}, and the uncertainty in peak positions is $\pm$ 1 cm^{-1}.

RESULTS

Previous studies have demonstrated that cytochrome *c* oxidase undergoes facile photoreduction when irradiated with Soret excitation, even when relatively low powers are employed (20 mW) (14,25). Because the pulsed enzyme, Compound C, and the 428/580 nm species contain reactive binuclear sites, prior to the examination of these intermediates by resonance Raman it was crucial to establish the requisite experimental conditions necessary to prevent photoreduction.

Resonance Raman spectra of the resting cytochrome *c* oxidase in the liquid state (273 K) and the solid state (153 K), are shown in Figure 2*a* and 2*b*. The use of 25 mW incident power induced extensive photoreduction as demonstrated by the dominant peaks at 1610 and 1622 cm^{-1}. These two bands have been previously assigned to vibrational modes of ferrous Fe_a, and have been observed under conditions where partial reduction of the enzyme occurred (14). In fact, the spectra in Figure 2 resemble the resonance Raman spectra of the formate-inhibited enzyme in the presence of mild reducing agents, which is known to consist of a high-spin ferric Fe_{a_3} and low-spin ferrous Fe_a. Even though Fe_a was probably entirely reduced, the oxidation state marker band (ν_4) at ~1370 cm^{-1} is still rather similar to that of the resting enzyme (1372 cm^{-1}). This is because with 406.7 nm excitation, the oxidation state marker band of Fe_a is not significantly enhanced. According to Babcock *et al.* (14), the oxidation state marker band is not a reliable indicator of photoreduction; therefore, we consistently monitored the spectral region near 1610-1625 cm^{-1} to ascertain whether photoreduction occurred in these experiments.

The peak positions of the vibrational bands observed in the RR spectrum of the frozen photoreduced sample, and the peak assignments are listed in Table I,

Figure 2

High frequency resonance Raman spectra of photoreduced cytochrome *c* oxidase at 273 K (*a*) and at 153 K (*b*). Conditions: excitation wavelength, 406.7 nm; laser power, 25 mW; scan rate, 1sec/1cm^{-1} (*a*,*b*); number of scans, 1 (*a*,*b*).

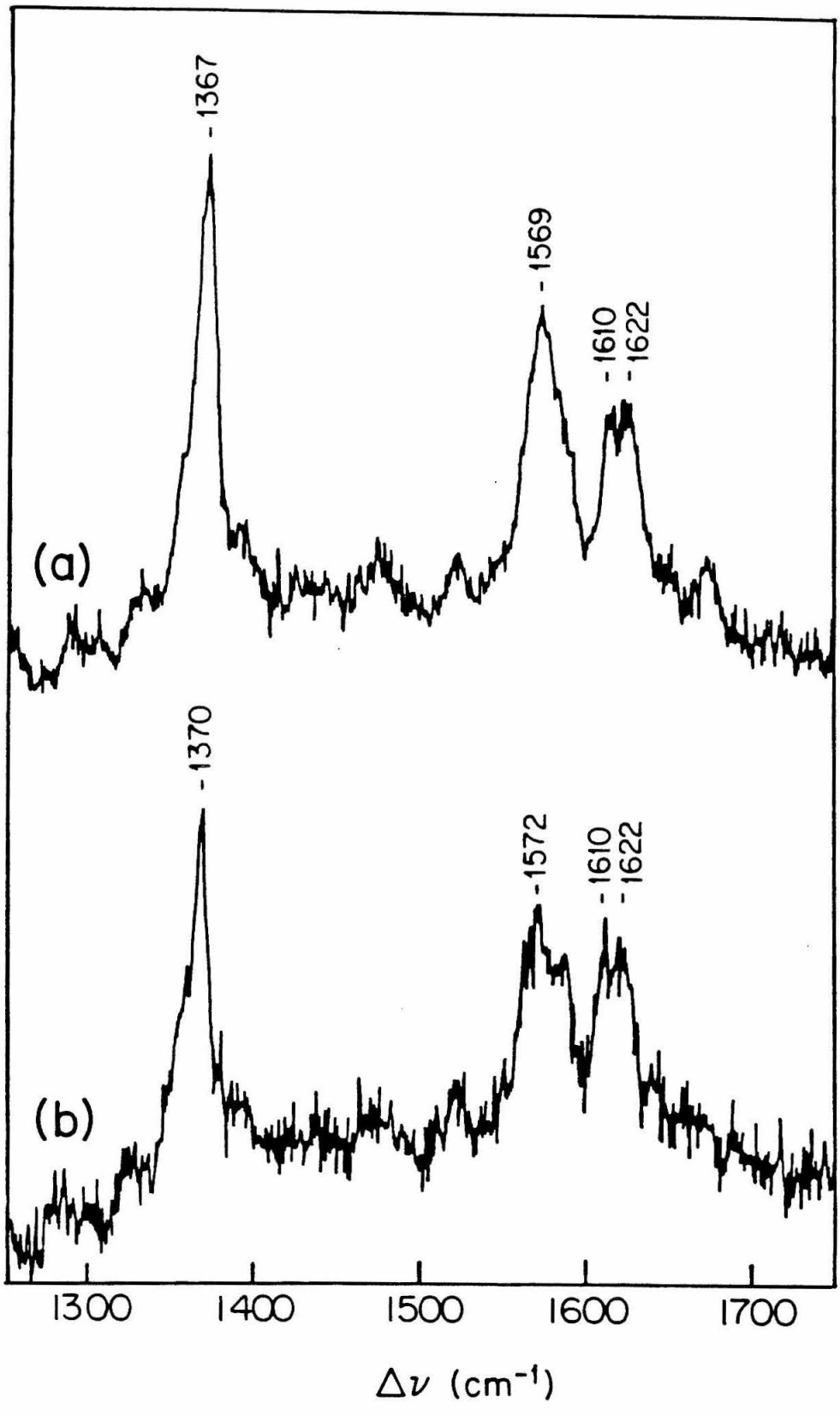
1367
1569
1610
1622
(a)
1370
1572
1610
1622
(b)
1300
1400
1500
1600
1700
Δν (cm⁻¹)

TABLE I

Soret excitation resonance Raman peaks (cm^{-1}) and assignments for the oxidized states of cytochrome *c* oxidase, i.e., resting, photoreduced, pulsed, Compound C, and the 428/580 nm species (580 nm). Data from low temperature study (150 K).

Soret Excitation Raman Peaks (cm-1) (frozen Samples)

Assignment	Resting	Photo-reduced	Pulsed	Cmpd C	580 nm
ν (C=O) a_3	1675	1672	1677	1675	1676
		1661			
ν_{10} (ls) +	1647	1640	1648	1650	1647
ν (C=O..H)			1645	1644	
ν (C=O) a^{II}		1622			
?	1625			1628	
ν_{10} (hs) a_3	1612	1610	1616	1613	
ν (C=O) a^{II} (ls)		1610			
+ ν_{10} a_3^{II}					
ν_2 (ls)	1589	1585	1595	1594	1595
ν_2 (hs) a_3	1575	1572	1573	1577	
?	1562	1551		1565	1562
ν_{11}	1511	1523	?1520	?1519	
ν_3 (ls)	1504		1504	1506	1505
ν_3 (ls) a_3		1482	1481	1488	
ν_{28}	1472	1471	1472	1478	1479
?	1439	1440	1437	1436	1440
?	1395	1394	1397	1395	1395
ν_4	1372	1370	1375	1374	1377
		1360	1364		
?	1335	1327	1338	1338	1337
?	1303	1302	1310	1309	1309
?	1289	1284	1284	1291	1291
?	1246		1250	1249	1253
?	1225		1228	1225	1225

Assignments are based on those of Choi et al. (1983) and Babcock (1986) according to the scheme of Abe *et al.* (1978).
a = cytochrome a heme, a_3 = cytochrome a_3 heme
Note: Rows without labels are a continuation of the one above and indicate 2 peaks with the same assignment (i.e., a_3 and a or inhomogeneous samples). (ls) = low-spin; (hs) = high-spin.

TABLE II

Heme A model compound data (reference 30).

Heme A Model Compounds* (cm^{-1})

(λ_{ex} = 406.7nm)

	Fe(II)		Fe(III)		
Mode	6 coordinate (low-spin)	5 coordinate (high-spin)	6 coordinate (low-spin)	6 coordinate (high-spin)	5 coordinate (high-spin)
$\nu C=O$	1642	1660	1670	1672	1576
$\nu C=O\ldots H_2O$	1633	1640	1656	-----	1656
$\nu C=C$	1622	------	------	------	------
ν_{10}	------	1607	1642	1615	1632
ν_{37}	1605	1565	------	------	------
ν_2	1587	1578	1590	1572	1581
ν_{19}	1583	------	------	------	------
$\nu_{38\,(1)}$	1563	------	------	------	1540
$\nu_{38\,(2)}$	------	------	------	------	1520
ν_{11}	1511	------	------	------	------
ν_3	1493	1473	1506	1482	1492
ν_{28}	1468	1455	1474	------	------
$\nu_{29/20}$	1391	1394	------	------	------
ν_4	1360	1357	1374	1373	1374
$\delta S=CH_2$	1329	1333	------	------	------
ν_{21}	1307	1314	1312	------	------

*Babcock, G.T. (1986) Biological Applications of Raman Spectroscopy (Spiro, T. ed.) Wiley, New York, in press.

along with the samples to be described below. Vibrational assignments are based on those of Abe *et al.* (26) and Choi *et al.* (27). For comparison, peak positions and assignments for the vibrational modes of heme A model compounds are listed in Table II. Our initial characterization of the resting enzyme revealed that it was necessary to use incident powers of 5 mW or less to avoid photoreduction.

High frequency resonance Raman spectra of resting cytochrome *c* oxidase, obtained with low incident power (~3 mW), are shown in Figure 3. The RR spectrum of the liquid sample (273 K) (Fig. 3*a*) is in agreement with previous reported studies of the resting enzyme (14,15,28). Vibrational modes from both heme centers are observed in the spectrum of the resting enzyme; however, several bands from Fe_{a_3} are more prominent (1372, 1572, and 1676 cm^{-1}) because its absorption band is in better resonance with the 406.7 nm excitation line than the low-spin ferric Fe_a (29). The frequency of ν_4 (1372 cm^{-1}) is consistent with a ferric Fe_{a_3} complex (Table II). A weak band is observed at approximately 1503 cm^{-1}, which has been assigned to a skeletal vibration (ν_3) of Fe_{a_3} (30). This band is a useful indicator of spin state. A comparison of the frequency of this band to the model compound data in Table II indicates that the band arises from a population of six-coordinate low-spin ferric heme (Fe_{a_3}). The intense band at ~1575 cm^{-1} (ν_2) is another skeletal mode of the Fe_{a_3} which is sensitive to the spin state of the iron (29). Inspection of the model compound data in Table II shows that the frequency of ν_2 is consistent with a six-coordinate ferric heme stabilized in the high-spin state. The band at 1649 cm^{-1} is a composite of several vibrational modes arising from Fe_a (30), whereas the band at 1676 cm^{-1} is the $\nu_{(C=O)}$ mode of Fe_{a_3} (29). Taken together, the frequencies and intensities of the skeletal modes in the high-frequency RR spectrum of the resting enzyme are consistent with the assignment of Fe_{a_3} as a six-coordinate, ferric high-spin complex, with only a minor subpopulation of low-spin species at the dioxygen reduction site, as evidenced by the negligible intensity of the mode at ~1505 cm^{-1}.

Figure 3

High frequency resonance Raman spectra of resting cytochrome *c* oxidase at 273 K (*a*) and at 153 K (*b*). Conditions: excitation wavelength, 406.7 nm; laser power, 3 mW; scan rate, 1sec/1cm^{-1} (*a*), 3sec/1cm^{-1} (*b*); number of scans, 1 (*a*), 3 (*b*).

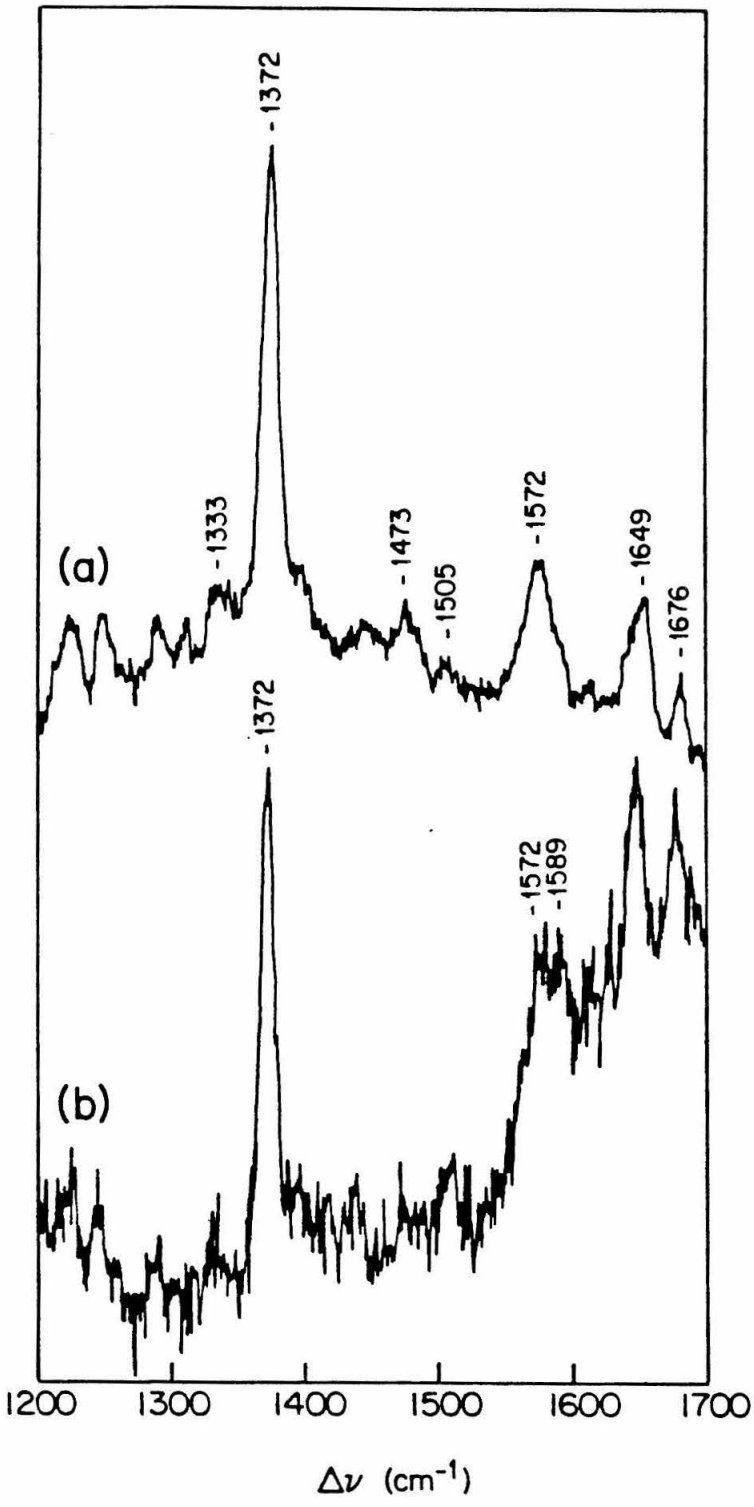
(a)
1372
1333
1473
1505
1572
1649
1676
(b)
1372
1572
1589
1200
1300
1400
1500
1600
1700
Δν (cm⁻¹)

A low-temperature RR spectrum of resting cytochrome *c* oxidase is shown in Figure 3b. Although the fluorescence background is much greater in the spectrum of the frozen sample, which resulted in a large non-linear sloping baseline, the low-temperature spectrum (153 K) of the resting enzyme retained several of the spectral features which are observed in the spectrum of the resting enzyme recorded at ice temperature. There were also some changes evident in the spectrum of the frozen sample relative to the spectrum of the liquid sample: (i) The band centered at 1648 cm^{-1}, which is a composite of several modes, is more symmetric and narrower than in the corresponding spectrum of the resting enzyme in the liquid state, (ii) the 1675 cm^{-1} peak, assigned to the formyl group associated with Fe_{a_3}, has increased in intensity, and (iii) there is more pronounced intensity at 1589 cm^{-1}, which is indicative of increased scattering from a low-spin ferric Fe_{a_3} species (Table II). A comparison of the spectrum of the frozen resting enzyme (Fig. 3*b*) to the spectra in Figure 2*a*,*b* shows that the extent of photoreduction was in fact negligible when low incident powers were utilized. Overall, the spectrum of the frozen sample was encouraging and indicated that most of the details observed from liquid samples are also observed when the samples are frozen.

Low-Temperature, High Frequency RR Spectra of Reactive Cytochrome c Oxidase Species. Our low-temperature RR spectra of the pulsed form of cytochrome *c* oxidase, the peroxidic adduct, Compound C, and the 428/580 nm species are shown in Figures 4, 5, and 6. To our advantage, we found that samples could be irradiated for an entire day without undergoing photoreduction if the samples were maintained at ca. 150 K, with low incident power (3-5 mW). In some cases we examined the reactive enzymatic species at 277 K and found that either rapid photoreduction occured during the course of the scanning, or the reactive intermediate converted to a more stable form of the enzyme, such as the resting enzyme, during the time period required to obtain the data (8-20 min).

We now focus attention on the low-temperature, high frequency RR spectra of these reactive states of cytochrome *c* oxidase.

Pulsed Cytochrome c Oxidase. Our high frequency resonance Raman spectrum of the pulsed form of cytochrome *c* oxidase is shown in Figure 4*a*. For comparison, the RR spectra of Compound C and resting cytochrome *c* oxidase are included in Figure 4. With 406.7 nm excitation of the pulsed enzyme (and Compound C), we expect selective enhancement of the vibrational modes of Fe_{a_3} since its absorption spectrum is in better resonance with the excitation wavelength than the absorption spectrum of Fe_a. Therefore, the vibrational modes ν_4, ν_3, and ν_2 probably are due primarily to Fe_{a_3}. The peak positions and the vibrational assignments for the different states of the enzyme shown in Figure 4 are tabulated in Table I.

We consistently observed that the pulsed enzyme displayed weaker Raman scattering than the resting enzyme, under identical conditions of enzyme concentration and incident power. The intense oxidation state marker band at 1375 cm^{-1} indicates that Fe_{a_3} is in the ferric oxidation state in the pulsed enzyme (Fig. 4*a*). A comparison of the RR spectra of the pulsed form of the enzyme (Fig. 4a) to the resting enzyme (Fig. 4*d*) in the spectral region between 1550-1600 cm^{-1} shows that the spectrum of the pulsed enzyme is quite unusual: In contrast to the fairly intense spin state marker band at 1572 cm^{-1} in the RR spectrum of the resting enzyme (Fig. 4*d*), which is diagnostic of a high-spin heme, the pulsed enzyme exhibits diminished intensity at 1572 cm^{-1}, yet unexpectedly, there is only negligible intensity of the band at 1590 cm^{-1}, which is characteristic of a low-spin species. These results are in agreement with the earlier RR (and MCD) study of the pulsed enzyme by Carter *et al.* (12), who concluded that the lack of appreciable intensity in the spin state marker region, and the observation that the addition of cyanide induces a conversion to a low-spin ferric Fe_{a_3} complex, suggests that ferric Fe_{a_3} is stabilized in the intermediate spin state (S = 3/2) in the pulsed enzyme.

Figure 4

High frequency resonance Raman spectra of pulsed cytochrome *c* oxidase, Compound C, and resting cytochrome *c* oxidase. Stoichiometrically reduced cytochrome *c* oxidase was reoxidized with 1 atm of O_2 to produce the pulsed form of the enzyme (*a*). The peroxidic adduct, Compound C, was prepared by two methods: (*b*) the addition of 1 atm of O_2 to a sample of the mixed-valence CO-inhibited form of the enzyme, followed by irradiation with intense visible light to photolyze carbon monoxide fron ferrous Fe_{a_3}; and (*c*) the addition of ~1 equiv of H_2O_2 to a sample of the pulsed form of cytochrome *c* oxidase. Resting cytochrome *c* oxidase (*d*). Conditions: excitation wavelength, 406.7 nm; laser power, 3 mW; scan rate, 5sec/1cm^{-1} (*a*,*b*,*c*), 3sec/1cm^{-1} (*d*); number of scans, 4 (*a*), 5 (*b*,*c*), 2 (*d*).

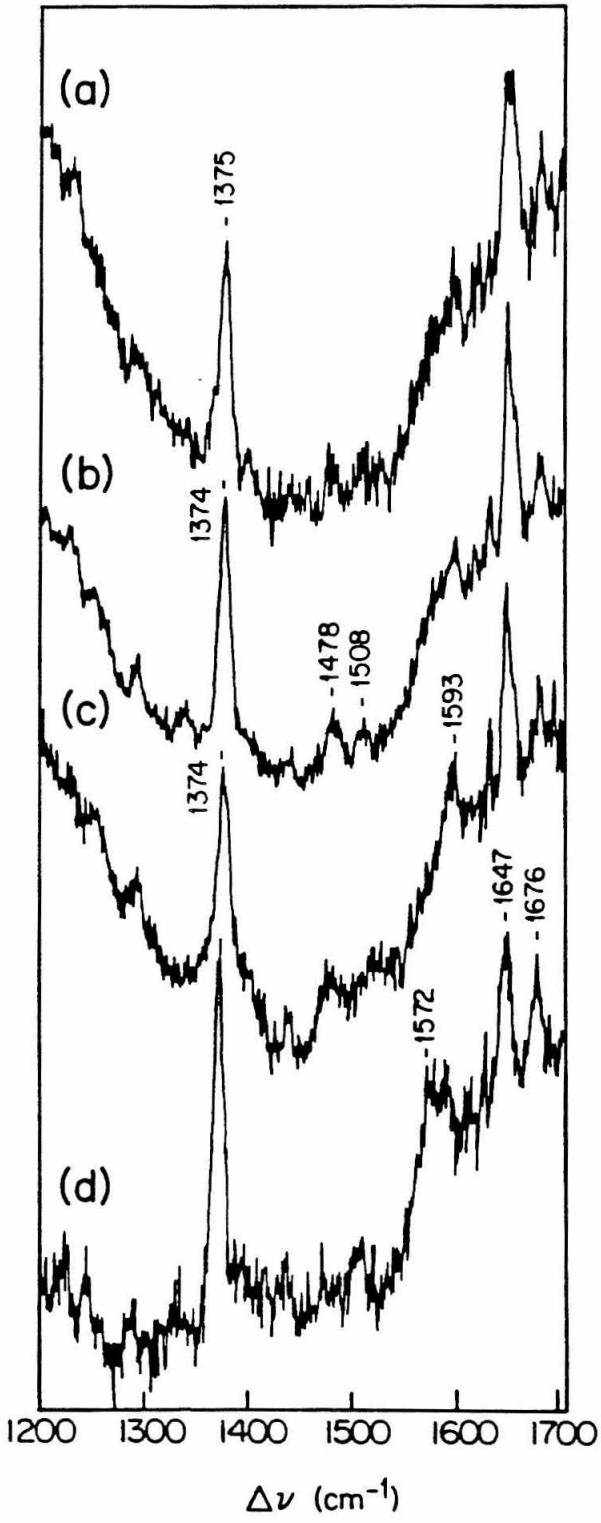
(a)
1375
(b)
1374
1478
1508
(c)
1374
1593
1647
1676
1572
(d)
1200
1300
1400
1500
1600
1700
Δν (cm⁻¹)

Compound C. When we examined a sample of Compound C at 277 K with Soret excitation (406.7 nm), the RR spectrum was nearly indistinguishable from the resonance Raman spectrum of the resting enzyme (data not shown). In fact, an optical spectrum of Compound C, recorded after completion of the scans, resembled the optical spectrum of the resting enzyme, verifying that rapid photoreduction of Compound C occurred when the sample was maintained in the liquid state. In order to retard the rate of photoreduction, the sample of Compound C was examined at low temperatures ($\sim$ 150 K).

The low temperature (150 K) spectrum of Compound C, produced upon the addition of O_2 to the mixed-valence CO-inhibited state of the enzyme and followed by brief illumination with intense visible light to photolyze the CO from ferrous Fe_{a_3}, is shown in Figure 4*b*. A companion sample of the peroxidic adduct was prepared by the addition of approximately one equivalent of hydrogen peroxide to the pulsed enzyme (Fig. 4*c*). Compound C samples produced by the two different methods showed similar but not identical results; both samples displayed weak Raman scattering intensity, similar to the weak scattering observed from the sample of the pulsed enzyme. A comparison of the spectra in Figure 4 to the spectra of the photoreduced enzyme in Figure 2 demonstrates that no appreciable photoreduction occurred over the course of the scans. The most pronounced differences between the two samples of Compound C are observed in the spin state marker region of the spectrum (1550-1600 cm^{-1}). The addition of $\sim$1 equiv of H_2O_2 to the pulsed form of the enzyme yielded a dioxygen reduction site that has a larger population of a low-spin ferric Fe_{a_3} species because of the increased intensity at $\sim$1590 cm^{-1} (Fig. 4*c*), which is indicative of a six-coordinate low-spin ferric heme, relative to the sample of Compound C produced by aerating the mixed-valence CO-inhibited form of the enzyme (Fig. 4*b*).

A comparison of the spectra in Figure 4 shows that the resonance Raman spectra of the two samples of Compound C (Fig. 4*b*,*c*) are nearly identical to the

spectrum of the pulsed enzyme (Fig. 4*a*). The only discernable differences are that the scattering is weaker for the sample of the pulsed enzyme, and the spectrum of the pulsed enzyme (Fig. 4*a*) is distinguished from Compound C (Fig. 4*b*) by a broad band at ~1676 cm^{-1} and the absence of the peak at 1628 cm^{-1}. All three spectra exhibit ν_4 at ~1374 cm^{-1}, which is diagnostic of the ferric oxidation state.

The 428/580 nm Species. Before attempting the low temperature experiments, we examined a sample of the 428/580 nm species at 277 K. The results for both temperatures are shown in Figure 5.

After approximately 20 min from the initial reoxidation of the reduced cytochrome *c* oxidase with excess H_2O_2, a RR spectrum of the 428/580 nm species was obtained at 277 K (Fig. 5a). The frequency of the intense oxidation state marker band at 1374 cm^{-1} is consistent with a Fe_{a_3} in the ferric oxidation state. An inspection of the spin state marker region shows a broad, asymmetric band centered at ~1589 cm^{-1}, with a shoulder at ~1575 cm^{-1}. The positions and intensities of these two overlapping bands are consistent with a predominant population of a low-spin Fe_{a_3} species (1590 cm^{-1}), with a minor contribution from a high-spin Fe_{a_3} species (1575 cm^{-1}). The position and intensity of ν_3, which is observed at ~1505 cm^{-1}, is also indicative of a population of a low-spin species at the binuclear dioxygen reduction site (Table II). This data illustrates that after 20 min of incubation at 277 K, the H_2O_2-treated enzyme is heterogeneous, with a population of a low-spin and high-spin ferric species at the binuclear dioxygen reduction site of cytochrome *c* oxidase. Finally, after ~ 90 min of continued irradition 277 K, another RR spectrum of the 428/580 nm species was recorded (Fig. 5*b*). The resultant RR spectrum is nearly identical to the spectrum of the resting enzyme shown in Figure 3*a*. This observation is in agreement with our previous optical and EPR experiments which demonstrated that the H_2O_2-treated enzyme eventually converts to the resting enzyme upon incubation at 277 K and higher.

When a sample of the 428/580 nm species was examined at low temperature,

Figure 5

High frequency resonance Raman spectra of H_2O_2-treated cytochrome *c* oxidase (428/580 nm species) at 273 K (*a*,*b*) and at 153 K (*c*). A resonance Raman spectrum of the 428/580 nm species was obtained after ~15-20 min (*a*) and ~90 min (*b*) from the initial reoxidation with excess H_2O_2. A sample of reduced cytochrome *c* oxidase was reoxidized with excess H_2O_2 (~ 5 mM), followed in 60 sec by the addition of a trace amount of catalase, and then frozen to 77 K (~120 sec from the addition of H_2O_2) (*c*). Conditions: excitation wavelength, 406.7 nm; laser power, 3 mW; scan rate, 1sec/1cm^{-1} (*a*,*b*), 5sec/1cm^{-1} and 2sec/cm^{-1} (*c*); number of scans, 1 (*a*,*b*), 1 and 2 (*c*).

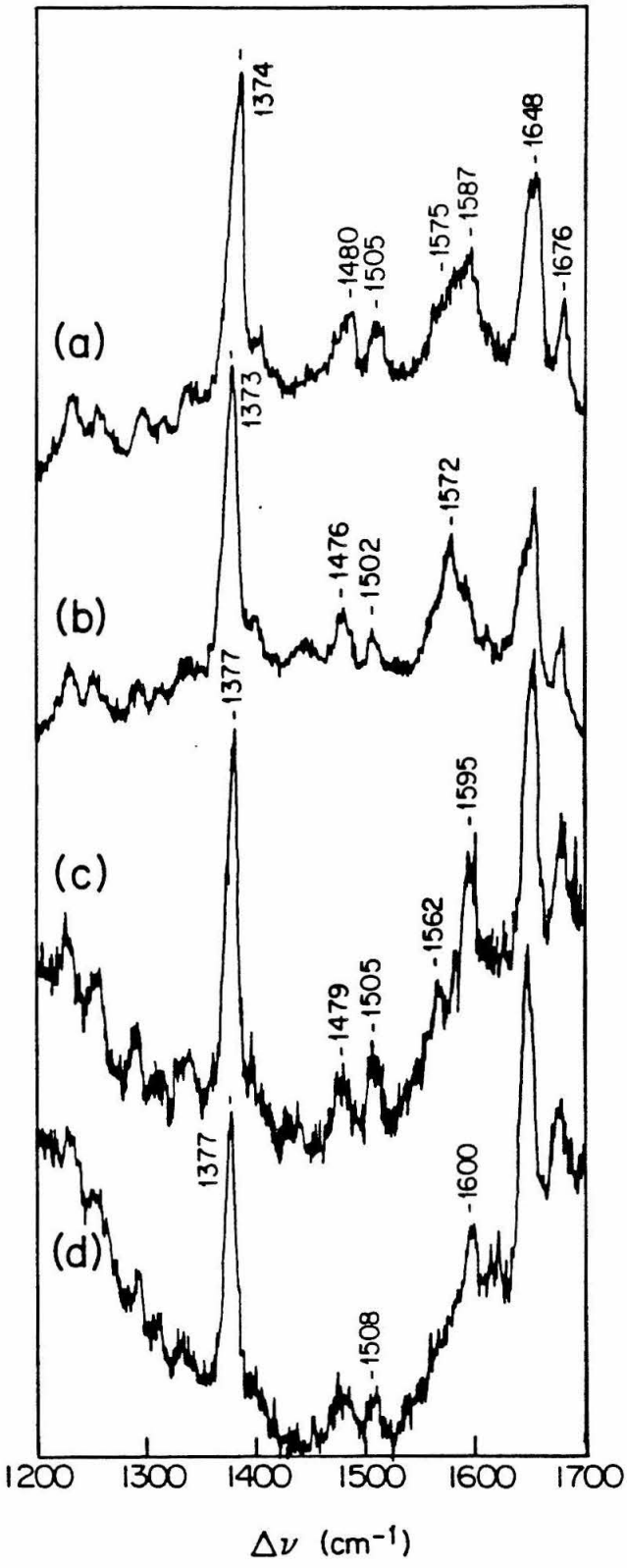
(a)
1374
1480
1505
1575
1587
1648
1676
(b)
1373
1476
1502
1572
(c)
1377
1479
1505
1562
1595
(d)
1377
1508
1600
1200
1300
1400
1500
1600
1700
Δν (cm⁻¹)

we found some quite intriguing results. The RR spectrum of the 428/580 nm species, obtained at 150 K, is shown in Figure 5*c*. We will focus attention on three diagnostic marker bands (ν_4, ν_3, and ν_2) in the low-temperature spectrum of the 428/580 nm species. An intense oxidation state marker band is observed at 1377 cm^{-1} (ν_4). The frequency of the oxidation state marker band is the highest frequency ever reported for any state of cytochrome *c* oxidase, and is indicative of a ferryl heme (Table VI), although we are aware of some anomolously high frequencies of ν_4 that have been reported for ferric and even ferrous hemes (vide infra). From the position and intensity of the two spin state marker bands we may draw an unambiguous conclusion: The frequency and intensity of ν_3 (1505 cm^{-1}) and ν_2 (1595 cm^{-1}) are only consistent with a low-spin (S = 1/2) ferric or low-spin (S = 1/2) ferryl (S = 1) Fe_{a_3} complex (see Table II and VI). In Figure 5*d* we can see that similar, but not identical, results were obtained for a sample of the 428/580 nm species which was dissolved in ~98 % D_2O. The structure-sensitive vibrational modes which arise mainly from Fe_{a_3} are observed at 1377 cm^{-1} (ν_4), 1508 cm^{-1} (ν_3), 1600 cm^{-1} (ν_2) and 1676 cm^{-1} ($\nu_{C=O}$).

In Figure 5 we also compare the RR spectra of the 428/580 nm species obtained at low temperature (*c*) and 277 K (*a*,*b*). In contrast to the intense sharp band at 1595-1600 cm^{-1}, which is diagnostic of a six-coordinate low-spin ferric or ferryl heme, we observe a relatively broad band in the spectrum of the 428/580 nm species in Figure 5*a*, indicating contributions from both high- and low-spin complexes. Based on these data we conclude that considerable conversion to the resting enzyme had already occurred before (or during) scans of the liquid sample of the 428/580 nm species, while maintaining the samples at 135-150 K retarded the rate of conversion of the 428/580 nm species to the pulsed (or resting) enzyme.

It is useful to compare the low-temperature RR spectra of the 428/580 nm species and the resting enzyme (Fig. 6*a*,*b*). Both samples displayed strong Raman scattering. The differences between the two states of the enzyme may be sum-

Figure 6

Low-temperature (153 K), high frequency resonance Raman spectra of H_2O_2-treated cytochrome *c* oxidase (428/580 nm species) (*a*) and resting cytochrome *c* oxidase (*b*) Sample conditions as described in the legend to Figure 5. Conditions: excitation wavelength, 406.7 nm; laser power, 3 mW; scan rate, 5sec/1cm^{-1} and 2sec/cm^{-1} (*a*), 3sec/1cm^{-1} (*b*); number of scans, 1 and 2 (*a*), 2 (*b*).

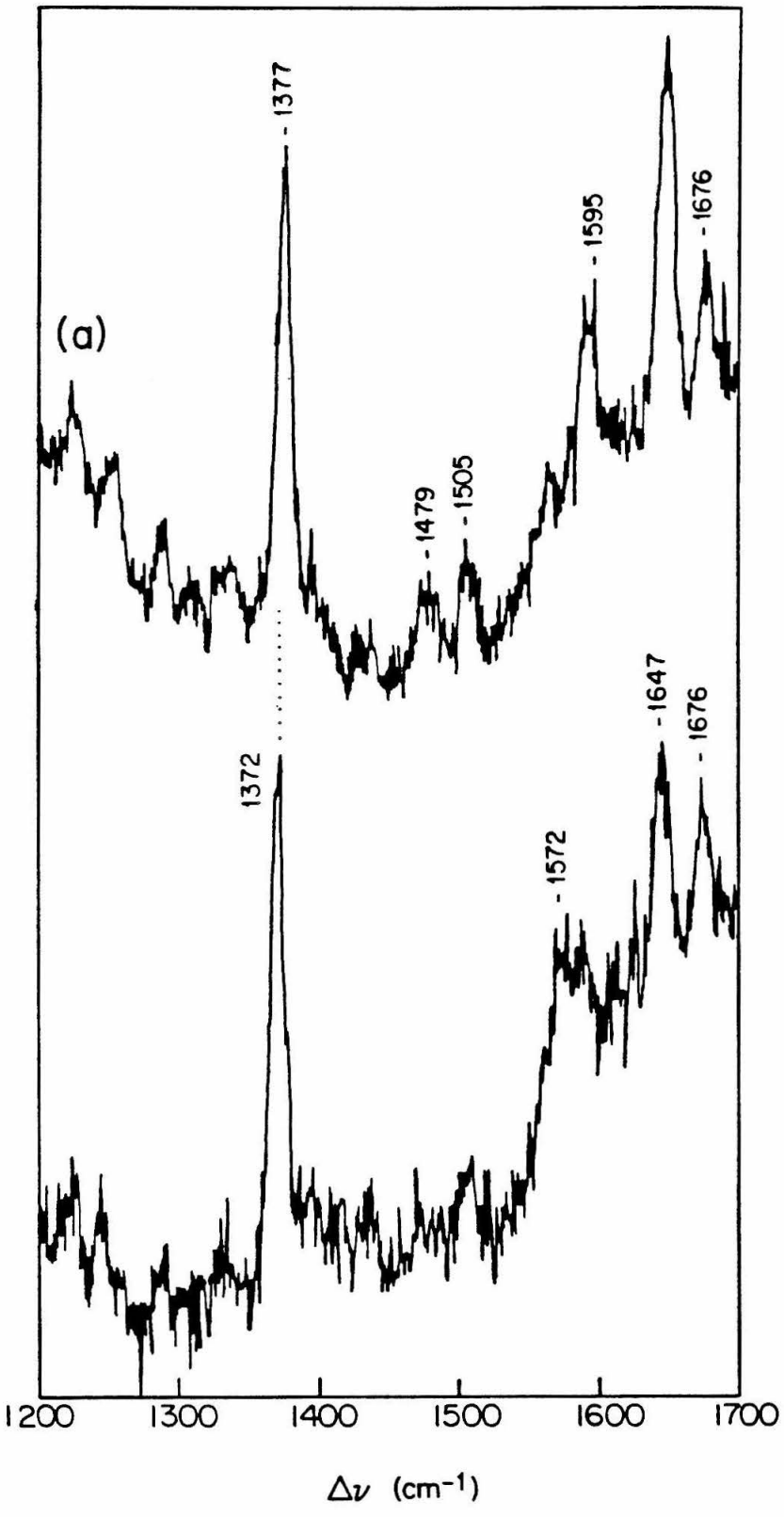
(a)
1377
1595
1676
1479
1505
1372
1647
1676
1572
1200
1300
1400
1500
1600
1700
Δν (cm⁻¹)

marized as follows. In the oxidation state marker region, the 428/580 nm species exhibits a ν_4 at 1377 cm^{-1}, while this mode appears at only 1372 cm^{-1} in the RR spectrum of the resting enzyme. The sizeable shift in the frequency of ν_4 is consistent with a decreased delocalization of electrons from the d-π orbitals of the iron to the porphyrin π^* molecular orbitals, which would result if there was an *increase* in the oxidation state of Fe_{a_3} from the ferric to the ferryl state. The spin state marker band, ν_3, is considerably more intense in the spectrum of the 428/580 nm species (ν_3 = 1505 cm^{-1}) (Fig. 6*a*), and is diagnostic of a six-coordinate low-spin Fe_{a_3} complex (Table II). Further support for a homogeneous population of a low-spin Fe_{a_3} complex at the dioxygen reduction site of the 428/580 nm species is obtained when we examine the spin state marker, ν_2, in the spectra shown in Figure 6. There is a complete conversion of the 428/580 nm species to a low-spin Fe_{a_3} complex (Fig. 6*a*) as evidenced by the increased intensity at 1595 cm^{-1}, relative to the spectrum of the resting enzyme (Fig. 6*b*). In contrast, the dioxygen reduction site of the resting enzyme is composed of a nearly homogeneous population of a six-coordinate ferric Fe_{a_3} species stabilized in the high-spin state, as evidenced by the appearance of ν_2 at ~1575 cm^{-1}, with only negligible intensity at ~1595 cm^{-1}.

Low frequency resonance Raman Spectrum of the 428/580 nm species. We observed strong scattering from the resting enzyme and the 428/580 nm species in the low-frequency region of the spectrum. The results are shown in Figures 7-9. In contrast, Compound C and the pulsed enzyme displayed weak scattering and little detail in the low frequency (150-1250 cm^{-1}) region (data not shown). Since we have proposed that the reactive binuclear site of the 428/580 nm species is composed of a ferryl Fe_{a_3}/cupric Cu_B couple, samples of the 428/580 nm species, reoxidized with $H_2{}^{16}O_2$ and $H_2{}^{18}O_2$, were examined in an attempt to identify the $\nu(Fe^{IV}{=}O)$ vibrational mode via an isotope shift. (A typical isotope shift for a $\nu(Fe^{IV}{=}O)$ vibrational mode is approximately 36 cm^{-1}, based on a simple

two-body harmonic oscillator, and $\nu(Fe^{IV}=O)$ usually falls in the spectral region between 750-850 cm^{-1}.) Resonance Raman spectra were obtained for the two different H_2O_2-treated samples over the entire frequency range from 150-1700 cm^{-1}. The spectra of both samples are shown only for the region of the spectrum where the $\nu(Fe^{IV}=O)$ band is likely to occur (Fig. 8*b*,*c*). H_2O_2-treated samples exhibited essentially identical spectral features in the spectral region between 150-700 cm^{-1} and 1200-1700 cm^{-1}.

150 – 700 cm^{-1}. Our resonance Raman spectra of the resting enzyme and the H_2O_2-treated enzyme in the spectral region between 150-700 cm^{-1} are shown in Figure 7*a*,*b*. The differences between these spectra are summarized as follows. The band at 347 cm^{-1} (ν_8) (Fig. 7*b*) has decreased in intensity and increased in frequency, relative to the spectrum of the resting enzyme (ν_8 = 341 cm^{-1}) (Fig. 7*a*). In addition, the peak at 376 cm^{-1} in the spectrum of the resting enzyme is absent in the spectrum of the 428/580 nm species.

650 – 800 cm^{-1}. Resonance Raman spectra of $H_2{}^{16}O_2$- and $H_2{}^{18}O_2$- treated cytochrome *c* oxidase and of the resting enzyme, in the spectral region between 650-800 cm^{-1}, are shown in Figure 8*a*-*c*. An examination of the RR spectrum of the H_2O_2-treated enzyme (Fig. 8*b*,*c*) reveals a loss of intensity at 765 and 795 cm^{-1} for the 428/580 nm species, with a concomitant increase in the intensity at ~749 cm^{-1}, relative to the spectrum of the resting enzyme (Fig. 8*c*). The only reproducible difference between the $H_2{}^{16,18}O_2$-treated samples (*b*,*c*) is the slightly higher intensity at ~749 cm^{-1} in the spectrum of the $H_2{}^{18}O_2$-treated enzyme. If the band at 749 cm^{-1} were the $\nu(Fe^{IV}={}^{18}O)$ stretching frequency, the corresponding $\nu(Fe^{IV}={}^{16}O)$ would be expected at ~785 cm^{-1}. However, the spectrum of the $H_2{}^{16}O_2$-treated enzyme (Fig. 8*b*) does not exhibit a band at ~785 cm^{-1}; therefore, we cannot yet assign the $\nu(Fe^{IV}=O)$ peak.

800 – 1250 cm^{-1}. To complete the characterization of the 428/580 nm species, we compare the RR spectrum of the 428/580 nm species to the spectrum

Figure 7

Low frequency resonance Raman spectra of resting and the 428/580 nm species of cytochrome *c* oxidase in the spectral region between 150-700 cm^{-1}. Conditions: excitation wavelength, 406.7 nm; laser power, 3 mW; scan rate, 4sec/1cm^{-1} (*a*), 3sec/cm^{-1} (*b*); number of scans, 1 (*a*), 3 (*b*); temperature, 153 K.

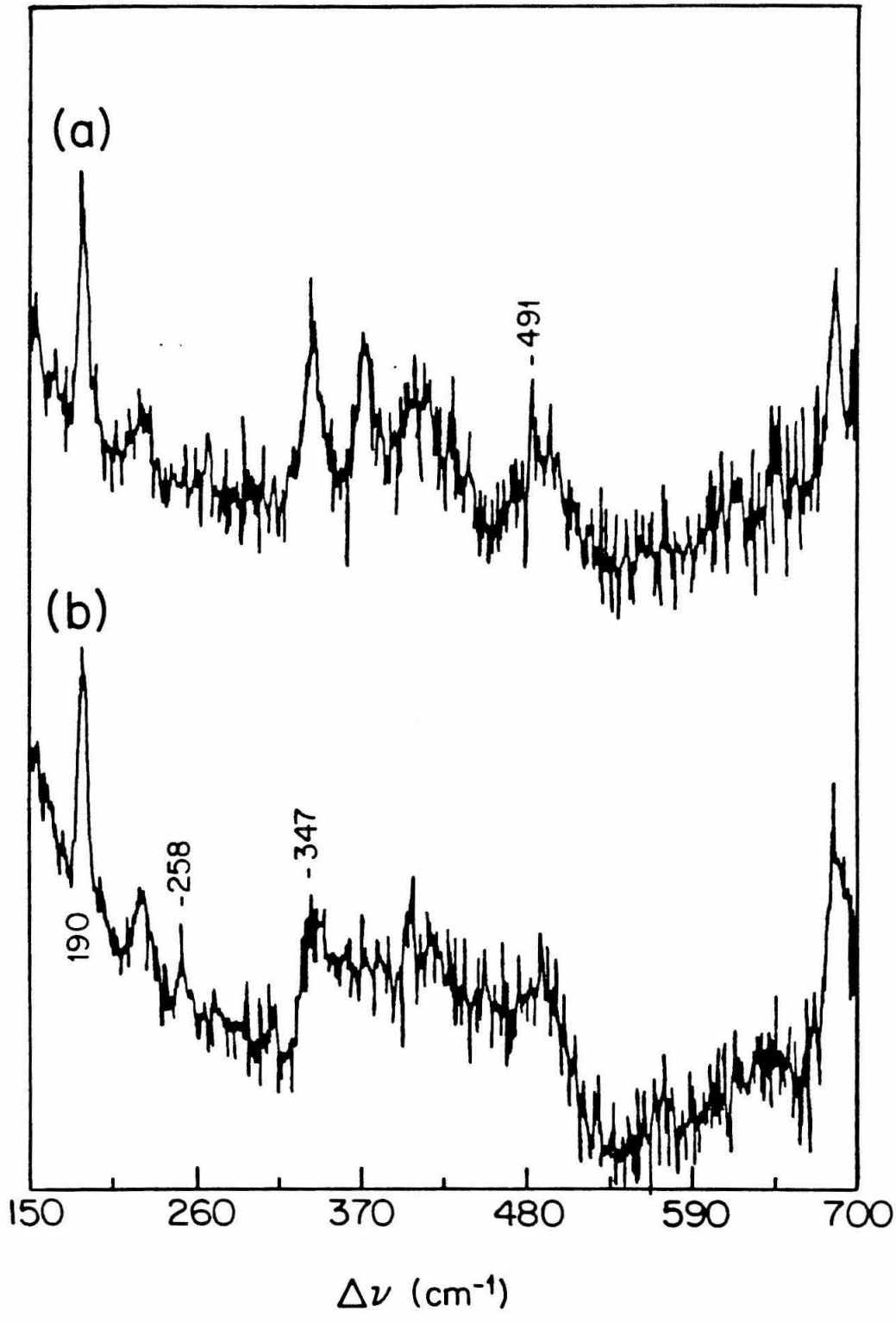
(a)
491
(b)
190
258
347
150
260
370
480
590
700
Δν (cm⁻¹)

Figure 8

Resonance Raman spectra of resting (*a*), $H_2{}^{16}O_2$-treated (*b*), and $H_2{}^{18}O_2$-treated (*c*) cytochrome *c* oxidase in the spectral region between 650-850 cm^{-1}. Samples of the 428/580 nm species were prepared according to the legends in Figure 5, with the exception that one sample was reoxidized with excess $H_2{}^{18}O_2$ (*c*). Conditions: excitation wavelength, 406.7 nm; laser power, 3 mW; scan rate, 3sec/1cm^{-1} (*a*), 5sec/cm^{-1} (*b*,*c*); number of scans, 3 (*a*), 5 (*b*,*c*); temperature, 153 K.

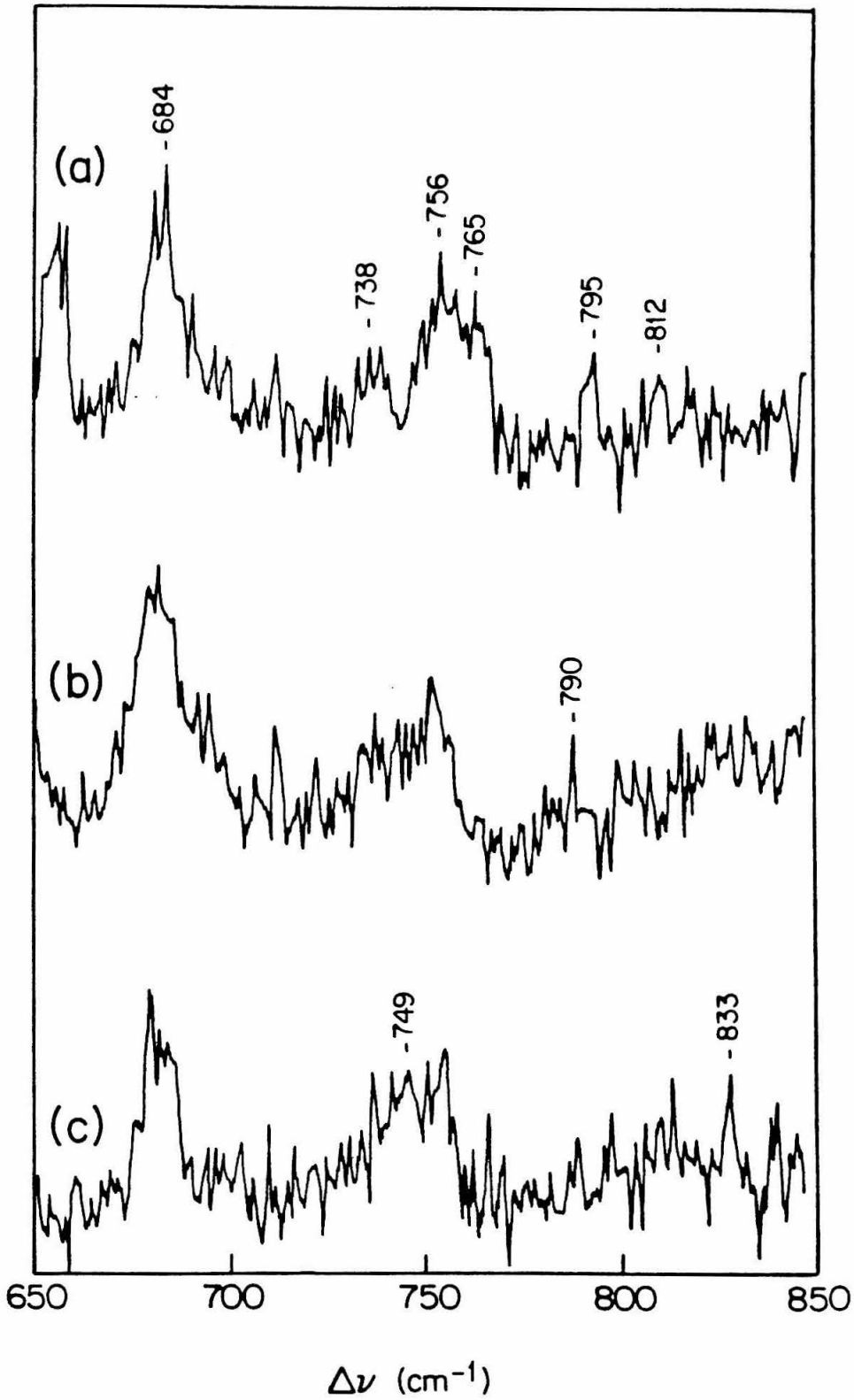
(a)
684
738
756
765
795
812
(b)
790
(c)
749
833
650
700
750
800
850
Δν (cm⁻¹)

Figure 9

Resonance Raman spectra of resting (*a*) and $H_2{}^{16}O_2$-treated (*b*) cytochrome *c* oxidase in the spectral region between 800-1250 cm^{-1}. Samples of the 428/580 nm species were prepared according to the legends in Figure 5, with the exception that one sample was reoxidized with excess $H_2{}^{18}O_2$ (*c*). Conditions: excitation wavelength, 406.7 nm; laser power, 3 mW; scan rate, 4sec/1cm^{-1} (*a*), 3sec/cm^{-1} (*b*); number of scans, 1 (*a*), 3 (*b*); temperature, 153 K.

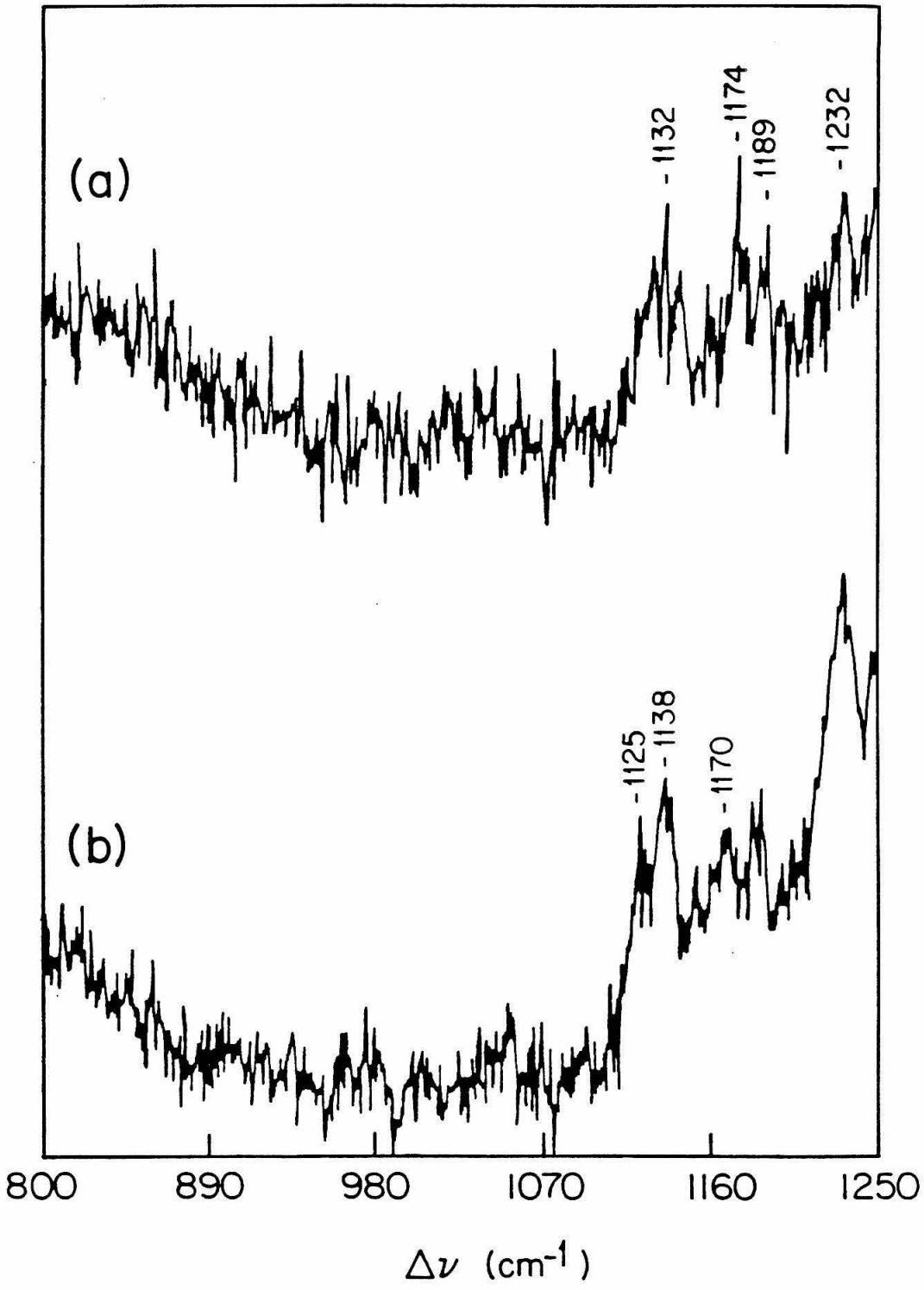
(a)
1132
1174
1189
1232
(b)
1125
1138
1170
800
890
980
1070
1160
1250
Δν (cm⁻¹)

TABLE III

Soret excitation resonance Raman peaks and assignments for the resting and the 428/580 nm states of cytochrome *c* oxidase (150-1250 cm^{-1}).

Assignment*	Resting CcO	428/580 nm species CcO
$\nu_{13}(a_3)$	1232	1233
?	1189	1188
ν_{30} or ν_{43}	1174	1170
$\nu_6 + \nu_8$	1138	1138
ν_{22}	1132	1125
$\nu_{32}(a_3)$	795	792
?	765	
$\nu_{16}(a_3)$	756	755
$\nu_{47}(a_3)$	738	741
?	713	716
?	700	703
$\nu_7(a_3)$	683	684
?	650	648
? a_3	420	422
* δc_b-c_α-c_β	412	------
$2\nu_{35}$ or $\delta c_b s$	376	------
$\nu_8(a_3)$	341	347
?	296	------
?	------	258
?	226	227

*Assignments based on those of Abe, *et al.* (1978). C_α and C_β are carbon atoms on the vinyl substituent to heme A (See Figure 1).

of the resting enzyme in the spectral region between 800-1250 cm^{-1}. In the RR spectrum of the 428/580 nm species (Fig. 9*b*) there is an increased intensity at 1138 and 1233 cm^{-1}, with a decreased intensity at ~1170 cm^{-1}, relative to the spectrum of the resting enzyme (Fig. 9*a*). The peak positions and vibrational assignments for the RR spectra shown in Figs. 7-9 are tabulated in Table III.

DISCUSSION

Photoreduction of frozen samples of cytochrome *c* oxidase under conditions of Soret excitation and high laser power was previously reported by Babcock *et al.* (14). The characteristic signs of photoreduction are evident in the spectra in Figure 2. Photoreduction is accompanied by an increase of the intensity of the bands at 1360, 1587, ~1520, 1610 and 1621 cm^{-1} and a diminution of intensity in the bands at ~1370, ~1646 and 1676 cm^{-1}. A comparison of the spectra in Figure 2 reveals an increased level of photoreduction in the frozen sample relative to the liquid sample at high laser power (~25 mW). This suggests that there is either an increase in the rate of photoreduction at low temperature (153 K), or a decreased rate of electron transfer between ferrous Fe_a and the dioxygen reduction site under the conditions of our experiment. At 173 K the half-time of the electron transfers from the low-potential centers to the dioxygen reduction site is on the order of minutes (21,38); therefore, a reasonable conclusion is that upon the photoreduction of Fe_a, which is thought to be mediated by endogenous flavins (14), the rate of electron transfer to the binuclear site is so slow that reduced Fe_a accumulates.

Since the samples of pulsed, Compound C, and the 428/580 nm species contain reactive binuclear dioxygen reduction sites, which convert to other species upon incubation at ice temperature, it was essential to examine the samples at low temperatures (and low powers), where the rate of interconversion between the various species would be significantly retarded. In order to determine whether

the freezing process caused a perturbation of the heme environment, we recorded resonance Raman spectra of a liquid and frozen sample of resting cytochrome *c* oxidase (Fig. 3). The similarity between the resonance Raman spectra of the liquid sample of the resting enzyme (273 K) (Fig. 3*a*) and the frozen sample (153 K) (Fig. 3*b*) assured us that the freezing process did not cause any significant perturbation of the heme environments in the resting enzyme. Except for the spectral region between 1550-1660 cm^{-1}, no significant changes are observed in the peak positions of the major bands in the spectrum of the resting enzyme in the solid and liquid state. The increased intensity at 1589 cm^{-1} evident in the spectrum of the frozen sample may signify an increased population of a low-spin species, relative to the liquid sample. A low-spin species, which would exhibit intensity at 1589 cm^{-1}, might arise as a result of photreducton, although the bands at 1647 and 1675 cm^{-1} and the relatively low intensity at 1610 and 1622 cm^{-1} are inconsistent with appreciable photoreduction.

Pulsed cytochrome c oxidase. The pulsed form of cytochrome *c* oxidase displayed overall weaker Raman scattering intensity than either the resting enzyme or the 428/580 nm species. A comparison of the low-temperature spectrum of the resting enzyme (Fig. 4*d*) to the low temperature spectrum of the pulsed enzyme (Fig. 4*a*) demonstrates the absence of appreciable intensity in the spin state marker region of the spectrum (1550-1590 cm^{-1}) of the pulsed enzyme. Our spectrum of the pulsed enzyme resembles the spectrum of the pulsed enzyme as reported by Carter *et al.* (12). In contrast, Copeland *et al.* (29) reported that the resonance Raman spectrum of the pulsed enzyme is nearly indistinguishable from the spectrum of the resting enzyme. Because the pulsed enzyme converts to the resting enzyme upon incubation at ice temperature, the differences in the reported resonance Raman spectra of the pulsed enzyme are probably due to varying subpopulations of the resting enzyme. Our samples of the pulsed enzyme were maintained at very low temperature; therefore, the rate of conversion from

the pulsed enzyme to the resting form of the enzyme was so slow that a large population of the pulsed enzyme was ensured in this study.

Since resonance Raman scattering is strongly dependent on the optical absorption spectrum, we must examine the differences in the optical properties of the pulsed (and Compound C) and the resting enzyme to gain insight into the differences in Raman scattering between the two species. What changes in the Soret band might account for the weaker scattering from the pulsed enzyme? The Soret absorption band of the pulsed enzyme is narrower and the absorption maximum occurs at a lower energy (424 nm) than the Soret maximum of the resting enzyme (~420 nm). These combined optical changes could result in a decrease in the absorptivity of the pulsed enzyme at the excitation line (406.7 nm), which would result in diminished scattering, relative to the resting enzyme. However, other factors must be important since the 428/580 nm species has a Soret band which is even more red-shifted than the pulsed enzyme, yet it displays fairly strong Raman scattering intensity with the 406.7 nm excitation.

A combination of spectroscopic studies of the pulsed enzyme have indicated that the principle difference between the pulsed and resting cytochrome *c* oxidase is that a ligand (X) which bridges Fe_{a_3} and Cu_B in the resting state of the enzyme, is absent in the pulsed state of the enzyme (31-32). The position of the oxidation state marker band (ν_4) in the RR spectrum of the pulsed enzyme indicates that Fe_{a_3} is in the ferric oxidation state in the pulsed enzyme. There is almost a complete absence of intensity of the spin state marker band, ν_2, at a position which is indicative of either a high-spin (~1575 cm^{-1}) or a low-spin (~1590 cm^{-1}) Fe_{a_3} complex, yet the addition of cyanide causes the formation of a homogeneous population of a low-spin ferric Fe_{a_3} complex (33); therefore, we reasonably conclude that the pulsed enzyme is composed of a dioxygen reduction site in which ferric Fe_{a_3} is stabilized in the intermediate spin state (S = 3/2).

The Peroxidic Adduct, Compound C. We examined two samples of

Compound C which were prepared by quite different procedures: (i) The addition of O_2 to the mixed-valence CO-inhibited state of the enzyme ($Fe_a^{III}, Cu_A^{II}, Fe_{a_s}^{II} - CO, Cu_B^{I}$), which was subjected to brief illumination with intense visible light in order to photolyze CO from ferrous Fe_{a_s}, and (ii) the addition of ca. one equiv of H_2O_2 to the pulsed enzyme. The two experimental procedures did not produce samples with identical optical absorption spectra. Typically, samples prepared as in (i) displayed a Soret maximum at 424 $\pm$ 1 nm, with an intense α band in the reoxidized minus resting difference spectrum at 607 nm. When the peroxidic adduct is prepared as in (ii), the sample exhibited a Soret maximum at 428 nm, with a moderately intense α band in the reoxidized minus resting difference spectrum at 603-605 nm. These observations indicate that the two different procedures produce different species, or more plausibly, the samples are heterogeneous.

The resonance Raman spectrum of the pulsed enzyme is remarkably similar to the RR spectrum of the peroxidic adduct, Compound C (Figure 4). The two most likely interpretations of the similarities between the resonance Raman spectra of these two species are: (i) The peroxidic adduct is rapidly photoreduced to the pulsed form of the enzyme on a time scale that is short with respect to the data acqusition time, or (ii) the two species share similar heme structures, *i.e.*, both contain an intermediate-spin (S = 3/2) ferric Fe_{a_s} complex. Unfortunately, because the frozen samples had only a limited surface area exposed to the laser irradiation, it was impossible to thaw the samples following the acquisition period in order to obtain optical spectra, which would have verified whether the sample had converted to another species. Therefore, we cannot rule out that the reactive peroxidic adduct was rapidly photoreduced, although we consider it unlikely under the experimental conditions that were employed in this study, *i.e.*, low incident powers and low temperature. Moreover, previous resonance Raman experiments on cytochrome *c* oxidase have sugested that the photoreduction of the

enzyme is mediated by flavins, and that the electrons enter the enzyme through Fe_a. Since electron transfer from the low-potential centers to the dioxygen reduction site is quite slow at 150 K, we consider it unlikely that the peroxidic adduct was reduced by electrons which originated from the low-potential center, Fe_a (14). Alternatively, there may be a mechanism whereby electrons may enter the reactive peroxidic adduct without mediation from Fe_a. In that case, the rate of the photoreduction could be very fast relative to the timescale of the data acquisition (~20 min).

If we accept that the peroxidic adduct was not rapidly photoreduced to the pulsed form of cytochrome *c* oxidase, we must conclude that Compound C and the pulsed enzyme have similar heme structures, even though the two species have remarkably different optical absorption spectra in the visible region of the spectrum. Although the pulsed form of cytochrome *c* oxidase and Compound C have quite different optical spectra in the visible region of the spectrum, recall that these two species have quite similar Soret bands. The Soret maxima of the pulsed enzyme and Compound C (MV-CO + O_2) are observed at 424 nm; therefore, the similarities in the RR spectra for these two species may not be that unusual.

Bickar and co-workers (19) demonstrated that resting (and pulsed) cytochrome *c* oxidase binds H_2O_2 reversibly at low concentrations of H_2O_2. The peroxidic adduct is EPR-silent, probably as a result of strong superexchange coupling between ferric Fe_{a_3} and cupric Cu_B, mediated by a bridging μ-peroxide group (34). Carter and co-workers (12) studied the peroxidic adduct and the pulsed enzyme by both the MCD and resonance Raman spectroscopies and also noted the similarities between the two species. They could not make an unambiguous assignment of the spin and redox states of Fe_{a_3} in these two derivatives. Based on their data and on chemical reasoning, they concluded that both the pulsed enzyme and Compound C are composed of an intermediate-spin ferric Fe_{a_3} species adjacent to cupric Cu_B. Our data also support the assignment of a ferric Fe_{a_3} complex stabi-

lized in the intermediate spin state for both the pulsed enzyme and Compound C. We believe that the disparate spectroscopic properties may be readily explained by the presence or absence of the bridging peroxidic group. Suppose the bridging peroxidic group mediates a strong superexchange coupling between ferric (S = 3/2) Fe_{a_3} and cupric Cu_B, rendering the site EPR-silent. If the bridging peroxidic group is deprotonated, a ligand to metal charge transfer transition might readily occur from the anionic peroxidic group to the ferric Fe_{a_3} center. This proposed interaction could explain the intense band at ~607 nm in the optical spectrum of Compound C. (Note that the bridging ligand is absent in the pulsed form of the enzyme.) It is possible that hydroxide is weakly coordinated to ferric Fe_{a_3}, stabilizing the metal center in the intermediate-spin state (S = 3/2). In this model, there would not be a significant ligand to metal charge transfer interaction since a hydroxyl ion is bound to the iron. More work is needed to characterize both the pulsed and the peroxidic adduct, Compound C, before we can make a definitive assignment of the spin and redox states of Fe_{a_3} in these two species. In the future, the low-temperature resonance Raman experiments must be coupled with optical absorption reflectance spectroscopy in order to monitor the optical changes, if any, upon Soret excitation.

The Nature of the Reactive Binuclear Dioxygen Reduction Site in the 428/580 nm Species. Optical absorption and EPR experiments previously established that the 428/580 nm species converts to the resting enzyme upon incubation at ice temperature, with a half-time of approximately 60 min. A RR spectrum recorded after approximately 20 min from the initial reoxidation with H_2O_2 exhibited spectral features that are characteristic of a mixture of low- and high-spin ferric Fe_{a_3} species. Normally, it would be expected that a sizeable population of the 428/580 nm species would be present after 20 min incubation at ice temperature; therefore, this result suggests that irradiation with 406.7 nm excitation accelerates the conversion of the 428/580 nm species to the resting state

of the enzyme, although in fact no appreciable photoreduction was observed. A spectrum recorded after 90 min of continued irradiation was practically indistinguishable from the spectrum of the resting enzyme. In contrast, the results from the frozen samples indicate that at 153 K, and with low incident laser power, no significant decomposition of the 428/580 nm occurred over an entire day of scans, since no significant changes were evident in the spectra over this period. Moreover, maintaining the samples at low temperature retarded the rate of conversion of the 428/580 nm species to the resting state of the enzyme and ensured us that a sizable population of the 428/580 nm species was studied.

We were unable to determine conclusively whether the binuclear dioxygen reduction site of the H_2O_2-treated cytochrome *c* oxidase contains a ferryl Fe_{a_3} intermediate because of the absence of an isotope-sensitive ν(FeO) strectching mode. This in itself is not significant since several factors could account for the absence of the ν(FeO) vibrational mode. It is intriguing that no ν(FeO) vibrational modes have been detected via an isotope shift for any of the "oxygenated" states of cytochrome *c* oxidase. The two factors which might preclude the observation of the ν(FeO) vibrational mode follow: (i) The proposed ν(FeO) vibration of the 428/580 nm species may not be resonance enhanced (with 406.7 nm excitation). (We also experimented with a 413.1 nm excitation wavelength and did not observe any improvement in the signal to noise in the low-frequency region of the spectrum.) Usually it is assumed that the ν(FeO) vibration is enhanced via coupling of the axial vibration with the motions of the porphyrin that contribute to the $\pi \rightarrow \pi^*$ electronic transition of the porphyrin (35), although the mechanism of the coupling is a subject of debate. In this model, one would expect the greatest enhancement of the ν(FeO) vibration with an excitation wavelength that closely matches the Soret maximum. Recently, Proniewicz *et al.* (36) suggested that the ν(FeO) vibration may be coupled to a charge transfer (CT) electronic transition along the Fe-O axis, which may have its maximal intensity at either higher or lower energy than the

Soret band. If the proposed ν(FeO) vibrational mode in the 428/580 nm species is in fact coupled to a CT electronic transition, the absorption maximum for the CT transition might not coincide with the Soret absorption band; therefore, future work should utilize a wider range of excitation wavelengths, *i.e.*, from 380-460 nm. (ii) The proposed ν(FeO) vibrational mode of the 428/580 nm species could be broadened beyond detection as a result of hydrogen bonding, which has been shown to occur for the ferryl form of horse radish peroxidase, referred to as HRP-II. For example, when a sample of horse radish peroxidase Compound II (HRP-II) (Fe^{IV}=O), which is buffered at pH 6.9, is examined by resonance Raman, the Fe^{IV}=O stretching mode is barely discernable from the baseline (37). In contrast, if HRP-II is examined at high pH (pH = 10), the Fe^{IV}=O stretching mode shifts to higher energy and increases in intensity by a factor of approximately 6. This effect has been interpreted to arise from broadening (at neutral pH) due to hydrogen bonding between the iron-oxo group and a distal histidine which is protonated below pH 8.8. Evidently, when the distal histidine is deprotonated, an intense Fe^{IV}=O stretching mode is observed. A similar effect might be responsible for the absence of the ν(FeO) vibrational mode in the RR spectrum of the 428/580 nm species. Blair *et al.* (38) proposed that a hydrogen bond between the oxy ferryl and a hydroxyl ion ligated to cupric Cu_B might provide enough superexchange coupling to render the site EPR-silent. The same hydrogen bonding interaction could reduce the intensity of the proposed ν(FeO) vibrational mode in the 428/580 nm species. Unlike many of the peroxidase enzymes, cytochrome *c* oxidase will tolerate only a very limited range of pH, *i.e.*, typically from ~6.5-8.5. This entire pH range should be investigated in the future.

The peak positions and intensities of the high-frequency structure-sensitive vibrational modes observed in the RR spectrum of the 428/580 nm species are only consistent with a homogeneous population of a low-spin Fe_{a_3} complex (Tables II, V, and VI). We must now examine the possible low-spin Fe_{a_3} complexes which

might exhibit these spectral features. The structures, however, must also be consistent with the observed optical, magnetic, and chemical properties of the 428/580 nm species. Three possible structures are listed in Table IV for our consideration.

TABLE IV

Fe(Spin)	SPECIES	
$S = 0$	$Fe_{a_3}^{II}$-O_2 (Cu_B^{II})	(A)
$S = 1/2$	$Fe_{a_3}^{III}$-L (Cu_B^{II})	(B)
$S = 1$	$Fe_{a_3}^{IV}$=O (Cu_B^{II})	(C)

(A) The high-frequency vibrational modes in the RR spectrum of the 428/580 nm species at 1595-1600 (ν_2), 1505-1508 (ν_3), and 1377 (ν_4) cm^{-1}, are actually quite similar to those reported for the oxy-complex of horse radish peroxidase (1581, 1506, and 1377 cm^{-1}) (39). The latter species contains iron protoporpyrin IX with a histidine-nitrogen and dioxygen as the fifth and sixth axial ligands (39). Are the optical and magnetic properties of the 428/580 nm species consistent with the expected properties of species (A)? A low-spin ferrous dioxygen adduct, trapped at the dioxygen reduction site of cytochrome *c* oxidase, would be

expected to produce considerable intensity in the absorption spectrum near 602 nm, because ferrous Fe_{a_3} is known to contribute intensity in that region of the spectrum. Furthermore, there is general agreement that the stabilization of ferrous Fe_{a_3} in the low-spin state by complexation of dioxygen produces a magnetically isolated cupric Cu_B, which is thought to give rise to a rhombic Cu_B EPR signal (40-41). (An analogous mixed-valence species, in which ferrous Fe_{a_3} is stabilized in the low-spin state by complexation with nitric oxide (NO) ($Fe^{II}_{a_3}$-NO Cu^{II}_B), was studied by Stevens *et al.* (42). This species exhibits a triplet EPR signal with hyperfine coupling in the half-field transition that is indicative of a cupric ion, and as expected for a ferrous Fe_{a_3} complex, there is considerable intensity near 600 nm in the optical absorption spectrum.) In contrast to the expected optical and EPR signatures for a low-spin ferrous Fe_{a_3}-O_2/cupric Cu_B species, the 428/580 nm species exhibits an unusually blue-shifted α band, with no EPR resonances from either Fe_{a_3} or Cu_B. We conclude that although the positions of the structure-sensitive vibrational modes in the RR spectrum of the H_2O_2-treated oxidase are similar to those reported for some ferrous hemes stabilized in the low-spin state by dioxygen, the optical and EPR properties of the 428/580 nm species are entirely inconsistent with this assignment.

(B) In Chapter III we focussed attention on the similar optical absorption properties of the 428/580 nm species and cyanide-inhibited cytochrome *c* oxidase (Fe^{III}_a,Cu^{II}_A,$Fe^{III}_{a_3}$-CN,Cu^{II}_B). Both species display a Soret maximum at 428 nm with intense, blue-shifted α and β bands, relative to the resting state of the enzyme. Based solely on these similar spectral features, we suggested that the reactive dioxygen reduction site in the 428/580 nm species is composed of a low-spin Fe_{a_3} complex, *i.e.*, either a low-spin (S = 1/2) ferric Fe_{a_3} complex, or a low-spin (S = 1) ferryl Fe_{a_3} complex. The results from our resonance Raman study confirm this observation. The positions of the two spin state marker bands, ν_3 (1505 cm^{-1}) and ν_2 (~1595 cm^{-1}), are in agreement with the values of these modes reported

for a six-coordinate low-spin ferric heme A model complex (Table II), as well as for those reported for low-spin (S = 1) ferryl hemes (Table VI). A comparison of the positions of the two spin state marker bands for the 428/580 nm species and the cyanide-inhibited form of the enzyme (Table V) reinforces our conclusion that the 428/580 nm species is composed of a low-spin species at the dioxygen reduction site. With regard to the oxidation state of Fe_{a_3} in the 428/580 nm species, the position of the oxidation state marker band, ν_4, clearly falls out of the range of observed frequencies for ferric heme A model complexes (Table II and V), and suggests that the dioxygen reduction site in the 428/580 nm species is composed of a ferryl Fe_{a_3} species.

Unfortunately, the position of the oxidation state marker is not always a reliable indicator of the oxidation state of the heme. This is exemplified by a series of experiments by Terner and co-workers on native heme protein, horse radish peroxidase, which is in the ferric oxidation state (43). At neutral pH, the structure-sensitive vibrational modes are observed at 1374 cm^{-1} (ν_4) and at 1572 cm^{-1} (ν_2), values characteristic of a high-spin ferric heme. Surprisingly, under alkaline conditions (pH = 10-11), ν_4 and ν_2 shifted to 1378-1379 cm^{-1} and 1505-1507 cm^{-1}, respectively, even though the enzyme remained in the ferric oxidation state. These latter frequencies are entirely consistent with a ferryl heme (Table VI). Terner and co-workers interpreted the changes in the resonance Raman spectrum as a complete conversion to a population of a ferric heme stabilized in the low-spin state by coordination by hydroxide. This example demonstrates that the frequency of the ν_4 vibrational mode is not completely insensitive to the spin state of the iron and admirably illustrates the hazards of basing an assignment of an oxidation state solely on the frequency of the oxidation state marker band. Because our samples of the 428/580 nm species were maintained at pH 7.4-8.1 (the brief treatment with H_2O_2 did not increase the pH of the medium), we consider it exceedingly unlikely that a homogeneous population of a low-spin ferric heme

TABLE V

Comparison of the structure-sensitive vibrational modes (ν_4, ν_3, and ν_2) for resting, pulsed, Compound C, cyanide-inhibited, and the 428/580 nm states of cytochrome *c* oxidase.

Soret Excitation Raman Peaks (cm^{-1})

(λ_{ex} = 406.7 nm)

	Resting	Pulsed	Compound C	* Cyanide-Inhibited	428/580 nm Species
Probable Spin-state	5/2	3/2	3/2	1/2	?
ν_4	1372	1375	1374	1374	1377
ν_3	----	----	1508	1505	1505
ν_2	1575	1595 (W)	1590	1590	1595

*Babcock, G.T., Callahan, P.M., Ondrias, M.R. and Salmeen, I. (1981) **Biochemistry** 20, 959-966.

(W) = weak

($Fe^{III}_{a_3}$-OH Cu^{II}_B) would be formed under the pH conditions of our experiments; however, given the documented variability of the frequency of ν_4, we cannot rule out that an unusual low-spin ferric Fe_{a_3} complex is produced at the binuclear dioxygen reduction site of cytochrome *c* oxidase upon treatment with excess H_2O_2.

The reactivity of the 428/580 nm species with carbon monoxide and the aerobic reductive titration provide strong evidence that the reactive dioxygen reduction site of the 428/580 nm species is composed of *three* oxidizing equivalents. A model which incorporates a low-spin ferric Fe_{a_3} necessitates the inclusion of a protein radical ($X^{\cdot}$) and cupric Cu_B in order to have three oxidizing equivalents at the dioxygen reduction site. An intriguing possibility is that the third oxidizing equivalent is located on a methionine radical (or some other amino acid radical) which might be situated in close proximity to the binuclear site or may even bridge ferric Fe_{a_3} and cupric Cu_B. A methionine residue has been implicated as a ligand to Cu_B in a recent extended X-ray absorption fine-structure study (44). Alternatively, it may be unreasonable to expect a cationic radical, such as a methionine radical, to have a ligand field strong enough to convert Fe_{a_3} to a homogeneous population of a low-spin ferric complex. We now direct attention to the final possible model for the reactive binuclear dioxygen reduction site of the 428/580 nm species.

(C) In Table VI we compare the observed frequencies of the oxidation state marker and spin state marker bands (ν_4, ν_3, and ν_2) from a variety of enzymatic species, including resting cytochrome *c* oxidase (CcO) and the 428/580 nm species. Several species which are known to contain a ferryl heme, such as ferryl horse radish peroxidase (HRP-II), ferryl cytochrome *c* peroxidase (CcP-II), and ferryl myoglobin (Myo-II) are included in Table VI.

The spin state marker bands are observed at 1506 cm^{-1} (ν_3) and 1595 cm^{-1} (ν_2) in the RR spectrum of the 428/580 nm species; these values are similar but not identical to those reported for low-spin (S = 1) ferryl hemes (Table VI).

TABLE VI

Comparison of the structure-sensitive vibrational modes (ν_4, ν_3, and ν_2) for the 428/580 nm form of cytochrome *c* oxidase and various ferryl enzymatic intermediates, i.e., horse radish peroxidase Compound II (HRP-II) (*P*Fe(IV)), cytochrome *c* peroxidase Compound II (*P*Fe(IV)), and myoglobin (*P*Fe(IV)). *P* = protoporphyrin IX.

Soret Excitation Raman Peaks (cm^{-1})

(λ_{ex} = 406.7 nm)

	Resting CcO	428/580 nm species CcO	HRP-II[a] (l.s.) Fe(IV)	CcP-II[b] (l.s.) Fe(IV)	Myo-II[c] (l.s.) Fe(IV)
ν_2	1575	1595	1589	1583	1585
ν_3	------	1506	1508	1509	1506
ν_4	1372	1377	1382	1378	1379

a Rakhit, *et al.* (1976) **Biochem. Biophys. Res. Comm.** 71, 803-808.

b Hashimoto, S., *et al.* (1986) **J. Biol. Chem.** 261, 11110-11118.

c Campbell, J.R. *et al.* (1980) **Inorg. Chimica Acta** 46, 77-84.

Moreover, since frequencies as low as 1376 cm^{-1} and as high as 1382 cm^{-1} have been reported for ferryl hemes (45), the frequency of the oxidation state marker band (ν_4 = 1377 cm^{-1}) in the RR spectrum of the 428/580 nm species is certainly in accord with the assignment of a ferryl Fe_{a_3}. Although the frequency of 1377 cm^{-1} (ν_4) appears to be slightly low for a ferryl heme (Table VI), the *absolute* frequency of ν_4 may not be the only diagnostic feature of the oxidation state marker. We should examine the frequency shift of ν_4 for some enzymatic species which are known to form stable intermediates in which the heme is in the ferryl oxidation state. The oxidation state marker band in the RR spectrum of native high-spin (S = 5/2) ferric cytochrome *c* peroxidase is observed at 1374 cm^{-1}, while the band shifts to only 1378 cm^{-1} upon formation of the ferryl species (CcP-II) (46). Similarly, for horse radish peroxidase, ν_4 is observed at 1375 cm^{-1} and shifts to 1382 cm^{-1} when the enzyme is oxidized to the ferryl oxidation state (HRP-II) (47). For the two cases cited, the oxidation state marker band shifts 4 cm^{-1} and 7 cm^{-1}, respectively, upon the oxidation from a Fe(III) to a Fe(IV) state. In fact, modest frequency shifts in the oxidation state marker band between ferric hemes and ferryl hemes are well documented (48). For samples of cytochrome *c* oxidase, we observed the oxidation state marker band at 1372 cm^{-1} in the RR spectrum of the resting enzyme and at 1377 cm^{-1} in the spectrum of the 428/580 nm species. This sizeable 5 cm^{-1} shift to higher energy in ν_4 is entirely consistent with a decrease in the overlap between the d-π orbitals on Fe_{a_3} and the porphyrin π^* molecular orbitals, which would result upon the oxidation of ferric Fe_{a_3} to ferryl Fe_{a_3}.

We conclude that the frequencies of the spin state and oxidation state marker bands provide support for the assignment of a low-spin (S = 1) ferryl Fe_{a_3} complex as the reactive species at the binuclear dioxygen reduction site of the 428/580 nm species. The alternative model, namely, a low-spin ferric Fe_{a_3}/X·/cupric Cu_B ion, cannot be ruled out as a possible candidate for the reactive binuclear site in the

428/580 nm species. In order to distinguish between the two proposed models, namely, a low-spin ferryl Fe_{a_3}/cupric Cu_B binuclear couple and the 428/580 nm species will have to be studied by a spectroscopic technique, such as Mössbauer spectroscopy, which is known to be quite sensitive to the redox state of iron.

REFERENCES

1. Spiro, T.G. (1983) in *Iron Porphyrins* (Lever, A.B.P. and Gray, H.B., eds.) Addison-Wesley, Reading, Ma. Vol. 2 p. 93.
2. Spiro, T.G. and Gaber, B.P. (1977) *Annu. Rev. Biochem.* **46**, 553.
3. Carey, P.R. (1982) *Biochemical Applications of Raman and Resonance Raman Spectroscopies*, (Academic Press, New York).
4. Makinen, M.W. and Churg, A.K. (1982) in *Physical BioInorganic Chemistry*, (A.B.P. Lever and H.B. Gray eds.), Addison-Wesley, Reading, Mass. (1982), Ch. 3, Vol. I.
5. Wikstrōm, M., Krab, K. and Saraste, M. (1981) *Cytochrome Oxidase - Synthesis*, (Academic Press, New York), p. 7.
6. Callahan, P.M. and Babcock, G.T. (1983) *Biochem.* **22**, 452-461.
7. Champion, P.M. and Albrecht, A.C. (1979) *J. Chem. Phys.* **71**, 1110-1121.
8. Spiro, T.G. and Strekas, T.C. (1974) *J. Am. Chem. Soc.* **96**, 338-345.
9. Woodruff, W.H., Kessler, R.J., Ferris, N.S., Dallinger, R.F., Carter, K.R., Antalis, T.M. and Palmer, G. (1982) *Adv. Chem. Ser.* **201**, 625-659.
10. Kitagawa, T., Ozaki, Y. and Kyogoku, Y. (1978) *Adv. Biophys.* **11**, 153.
11. Spiro, T.G. and Burke, J.M. (1976) *J. Am. Chem. Soc.* **98**, 5482-5489.
12. Carter, K.R., Antalis, T.M., Palmer, G., Ferris, N.S. and Woodruff, W.H. (1981) *Proc. Natl. Acad. Sci. USA* **78**, 1652-1655.
13. Spiro, T.G. (1983) in *Iron Porphyrins* (Lever, A.B.P. and Gray, H.B., eds.) Addison-Wesley, Reading, Ma. Vol. 2 p. 134-138.
14. Babcock, G.T., Callahan, P.M., Ondrias, M.R. and Salmeen, I. (1981) *Biochem.* **20**, 959-966.
15. Woodruff, W.H., Dallinger, R.F., Antalis, T.M. and Palmer, G. *Biochem.* **20**, 1332-1338.
16. Vanneste, W.H. (1966) *Biochem.* **5**, 838-848.
17. Hartzell, C.R. and Bienert, H. (1974) *Biochim. Biophys. Acta* **368**, 318-338.

18. Cotton, M.L. and Dunford, H.B. (1973) *Can. J. Chem.* **51**, 582-587.

19. Bickar, D., Bonaventura, J. and Bonaventura, C. (1982) *Biochem.* **21**, 2661-2666.

20. Wrigglesworth, J.M. (1984) *Biochem. J.* **217**, 715-719.

21. Chance, B., Saronio, C and Leigh, J.S. (1975) *J. Biol. Chem.* **250**, 9226-9237.

22. Nicholls, P. and Chanady, G. (1981) *Biochim. Biophys. Acta* **634**, 256-265.

23. Bickar, D., Bonaventura, C. and Bonaventura, J. (1984) *J. Biol. Chem.* **259**, 10777-10783.

24. Farrell, J.K. (1960) *Chem. Abstr.* **54**, p. 3890.

25. Bocian, D.F., Lemley, A.T., Petersen, N.O., Brudvig, G.W. and Chan, S.I. (1979) *Biochem.* **18**, 4386-4402.

26. Abe, M., Kitagawa, T. and Kyogoku, Y. (1978) *J. Chem. Phys.* **69**, 4526-4534.

27. Choi, S., Lee, J.J., Wei, Y.H. and Spiro, T.G. (1983) *J. Am. Chem. Soc.* **105**, 3692-3707.

28. Copeland, R.A., Naqui, A., Chance, B. and Spiro, T.G. (1985) *FEBS Lett.* **182**, 375-379.

29. Ondrias, M.R. and Babcock, G.T. (1980) *Biochem. Biophys. Res. Comm.* **93**, 29-35.

30. Babcock, G.T. (1986) in *Biological Applications of Raman Spectroscopy*, (Spiro, T.G., ed.) Wiley, New York, *in press.*

31. Brudvig, G.W., Stevens, T.H., Morse, R.H. and Chan, S.I. (1981) *Biochem.* **20**, 3912-3921.

32. Powers, L., Chance, B., Ching, Y. and Angiollio, P. (1981) *Biophys. J.* **34**, 465-498.

33. Shaw, R.W., Hansen, R.E. and Beinert, H. (1978) *J. Biol. Chem.* **253**, 6637-6640.

34. Wikström, M., Krab, K. and Saraste, M. (1981) *Cytochrome Oxidase - Synthesis*, (Academic Press, New York), p. 126.

35. Spiro, T.G. (1983) in *Iron Porphyrins* (Lever, A.B.P. and Gray, H.B., eds.) Addison-Wesley, Reading, Ma. Vol. 2 p. 91.

36. Proniewicz, L.M., Bajdor, K. and Nakamoto, K. (1986) *J. Phys. Chem.* **90**, 1760-1766.

37. Sitter, A.J., Reczek, C.M. and Terner, J. (1985) *J. Biol. Chem.* **260**, 7515-7522.

38. Blair, D.F., Witt, S.N. and Chan, S.N. (1985) *J. Am. Chem. Soc.* **105**, 7389-7399.

39. Van Wart, H.E. and Zimmer, J. (1985) *J. Biol. Chem.* **260**, 8372-8377.

40. Karlsson, B. and Andréasson, L.-E. (1981) *Biochim. Biophys. Acta* **635**, 73-80.

41. Blair, D.F., Martin, C.T., Gelles, J., Wang, H., Brudvig, G.W., Stevens, T.H. and Chan, S.I. (1983) *Chemica Scripta* **21**, 43-53.

42. Stevens, T.H., Brudvig, G.W., Bocian, D.F. and Chan, S.I. (1979) *Proc. Natl. Acad. Sci. USA* **76**, 3320-3324.

43. Terner, J. and Reed, D.E. (1984) *Biochim. Biophys. Acta* **789**, 80-86.

44. Li, P.M., Gelles, J., Chan, S.I., Sullivan, R.J. and Scott, R.A. (1987) *Biochem.* **26**, 2091-2095.

45. Felton, R.H., Romans, A.Y., Yu, N.-J. and Schonbaum, G.R. (1976) *Biochim. Biophys. Acta* **434**, 82-89.

46. Hashimoto, S., Teraoka, J., Inubushi, T., Yonetani, T. and Kitagawa, T. (1986) *J. Biol. Chem.* **261**, 11110-11118.

47. Rakhit,G., Spiro, T.G. and Uyeda, M. (1976) *Biochem. Biophys. Res. Comm.* **71**, 803-808.

48. Kitagawa, T. (1986) in *Spectroscopy of Biological Systems*, (Clark, R.J.H. and Hester, R.E., eds.) Wiley, New York, p. 450.

CHAPTER V

The Structure of Cu_B

Introduction

The mixed-metal (Fe-Cu) binuclear dioxygen reduction site of cytochrome *c* oxidase displays remarkably diverse catalytic activity, as manifested by its oxidase (1), catalase (2), superoxide dismutase (3) and carbon monoxide oxygenase activities (4). The two metal centers which comprise the binuclear site are referred to as Fe_{a_3} and Cu_B. Due to the importance of the binuclear dioxygen reduction site to the overall mechanism of dioxygen reduction by cytochrome *c* oxidase, it is essential to elucidate the intermetal distance, geometries and the ligands to these metal centers, for these structural elements impart the unique reactivity to the site.

The structural and spectroscopic features of Fe_{a_3} were discussed at length in Chapter I. This chapter will focus on the unusual metal center, namely, Cu_B. Since Cu_B does not contribute to the absorption spectrum of cytochrome *c* oxidase, and because it is usually EPR-silent under most experimental conditions, structural

information regarding this metal center has been elusive. EXAFS studies have provided some insight into the nature of the ligands to Cu_B (see Chapter I), however the analysis of EXAFS data from cytochrome *c* oxidase is complicated due to the presence of another copper in the enzyme, namely, Cu_A. Recently, an EXAFS study was conducted on a Cu_A-depleted derivative of cytochrome *c* oxidase. The results from that study are consistent with a $Cu(N,O)_3(S,Cl)$ ligand structure for Cu_B (5).

In Chapter III we showed that upon the addition of CO to the 428/580 nm species a large population of a Cu_B EPR signal is produced. The signal has been observed under a variety of experimental conditions (6-9), and the signal has been reasonably assigned to a magnetically isolated cupric Cu_B ion adjacent to a ferrous-dioxygen (or CO) low-spin Fe_{a_3} adduct (7,10). In this chapter, we exploit the novel reactivity of 428/580 nm species with carbon monoxide to generate large populations of the rhombic Cu_B EPR signal. We then examined the rhombic Cu_B EPR signal using electron nuclear double resonance, referred to as ENDOR, which enabled us to resolve superhyperfine coupling between Cu_B and its associated ligands. This approach has enabled us to confirm a previously observed superhyperfine coupling due to a ^{14}N ligand (11), with a ligand hyperfine coupling of 34 MHz. Furthermore, preliminary data is reported for the identification of a second ^{14}N ligand with hyperfine coupling of 41 MHz. We complimented this study with experiments designed to test whether an oxygen-containing ligand is coordinated to Cu_B in the species which gives rise to the rhombic Cu_B EPR signal. This was accomplished by employing $H_2O_2^{17}$ to prepare the 428/580 nm species of cytochrome *c* oxidase. When carbon monoxide is added to the $H_2O_2^{17}$-treated enzyme, we in fact observed a 10 Gauss broadening of the rhombic Cu_B EPR signal, suggesting an interaction between a ^{17}O-labeled species and the cupric Cu_B ion. The EPR and ENDOR results will be presented, and then we discuss a model for the structure of Cu_B which is consistent with the reported results.

Materials and Methods

Beef-heart cytochrome *c* oxidase was prepared by the method of Hartzell and Beinert (12). The enzyme was suspended in a 50 mM phosphate buffer containing 0.5 % Tween-20 at pH = 7.8-8.0. The concentration of the enzyme was determined spectrophotometrically ($\Delta\epsilon$(604 nm) = 24 mM^{-1} cm^{-1}) (13). Enzyme activity was measured polarographically and was typically 120-125 moles ferrocytochrome *c* (mole of oxidase)$^{-1}$ sec^{-1}. Some samples were prepared in ^2H_2O (containing 50 mM phosphate with 0.5 % Tween-20) at pD = 8.0. In that case, the enzyme was dialyzed for 6 hours into the deuterated, buffered solvent. To ensure that the dioxygen reduction site became completely exposed to deuterium, enough NADH (8 e^-/molecule) (plus mediator, phenazine methosulfate) was admitted to the oxygenated sample such that two reductive cycles were carried out.

ENDOR studies require very concentrated enzyme solutions, typically 1 mM. Cytochrome *c* oxidase was concentrated by a centrifugation technique, employing an Amicon microconcentrator. The microconcentrator has a porous membrane which allows the passage of any molecule with a molecular weight < 15 KD through the membrane upon centrifugation at 5 K RPM. After a 4 hours of centrifugation at 5 K RPM, we found that the enzyme was sufficiently concentrated (~0.9-1.2 mM) for the ENDOR study.

EPR and ENDOR samples were prepared in thick walled (5 mm O.D., 3.4 mm I.D.) quartz EPR tubes. The concentrated samples were thoroughly deoxygenated by repeated flushing with argon which had been deoxygenated by passage through a 1-m long column of manganous dioxide supported on vermiculite. Normally, 5-7 flushing cycles were performed. Deoxygenated oxidase samples were reduced by the addition of a two-fold excess of thoroughly deoxygenated NADH. Samples were then incubated for 40-65 hours at ice temperature to ensure complete reduction. Activation to the proposed ferryl Fe_{a_3}-containing state of cytochrome *c* oxidase was accomplished by the addition of excess hydrogen peroxide (4-6 mM) (either $H_2O_2^{16}$

or $H_2O_2^{17}$) to the reduced sample. After a brief incubation with the hydrogen peroxide (60 sec), a trace amount of catalase was added to remove the residual hydrogen peroxide. The catalase reaction produces $^{16}O_2$ (or $^{17}O_2$) and H_2O^{16} (or H_2O^{17}) (14). After the reoxidation procedure, the sample was immediately frozen to 77 K. Carbon monoxide was admitted to the frozen sample by the following procedure. The sample was evacuated while the sample end of the EPR tube was immersed in liquid nitrogen. Carbon monoxide (1 atm) was then admitted to the evacuated EPR tube. In some cases, we even condensed carbon monoxide into the EPR tube in order to increase the concentration of CO in the enzyme solution. We estimate that from 2-5 atm of CO were added by the latter procedure. Samples were rapidly thawed ($\sim$ 20 sec) by flowing tap water over the outside of the EPR tubes. This procedure prevented the rupture of the sample tube. After the sample tube was shaken, the sample was immediately frozen to 77 K for examination by EPR ($\sim$90 sec from thawing).

Hydrogen peroxide solutions were prepared by diluting a 30 % stock solution of hydrogen peroxide (Baker) into a buffered solution (50 mM phosphate, 1 mM EDTA (Baker)). If necessary, the hydrogen peroxide was diluted in a deuterated buffer in order to reoxidize samples contained in ^2H_2O. Isotopically enriched ^{17}O-labeled hydrogen peroxide was purchased commercially; the ^{17}O enrichment was 80 %. The concentration of the hydrogen peroxide solution was determined by employing an enzymatic assay (15).

EPR– EPR spectra were recorded on a Varian E-Line Century Series X-band spectrometer. Samples were examined at 77 K by the use of a liquid nitrogen finger dewar, which was inserted into the cavity. Conditions for obtaining the spectra are given in the figure legends.

ENDOR– The ENDOR experiments were conducted at T$<$ 2.1 K, employing 100 KHz detection (16). The operating frequency and power were typically 9.575 GHz and 45 dB, respectively. The conditions for the individual spectra are given

in the figure legends.

In many cases, the linewidth of the superhyperfine coupling between a paramagnetic center and a ligand is so small, relative to the large linewidths of EPR signals, that the couplings are unobservable by EPR. ENDOR spectroscopy, however, enables splittings in the megahertz range to be detected (17). In the ENDOR experiment, nuclear transitions are induced with a frequency swept RF-field at a constant external field H_o (18). Upon a nuclear transition of an interacting nucleus, there is a transient relief of the saturation of the EPR transition, which is manifested as an increase in the intensity of the EPR signal. Since changes in the EPR intensity are monitored, only nuclear transitions are observed for those nuclei which are coupled to the paramagnetic center.

A set of magnetically equivalent protons will give rise to a characteristic pair of lines (Eqn. 1) in the ENDOR spectrum. The pair of signals are separated by the hyperfine coupling constant (A^H), and the pattern is centered at the free proton Larmor frequency ($\nu_H = g_H\beta_H H_o/h$) (19-20).

$$\nu^H = \nu_H \pm A^H/2 \qquad (1)$$

As evidenced by Equation 1, the magnitude of the hyperfine coupling constant is independent of the external field H_o. However, the position of the doublet is dependent on the microwave frequency. For ^{14}N nuclei, the typical ENDOR pattern for a set of magnetically equivalent ^{14}N nuclei is given by Equation 2 (19-20)

$$\nu^N = A^N/2 \pm P^N \pm \nu_N \,, \qquad (2)$$

where P^N is the quadrupolar coupling constant. In contrast to the set of magnetically equivalent protons, the position of the ENDOR pattern for ^{14}N nuclei is independent of the microwave frequency. Equation 2 predicts a rather complicated ENDOR pattern. However, the quadrupolar coupling is usually unresolved in biological systems; typically, a simple two line ENDOR pattern is observed for ^{14}N nuclei, which is centered at $A^N/2$ (11).

RESULTS

EPR- In Figure 1 we show EPR spectra of the rhombic Cu_B EPR signal of cytochrome *c* oxidase, under a variety of experimental conditions: (*b*) ^1H_2O ($H_2O_2^{16}$-reoxidized), (*c*) ^2H_2O ($H_2O_2^{16}$-reoxidized) and (*d*) ^2H_2O ($H_2O_2^{17}$-reoxidized). Also shown for reference is an EPR spectrum of Cu_A (*a*). In Figure 1 *b*-*d*, the observed EPR signal is a superposition of two EPR signals, one from Cu_A and the other from Cu_B. The *g* tensor of Cu_A is $g_z = 2.18$, $g_y = 2.03$ and $g_x = 1.99$ (21). The Cu_A EPR signal exhibits no resolvable hyperfine coupling as shown in Figure 1*a*. The *g* tensor of the rhombic Cu_B EPR signal is $g_z = 2.28$, $g_y = 2.109$ and $g_x = 2.052$, with $A_{||} = 0.0102$ cm^{-1} (6). In the low-field region of the EPR spectra shown in Figure 1 *b*-*d*, two completely resolved hyperfine lines are observed which are due to Cu_B. A consequence of the superposition of the rhombic Cu_B EPR signal with the signal from Cu_A is that the positive feature of the Cu_A EPR signal at $g = 2.08$ is reduced in intensity due to overlap with the negative feature of the rhombic Cu_B EPR signal at $g = 2.07$ (6). The field position which was employed in this ENDOR study is indicated in Figure 1. At the designated field position there are no contributions due to Cu_A, therefore the ENDOR spectrum will be free from resonances associated with Cu_A. Furthermore, when the field is set to the g_z region of the rhombic Cu_B EPR signal, only those molecules oriented with their *z* axis parallel to the magnetic field will be probed, thus single crystal-like spectra are obtained (11).

Comparison of the rhombic Cu_B EPR signal in ^1H_2O (Fig. 1*b*) and ^2H_2O (Fig. 1*c*) reveals that there are no obvious differences between these two spectra which can be attributed to an isotope effect. In contrast, the $H_2O_2^{17}$-treated sample (in ^2H_2O) is broadened by 10 Gauss (Fig.1*d*), relative to the spectrum shown in either trace *b* or *c*. Although the broadening is most apparent in the parallel region of the spectrum (*inset e*), the consequences of this effect are also manifested in the high-field region where the superposition of Cu_A and Cu_B is most evident

Figure 1

EPR spectra of Cu_B at 77 K. After the reoxidation of fully reduced cytochrome *c* oxidase with excess $H_2O_2^{16}$, the spectrum shown in *a* was obtained. The rhombic Cu_B EPR signal of cytochrome *c* oxidase in ^1H_2O (*b*) and ^2H_2O (*c*). After the reoxidation of a reduced sample of cytochrome *c* oxidase with $H_2O_2^{17}$, followed by the addition of catalase and then 1-3 atm of CO, the EPR spectrum shown in *d* was obtained. The *inset* (*e*) compares the low-field hyperfine lines of the ^{16}O reoxidized sample (*c*) and the ^{17}O reoxidized sample (*d*). Conditions: Temperature, 77 K; microwave power, 4 mW (*a-d*) 16 mW (*e*); modulation amplitude, 10 Gauss (*a-e*); gain, 1.25 x 10^4 (*a*), 4 x 10^3 (*b*), 5 x 10^3 (*c-d*) and 8 x 10^3 (*e*); sample concentration, ~.35 mM (*a*), 0.9 mM (*b-e*).

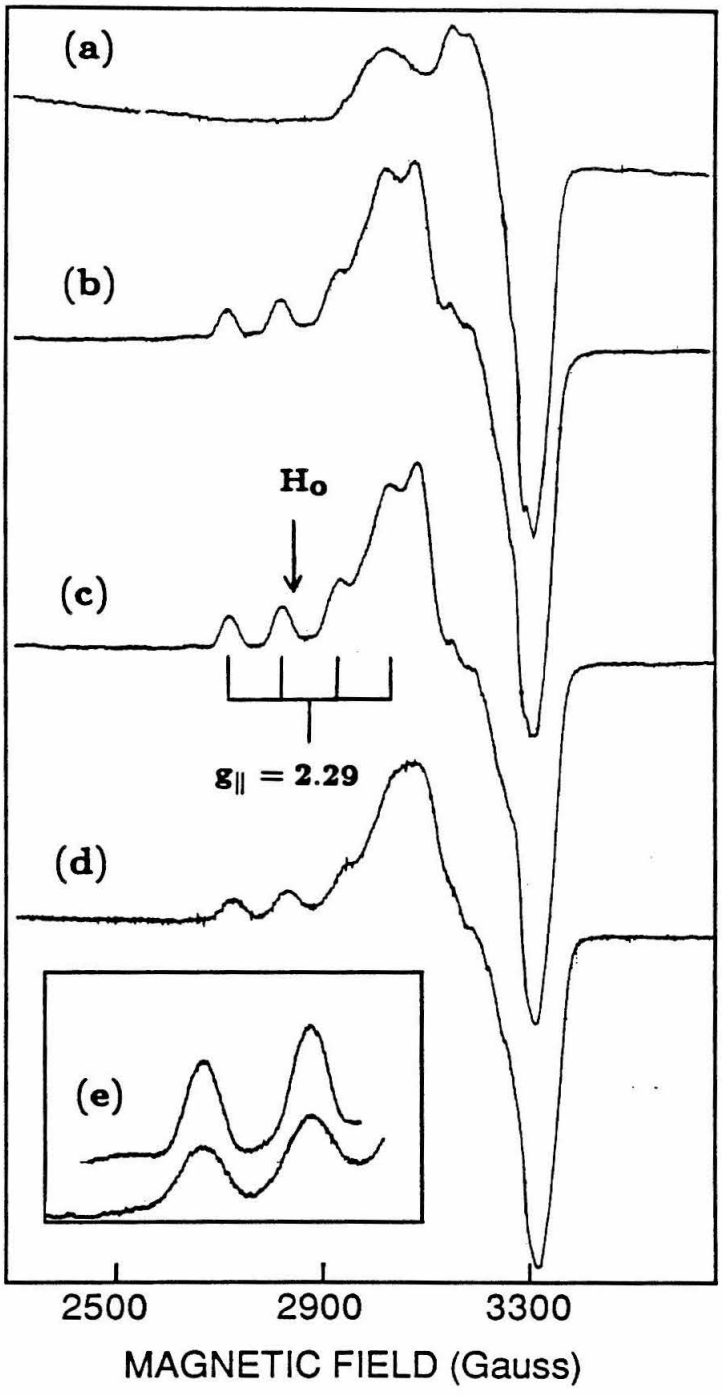
(a)
(b)
H_o
(c)
$g_{\|} = 2.29$
(d)
(e)
2500
2900
3300
MAGNETIC FIELD (Gauss)

(Fig. 1*d*). These EPR results suggest that there is a ligand hyperfine interaction between an ^{17}O-labeled ligand and the cupric Cu_B ion.

We examined the three different samples shown in Figure 1 by ENDOR in order to determine (i) the ligands to Cu_B which are associated with the apoprotein and (ii) to ascertain whether coupling to the ^{17}O-labeled ligand can be resolved.

^{14}N ENDOR of Cu_B in Native Cytochrome *c* Oxidase. ENDOR spectra of Cu_B, under a variety of experimental conditions, are shown in Figure 2. The field was fixed to the g_z region of the spectrum, hence only those orientations with the z axis parallel to the magnetic field are observed (11). The ENDOR spectrum of Cu_B in ^1H_2O is shown in Fig. 2*a*. The two well resolved signals at 17.9 and 16.1 MHz are separated by twice the expected ^{14}N Zeeman energy ($2\nu_N$ = 1.78 MHz), therefore the doublet is assigned to a ^{14}N hyperfine coupling of 34 MHz. The expanded spectrum of the high-frequency region of the spectrum is also shown in Figure 2. The expanded spectrum reveals two poorly resolved signals at approximately 21.5 and 19.7 MHz, which are split by the expected ^{14}N Zeeman energy of 1.78 MHz. Accordingly, we assign this weak doublet to a ^{14}N hyperfine coupling of 41 MHz. The doublet is so poorly resolved that in order to rule out that the signals are not due to ^1H, this assigment will have to be confirmed by repeating the experiment with another microwave frequency. If the signals at 21.5 and 19.7 are indeed due to ^{14}N, the center of the doublet will be invariant with a change in the microwave frequency; whereas, if the doublet is due to coupling to ^1H, the center of the doublet will shift with a change in the microwave frequency (Eqn. 1).

A broadband ENDOR spectrum of Cu_B is shown in Figure 3. The spectrum includes a lower-frequency region of the ENDOR spectrum, not observed in the spectrum in Figure 2. Inspection of Figure 3 reveals coupling to only one ^{14}N which is clearly resolved and is centered at $A_z/2 = 17$ MHz. The poorly resolved doublet, which is observed in the expanded spectrum (Fig. 2), is not seen in the broadband

Figure 2

ENDOR spectrum of Cu_B (^1H_2O) observed at $g = 2.33$. Sample is the same as shown in Figure 1 *b*. Conditions: Temperature, 2 K; microwave frequency, 9.575 GHz; microwave power, 50 dB; RF power, 20 watts; RF scan rate, 6.5 MHz/sec; number of scans, 200.

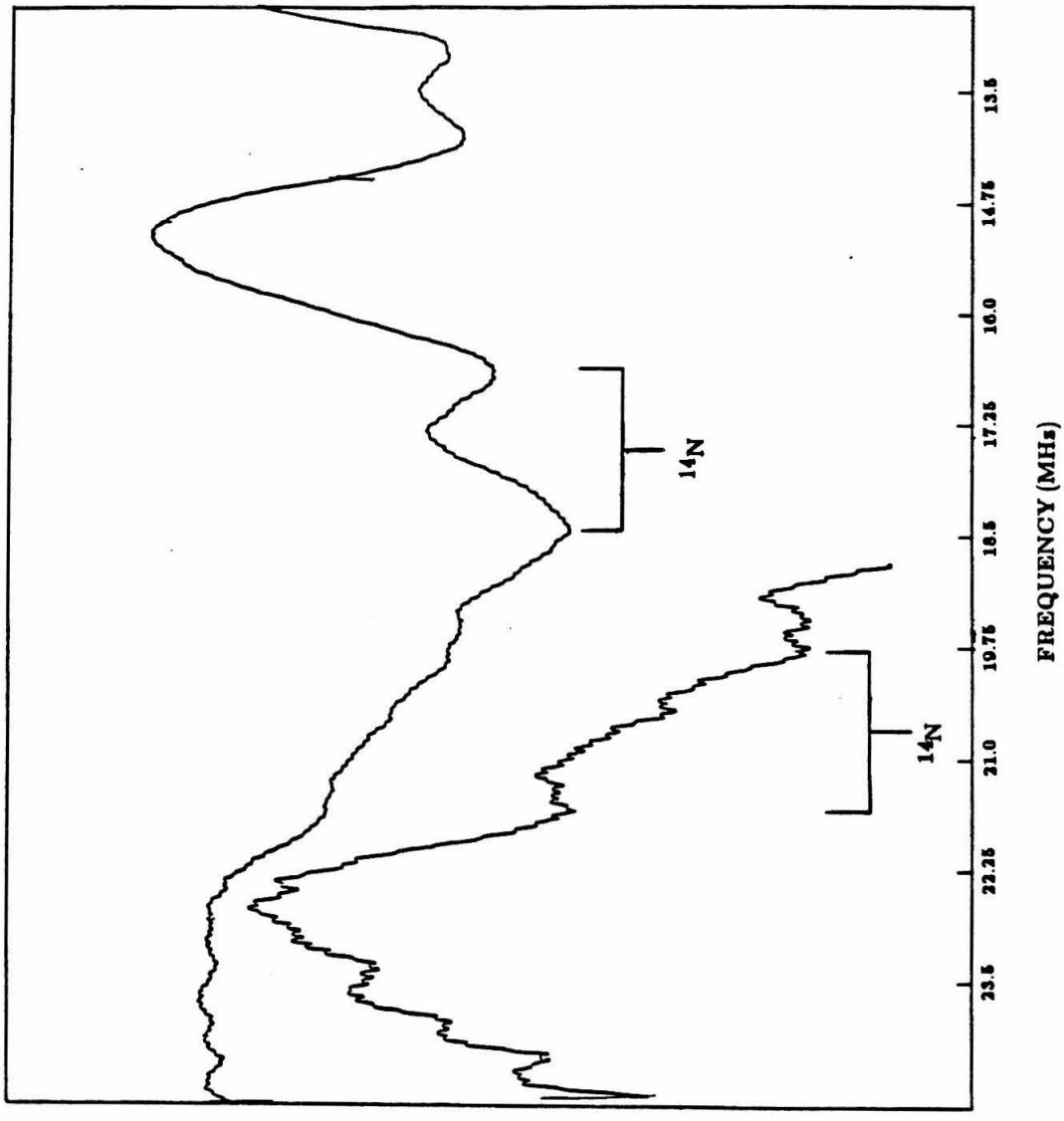
^{14}N
^{14}N
23.5
22.25
21.0
19.75
18.5
17.25
16.0
14.75
13.5
FREQUENCY (MHz)

Figure 3

Broadband ENDOR spectrum of Cu_B (^1H_2O) observed at $g = 2.33$. Conditions: Temperature, 2 K; microwave frequency, 9.575 GHz; microwave power, 50 dB; RF power, 20 watts; RF scan rate, 6.5 MHz/sec; number of scans, 400.

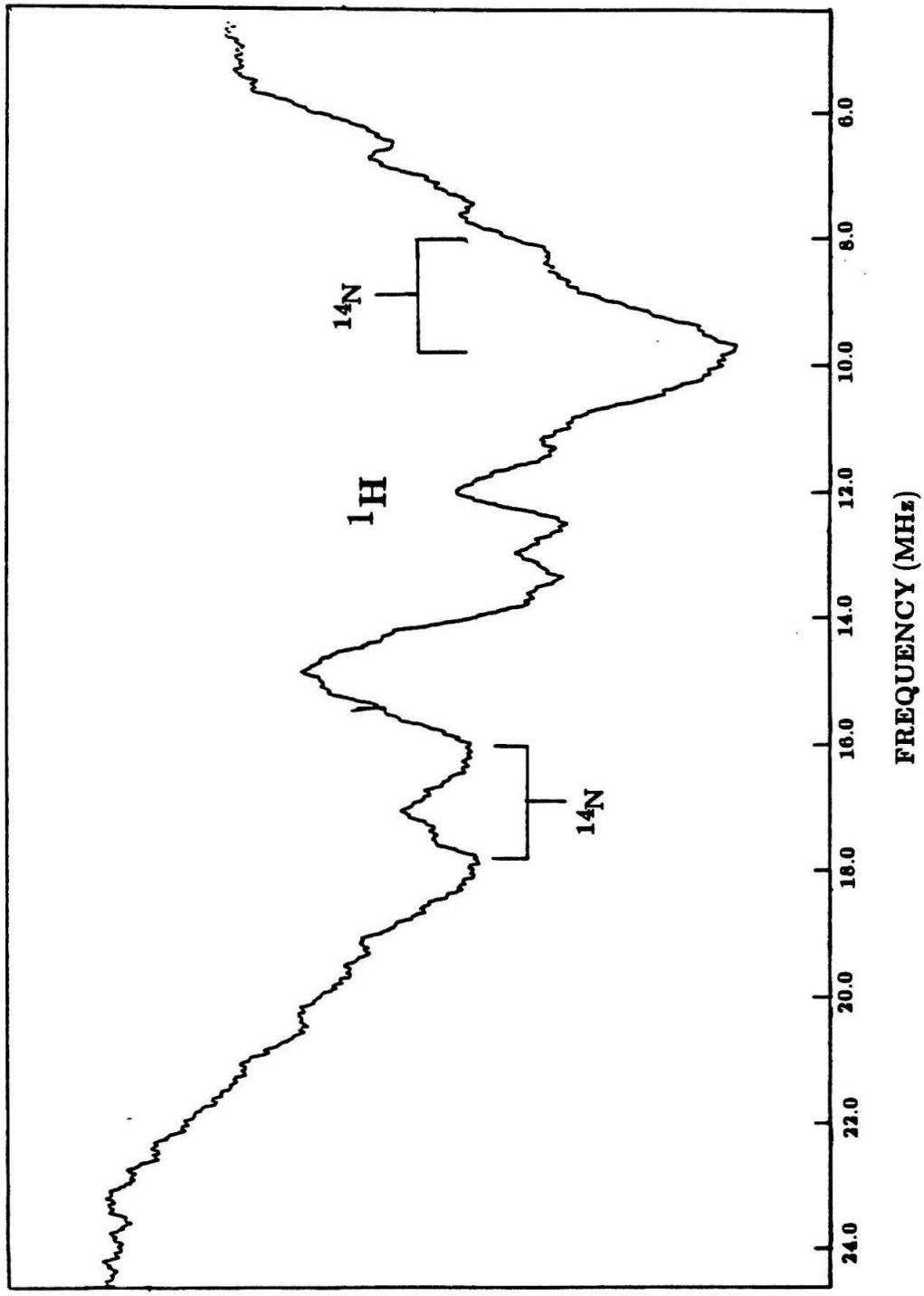
^{14}N
^{1}H
^{14}N
6.0
8.0
10.0
12.0
14.0
16.0
18.0
20.0
22.0
24.0
FREQUENCY (MHz)

spectrum (Fig. 3). In the low frequency region of the spectrum in Figure 3 we see evidence for a possible third ^{14}N coupling. The doublet is centered at a rather low frequency of ~9 MHz. The low-frequency resonance, expected at ~8 MHz, is probably obscured from overlap with proton resonances. More experimentation will be required before this tentative assignment can be confirmed. Specifically, different frequencies will be required which enable the protons to shift out of the spectral region surrounding 7 MHz, as predicted by Equation 1

^{17}O ENDOR of Cu_B. The ^{17}O-broadened sample of the rhombic Cu_B EPR signal was examined by the X-band ENDOR technique. The results are shown in Figures 4 and 5. Included in both figures are ENDOR spectra of Cu_B in ^2H_2O with the normal ^{16}O-oxygen isotope. Comparison of the two traces in Figure 4 reveals a signal at ~7 MHz in the ^{17}O-labeled sample (Fig. 4*a*), which is absent in the companion sample (Fig. 4*b*). (The feature is denoted in the Figure 4 by an arrow.) If this signal is due to hyperfine coupling from ^{17}O, we expect two sets of $2I = 5$ lines centered around the putative ν_O^{17} (22). However, the signal to noise level is so poor that we cannot resolve any of the quadrupolar splitting.

In Figure 5 we show the broadband ENDOR spectrum of the ^{17}O-labeled Cu_B. Once again, we see a reproducible feature in the ENDOR spectrum of the ^{17}O-labeled sample at ~7 MHz (Fig. 5*a*), which is absent in the spectrum of the normal isotope sample shown in Figure 5*b*. Under the conditions of the experiment in Figure 5 (2940 G, 9.575 GHz), the free proton Larmor frequency is 12.5 MHz. Hence we expect resonances due to protons which are coupled to the cupric ion to be centered around 12.5 MHz. However, some of interacting protons may have their low-frequency signal in the spectral region at ~7 MHz. Because of the expected overlapping signals due to protons resonances in this spectral region, without examining the signal at other microwave frequencies, we cannot make a definitive assignment of the signal at 7 MHz.

Figure 4

ENDOR spectrum of ^{17}O-labeled Cu_B (*a*) and ^{16}O-labeled (*b*) Cu_B observed at $g = 2.33$. Same samples as shown in Figure 1*c*,*d*. Conditions (*a* and *b*): Temperature, 2 K; microwave frequency, 9.575 GHz; microwave power, 45 dB; RF power, 20 watts; RF scan rate, 3.0 MHz/sec.

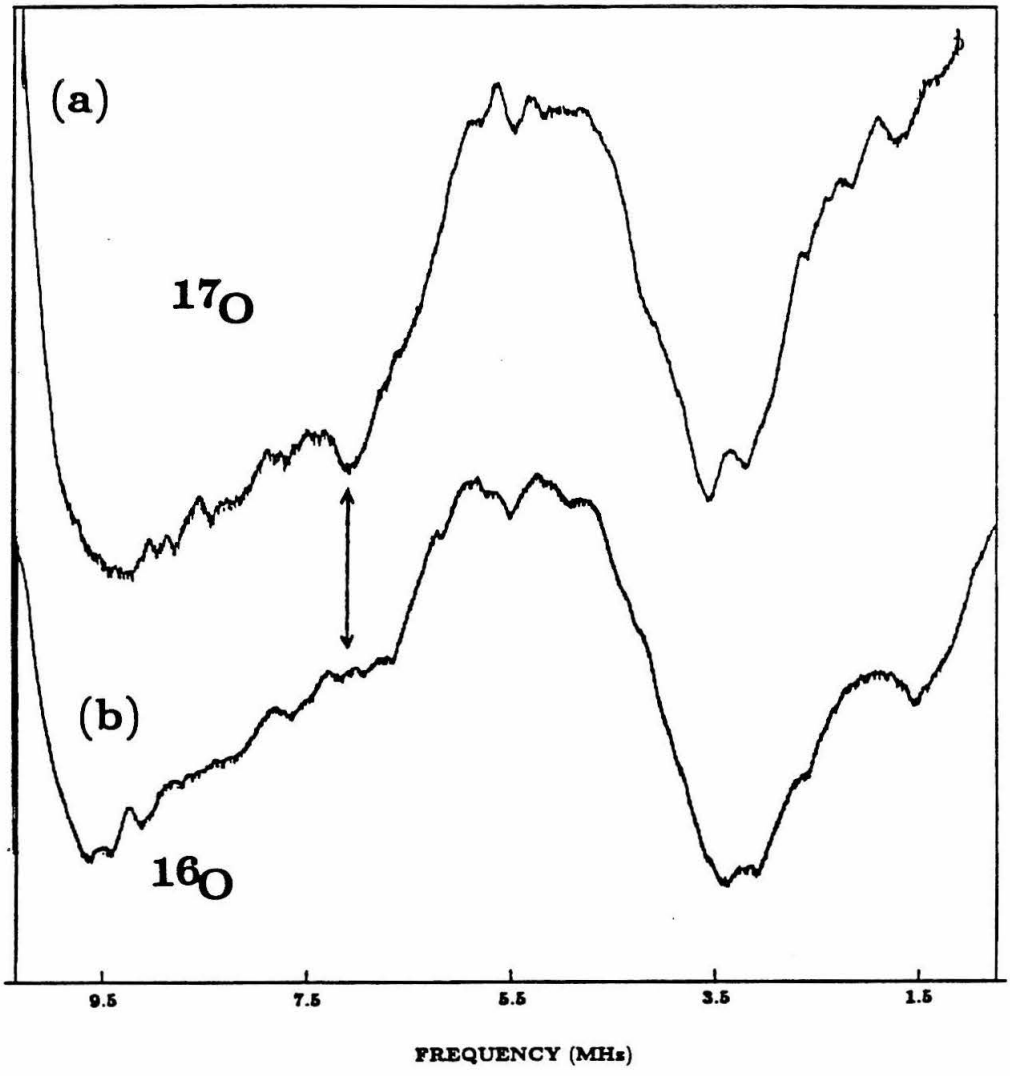
(a)
^{17}O
(b)
^{16}O
9.5
7.5
5.5
3.5
1.5
FREQUENCY (MHz)

Figure 5

Broadband ENDOR spectrum of ^{17}O-labeled Cu_B (*a*) and ^{16}O-labeled (*b*) Cu_B observed at $g = 2.33$. Same samples as in Figure 1*c*,*d*. Conditions (*a* and *b*): Temperature, 2 K; microwave frequency, 9.575 GHz; microwave power, 45 dB; RF power, 20 watts; RF scan rate, 3.0 MHz/sec; number of scans, 720.

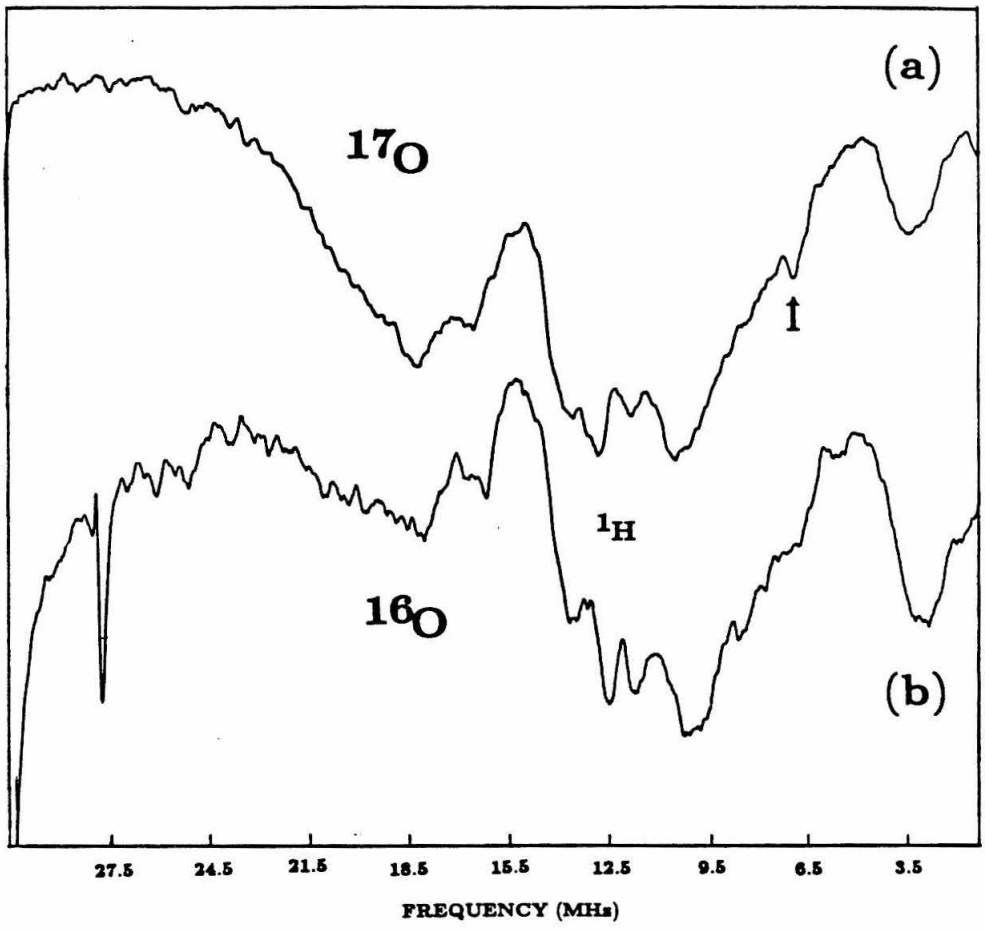
(a)
^{17}O
^{1}H
^{16}O
(b)
27.5
24.5
21.5
18.5
15.5
12.5
9.5
6.5
3.5
FREQUENCY (MHz)

DISCUSSION

Our ENDOR study of native beef-heart cytochrome *c* oxidase shows that there are two nitrogen ligands to Cu_B. We confirmed the previously reported well-resolved doublet, with the characteristic splitting due to ^{14}N, which has a ligand hyperfine coupling of 34 MHz (11). We discovered a poorly resolved doublet centered at 20.5 MHz, which is split by twice the characteristic ^{14}N Zeeman energy. Accordingly, this doublet is assigned to an ^{14}N hyperfine coupling of 41 MHz. Evidence for a third nitrogen coupling was also obtained in this work. There is a poorly resolved doublet centered at 9 MHz. Under the conditions of our experiment, the doublet cannot be due to Cu_A, and because of the large *g*-anisotropy of the Fe_a EPR signal, it is unlikely that the coupling is due to a ligand to Fe_a. Clearly, more experimentation is required to confirm that these latter resonances are due to ^{14}N.

A recent EXAFS study of the Cu_A-depleted cytochrome *c* oxidase showed that a $Cu(N,O)_3(S,Cl)$ coordination structure is most consistent with the EXAFS scattering pattern (5). The results reported here enable us to conclude that Cu_B has at least one, probably two, nitrogen ligands, i.e., $CuN_2(N,O)(S,Cl)$. With regard to the identity of the residues which contribute the nitrogen ligands to Cu_B, the magnitudes of the superhyperfine couplings are consistent with the histidine nitrogens (23). In order to unambiguously determine the nature of the amino acids which donate these nitrogenous ligands, isotopically labeled amino acids will have to be incorporated into the oxidase (24).

The ENDOR experiments on the broadened rhombic Cu_B EPR signal of cytochrome *c* oxidase suggest coupling to a ^{17}O-labeled ligand at $\sim$7 MHz. However, because this region of the spectrum contains overlapping signals from protons and nitrogens, and because the signal is so weak, it would be premature to assign the signal at $\sim$7 MHz to ^{17}O coupling. In order to confirm the putative coupling to an ^{17}O-containing ligand, ENDOR experiments will have to be conducted at

different microwave frequencies, frequencies that shift the proton resonances out of the spectral region surrounding 7 MHz.

The Nature of Cu_B

The g tensor and hyperfine coupling constant of the rhombic Cu_B EPR signal are strikingly similar to those reported for (i) native superoxide dismutase (and its various metallated derivatives) (25-26), (ii) the type-3 copper site in partially reduced tree and fungal laccase (6) and (iii) the type-3 site in partially reduced hemocyanin (6,27). The g tensors of the EPR signals from these disparate species are definitely rhombic. Regarding the magnitude of the hyperfine coupling constant ($A_{||}$), the hyperfine coupling constants in the parallel region of the spectra are larger than those observed for the type-1 "blue-copper" proteins, yet the coupling is smaller than that typically observed for inorganic copper complexes, or type-2 copper complexes (25). The similarities in the g tensors and the hyperfine coupling constants for species (i-iii) and for the rhombic Cu_B EPR signal of cytochrome c oxidase suggest that these disparate enzymatic states have similar coordination environments for the copper centers. An examination of the coordination structure of the copper center in superoxide dismutase and one of its metal-substituted derivatives may lend insight into the coordination structure of Cu_B.

X-ray crystallographic studies have demonstrated that native superoxide dismutase contains a binuclear active site composed of a cupric ion separated from a neighboring zinc ion by ~6Å (28-29). In the oxidized state of the enzyme, the copper center is penta-coordinate, with four histidine nitrogen ligands comprising a distorted plane. A water molecule is the fifth, axial ligand. The zinc ion is stabilized in a distorted tetrahedral environment by three histidine nitrogen ligands and by a nitrogen donated from an aspartate residue (28-29). Regarding the EPR signature of native superoxide dismutase, the native enzyme exhibits a rhombic

copper EPR signal ($g_z = 2.257$, $g_z = 2.103$ and $g_z = 2.025$, with $A_{||} = .0132$ cm^{-1}) (25). It is intriguing that when copper is substituted into the zinc site of superoxide dismutase (with zinc in the copper site) (25), the hyperfine coupling constant ($A_{||}$) ($g_z = 2.289$, $g_y = 2.15$, $g_z = 2.01$ and $A_{||} = 0.0102$ cm^{-1}) is almost identical to that reported for the Cu_B EPR signal of cytochrome *c* oxidase, *e.g.*, $g_z = 2.278$, $g_y = 2.109$, $g_x = 2.052$ and $A_{||} = 0.0102$ cm^{-1} (6). This correspondence suggests that Cu_B may have a distorted tetrahedral environment, similar to that of the zinc site of superoxide dismutase. (The underlying assumption is that when copper is substituted into the zinc site, the site retains its distorted tetrahedral structure, although certainly H_2O might coordinate to the copper ion which occupies the zinc site.)

Before discussing a model for the structure of the Cu_B site in cytochrome *c* oxidase, we should examine the implications of the observed broadening of the rhombic Cu_B EPR signal by an ^{17}O-labeled ligand. The 428/580 nm state of cytochrome *c* oxidase was prepared by reoxidation of the fully reduced enzyme with excess $H_2O_2^{17}$ in $^2H_2O^{16}$. The reoxidation of the fully reduced enzyme by ^{17}O-labeled hydogen peroxide and the resultant activation to the proposed ferryl Fe_{a_3}/cupric Cu_B state of the enzyme results in the production of $O^{17}H^-$. Before the addition of carbon monoxide, catalase is added to the sample to remove the residual hydrogen peroxide. The catalase reaction produces H_2O^{17} and O_2^{17}. Therefore, it is plausible that the rhombic Cu_B EPR signal is broadened as a result of an interaction with either ^{17}O-hydroxide or even by an oxygen atom derived from ^{17}O-dioxygen.

A proposed structure of Cu_B in the resting state of cytochrome *c* oxidase is shown in Scheme I. The model is based on a four coordinate copper ion, although we cannot rule out that the site is five-coordinate. Cu_B has two nitrogen ligands, and possibly a third nitrogen, with superhyperfine couplings suggestive of two histidine nitrogens. Moreover, the rhombic *g* tensor is consistent with a site of

Scheme I

Proposed scheme for the structure of the binuclear dioxygen reduction site of cytochrome *c* oxidase and for the formation of the half-reduced dioxygen reduction site, *i.e.*, the state which gives rise to the rhombic Cu_B EPR signal.

SCHEME I

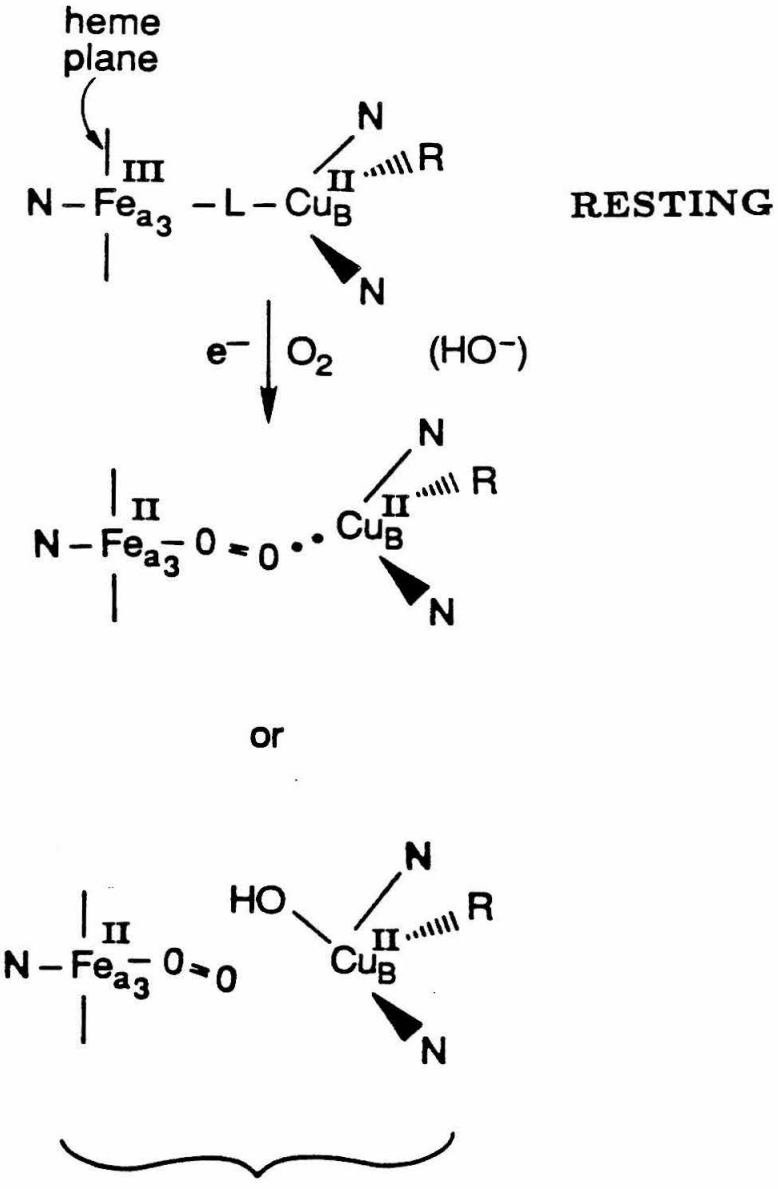

HALF-REDUCED DIOXYGEN REDUCTION SITE

(rhombic Cu_B EPR signal)

low symmetry. Thus, we propose that the Cu_B site has a distorted tetrahedral structure, which is akin to the structure of the superoxide dismutase zinc site, with possibly chloride as a bridging ligand (5) between the copper ion and Fe_{a_3}. Formation of the species which gives rise to the rhombic Cu_B EPR signal may result upon the one-electron reduction of the enzyme (6-7), as shown in Scheme I, or upon the addition of CO to the 428/580 nm state of the enzyme (Chap. III, Scheme IV). The results reported here offer two possibilities for the oxygen-containing ligand to Cu_B: (i) A hydroxyl ligand may be directly coordinated to cupric Cu_B as shown in Scheme I, or (ii) an intriguing possibility is that the distal oxygen atom of the Fe_{a_3}-bound dioxygen molecule interacts with Cu_B, *i.e.*, dioxygen bridges the half-reduced binuclear dioxygen reduction site. Both of these proposed species would be expected to give rise to the rhombic Cu_B EPR signal as long as ferrous Fe_{a_3} is stabilized in the low-spin state by dioxygen.

The proposed interaction between the distal oxygen atom of dioxygen and cupric Cu_B might be facilitated by charge transfer from the ferrous Fe_{a_3} to the dioxygen molecule ($Fe^{II+\delta}_{a_3}$-O=O$^{-\delta}$ Cu^{II}_B). In this case, cupric Cu_B may then act like a strong Lewis acid and interact with the distal oxygen atom. Conceivably, the proposed mixed-valence bridged-dioxygen complex of the binuclear dioxygen reduction site of cytochrome *c* oxidase may have physiological significance. For example, the suggested interaction between the distal oxygen atom of the dioxygen molecule and cupric Cu_B would serve to *anchor* the dioxygen molecule to the dioxygen reduction site when only one electron is at the site. Moreover, upon the transfer of the second electron to the site, there would be minimal rearrangement necessary to accomodate the peroxidic species which is also thought to bridge Fe_{a_3} and Cu_B (30). In the future, experiments may be designed to test whether dioxygen bridges the binuclear dioxygen reduction site in the species which gives rise to the rhombic Cu_B EPR signal, or whether hydroxide is coordinated to Cu_B. Moreover, the novel reaction between the 428/580 nm state of cytochrome

c oxidase and carbon monoxide proved to be a valuable route to large populations of the rhombic Cu_B EPR signal. This method should be exploited in future experiments.

REFERENCES

1. Wikström, M., Krab, K. and Saraste, M. (1981) *Cytochrome Oxidase - Synthesis*, (Academic Press, New York), p. 7.
2. Orii, Y. (1963) *J. Biochem.* **54**, 207-213.
3. Markossian, K.A., Poghossian, F.A., Paitain, N.A. and Nalbandyan, R.M. (1978) *Biochim. Biophys. Res. Commun.* **81**, 1336-1343.
4. Nicholls, P. and Chanady, G. (1981) *Biochim. Biophys. Acta* **634**, 256-265.
5. Li, P.M., Gelles, J., Chan, S.I., Sullivan, R.J. and Scott, R.A. (1987) *Biochem.* **26**, 2091-2095.
6. Reinhammer, B., Malkin, R., Jensen, P., Karlsson, B., Andréasson, L.-E., Aasa, R., Vänngård, T. and Malmström, B. (1980) *J. Biol. Chem.* **255**, 5000-5003.
7. Karlsson, B. and Andréasson, L.-E. (1981) *Biochim. Biophys. Acta* **635**, 73-83.
8. Blair, D.F., Witt, S.N. and Chan, S.I. (1985) *J. Am. Chem. Soc.* **107**, 7389-7399.
9. Witt, S.N. and Chan, S.I. (1987) *J. Biol. Chem.* **262**, 1446-1448.
10. Blair, D.F., Martin, C.T., Gelles, J, Wang, H., Brudvig, G.W., Stevens, T.H. and Chan, S.I. (1983) *Chemica Scripta* **21**, 43-53.
11. Cline, J., Reinhammer, B., Jensen, P., Venters, R. and Hoffman, B.M. (1983) *J. Biol. Chem.* **258**, 5124-5128.
12. Hartzell, C.R. and Bienert, H. (1974) *Biochim. Biophys. Acta* **368**, 318-338.
13. Blair, D.F., Bocian, D.F., Babcock, G.T. and Chan, S.I. (1982) *Biochem.* **21**, 6928-6935.

14. Schonbaum, G.R. and Chance, B. (1976) in *The Enzymes*, (Boyer, ed.) Vol. XIII, pp. 363-408.

15. Cotton, M.L. and Dunford, H.B. (1973) *Can. J. Chem.* **51**, 582-587.

16. Hoffman, B.M., Roberts, J.E., Kang, C.H. and Margoliash, E. (1981) *J. Biol. Chem.* **256**, 6556-6564.

17. Hütterman, J. and Kappl, R. (1987) *Metal Ions in Biol.*, Vol. 22, pp. 1-80.

18. Roberts, J.E., Hoffman, B.M., Rutter, R. and Hager, L.P. (1981) *J. Biol. Chem.* **256**, 2118-2121.

19. Atherton, N.M. (1973) *Electron Spin Resonance*, Wiley, New York.

20. Carrington, A. and McLachlan. A.P. (1967) *Intro. to Magnetic Resonance*, Harper and Row, New York.

21. Aasa, R., Albracht, S.P.J., Falk, K.-E., Lanne, B. and Vänngård, T. (1976) *Biochim. Biophys. Acta* **422**, 260-272.

22. Telser, J., Emptage, M.H., Merkle, H., Kennedy, M.C., Beinert, H. and Hoffman, B.M. (1986) *J. Biol. Chem.* **261**, 4840-4846.

23. Roberts, J.E., Brown, T.G., Hoffman, B.M. and Peisach, J. (1980) *J. Am. Chem. Soc.* **102**, 825-829.

24. Stevens, T.H., Martin, C.T., Wang, H., Brudvig, G.W., Scholes, C.P. and Chan, S.I. (1982) *J. Biol. Chem.* **257**, 12106-12113.

25. Pantoliano, M.W., Valentine, J.S. and Nafie, L.A. (1982) *J. Am. Chem. Soc.* **104**, 6310-6317.

26. Pantoliano, M.W., Valentine, J.S., Mammone, R.J. and Scholler, D.M. (1982) *J. Am. Chem. Soc.* **102**, 1717-1723.

27. Himmelwright, R.S., Eickman, N.C. and Solomon, E.I. (1978) *Biochem. Biophys. Res. Commun.* **81**, 243-247.

28. Richardson, J.S., Thomas, K.A., Rubin, B.H. and Richardson, D.C. (1975) *Proc. Natl. Acad. Sci. USA* **72**, 1349-1353.

29. Beem, K.M., Richardson, D.C. and Ragagopalan, K.V. (1977) *Biochem.* **16**,

1930-1936.

30. Wikström, M., Krab, K. and Saraste, M. (1981) *Cytochrome Oxidase- A Synthesis*, Academic Press, New York, pp. 124-128.